

**METHODOLOGY TO PREDICT NATURAL
GAS IN LOADING AND UNLOADING OF
COMPRESSED NATURAL GAS (CNG)
OPERATIONS**

by

Erika Beronich

PhD Thesis

Faculty of Engineering and Applied Science

Memorial University of Newfoundland

October 2014

St John's

Newfoundland

ABSTRACT

Exploiting stranded gas reservoirs, associate gas from offshore production platforms, condensate gas reservoirs may not be feasible using traditional approaches (i.e. pipelines) due to gas volumes, composition, location and/or climate. Marine Compressed Natural Gas (CNG) technology is a possible alternative; however, the required gas quality for CNG remains a challenge in commercial deployment. The optimal design conditions to safely and efficiently load, store, and unload CNG vessels are highly dependent on the quality of the gas. The objective of this work was to evaluate the impact of moderate/rich gases in CNG technology by performing dynamic simulations of the loading and unloading operations. It was demonstrated that existing Equations of State (EOS) are limited in accurately predicting the behaviour of the gas under load/unload conditions, particularly for gases with large heavy hydrocarbons content. Experiments with laboratory-synthesized gas samples were conducted using a PVT cell. The accuracy of the EOSs in predicting dew points, liquid dropout percentages, and gas densities was evaluated using the experimental data from the laboratory and literature. After tuning Peng-Robinson (PR) and Soave-Redlich-Kwong (SRK) equations to improve their predictions, their performance was evaluated using the HYSYS process simulator. A marked improvement in the EOS predictions was achieved by modifying a few EOS parameters. Dew point predictions were improved by adjusting binary interaction parameters (k_{ij}), the density predictions were improved by modifying the Peneloux parameters, and modifying both k_{ij} and Peneloux parameters enhanced the liquid dropout predictions. Dynamic simulations of the loading and unloading operations of a CNG tank

were then performed to evaluate the effect of the heavy hydrocarbon content of the gases. Overall, removing all the heavier hydrocarbons appeared to produce very low temperatures during the unloading operation, while not removing these components caused an accumulation of liquids inside the tank at keel pressure. In addition, the simulation of the loading and unloading of a CNG tank was attempted in the laboratory using the PVT system; however, the attempt was unsuccessful as the system would require major modifications.

ACKNOWLEDGMENTS

First, I would like to deeply thank my supervisors Dr. Majid Abdi and Dr. Kelly Hawboldt, who believed in me and gave this great opportunity. They provided me with useful and helpful assistance, experimental equipment and support.

This thesis has received financial support from the National Research Council of Canada NRC, Atlantic Canada Opportunity Agency (ACOA) through the Centre for Marine CNG Inc., as well support from the National Science and Engineering Research Council of Canada (NSERC), and School of Graduate Studies of Memorial University of Newfoundland.

I would also like to thank Ms Moya Crocker, Secretary to the Associated Dean of Graduate Studies and Research, and Dr. Leonard Lye, Associated Dean of Graduate Studies and Research, for their efficiency and kindness.

TABLE OF CONTENTS

ABSTRACT	i
ACKNOWLEDGMENTS.....	iii
TABLE OF CONTENTS	iv
LIST OF FIGURES	x
LIST OF TABLES	xvii
NOMENCLATURE.....	xxi
CHAPTER 1	1
INTRODUCTION	1
1.1 Background information	1
1.2 Challenges in CNG loading and unloading operations.....	4
1.3 CNG and condensate reservoirs.....	5
1.4 Applications for liquid yield prediction of gas condensates.....	6
1.5 Objectives of Research.....	7
1.6 Outline of Thesis.....	8
CHAPTER 2.....	10
LITERATURE REVIEW.....	10
2.1 Marine CNG transportation	10
2.1.1 Existing Marine CNG Technologies.....	11
2.2 Classification of Gas Samples	14
2.2.1 Plus Fractions Characterization	15

2.3 Development of the Equation of States (Thermodynamic models).....	16
2.4 Review of EOS Predictions	19
2.4.1 Dew Points Prediction.....	20
2.4.2 Liquid Dropout Prediction	22
2.5 Tuning EOS to Improve Predictions of Gas Condensates	23
2.6 Prediction of Phase Behaviour.....	24
2.7 Application of Research to Marine CNG Technologies	27
2.8 Conclusions.....	28
CHAPTER 3.....	29
EXPERIMENTAL WORK.....	29
3.1 Set up Description.....	30
3.1.1 Gas Chromatography	30
3.1.2 Fluid Phase Behaviour or PVT System	31
3.1.3 Densitometer	34
3.2 Preparation of gas mixtures.....	35
3.2.1 Transferring the gas mixture	38
3.3 Experimental procedures	43
3.3.1 Constant Composition Expansion (CCE)	44
3.3.2 Constant Volume Depletion (CVD).....	46
3.4 Experimental Errors	49
3.4.1 Limitations in performing PVT experiments.....	53
3.4.2 Validation of PVT Experimental Test Results.....	54
3.5 Simulation of the filling of a CNG tank in the laboratory	57

3.6 Tuning the EOS.....	62
3.7 Conclusions.....	63
CHAPTER 4.....	65
EVALUATION OF EQUATIONS OF STATE	65
4.1 Dew Points	65
4.1.1 Deviation of EOS predictions for synthetic gas samples.....	67
4.1.2 Deviation of EOS predictions for field natural gas samples.....	82
4.2 Liquid Dropout.....	84
4.3 Density	88
4.3.1 Density in the supercritical fluid region.....	89
4.3.2 Gas Densities in the two phase region	94
4.4 Compressibility in the supercritical region	97
4.5 Conclusions.....	99
CHAPTER 5.....	101
MATHEMATICAL MODEL	101
5.1 Mathematical Models descriptions	101
5.2 Equation Tuning Process based on Experimental Results	105
5.2.1 Method to tune parameters of EOS.....	105
5.2.2 Steps in tuning EOS	107
5.2.2 Mathematical model solution.....	112
5.3 Conclusion	112
CHAPTER 6.....	114
PROPOSED APPROACH FOR IMPROVEMENT OF THE EOS PREDICTIONS	114

6.1 Dew Points	114
6.2 Liquid Dropout.....	124
6.3 EOS Parameter modified for improvement of the dew point and liquid dropout predictions	129
6.4 Density	131
6.5 Compressibility	133
6.6 Conclusion	136
CHAPTER 7	137
DYNAMIC SIMULATION OF LOADING AND UNLOADING CNG TANKS	137
7.1 Methods to Adjust Gas Composition	138
7.2 Dynamic Simulations of Loading and Unloading a CNG Tank	138
7.2.1 Principal assumption to perform the dynamic simulations.....	138
7.2.2 Conservation Relationships	140
7.3 Dynamic Simulation Conditions.....	143
7.4 Simulations of Loading Operation of a CNG Tank	146
7.4.1 Feed Pressure for the loading of a CNG tank	147
7.4.2 Feed Temperature	153
7.4.3 Molar Flow.....	157
7.4.4 Gas Composition.....	159
7.5 Unloading Conditions	161
7.5.1 Effect of initial temperature	163
7.5.2 Effect of gas composition	166
7.5.3 Effect of molar flow.....	169

7.6 Impact of Gas Composition	170
7.6.1 Consequences of an incorrect prediction by the EOS when flashing a rich gas.	171
7.7 Original vs Tuned EOSs	174
7.8 Conclusions.....	175
CHAPTER 8.....	178
CONCLUSIONS AND RECOMMENDATIONS.....	178
8.1 Concluding Summary	178
8.1.1 Dynamic Simulations of Loading and Unloading a CNG tank	179
8.1.2 Experimental Approach	181
8.1.3 EOS Performance.....	182
8.1.4 Method to Improve EOS predictions	186
8.2 Objectives Reached.....	188
8.3 Mayor Contributions	190
8.4 Recommendations.....	191
REFERENCES	194
APPENDIX A.....	202
A.1 Initial Mass Balance for first CVD sample using experimental data.....	202
A.1.1 System of equations to solve unknown.....	203
A.1.2 Result of Mass balance using experimental data for First CVD sample.....	204
A.1.3 Checking consistency of the data	205
A.1.4 New K-values to re-calculate the mass balance	206
A.2 Experimental Procedures	207
APPENDIX B.....	212

APPENDIX C.....	216
C.1 Experimental Errors of the data of synthetic gas samples obtained from the literature	216
C.1.1 Experimental data obtained from literature for evaluating Dew Points.....	216
C.2 Experimental Errors of the data of natural gas samples obtained from the literature	221
C.2.1 Experimental data obtained from literature for evaluating Dew Points.....	221
APPENDIX D.....	222
APPENDIX E.....	232
E.1 Binary Interaction Parameters (k_{ij}).....	232
E.1.1 Original k_{ij} for PR and SRK used for synthetic gas samples.....	232
E.1.2 k_{ij} for PR used for NG3 sample.....	232
E.1.3 Volume translation parameters.....	233

LIST OF FIGURES

Figure 2.1:	Schematic diagram of a typical marine CNG transport chain (TransCanada, 2007)	12
Figure 2.2:	Phase envelope diagram for a typical natural gas composition	26
Figure 3.1:	Schematic of PVT systems	32
Figure 3.2:	Schematic of a tapered piston	33
Figure 3.3:	Flow diagram of the set up for gas mixtures preparation	37
Figure 3.4:	Picture of the panel for gas mixtures preparation	38
Figure 3.5:	Flow diagram of the system to transfer gas mixtures to PVT cell	41
Figure 3.6:	Picture of the system to transfer gas mixtures to PVT cell	42
Figure 3.7:	The liquid dropout percentages of the diverse CCE tests for Mix 5 at 60 °C	52
Figure 3.8:	Schematic of the glass tube inside the PVT cell, where the gas is charged	59
Figure 3.9:	Change of pressure and temperature inside of the PVT Cell with time during the loading and unloading of the cell with gas.	61
Figure 3.10:	Schematic showing the glass tube and the steel cell relative radius.	62
Figure 4.1:	Experimental and predicted dew point curves for Mix 3	70
Figure 4.2:	Experimental and predicted dew point curves for Mix 4	72
Figure 4.3:	Experimental and predicted dew point curves for SNG1	74
Figure 4.4:	Experimental and predicted dew point curves for SNG2	75
Figure 4.5:	Experimental and predicted dew point curves for SNG3	76
Figure 4.6:	Experimental and predicted dew point curves for SNG4	77
Figure 4.7:	Experimental and predicted dew point curves for SNG5	77
Figure 4.8:	Experimental and predicted dew point curves for SNG6	78
Figure 4.9:	Experimental and predicted dew point curves for SNG8	78
Figure 4.10:	Experimental and predicted dew point curves for SNG7	79

Figure 4.11:	Experimental and predicted dew point curves for SNG9	80
Figure 4.12:	Experimental and predicted dew point curves for SNG10	81
Figure 4.13:	Predicted liquid dropout of PR and SRK versus pressure for the synthetic gas at 40 °C	85
Figure 4.14:	Predicted liquid dropout of PR and SRK versus pressure for the synthetic gas at 60 °C.	86
Figure 4.15:	Predicted liquid dropout of PR and SRK versus pressure for the natural gas sample at 156 °C.	87
Figure 4.16:	Percentage errors of molar density predictions of PR in supercritical region as a function of temperatures for RG2 gas sample.	91
Figure 4.17:	Percentage errors of molar density predictions of SRK in supercritical region as function of temperatures for RG2 gas sample.	91
Figure 4.18:	Average percentage errors of PR and SRK in predicting gas densities during CVD Test for Mix 5 at 40 °C.	96
Figure 4.19:	Average percentage errors of PR and SRK in predicting gas densities during CVD Test for Mix 5 at 60 °C.	96
Figure 4.20:	Average percentage errors of PR and SRK in predicting compressibility of natural gas sample NG3 in the supercritical region as function of temperatures.	98
Figure 5.1:	Screenshot of PVTPro.5.1 software where the data for tuning are selected and the relative weight percentages are designated.	111
Figure 6.1:	Dew point curves of PR and SRK before and after tuning together with the experimental values for samples SNG1	116
Figure 6.2:	Dew point curves of PR and SRK before and after tuning together with the experimental values for samples SNG5	116
Figure 6.3:	Absolute percentage errors of the temperature predicted at the experimental saturated pressure of PR and SRK for SNG5.	117
Figure 6.4:	Dew point curves of PR and SRK before and after tuning	118

	together with the experimental values for samples SNG4	
Figure 6.5:	Dew point curves of PR and SRK before and after tuning together with the experimental values for samples SNG6	119
Figure 6.6:	Absolute percentage errors of the temperature predicted at the experimental saturated pressure of PR and SRK for SNG6.	120
Figure 6.7:	Dew point curves of PR and SRK before and after tuning together with the experimental values for samples SNG8	120
Figure 6.8:	PR and SRK predicted dew point curves for NG3 before and after tuning together with the experimental values	123
Figure 6.9:	Absolute percentage errors of the temperature predicted at the experimental saturated pressure of PR and SRK for NG3.	123
Figure 6.10:	Absolute percentage of error for Liquid dropout during CCE Tests at 40 °C for Mix 5	125
Figure 6.11:	Absolute percentage of error for Liquid dropout percentage during CCE Tests at 50 °C for Mix 5	125
Figure 6.12:	Absolute percentage of error for Liquid dropout percentage during CCE Tests at 55 °C for Mix 5	126
Figure 6.13:	Liquid dropout percentages versus pressures during CCE Tests at different temperatures for the natural gas sample. (Left top: 117 °C, right top: 136 °C, left bottom: 156 °C, right bottom: 177 °C)	128
Figure 6.14:	Absolute percentage errors of gas density predictions of PR and SRK for Mix 4 during CVD test at 0 °C	132
Figure 6.15:	Absolute percentage errors of gas density predictions of PR and SRK for Mix 5 during CVD test at 40 °C	132
Figure 6.16:	Absolute percentage errors of gas density predictions of PR and SRK for Mix 5 during CVD test at 60 °C	133
Figure 6.17:	Absolute percentage errors of compressibility predictions of PR for NG3	134

Figure 6.18:	Absolute percentage errors of compressibility predictions of SRK for NG3	135
Figure 7.1:	Dew point curves of the original gas samples before flashing employed for the study of the dynamic loading and unloading of a CNG tank.	145
Figure 7.2:	Flow diagram of loading a CNG tank with one feed stream a constant high pressure (arrangement named 1P)	148
Figure 7.3:	Flow diagram of loading a CNG tank with two feed streams in series, one with a low pressure and the other one with a high pressure (arrangement named 2P)	148
Figure 7.4:	Flow diagram of loading a CNG tank with three feed streams in series, one with a low pressure, the second one with a medium pressure and the last one with a high pressure (arrangement named 3P)	149
Figure 7.5:	Pressure trends of the SNG1 inside a CNG tank during the loading operation with a Feed Stream Temperature of 20 °C using diverse loading alternatives (1P, 2P, 3P)	151
Figure 7.6:	Temperatures trends of the loading of a CNG tank with SNG1 sample at a Feed Temperature of 20 °C using diverse feed alternatives (1P, 2P, 3P)	152
Figure 7.7:	Liquid Dropout trends of the loading of a CNG tank with SNG1 sample at a Feed Temperature of 20 °C using diverse feed alternatives (1P, 2P, 3P)	152
Figure 7.8	Temperatures trends of the loading of a CNG tank with SNG1 sample at a Feed Temperature of 20 and 80 °C	153
Figure 7.9:	Liquid dropout trends of the SNG1 inside a CNG tank during the loading operation with a Feed Stream Temperature of 20 and 80 °C	155

Figure 7.10:	Pressure trends of the SNG1 inside a CNG tank during the loading operation with a Feed Stream Temperature of 20 and 80 °C	155
Figure 7.11:	Pressure trends of SNG1 inside a CNG tank during loading it with a Feed Molar Flow of 5 and 10 kgmol/hr and 40 °C.	158
Figure 7.12:	Temperature trends of SNG1 inside a CNG tank during the loading operation with a Feed Molar Flow of 5 and 10 kgmol/hr and 40 °C.	158
Figure 7.13:	Liquid Dropout trends of SNG1 inside a CNG tank during the loading operation with a Feed Molar Flow of 5 and 10 kgmol/hr and 40 °C.	159
Figure 7.14:	Temperature trends of the three different gases: NG2, SNG1, and SNG2	160
Figure 7.15:	Pressure trends of the loading of a CNG tank with three different gases: SNG 1, SNG 2 after flashing with two separators, and NG after flashing with four separators. The Feed Flow was 5 kgmol/hr and feed temperature 40 °C.	160
Figure 7.16:	Temperature trends for SNG1 inside the CNG tank during the unloading operation for two initial gas temperatures, which values were 20 and 33 °C.	164
Figure 7.17:	Liquid dropout trends for two initial gas temperatures during the unloading operations of SNG1. The initial temperatures are 20 and 33 °C.	165
Figure 7.18:	Pressure trends for two initial gas temperatures during the unloading operations of SNG1. The initial temperatures are 20 and 33 °C.	165
Figure 7.19:	Temperature trends during the unloading of SNG2 and NG2. Initial gas temperature and pressure are 20 °C and 26,206 kPa (3800 psia).	167

Figure 7.20:	Liquid dropout trends during the unloading of SNG2 and NG2. Initial gas temperature and pressure are 20 °C and 26,206 kPa (3800 psia).	167
Figure 7.21:	Liquid dropout trends during the unloading operation for the original gas sample SNG2 and the same sample but after flashing it.	168
Figure 7.22:	Temperature trends during the unloading of CNG tank with SNG1 for two discharge molar flow rates of 5 and 10 kgmol/hr.	170
Figure 7.23:	Process flow diagram of flashing a NG1 sample at 35 °C and 6,897 kPa (the molar flows are the one obtained with the original PR)	172
Figure A.1:	Block diagram of the streams involved in a CVD test	202
Figure A.2:	Plot of the K values obtained through the material balance procedure versus pressure.	205
Figure A.3:	Plot of Log K versus Normal Boiling Point to check consistency of the data	206
Figure A.4:	Correction graph of Log K _j versus normal boiling points.	207
Figure B.1:	Nitrogen density curves for diverse temperatures	212
Figure B.2:	Dependency of the slope with the temperature	214
Figure B.3:	Dependency of the constant with the temperature	214
Figure D.1:	Percentage errors of mass density predictions of PR in supercritical region at diverse temperatures for Mix 5	222
Figure D.2:	Percentage errors of mass density predictions of SRK in supercritical region at diverse temperature for Mix 5	222
Figure D.3:	Percentage errors of mass density predictions of PR in supercritical region at diverse temperature for Mix 4	223
Figure D.4:	Percentage errors of mass density predictions of SRK in supercritical region at diverse temperature for Mix 4	223
Figure D.5:	Percentage errors of molar density predictions of PR in supercritical region at diverse temperature for RG2	224

Figure D.6:	Percentage errors of molar density predictions of SRK in supercritical region at diverse temperature for RG2	224
Figure D.7:	Percentage errors of mass density predictions of PR in supercritical region at diverse temperature for Gas2	225
Figure D.8:	Percentage errors of mass density predictions of SRK in supercritical region at diverse temperature for Gas2	225
Figure D.9:	Percentage errors of molar density predictions of PR in supercritical region at diverse temperature for GU2	226
Figure D.10:	Percentage errors of molar density predictions of SRK in supercritical region at diverse temperature for GU2	226
Figure D.11:	Percentage errors of molar density predictions of PR in supercritical region at diverse temperature for GU1	227
Figure D.12:	Percentage errors of molar density predictions of SRK in supercritical region at diverse temperature for GU1	227
Figure D.13:	Percentage errors of molar density predictions of PR in supercritical region at diverse temperature for NIST1	228
Figure D.14:	Percentage errors of molar density predictions of SRK in supercritical region at diverse temperature for NIST1	228
Figure D.15:	Percentage errors of molar density predictions of PR in supercritical region at diverse temperature for Gas3	229
Figure D.16:	Percentage errors of molar density predictions of SRK in supercritical region at diverse temperature for Gas3	229
Figure D.17:	Phase envelopes of the synthetic gas samples used in this study are indicated together with the isothermal where densities were measured.	230
Figure D.18:	Phase envelopes of the synthetic gas samples used in this study are indicated together with the isothermal where densities were measured.	231

LIST OF TABLES

Table 2.1:	Marine CNG transport technologies	14
Table 3.1:	Dimensions of the PVT cell and quartz tube	33
Table 3.2:	Composition of five mixtures prepared using the gas preparation set up	43
Table 3.3:	Variability in the measurement of the dew point pressures taken in the laboratory.	51
Table 3.4:	Percentage difference in the measurement of the dew point pressures taken in the laboratory.	52
Table 3.5:	Molar composition of the gas charged to the PVT cell for the simulation of the loading and unloading of a CNG tank	59
Table 4.1	Compositions of synthetic gas samples prepared in our laboratory	68
Table 4.2:	Composition of synthetic gas mixtures in molar percentages from literature	69
Table 4.3:	Dew points predicted by PR and SRK vs data measured for Mix 3 at diverse temperatures during CCE tests	71
Table 4.4:	Dew points predicted by PR and SRK vs data measured for Mix 4 at 0 and 10 °C during CCE tests.	72
Table 4.5:	Composition of natural gas samples in molar percentages	82
Table 4.6:	Absolute percentage of error for PR and SRK dew point predictions for natural gas samples.	83
Table 4.7:	Compositions of the gas samples employed to study the performance of the PR and SRK models for liquid dropout prediction.	85
Table 4.8:	Compositions of synthetic gas samples, together with their molecular weights and propane and pentanes plus fractions	89
Table 4.9:	Average absolute percentage errors of PR and SRK in predicting gas densities for gas samples.	92
Table 4.10:	Average percentage errors of PR and SRK in predicting gas densities for Mix 3 during CVD tests at 10 and 0 °C	94

Table 4.11:	Average percentage errors of PR and SRK in predicting gas densities for Mix 4 during CVD tests at 0 °C	95
Table 5.1:	Expression of volume correction parameters for generalized EOS equation 5.1.	102
Table 5.2:	Values of the constant of the EOS parameters	103
Table 6.1	The k_{ij} tuned values involved in improving the predictions of the dew points for PR	121
Table 6.2	The k_{ij} tuned values involved in improving the predictions of the dew points for SRK	121
Table 6.3	Average percentage of errors for liquid dropout calculations for the PR and SRK predictions for Mix 5 during CCE Tests at diverse temperatures	126
Table 6.4	Average percentage errors of PR and SRK in predicting liquid dropout for a field gas sample during CCE Tests at diverse temperatures	129
Table 6.5:	Diverse combination of new k_{ij} values for C ₃ -nC ₅ , C ₃ -nC ₆ , and C ₃ -nC ₈ when PR was tuned	130
Table 6.6:	Diverse combination of new k_{ij} values for C ₃ -nC ₅ , C ₃ -iC ₅ when SRK was tuned	130
Table 6.7:	Absolute percentage errors of PR and SRK in predicting compressibility	135
Table 7.1:	Compositions of the gas samples	144
Table 7.2:	Conditions of the feed stream for simulating (dynamically) the loading of a CNG tank using 1P arrangement to evaluate the feed pressure arrangement.	149
Table 7.3:	Conditions of the feed stream for simulating (dynamically) the loading of a CNG tank using 2P arrangement to evaluate the feed pressure arrangement.	150

Table 7.4:	Conditions of the feed stream for simulating (dynamically) the loading of a CNG tank using 3P arrangement to evaluate the feed pressure arrangement.	150
Table 7.5:	Gas density of the diverse gases at the final pressure inside the CNG tank (26200 kPa) and 40 °C as well as the total moles loaded inside the tank	161
Table 7.6:	Results of flashing NG1sample (composition in Table 7.1) at 35 °C and 6,897 kPa in an equilibrium flash separator	173
Table A.1:	Mass Balance Results for First CVD sample	204
Table A.2:	Liquid fractions and K-values resulting from mass balance	204
Table A.3:	Recalculation of the K-values using the least squares straight line illustrated in Figure 3.	211
Table B.1:	Equations of the calibration curves of Nitrogen at diverse temperatures	213
Table C.1:	Gas compositions	217
Table C.2:	Composition of Synthetic Natural Gases (SNG2 and SNG10) in % mol and Relative Accuracy Specified by the Supplier	218
Table C.3:	Composition of Synthetic Natural Gases (% mol) and Absolute or relative Accuracy by the supplier	219
Table E.1:	k_{ij} for PR equation	232
Table E.2:	k_{ij} for SRK equation	232
Table E.3:	k_{ij} for PR equation for sample NG3	233
Table E.4:	k_{ij} for PR equation after tuning	233
Table E.5:	Volume translation parameters of each component for PR equation before and after tuning for Mix 5	234
Table E.6:	Volume translation parameters of each component for PR equation	234

before and after tuning for NG3

NOMENCLATURE

Units

bbls/d: barrel/day

°C: Celsius degrees

cc: cubic centimetres

cc/hr: cubic centimetres per hour

cm: centimetres

GPM: gallons of condensate per thousand standard cubic feet of gas

GPM/mmscf : gallons of condensate per thousand standard cubic feet of gas

K: degree Kelvin

kg/m³: kilogram per cubic meter

kg/kgmol : kilograms / kilograms mol

kPa: kilo Pascal

m³: cubic meter

m³/Msm³: cubic meters of condensate per thousand standard cubic meter of gas

mol/s: mol per seconds

MPa: Mega Pascals

MSCF: thousand standard cubic feet

STDm³/d: standard cubic meters per day

Letters

APE: absolute percentage error

Ar: Argon

b : volume correction or molecular co-volume parameter of the cubic equations of state

BIP: binary interaction parameter between components

c : volume translation or volume shift parameter

C: volume shift parameter

C₁: methane

C₂: ethane

C₃₊: ethane plus components

C₅₊: pentane plus components

C₆₊: hexane plus components

C₇₊: heptane plus components

C₁-C₆: light hydrocarbons from methane to hexane

CCE: constant composition expansion test

CNG: Compressed natural gas

CVD: constant volume depletion test

CO₂: Carbon dioxide

d_1 and d_2 : adjustable parameters of the dimensionless volume shift parameter

DL: differential liberation test

DPT: Dense Phase Tuning parameter

e^{exp} : experimental values

e^{cal} : calculated values

EOS: equation of state

F: objective function

FID: Flame Ionization Detector

GD: Guo and Du

H₂S: Hydrogen sulfide

K_i: equilibrium constant

k_{ij} : dimensionless binary interaction coefficient between hydrocarbon components i and j

L: liquid

LNG: liquefied natural gas

M: number of data points

MW: molecular weight (kg/kgmol)

N: number of adjustable parameters

N: total number of components

n: number of moles

N₂: Nitrogen

NG: natural gas

O₂: Oxygen

P: pressure

P_{sat}: saturation pressure

P_C: critical pressure

PFPD: Pulsed Flame Photometric Detector

PR: Peng-Robinson

PRD: Peng-Robinson modified versions by Danesh

PRF: Peng-Robinson modified versions by Floter
PRG: Peng-Robinson modified versions by Gasem
PRT: Peng-Robinson modified versions by Twu
PT: Patel and Teja
P-T: Pressure-Temperature
PTV: Patel and Teja modified by Valderrama
PVT: Pressure-Volume-Temperature
R: gas constant ($\text{m}^3 \text{kPa/ K mol}$)
RK: Redlich-Kwong
RKSS: Redlich-Kwong modified version by Souahi
RKT: Redlich-Kwong modified version by Twu
SCN: single carbon number
SEP: separator test
SNG: synthetic natural gas
SRK: Soave-Redlich-Kwong
SW: Schmidt and Wenzel
TBS: Trebble-Bishnoi-Salim
T: temperature ($^{\circ}\text{C}$)
 T_b : boiling temperature
 T_c : critical temperature
TCD: Thermal Conductivity Detector
 v = molar volume
V: volume

V_C : critical molar volume

VLE: vapour liquid equilibrium

V_{sat} : saturated volume

V' : dimensionless volume shift parameter

x : vector of adjustable parameters with N (number of adjustable parameters) dimension

x_i : liquid molar fraction of component i

X = the adjustable parameters

X_{min} = the lower bound

X_{max} = the upper bound

w_i : weighing factor

y_i : vapour molar fraction of component i

Z : compressibility factor

Z_{RA} : Rackett compressibility factor

Greek

α_c : attractive parameter at the critical temperature

ρ : gas density (kg/m^3)

θ : power in the binary interaction coefficient correlation between hydrocarbons

ω : acentric factor

α : attractive parameter temperature dependence

v_1, v_2 and v_3 : volume correction parameters

Subscripts

min: minimum

max: maximum

i and j: components

Superscripts

exp: experimental values

cal: calculated values

CHAPTER 1

INTRODUCTION

The intention of this chapter is to introduce the reader into the context of the research topic and provide the objectives and problem statements. A brief description of the topics developed in each chapter is provided as a reference for the reader.

1.1 Background information

Natural gas is a mixture of methane and other gases, which can include heavier hydrocarbon components (normally with carbon atoms of three or greater also known as natural gas liquids or NGLs), water vapour, inert gases, CO₂ and H₂S. As a source of energy, natural gas is very attractive from an environmental perspective. Upon combustion, its emissions of carbon dioxide, nitrogen oxides, and particulates are significantly lower in comparison with oil and coal combustion emissions. The low emissions associated with natural gas extraction, processing, and use make it a preferred fuel for nations interested in reducing greenhouse gas and associated emissions. The electric power sector leans towards the use of natural gas due to its low capital cost and fuel efficiency (EIA 2011). The market for natural gas has been rapidly increasing and it is becoming one of the most important sources of energy in the world. Several factors

contribute to this trend including an expected energy demand increase of 53 % from 2008 to 2035 (EIA, 2011).

Currently, natural gas is transported through pipelines and to a lesser degree as liquefied natural gas (LNG). The use of pipelines is more suitable for onshore transportation; however, in transportation from remote offshore locations pipelines may be challenged due to distance to destination, depth of water, and/or oceanic conditions such as iceberg traffic. Conversion of gas to LNG has been the most used alternative for long distance and overseas transportation. Nevertheless, pipelines have been also an alternative for long distance, such as the case of Russia's terrestrial pipelines. The LNG technologies however are only economical if the amount of gas in a remote reservoir warrants the high cost of LNG projects.

The natural gas reserves are estimated at 169.9 trillion standard cubic meter (6,000 trillion standard cubic feet (tcf)) of which one third is currently considered stranded due to their remote locations, small deposits, or harsh environments (Hanrahan, 2008). The conditions of stranded reserves make it challenging to develop or produce them using current technologies, such as LNG transportation. An alternative technology for developing these reserves is marine Compressed Natural Gas (CNG) transportation. This technology transports the gas at elevated pressures, typically between 13 and 25 MPa, in high-pressure storage containers inside specially designed ships. In the past decade, the interest in marine CNG has been increasing and, as a result, a number of methods have

been developed to improve its efficiency. A number of publications have addressed the CNG cargo and ship design (Valsgård et al., 2004; and Rynn et al., 2007). However, the information available on gas quality (i.e. hydrocarbon composition and contaminant levels) for marine CNG transportation is very limited. The construction of gas conditioning facilities in remote and offshore locations has significant cost implications. Therefore any gas transport technology requiring minimum offshore gas treatment will have an advantage over competing technologies. As such, it is important to determine the extent of gas conditioning required for specific gas transportation technologies. To transport the gas through pipeline the gas needs to be treated to a minimum pipeline quality. The gas pre-treatment for LNG production is significantly more complex since the gas is transported at -160 C at atmospheric pressure. Heavy hydrocarbons (from propanes) and contaminants (such as carbon dioxide and sulphur components) should be removed to avoid damaging equipment, freezing up, and to meet pipeline specifications at the delivery point. Since the gas is not flowing during the transport in CNG containers and no strict processing is required for cryogenic liquefaction, the gas treatment for CNG transport is less severe than for LNG transport. For example, larger amount of heavy hydrocarbon components are allowed. The optimal design conditions to safely and efficiently load, store, and unload CNG tanks on ships are highly dependent on the state and constituents of natural gas. The amount of condensate that could be charged into a CNG tank needs to be evaluated since it could bring several complications for the unloading operations. For instance, not all equipment is designed to handle liquids in a natural gas gathering center or gas booster station. In some cases, it was observed that

compressors experienced vibration problems due to the large amount of liquid condensate in the flowline caused by abrupt changes in pressure and temperature (Esmail, 2009)

Process simulation tools can be employed to predict the behaviour of gas during CNG loading and unloading operations. However, the existing thermodynamic models (such as equations of state) present predictions that preclude a sound analysis of the behaviour of natural gas under loading and unloading conditions. To properly simulate the upload/unload operations of CNG and to develop safe operating procedures, an accurate prediction of gas behaviour, including liquid drop out (heavy hydrocarbons condensation) potential and cooling/heating effects during load and unload operations, is required.

1.2 Challenges in CNG loading and unloading operations

The successful design of CNG loading and unloading operations requires a complete understanding of natural gas phase behaviour. Gas composition is the governing factor to determine operating parameters such as pressures and temperatures in these processes. For instance, higher loading temperatures will be chosen if the gas loaded contains a large amount of heavy hydrocarbons, so the liquid condensation is minimized during this operation. Current thermodynamic models lack the ability to predict gas behaviour accurately in the pressure and temperature ranges of interest to CNG transport

technologies. This problem is compounded as the amount of heavy hydrocarbons increases in the natural gas. To be able to dynamically model the loading and unloading operations it is extremely important to develop a thermodynamic model capable of predicting the phase behaviour of natural gas.

1.3 CNG and condensate reservoirs

A condensate reservoir has both condensate and gas coexisting in one homogeneous phase, and when fluid is brought up to surface, the pressure decreases below the critical level, a liquid phase appears. Some natural gas reserves in remote locations contain large amounts of condensates. This is the case of stranded gas reservoirs found in offshore Newfoundland and Labrador. Marine CNG technology could be an option to exploit such reserves; however, the behaviour of the gas loaded with heavier hydrocarbons needs to be studied.

As mentioned in the previous section, existing thermodynamic models lack the capability to accurately predict the behavior of the rich gases, especially at as above critical or cricondenbar conditions. Therefore, in order to evaluate the possibility of producing gas from condensate reservoirs using marine CNG technology, the models need to be tuned. Tuning a thermodynamic model involves modifying some of its parameters to achieve better predictions. Once the models are improved by the tuning, reliable dynamic simulations of the CNG loading and unloading operations can be performed. Dynamic

simulation represents the time varying behavior of a process; therefore, the time-dependent description, prediction and control of real processes can be represented in real time. The accurate loading and unloading simulation tools will allow predicting the behaviour of gas with diverse compositions leading to the extension of the possible reservoirs to be exploited such as remote retrograde condensate and heavy hydrocarbon rich gas reservoirs.

1.4 Applications for liquid yield prediction of gas condensates

Retrograde condensation is associated with the behavior of hydrocarbon mixture nearness the critical region, where at constant temperature the vapor phase will partially condensate by decreasing the pressure, or at constant pressure the vapor phase will partially condensed by increasing the temperature. Most of the gas-condensate reservoirs experience retrograde condensation at the end of the primary production. The withdrawn gas contains heavy hydrocarbons. In order to prevent hydrocarbon condensation in the gathering and pipeline systems, the gas needs to be processed to remove the heavy components. Large volumes of liquid can be produced from the withdrawn gas, and thus the proper design of surface and processing facilities is essential for reliable transport of the gas. The optimum design and operation of process facilities depends on the volumetric performance of the gas, which is strongly composition-dependent. The volumetric performance of the gas refers to volume ratios between liquid and gas phases during the loading and unloading operations. When hydrocarbons condense, they

produce an incremental pressure drop in the transmission line due to the two phase flow in the pipeline (Morch et al., 2006). Thus, an appropriate prediction of the behaviour of the gas under different conditions of pressure and temperature is critical (Aminian et. al., 2004) for the design and operation of CNG facilities.

For single phase transport of gas in transmission pipelines, the lowest pressure must remain above the cricondenbar. Single phase transportation is also possible if the gas temperature in the pipeline is kept above the cricondentherm (Morch et. al., 2006). In order to properly design production and transmission systems, it is critical to accurately predict the phase behaviour of natural gases both near the cricondentherm and cricondenbar. Particularly, natural gas dew points predicted by equation of state (EOS) are often inaccurate, especially for pressures above the cricondentherm temperature (Morch et al., 2006).

1.5 Objectives of Research

The purpose of this research is to improve the understanding of the behaviour of natural gas under CNG loading and unloading conditions. In order to accomplish this, the following main objectives are addressed:

- To assess current thermodynamic models in accurately predicting natural gas phase behaviour under CNG conditions and particular temperatures and pressures where the models are limited.

- To evaluate the impact of condensates on the accuracy of the thermodynamic models predictions.
- To determine the conditions of temperature and pressure under which the thermodynamic models have large deviations with respect to experimental data.
- To establish a methodology to improve the predictions of gas behaviour.
- To examine the effect of erroneous gas behaviour predictions on the dynamic modelling of CNG loading and unloading operations.
- To demonstrate the impact of heavy hydrocarbon content of a gas on the CNG loading and unloading operations.
- To experimentally simulate the loading and unloading of a CNG tank in the lab in order to assess the accuracy of temperature and pressure profiles modelling predictions during gas loading and unloading operations.

1.6 Outline of Thesis

Chapter 1 presents an introduction and overview of the research topic, and establishes the main objectives of the research.

Chapter 2 provides an introduction to marine transportation of Compressed Natural Gas (CNG) and reviews the literature related to equations of state and thermodynamic properties predictions.

Chapter 3 explains the laboratory set-up employed to obtain experimental data for this research.

Chapter 4 presents an evaluation of the two most widely used thermodynamic models in the oil and gas industry, i.e., the Peng-Robinson (PR) and the Soave-Redlich-Kwong (SRK) equations of state (EOS).

Chapter 5 provides a complete explanation of the regression process built in the PVT software used to tune the PR and SRK thermodynamic models.

Chapter 6 presents a methodology to improve EOS predictions.

Chapter 7 addresses the importance of properly predicting liquid dropouts for CNG technologies, particularly in cases when rich gases are transported.

Chapter 8 summarizes the findings of this research and suggests areas that need to be further investigated.

CHAPTER 2

LITERATURE REVIEW

Marine CNG has been identified as a potential technology to monetize stranded natural gas. While marine CNG technology is not currently commercialized, several studies have examined the cargo and ship design. The cargo is the containment system and the main focus in the development design was to reduce its weight and increase its capacity to host larger amount of gas. Nevertheless, few studies have evaluated gas thermodynamic behaviour during the loading and unloading operations of a CNG tank (Abdi et al, 2006). The optimal design conditions for these operations are highly dependent on the state and constituents of natural gas. The existing thermodynamic models may fail to accurately predict the behaviour of the gas under certain temperature and pressure conditions (typical of marine CNG operations), especially when the gas contains large amounts of heavy hydrocarbons.

2.1 Marine CNG transportation

Marine CNG transportation technologies represent an opportunity to develop stranded gas reservoirs, where other alternative technologies, such as LNG or pipelines, are not economically, environmentally as technically feasible. The effective economic and technical ranges for LNG are for large reserves and long distances, whereas pipelines are

for shorter distances with minimal hurdles in the path. While Marine CNG is not currently a commercial operation in the world, it is nevertheless a promising technology. Moreover, Marine CNG is presently under evaluation for the development of gas reserves near the Caribbean island of Tobago, and the company (Centrica Energy) expects to finalise an agreement in the near future (Hine L, 2011).

Unlike pipeline and LNG liquefaction systems that are fixed investments, the majority of the cost of CNG transportation projects is mobile and therefore is less sensitive to the size of the reservoir (Economides et al., 2007). The key advantages of CNG technologies are scalability, simplified production process, mobile capital investment (ship), ability for gas recovery and export from oil and gas producing platforms (associated gas), and suitability for deepwater implementation. Conversely, CNG technology can only reach a reduction of 200 times the volume of natural gas, while LNG obtains a reduction of 600 times the volume of the natural gas.

2.1.1 Existing Marine CNG Technologies

Figure 2.1 outlines a typical operations chain for the marine transport of CNG. In a standard gas processing operation, the first step is to dehydrate the gas to prevent hydrate formation and to prevent corrosion. Hydrate is a water–hydrocarbon gas hybrid crystalline structure formed under certain conditions (temperature, pressure, and gas composition). This solid can plug the equipment or pipelines causing diverse operating problems. The amount of water allowed in the gas composition is related to the final

temperature of the high pressure gas. In other words, the formation of hydrates can be avoided if the temperature of the gas is kept above the hydrate formation temperature. In addition, acid gases (CO_2 and H_2S) present in natural gas in combination with free water can cause severe corrosion to gas handling equipment and flowlines. The amount of acid gases allowed in natural gas is directly related to the amount of water content in it; lower amount of water permit the composition to handle larger amounts of acid gases. The risk of condensation and formation of free water increases with the water content of the gas. In the second step of the process the gas is compressed and then cooled. In some processes, the gas is cooled further to reduce the required pressure. The gas is finally loaded into a carrier ship containing a large number of pressure vessels, transported to the desired destination, and offloaded afterwards.

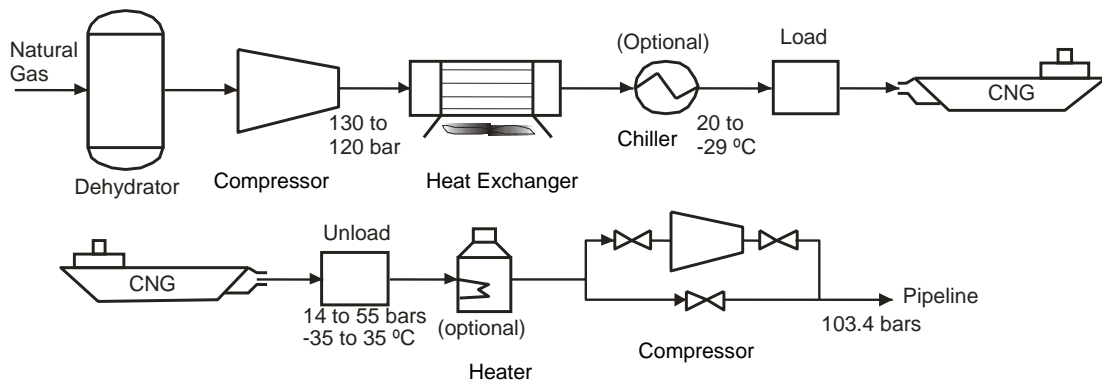


Figure 2.1: Schematic diagram of a typical marine CNG transport chain (TransCanada, 2007)

Several systems are proposed for ship-based transport of CNG (Economides et al., 2007; Wagner & Wagenveld, 2002). In general, Marine CNG systems are based on loading and unloading the tanks with gases under variable pressure conditions, with the exception of one system in which the loading and unloading of the tanks take place under isobaric conditions (Britton, 2004).

The number of ships needed to develop a reservoir can be related to the gas production rate, volume of the ship gas containment system, distance between reservoir and destination, and loading and unloading periods. Since it is difficult to store gas at an offshore gas production site, a ship must always remain on standby at the loading point. For small production systems, three ships are necessary: one ship at sea transporting the CNG cargo, another at the reservoir being loaded with gas, and the third one to take over if there is any disability to the other two ships. As the production increases, additional ships or ships with larger carrying capacity are required in order to keep the reservoir producing at a constant flow. Several technologies have been developed, which use different methodologies for compression and storage. The gas storage concepts employed by the CNG companies are storing compressed gas (Biopact Team, 2007):

- 1) in coselles, which are large coils of pipe roll inside cylindrical vessels
- 2) in stacked pressure cylindrical containers made from light weight composites
- 3) in moveable storage containers containing pipe sections or pressure vessels (made of steel or composite) that can be manipulated as regular shipping container and can be integrated into intermodal transport chains.

The technologies under development for CNG transportation are summarized in Table 2.1 (Hanssen, 2005).

Table 2.1: Marine CNG transport technologies

Transport Technology	Material	Arrangement	Temperature (°C)	Pressure (bar)
EnerSea	steel	vertical pipe	- 29	130
Sea NG (Coselle)	steel	coiled	ambient	275
Knutsen	steel	vertical pipe	ambient	250
CETech	steel	horizontal pipe	ambient	140-275
TransCanada	wrapped steel liner	horizontal pipe	ambient	200
Trans Ocean Gas	Composite (FRP)	modular cassettes	ambient	200-250

FRP: Fiber Reinforced Plastic

2.2 Classification of Gas Samples

Natural gas can be classified as lean, moderately rich or rich. The difference among them is the amount of condensates per thousand standard cubic feet (MSCF) (Manning, F. S. and Thompson, 1991),

- A lean gas presents an amount lower than 7.5 cubic meters of condensate per thousand standard cubic meter of gas (m³/Msm³) (2.5 gallons of condensate per thousand standard cubic feet of gas (GPM/mmscf))
- A moderately rich gas has between 7.5 and 15 m³/Msm³ (2.5 and 5 GPM/mmscf)
- A rich gas has larger values than 15 m³/Msm³ (5 GPM/mmscf)

2.2.1 Plus Fractions Characterization

Natural gas samples containing a hydrocarbon plus fraction (C_7^+) that requires a characterization procedure for the EOS to be able to describe properly the phase behavior and thermodynamic properties (Liang et al., 2011). In general, the specific gravity and molecular weight of this fraction are available for many gas samples; however, the critical properties and acentric factor are generally unavailable and need to be estimated. The correct estimation of these properties is essential to obtain accurate predictions when using EOS. In particular, the proper characterization of the heavy end is of great significance in simulating the phase behaviour of gas condensate fluids, because their phase behaviour and liquid drop-out characteristics are controlled by the heavy end (Dandekar, 2007). There is an optimum number of components after lumping (usually between 6 and 12), since having a large number of components typically causes unaffordable computational time, while few components cause deviations from fluid characterization (Liang et al., 2011).

Dandekar (2008) studied the effect of fluid characterization on liquid drop-out predictions of gas condensate fluids using the Peng-Robinson EOS model. This study involved 11 different gas condensate fluids with diverse fluid compositions and C_7^+ plus fraction properties. Two sets of predicted data were obtained, one with the C_7^+ fractions uncharacterized and the other with all C_7^+ fractions characterized. The study indicated that the EOS predictions were superior when the C_7^+ fraction was characterized by

dividing it into several pseudo-components rather than treating it as a single lumped component.

The Pedersen characterization method for the plus fractions seems to be the best method since it, in general, is more accurate in predicting thermodynamic properties. Zuo et al. (2001) evaluated the Pedersen method and the Whitson characterization procedures (Pedersen et al., 1989; and Whitson et al, 1989, 1990) using PR EOS against experimental data. Zuo's study determined that the characterization method of Pedersen provided better predictions. Elsharkawy (2001) also found Pedersen characterization method more accurate when comparing it with other characterization methods.

2.3 Development of the Equation of States (Thermodynamic models)

EOSs are commonly used in the oil and gas industry to predict the properties and behaviours of gas and oil mixtures.

The first EOS to address the non-ideality of gases was introduced by Van der Waals in 1873. This equation incorporated two constants, "a" and "b" into the ideal gas equation. The ideal gas and the Van der Waals equations are illustrated in Equation 2.1 and 2.2, respectively. The constant "b" that appears in the Van de Waals equation refers to the size of each molecule, and constant "a" considers the intermolecular attractive forces between the molecules. These two constant are positive and their values depend on the

gas composition, being close to zero when the gas exhibits an ideal behaviour. The Van de Waals equation is effectively limited to the phase behaviour of pure components. This equation is a cubic equation in terms of molar volume (V/n). Subsequent equations based on the Van der Waals equation were called cubic EOS, and were developed to improve the prediction of either the vapour pressure or phase properties. Cubic EOS can be arranged into cubic polynomial terms of the variable volume (V) or compressibility factor (Z). The compressibility factor (Z) is a thermodynamic property that describes the deviation of the behaviour of a real gas from the behaviour of an ideal gas. It can be seen as the ratio of the molar volume of a real gas to the molar volume of an ideal gas at the same temperature and pressure. For an ideal gas, Z always has a value of 1, and for real gases, the value could deviate positively or negatively. The deviations become larger as the gas is under conditions close to its critical point or its saturation point.

$$PV = nRT$$

(2.1)

$$\left[P + a \left(\frac{n}{V} \right)^2 \right] \left(\frac{V}{n} - b \right) = RT \quad (2.2)$$

Where, R is the gas constant; T is temperature; P is pressure; V is molar volume; and n is number of moles.

The Soave-Redlich-Kwong (SRK) equation was developed in 1972 to improve the vapour pressure prediction of pure components. In 1976, the Peng-Robinson (PR) equation was developed to improve the liquid-phase densities predicted by the SRK equation, since SRK had predicted the pure component critical compressibility factor as 0.333 which is larger than the experimental values (descriptions of PR and SRK equations are provided in Chapter 3). Later, Peneloux et al. (1982) and Jhaveri & Youngren (1988) added a volume translation parameter, called “c,” to the SRK and PR equations to improve the liquid and vapour density predictions, illustrated in Equations 2.3 and 2.4, respectively. It is important to note that the parameter “c” does not alter the gas-liquid phase equilibrium calculations of the SRK and PR equations. Several cubic equations of state were developed to include three different volumetric correction parameters. While the Adachi-Lu-Sugie (ALS) equation (Adachi et al., 1983) presents more flexibility than the PR and SRK equations, it never gained popularity in the oil industry due to the large amount of parameters. The SRK and PR are the two most accepted equations in the industry to predict phase equilibrium and properties of gas and oil (Pedersen & Christensen, 2007) since they are simple and accurate.

$$P = \frac{RT}{(V-b)} - \frac{a_c \alpha(T)}{(V+c)(V+b+2c)} \quad (2.1)$$

$$P = \frac{RT}{(V-b)} - \frac{a_c \alpha(T)}{\left[V + (c + (1 + \sqrt{2})(b+c)) \right] \left[V + (c + (1 - \sqrt{2})(b+c)) \right]} \quad (2.2)$$

Where a_c is the attractive parameter at the critical temperature, $\alpha(T)$ is the attractive parameter temperature dependence, and V denotes the molar volume.

2.4 Review of EOS Predictions

Nasrifar & Bolland (2005) compared 15 EOS for predicting the vapour liquid equilibrium (VLE) of several gas mixtures. These equations included two-parameter, three-parameter, and four-parameter EOSs. The two-parameter EOSs included the PR and RK families. The RK family was composed of the modified versions by Soave (SRK), Twu (RKT), and Souahi (RKSS). The PR family was composed of the original PR and the modified versions of Danesh (PRD), Twu (PRT), Floter (PRF), and Gasem (PRG). The three-parameter EOSs included Schmidt and Wenzel (SW); Guo and Du (GD); Patel and Teja (PT); a modified PT by Valderrama (PTV); and Mohsen-Nia, Modarress, and Mansoori (MMM). The only four-parameter EOS included was the Trebble-Bishnoi-Salim (TBS) equation. In order to compare the accuracy of the equations, several properties were evaluated. One of the properties compared was the supercritical behaviour of methane and nitrogen in terms of the fugacity parameter. This property reflects the accuracy of EOSs in characterizing natural gas mixtures, and the PT EOS was the most accurate equation in predicting fugacity followed by the PTV, GD, and PRF EOSs. When comparing the two main families, the RK family proved to predict better than the PR family, with SRK being the best equation followed by RKT, RKSS. In the PR family, PRF and PRT were better than the others. The prediction of vapour

pressure of several pure components was also analysed. In this case, the RK family showed a better accuracy in their predictions than PR family, except for the PRT EOS.

2.4.1 Dew Points Prediction

For the purpose of this thesis, dew point and liquid dropout are the most important thermodynamic property predictions. Nasrifar et al. (2005) evaluated the dew points of several natural gas mixtures. It was reported that, in the case of lean gas mixtures, dew points predictions were more accurate with the RKS, RKSS, RKT, and SW equations. Also PRT and GD showed good predictions. In the case of rich natural gases, the three-parameter EOSs demonstrated a better accuracy, with PTV, PT, and GD the most accurate. In terms of the characterization of the C_7^+ fraction, exponential distribution of Pedersen & Christensen (2007) was used with 12 single carbon number (SCN) groups, and Twu correlation was used to calculate the critical properties of the SCN groups.

Elsharkawy (2001) evaluated (using EOS) the effect of temperature, gas condensate composition, and properties of the plus fraction on dew point pressure using experimental data of gas condensates and lean gas samples. Several observations were obtained from this study. As the molecular weight (MW) of C_7^+ increases in the gas sample, the cricondenbar point moves to higher pressure values (as well as dew points) and the cricondenthem point moves to higher temperature values. When the density of the plus fraction increases, the cricondenbar point moves to higher pressure values, while the cricondenthem point moves to higher temperature values (though not as markedly as

the increase as the cricondenbar point). As well, larger amounts of C_7^+ in the gas sample move the cricondenthem to higher temperatures but not as much as the cricondenbar is moved to higher pressures. It was also found that the ratio of light to heavy hydrocarbons (C_1/C_7^+) affect the shape of the phase envelop. As this ratio increases in the gas sample, the cricondenthem point is reduced to lower temperatures but the cricondenbar point increases to higher pressures. Dew point pressure decreases enormously when the amount of intermediate components (propane through hexane) molecular weight (MW) is increased. Moreover, the MW of the intermediate component fractions have larger influence over the dew point pressure than the light MW fraction (methane and ethane), and non-hydrocarbons. Particularly, it was found that non-hydrocarbon components have the least influence in controlling the dew point pressure when compared with the influence of the other components.

Elsharkawy (2001) also compared the dew point pressure predictions of PR and SRK for gas condensate samples against experimental data. This study found that PR together with the Pedersen characterization method had smaller errors when predicting the dew point pressures of gas condensates. This study illustrated the sensitivity of the predicted dew point pressure with the chosen characterization method of the plus fraction and with the number of pseudo-components considered in splitting the plus fraction. Although the study indicated that splitting the plus fraction into 10 to 12 pseudo-components resulted in minimum absolute deviation for most gas condensate samples, the optimum number of pseudo-components of the plus fraction varied from one sample to another.

A study performed by Dandekar in 2008 compared experimental and predicted dew points using PR EOS for diverse natural gas samples with high contents of heavy hydrocarbons. In some cases, a bubble point pressure was predicted instead of the dew point pressure. This erroneous prediction was due to the large amount of heavy hydrocarbons (among 10 and 12.4% of C_7^+ mole percentages). The mistaken predictions are avoided by characterizing the C_7^+ fractions. After characterizing the C_7^+ fraction, PR predicted dew point pressures for most of the gas samples, and not bubble point pressures. When the heavy hydrocarbon fraction (C_7^+) was not characterized the average absolute deviation was 17.5%, and the dew points were underestimated. On the other hand, when C_7^+ fractions were characterized, this deviation was reduced to 11% but the dew points were overestimated.

2.4.2 Liquid Dropout Prediction

Dandekar (2008) also evaluated the liquid drop out predictions of PR EOS and compared them with his experimental data. Overall, the results by using PR indicated large inaccuracies in predicting liquid drop out when modeling gas condensate systems by using the uncharacterized plus fraction such as C_7^+ . The liquid drop out predictions improved when the C_7^+ fraction was characterized, but still the predictions were not accurate.

2.5 Tuning EOS to Improve Predictions of Gas Condensates

It is well known that EOSs present inaccuracies when predicting phase behaviors of reservoir fluids, especially for gas condensates and for near critical reservoir properties. Therefore, the parameters in the EOS require modification to improve their predictions. A study proposed by Dandekar et al. (2007) tuned the PR EOS to improve liquid dropout predictions by matching experimental dew points of gas condensate. For the tuning process, the experimental data was used with the plus fraction both uncharacterized and characterized in order to evaluate the effect of characterizing the plus fraction on the prediction of the tuned EOS. Then, four tuned PR EOS models were obtained by altering: the properties of C_7^+ fraction, the properties of methane in the uncharacterized fluid, the properties of C_{40}^+ fraction (or C_{20}^+), and the properties of methane in the characterized fluid. As a result, the study indicated that the characterization of the plus fraction played a key role in the accuracy of the tuned models. Therefore it is always recommended to characterize the plus fraction of the fluids before using them in EOS modeling. Modifications of either the methane properties or the properties of the plus fraction (C_{40}^+ or C_{20}^+) in the characterized fluid resulted in an improvement of the PR EOS liquid dropout predictions. Nevertheless, modifying the plus fraction properties is highly recommended since methane is a well defined component and the plus fractions vary in each sample. The parameter modified after tuning to improve the prediction was the critical temperature of the extended heavy end plus fraction. In addition, this study performed the characterization of the plus fraction with the simple method proposed by Katz (1983), which was designed specifically to handle the plus fraction of gas

condensates. As mentioned previously (section 2.2.1), the characterization method chosen is relevant to the level of accuracy reached after tuning. Although, Katz' characterization method was designed specifically for handling the plus fraction of gas condensates, this is an older method.

In order to build a robust PVT model for compositional reservoir simulation, Liang (2011) expounds that fluid analysis and EOS model tuning to experimental data are critical. In this study, gas condensate predictions are tuned by adjusting the boiling point for C_7^+ and density, varying the binary interaction parameter (BIP) for C_1 and C_7^+ , and generating gas viscosity by the Lohrenz-Bray-Clark correlation.

2.6 Prediction of Phase Behaviour

Phase equilibrium refers to two or more phases that coexist and have no tendency for a phase change. Mechanical equilibrium refers to equal pressures among the phases that form the system, while thermal equilibrium refers to equal temperatures between the system composed for two or more phases and the surroundings. Having phase, mechanical, and thermal equilibrium in a system means that there is no driving force that can produce any type of change (Koretsky, 2004).

During the loading and unloading operations of a CNG tank, the gas will experience different conditions of pressure and temperature. Its state may therefore vary between

one or two phases. Therefore, it is crucial to have accurate predictions of these changes for the proper design of the operations. For example, if a thermodynamic model predicts, at a certain condition of pressure and temperature, that a fluid behave as a liquid instead of a gas and it is actually behaving as a gas, the design of the loading operation could be incorrect. This miscalculation may have an economic consequence by loading a smaller amount of fluid into a CNG tank.

When the gas is at high pressure and relatively low temperatures, the fluid phase behaviour prediction could be challenging for some process simulators. There are different criteria to determine whether the fluid is in liquid, gas, or supercritical states (Pedersen & Christensen, 2007). One simple criterion is to assume that above the critical pressure, and below the critical temperature, there is always a liquid phase; while above the critical temperature there is always a single supercritical gas phase. However, this criterion could not be extended to all applications since the critical point, and possibly the dew or bubble point temperatures at the actual pressure are not known (Pedersen & Christensen, 2007). This becomes important when computational times matters. Another criterion to determine the difference between liquid and gas phases is based on the ratio of the molar volume (v) and the parameter b (volume correction or molecular co-volume parameter of the cubic EOS). If the ratio (v/b) is larger than a certain constant, which is a characteristic of each EOS, the mixture is assumed to be in the liquid phase; if the ratio is smaller than the constant the mixture is considered to be in the gas phase. In the case of

PR and SRK equations, the value of the constant is 1.75 (Pedersen & Christensen, 2007).

A more detailed description of these EOSs is provided in Chapter 5.

A 2006 study by Abdi et al. regarding dynamic simulations of natural gas loading and unloading operations of a CNG tank indicated that the available thermodynamic models (in commercial process simulation packages) predicted phase behaviour that did not correspond well with the published data. The models tended to disagree with each other at high pressure (above the two-phase region of the phase envelope) conditions. The supercritical region is the most difficult area for which to predict the behaviour of natural gas using commercial process simulators (such as Hysys). The region is shown in Figure 2.2 above the critical point.

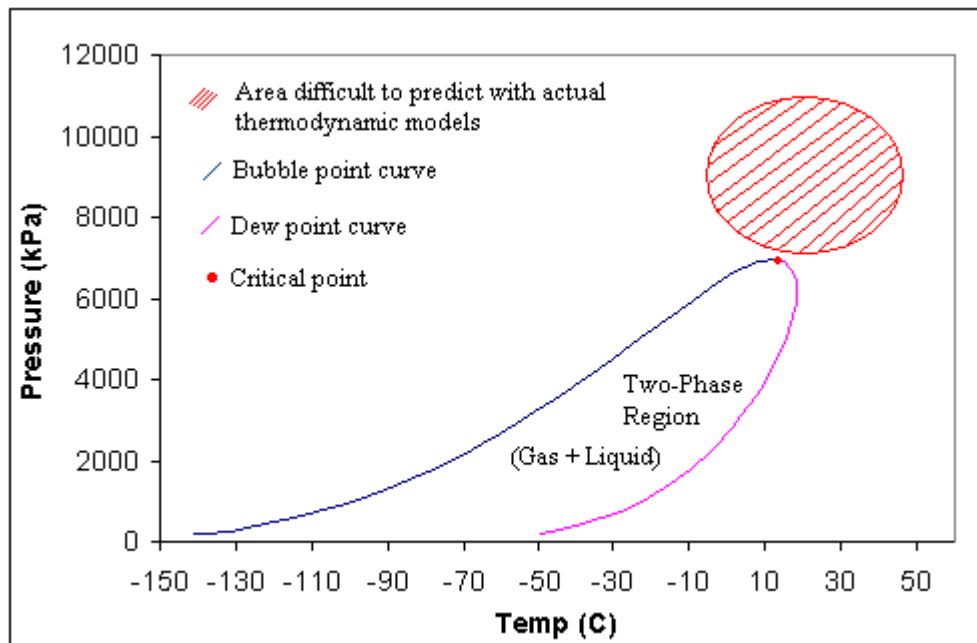


Figure 2.2: Phase envelope diagram for a typical natural gas composition

Theoretically, in the supercritical region there is no distinction between liquid or vapor phases. Nevertheless, the process simulator software needs to decide between a liquid and vapor phase in order to calculate some of the thermodynamic properties. Depending on the phase, the software calculates properties using a certain set of specific phase models. Hysys performs flash calculations and uses compressibility factors to determine whether the phase is liquid or vapor (refer to HYSYS Manuals “Properties Methods and Calculations” section A7 for details). When a depressurization process is simulated, these calculations cause instability in the predicted results. In order to reduce this instability, a Dense Phase Tuning (DPT) parameter was introduced in the latest version (HYSYS v7.2). This parameter can be modified to alter the predicted liquid and vapor phase boundaries in the supercritical region.

2.7 Application of Research to Marine CNG Technologies

The objective of this research is to aid in the development of marine CNG technology in order to produce stranded gas condensate reservoir which could otherwise not be monetized due to a lack of suitable technologies. The proper design of the loading and unloading operations requires accurate phase behavior predictions of the gas charged into and withdrawn from CNG tanks. This research will evaluate the current errors of the EOS in their predictions, and will further propose a methodology to apply for improvement.

2.8 Conclusions

In this chapter a literature review of the main topics involved in this research was presented. It was demonstrated how the lack of accuracy of the EOS in predicting thermodynamic behavior of natural gas, especially when it contains large amount of heavy hydrocarbons could impact the proper modeling of loading and unloading cycles for CNG transportation of natural gas. The necessity of a tuning process for the current EOS was illustrated along with diverse studies mentioned in this literature review. By improving the EOS predictions, marine CNG technology can be properly designed. Also, the range of applicability of marine CNG technologies could be studied. For instance, stranded gas condensate reservoirs could be produced using CNG technologies.

CHAPTER 3

EXPERIMENTAL WORK

Experimental data are required to evaluate the performance of thermodynamic models and are used for process simulations. Standard reservoir fluid analysis tests are traditionally performed to obtain information on the behaviour of reservoir fluids for reservoir engineering and maintenance applications. The two standard tests mainly used in the laboratory to collect experimental data are Constant Composition Expansion (CCE) and Constant Volume Depletion (CVD). Brief descriptions of the equipment and techniques employed in the laboratory are provided in the following sections as well as the experimental errors involved in the tests. In addition, a description of the methodology developed to make the gas samples is also provided.

In order to use the experimental data to evaluate the performance of thermodynamic models, a compositional validation needs to be conducted in order to check the consistency of the results. In case of inconsistencies, corrections are required to obtain a true description of the fluid under study. A description of this procedure will also be presented.

In order to simulate the filling of a CNG tank in a laboratory setting, an experimental apparatus that incorporated a PVT (pressure-volume-temperature) cell was used.

However, the results were unsuccessful due to excessive heating loss during the experiments, and therefore it was not possible to measure the temperature change of the gas while filling a container. A description of this apparatus, together with an explanation of the reason for the failure, is provided in the last part of this chapter.

3.1 Set up Description

The main pieces of equipment employed in the laboratory are a gas chromatograph, which was specially designed to analyse natural gas samples, a high pressure fluid analysis, set up for PVT system, and a densitometer.

3.1.1 Gas Chromatography

A gas chromatograph CP-3800 from Varian Inc. was employed in the laboratory to characterize and quantify the components present in the sample. This chromatograph is capable of analysing gas samples as well as hydrocarbon liquid samples.

The chromatograph has three detectors operating simultaneously: Thermal Conductivity Detector (TCD), Flame Ionization Detector (FID), and Pulsed Flame Photometric Detector (PFPD). Light gases (including nitrogen, methane, CO₂) are separated isothermally using packed columns and measured with the TCD detector. Hydrocarbons and methane (through heavy end components) are separated with a capillary column using temperature programming and are measured using an FID detector. The presence

of sulphur compounds in natural gas is analyzed by a PFPD detector. The chromatograph is connected to a computer, where the Star Workstation software processes the data from the three detectors and provides a single report with the composition of the sample injected into the equipment.

In order to determine the characteristic peaks of the main components of natural gas, calibration standards were used. Standards covered methane to normal decane.

3.1.2 Fluid Phase Behaviour or PVT System

A PVT cell (DBR Series II Phase Behavior Apparatus, Schlumberger, OilPhase-DBR) was used to measure fluid properties and to study the behaviour of high pressure fluid mixtures. The operations pressure and temperature ranges of the PVT system are 0 to 100 MPa (15,000 psi) and -35 to 200 °C, respectively. These wide ranges allow conducting diverse studies for the oil and gas industry. Accurate measurements and sampling of various fluid phases at a specific temperature can be performed with the PVT cell. For instance, measurements of phase equilibrium at high pressure, gas and liquid densities, vapour-liquid ratios, and dew or bubble points can be accomplished using this equipment.

The PVT cell contains a glass tube, which is surrounded by a thin layer of hydraulic oil and then by a massive steel structure. The high pressure cell is equipped with a magnetic stirrer that helps to establish equilibrium among phases more quickly than a system that

does not use a magnetic stirrer. The pressure inside the cell is controlled by a positive displacement pump controlled by computer software. The PVT equipment also contains a video based cathetometer to obtain a precise quantification of the height of the liquid and gas phases. The schematic of the PVT system is outlined in Figure 3.1.

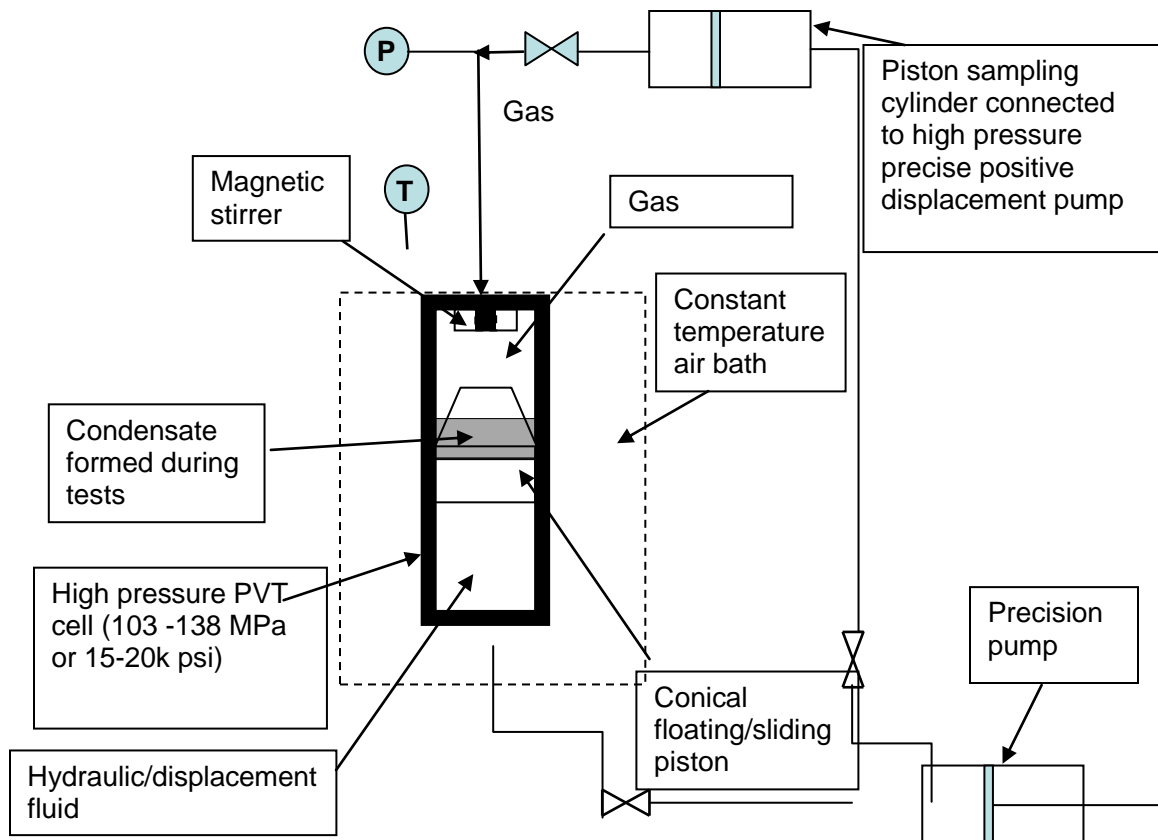


Figure 3.1: Schematic of PVT systems

The dimensions of the cell together with the quartz tube are indicated in Table 3.1.

Table 3.1: Dimensions of the PVT cell and quartz tube

Component	Measurement
Diameter steel cell	0.254 m
Height steel cell	0.413 m
Weight cell	117.94 kg
Quartz tube height	0.178 m
Inside diameter of quartz tube	0.064 m
Outside diameter of quartz tube	0.102 m

Two types of pistons are generally used for experiment with the PVT cell; flat piston and tapered piston. Flat pistons are mainly used when the amount of liquid collected during the tests is large (predominantly crude samples) and conical pistons when it is small (gas samples). Since the gas samples used for the experimental tests did not present a large amount of condensate, a conical piston was selected. Figure 3.2 illustrates the dimensions of the conical piston.

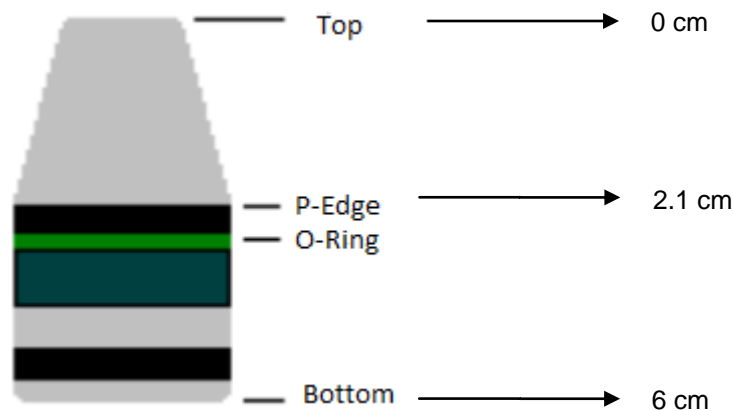


Figure 3.2: Schematic of a tapered piston

In order to determine the volume of the collected liquid into the annular space around the piston, a calibration curve is required. The calibration is performed with the glass tube extracted from the PVT cell with the tapered piston placed inside the tube. Small known volumes (from 0.02 to 0.1 cc) of a solvent are added inside the annular space around the piston using pipettes. The solvent employed for the calibration should be slightly colored, non-volatile, and with low viscosity and surface tension. The cathetometer of the PVT cell is used to measure the height of the volumes added. Small amounts of solvent are added until the liquid level reaches the top of the coned piston and cumulative volumes added at each increment and the height increase recorded. This data is used to plot total volume (cc) against height (cm), and from the plotted data an equation could be regressed. This equation was used to determine the corresponding volume in the annular space of the coned piston from a height measurement. The equation obtained in the calibration is shown in Equation 3.1.

$$V = a.h^2 + b.h + c \quad (3.1)$$

Where a , b and c are the coefficients obtained from the plotted data, h is the measured height in cm, and V is the volume of the liquid in cc.

3.1.3 Densitometer

An Anton Parr densitometer model mPDS 2000 v3 was integrated into the PVT system. The densitometer was placed inside of the oven of the PVT cell to ensure equilibrium

temperature of the densitometer and cell. The densitometer is able to operate under temperatures and pressures ranging from -10 to 200 °C and from 0 to 140,000 kPa (0 to 20,300 psi), respectively (Anton Paar, 2005a). It measures the period of an oscillating U-tube that contains the sample with the frequency depending on the sample density. A low density fluid has a high oscillation frequency, and a high density fluid has a low frequency (Anton Paar, 2005b). The gas is sent into the U-tube, which is under continuous oscillation by means of a magneto-electrical system. In order to relate the period/frequency signals with the density of the sample, a calibration procedure is needed for each temperature.

3.2 Preparation of gas mixtures

A method to prepare natural gas mixtures with known composition for different experiments was developed in our laboratory. The accuracy of the method was deemed acceptable, based on the percentage errors between the designed and the obtained composition approximately 10% for the light components (C₁-C₃) and 20% for the heavy components (from C₄-C₈). The method uses a combination of process simulator software (HYSYS), high pressure sample containers, a laboratory mass balance, several pressure gauges, and a gas chromatograph. The process simulator software is used to predict the pressure inside the high pressure sample container as the gas components are added. A mass balance is used to confirm that the amount of mass sent into the sample cylinder matches the required composition. The pressure gauges are used for two

purposes: to control the pressure of the sampling container when individual components are added, and to control the pressure of the pure gas cylinder from which the individual gases are sent. The preparation consists of adding first the liquid hydrocarbon components (pentanes, normal hexane, normal heptane, and normal octane). Then, the gaseous components are added in an ascending vapour pressure order, starting from butanes, propane, ethane, continuing with carbon dioxide, nitrogen, and finally methane. An accurate gas and liquid chromatography analysis is required to quantify the components of the final mixture.

A gas preparation system was arranged to introduce the gas components individually into the sample cylinder. Figure 3.3 shows a flow diagram of the set up for the gas mixture preparations, and Figure 3.4 illustrate a picture of this set up used in the laboratory. The system contains valves and gas manifold lines connected to the pure gas cylinders as well as to a flow control valve. The purpose of the flow control valve is to control the pressure of the gas added since some of the pure gas cylinders could have significantly higher pressure than required. In order to read the pressure of the gas added, the flow control valve is connected to a three way valve that joins two pressure gauges (with different maximum handling pressures) and a line to the sample cylinder, where the gases are mixed. The low pressure gauge (with 60 psig or 0.4 MPa max pressure) is used when the low vapour pressure components (butanes and propane depending the pressure required) are added. This pressure gauge is then isolated by closing a valve to avoid its contact with a high pressure gas and subsequent damage. The high pressure gauge (with 6.9 MPa

or 1,000 psig max pressure) is used for adding the rest of the gas components with a maximum pure cylinder pressure of 6.9 MPa (1,000 psig). The steps that need to be followed to prepare a gas sample are indicated in Appendix A.

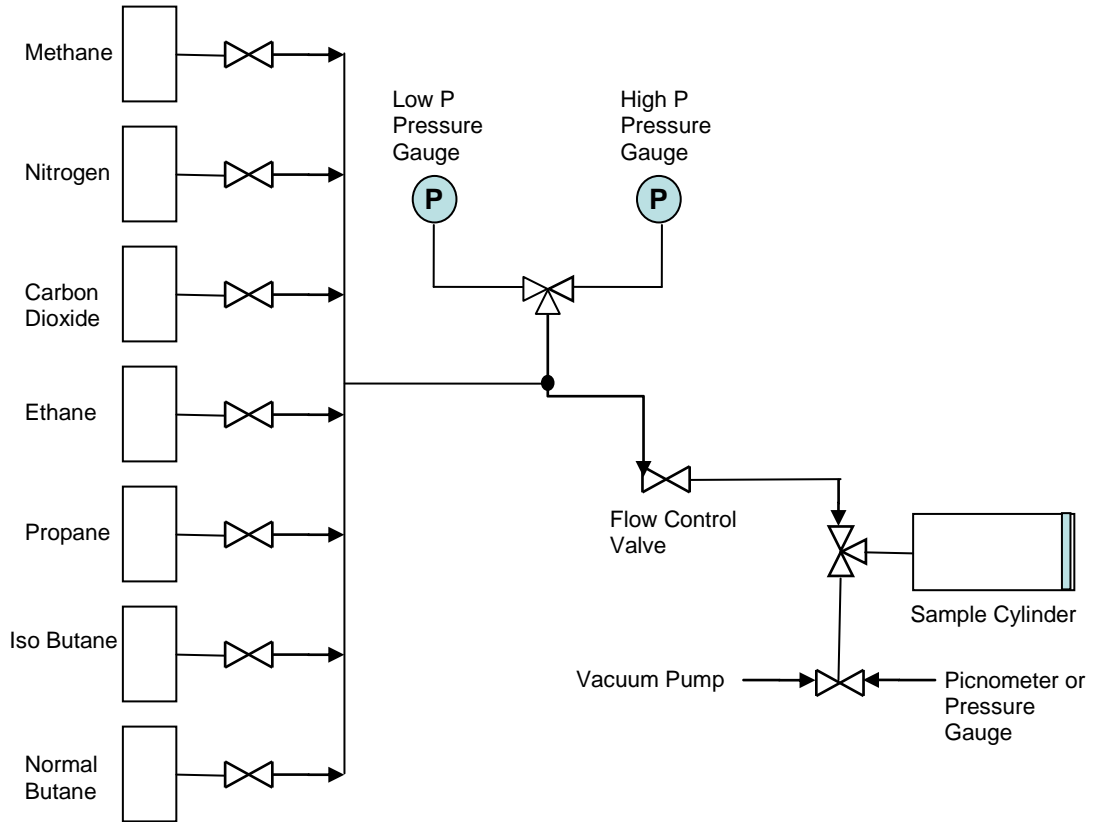


Figure 3.3: Flow diagram of the set up for gas mixtures preparation

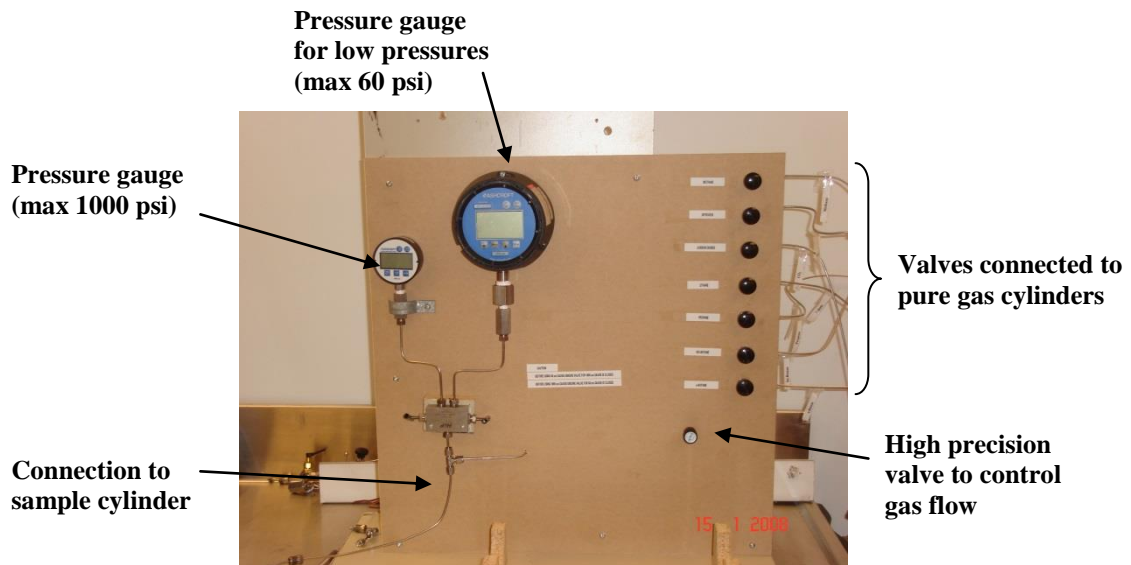


Figure 3.4: Picture of the panel for gas mixtures preparation

Hysys was used as a reference to prepare the gas samples. The method used to prepare a gas sample in this research was not highly precise but accurate for the purpose of this research. The final composition of the gas sample prepared in the laboratory was obtained with gas chromatography.

3.2.1 Transferring the gas mixture

After obtaining the exact composition of the gas mixture prepared in the laboratory, the gas sample was ready to be used for tests in the PVT system. The gas mixture was transferred from the pistoned sampling cylinder (which contained the gas sample on one side and water on the other) to the PVT cell using another pistoned cylinder (which contained water and oil in each side of the piston). Two pumps were employed for

transferring the gas sample, a high pressure precision positive displacement pump and a manual oil pump. The high pressure precision positive displacement pump was connected to the PVT cell and set in pressure mode to keep constant pressure inside the cell. The manual oil pump was connected to the extra pistoned cylinder, which was connected to the sample cylinder through the water side. In addition, the PVT cell was placed with the mixer down and with the piston almost touching the mixer. The purpose was to minimize the pressure drop of the gas entering into the cell by reducing the available volume. It is important to mention that all the lines and PVT cell should be evacuated using the vacuum pump before transferring gas sample into it.

The gas volume entering into the cell could be determined by calculations or by indirect measurement. The calculations requires measurement of the initial and final positions of the piston (taken with the camera of the PVT system) and then multiply the difference between these two positions by the inner area of the quartz tube. The indirect measurement is considering the volume of the oil displaced by the high pressure precision positive displacement pump when transferring the gas into the cell; the oil can be assumed as incompressible fluid so its volume can be used as a reference.

Before sending the gas mixture to the PVT cell, the pressure of the mixture inside the sample cylinder was raised to a high value to ensure one single phase. To avoid condensation during the transfer, the PVT cell temperature was set to a value higher than 50 °C and the lines were wrapped with heating tape. The gas was transferred into the

PVT cell at a constant pressure using the control system on the hydraulic pump. The differential pressure while sending the sample into the PVT cell should be small to avoid the rupture of the glass tube of the PVT system. While the high pressure precision pump was set on pressure mode at a constant pressure, the manual oil pump was operated in order to maintain a higher pressure inside the sample cylinder so the gas was transferred toward the PVT cell.

The density of the gas transferred is measured in the densitometer at the same final temperature and pressure inside the cell. Knowing the volume and the mass density, the total mass of the gas inside the cell can be calculated and used as a starting data for the CVD tests.

A flow diagram of the system is shown in Figure 3.5. Figure 3.6 shows a picture of the two pistoned sample cylinders employed to transfer the gas sample into the PVT cell and the lines wrapped with heating tape to avoid condensation. The pressure gauge connected to the sample cylinder which was used to check precisely the pressure inside can also be observed.

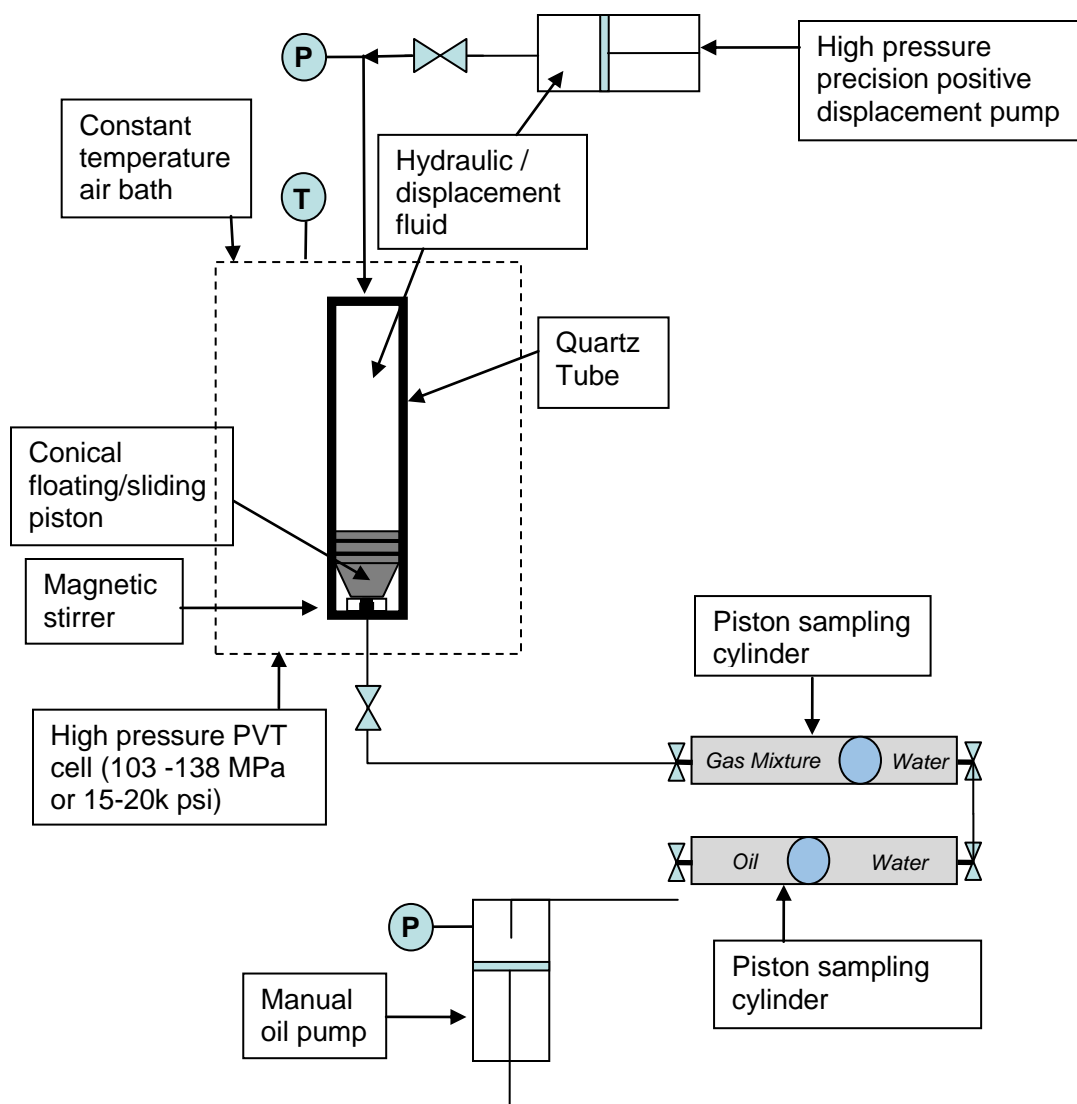


Figure 3.5: Flow diagram of the system to transfer gas mixtures to PVT cell

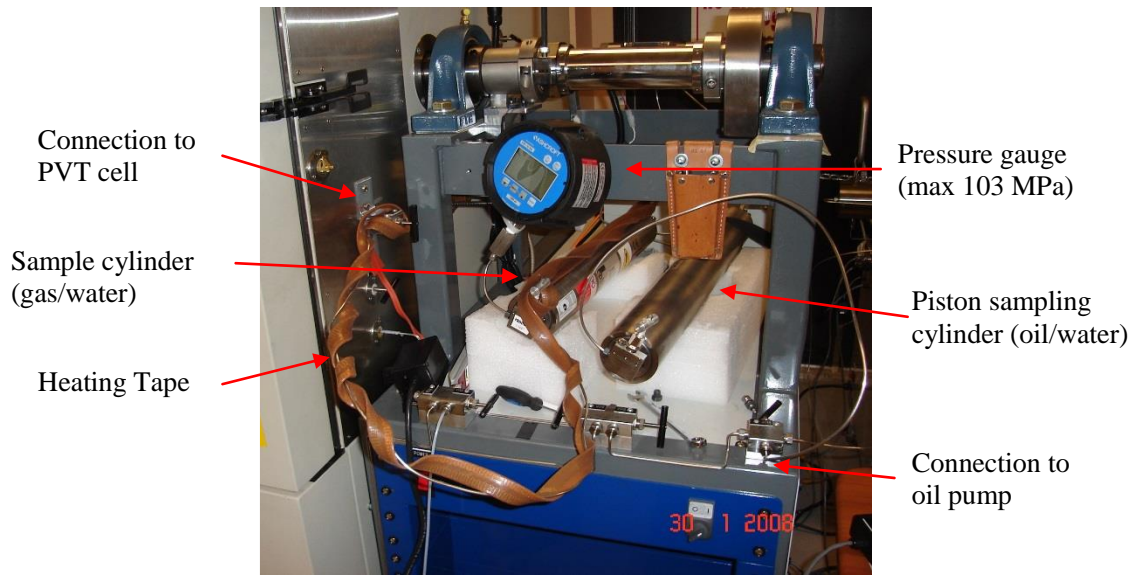


Figure 3.6: Picture of the system to transfer gas mixtures to PVT cell

Five synthetic gas mixtures were prepared in our laboratory (Mix 1, Mix 2, Mix 3, Mix 4, and Mix 5; their compositions are shown in Table 3.2. These particular compositions reflect gases with relatively large amount of condensate, and therefore the liquid dropout percentages and densities could be evaluated. One of the objectives of the research was to evaluate the impact of condensate on CNG loading and unloading operations. The compositions were selected as tests were performed. Employing the first gas compositions (Mix 1, Mix 2 and Mix 3) the amount of condensates obtained during the CCE and CVD tests were not enough, so the amount of heavy hydrocarbons was increased for Mix 4 and Mix 5

Table 3.2: Composition of five mixtures prepared using the gas preparation set up

	Mix 1	Mix 2	Mix 3	Mix 4	Mix 5
Component	% Molar				
Methane	36.57	49.164	84.083	83.687	64.414
Ethane	57.65	38.413	7.223	7.595	10.979
Propane	4.74	12.281	4.441	4.748	12.819
i-Butane	0.44	0.094	1.042	0.231	2.480
n-Butane	0.5	0.007	---	1.450	3.290
i-Pentane	0.08	---	0.423	0.316	2.150
n-Pentane	0.02	---	0.493	0.331	1.800
n-Hexane	---	---	0.658	0.037	1.100
n- heptane	---	---	---	0.045	0.430
n-Octane	---	---	---	0.058	0.538
O ₂ /Ar	---	0.042	---	---	---
CO ₂	---	---	1.637	1.111	---
Nitrogen	---	---	---	0.391	---

3.3 Experimental procedures

Two main phase behaviour tests were performed in this research. These two standard tests are Constant Composition Expansion (CCE) and Constant Volume depletion (CVD), and they are used to determine fluids properties under the conditions of interest. Traditionally, these standard reservoir fluid analysis tests are performed to obtain information on the behaviour of reservoir fluids for reservoir engineering and maintenance applications. The results obtained from them provide important thermodynamic properties including saturation pressures and temperatures, and data on vapour-liquid equilibria, which can be used for thermodynamic data regression analyses or to verify tuned thermodynamic models. Brief descriptions of these tests are provided in the following sections.

3.3.1 Constant Composition Expansion (CCE)

In a CCE test, the saturation pressure and the relative amounts of gas and condensate at various pressures are measured for a specific temperature. The experiment starts at a high pressure and then reduced in incremental steps as necessary. If the temperature chosen for the test falls inside the two phase region, a liquid formation will be observed when the pressure reaches the saturation point (dew point or bubble point). Knowing the phase envelop diagram of the gas used will help to choose the right conditions of pressure and temperature for the test. Although the CCE test could be used to calculate the compressibility factor (Z) of a gas, it is commonly used to evaluate the liquid to gas ratio below the saturation pressure (dew or bubble point) at a specific temperature.

During CCE tests, as the pressure is reduced in steps, the total cell volume and the volumes of the two phases (liquid and gas) are recorded at each step alongside the cell pressure. The pressure is reduced until the saturation pressure is reached. At this pressure the cell volume is recorded (V_{sat}) and used as the reference volume in subsequent tests. Below the dew point, the relative phase volumes and the liquid percentages in the cell are calculated for each pressure stage. The relative volume is the ratio of total volume of condensed liquid and the saturated volume (V_{sat}). The percentages of liquid volumes vs. pressure are plotted, and this information is later used to decide on the pressures at which the gas sample should be taken during the CVD test. In addition, the ratio of vapour to liquid can be calculated (V/L) from the CCE test (Pedersen & Christensen, 2007).

Steps to perform the CCE Test

- 1- HYSYS is used to develop the phase envelop of the gas sample (using both PR and SRK equations) and to obtain estimates of the main areas of the phase envelop (such as dew point and bubble point curves, retrograde condensation, critical point). This diagram will help to determine the temperature for the CCE test.
- 2- The PVT cell is placed with the mixer on the top so that the liquid accumulation falls over the piston in order to be measured precisely. For gas samples, conical piston is employed so slight amount of liquids can be measured.
- 3- The pressure of the PVT cell is raised high enough to ensure only one phase (use phase envelop as a guide).
- 4- The PVT oven temperature is set to the temperature selected for the CCE test and wait until this temperature is reached.
- 5- The initial position of the piston, temperature, and pressure of the PVT cell is observed.
- 6- The pressure to the first step is reduced, which will be 0.34 MPa (50 psig) lower than the initial pressure. In order to avoid sudden changes, the PVT cell pump is set in volume mode. The reduction in pressure is started at a low speed (20-50 cc/hr) and stoped when the desired pressure is reached. While reducing the pressure, the mixer always left on so that small condensations over the tube can be captured by observation.
- 7- Wait 30 minutes in every pressure step to ensure there is not any condensation.

- 8- When the saturation pressure (dew point) is reached, the gas mixture becomes foggy and after few seconds a drop travelling along the wall of the tube can be observed. The mixer tuned on is quiet important to detect the first drop traveling along the tube, otherwise the human eye will not be able to perceive it. The pressure is registered as saturation pressure, and the saturation volume is calculated using the height of the piston at the temperature of the test and the inner cross area of the glass tube.
- 9- After the dew point, the pressure is further reduced in steps. In each step, the mixer is turned off for 30 minutes and the height of the liquid accumulated is measured. The the mixer must be turned off in order to allow the two phases to split, as a wrong measurement could be taken if not enough time is allowed for the phases to separate.
- 10- The pressure continues to be reduced until the piston reached the bottom of the cell and it cannot go any further. Reducing the pressure in small steps will provide more accuracy and additional data points.

3.3.2 Constant Volume Depletion (CVD)

The test begins at the saturation pressure (P_{sat}), which is recorded together with the saturation volume (V_{sat}). These data are obtained from a CCE test previously performed at the same temperature. The volume of the sample is expanded to pressures below the saturation pressure to obtain a clear liquid formation, and the liquid and gas volumes recorded. The two-phase total volume is then reduced to the original V_{sat} at the constant

selected pressure by removing excess gas through a valve. The density, volume, as well as the composition (by gas chromatography) of the excess gas is then measured. The molar amount of the depleted gas is determined from a mass balance calculation from the original moles in the cell. The compressibility factor (Z) of the depleted gas is calculated using Equation 3.2 at the cell conditions (Pedersen & Christensen, 2007).

$$Z = \frac{PV}{RT} \quad (3.2)$$

CVD tests were originally designed to obtain information about the change in properties with time of gas condensate or volatile oil in the reservoir. The reservoir usually has a constant volume and temperature. When the reservoir goes to production mode, the reservoir pressure is reduced as the amount of material decreases; however, the reservoir volume remains constant. After a certain time, the pressure of the reservoir reaches the saturation pressure and liquid starts to form. In the case of this research, the main purpose of the CVD test was to obtain as many equilibrium samples as possible to provide information about equilibrium mixtures that will be used to tune the equation of state.

Steps to perform a CVD Test

- 1- The following data is collected prior to testing: the composition of the gas mixture, the initial mass of the gas inside the cell (which is calculated using the volume and the mass density obtained in the transferring process), the saturation

pressure (P_{sat}) and the saturation volume (V_{sat}) at the temperature selected for the test.

- 2- The PVT cell temperature and cell pressure is set to the selected temperature for the CVD test and to the saturation pressure (P_{sat}) respectively.
- 3- The PVT cell is placed in the same position than for a CCE test, with the mixer on the top, so the liquids accumulate over the conical piston.
- 4- The top of the piston position is set to the corresponding height of the saturation point obtained in the CCE test, and the value is taken as reference. The volume of the sample is then expanded to a pressure below the saturation pressure at which a clear liquid formation can be detected (the information obtained from the CCE test is used). While the pressure is being reduced, the mixer is left on until the desired pressure is reached. The mixer is then tuned it off for 30 minutes, and the liquid and gas volumes recorded.
- 5- In order to remove part of the gas phase so the original V_{sat} can be reached, the PVT cell pressure is increased to 0.34 MPa (50 psig). The reason of this pressure increment is to avoid a large pressure drop inside the cell when the valve is opened. If the pressure inside the cell goes below the selected pressure, the compositions of the phases may change and the gas sample (taken for analysis) may be incorrect. Increasing the pressure to 0.34 MPa is a common practice when working with gas samples and it will not change the composition of the two phases, since reaching the equilibrium at the new pressure will take a long time.

- 6- Part of the excess gas is sent to the densitometer to measure its density, another portion is used to take a sample in a picnometer for GC analysis, and the rest is purged.
- 7- The total molar amount of the depleted gas is calculated from a mass balance calculation from the original moles in the cell. The compressibility factor (Z) of the depleted gas can also be calculated. In Appendix A, in the Table A.1, the data obtained and calculated in a CVD test is illustrated.
- 8- After removing all the excess gas to reach the reference volume, the valve is closed and the mixer is turned on to mix the phases in order to get the mixture ready for the next pressure reduction.
- 9- The steps 2 to 6 are repeated multiple times. The liquid accumulation will first increase and then decrease as the pressure is reduced.

In Appendix A, the equations to obtain the mass balance of the first pressure step in a CVD test are indicated.

3.4 Experimental Errors

The PVT tests performed in this research involved gas density measurements, dew points determination, gas and liquid volume measurements, and gas compositions analysis. All these measurements have certain experimental errors due to equipment or human errors.

The experimental errors involved in each of these measurements are discussed in the following sections.

a) Experimental errors in density measurements

The gas density was measured in an Anton Parr densitometer (described in Section 3.1.1) The Anton Parr device measures the period of an oscillating U-tube produced by gas inside of it. The density data can be regressed using a calibration equation that takes into account the temperature and period of the gas sample. The densitometer was calibrated using pure gas samples of known density (such as nitrogen). The calibration gas densities were measured maintaining the temperature constant under changing pressure. A detailed explanation of the calibration method for the densitometer can be found in Appendix C. The period produced by the gas sample was measured five times with intervals of 5 minutes and the average period was taken to obtain the density. The overall percentage error, calculated as the ratio of standard deviation and the average measured densities, was 0.02%.

b) Experimental variability in dew point measurements

The dew point of the gas samples at a specific temperature was measured three times and then the average value was taken. The dew points were measured in the CCE test and the tests were repeated several times. Since the same procedure was followed for all samples, the dew point percentage variability for one test is illustrated here. The selected sample is

Mix 5 and the dew point pressure was measured at 60°C. Table 3.3 shows the dew point pressure values and the percentage variability.

Table 3.3: Variability in the measurement of the dew point pressures taken in the laboratory.

	Dew point pressure measured (kPa)
Test 1 - Mix 5 at 60 °C	11,880
Test 2 - Mix 5 at 60 °C	11,969
Test 3 - Mix 5 at 60 °C	11,831
Test 4 - Mix 5 at 60 °C	11,790
Average value	11,868
Standard Deviation	77

c) Experimental variability in liquid dropout measurements

The liquid dropout percentages (V_{liq}/V_{tot} %) of a gas sample were measured at different pressures during CCE tests for a particular temperature of interest. These measurements were repeated 2 or 3 times for some samples and the percentage difference of the liquid dropout were calculated. Table 3.4 indicates the average liquid dropout percentage values, their standard deviation and the percentage difference for a gas sample of Mix 5 at 60 °C. The liquid dropout percentages of the diverse CCE tests for Mix 5 at 60 °C are illustrated in Figure 3.7.

Table 3.4: Percentage difference in the measurement of the dew point pressures taken in the laboratory.

Liquid dropout values for Mix 5 at 60 °C			
Pressure (kPa)	Average value of Liquid Dropout (Vliq/Vtot %)	Standard Deviation (σ)	% difference
11,625	1.67	0.043	2.6
11,287	4.91	0.169	3.4
10,942	6.19	0.144	2.3
10,831	6.25	0.030	0.5
10,576	6.77	0.103	1.5
10,212	6.93	0.044	0.6
10,135	6.90	0.098	1.4
9,874	6.78	0.114	1.7

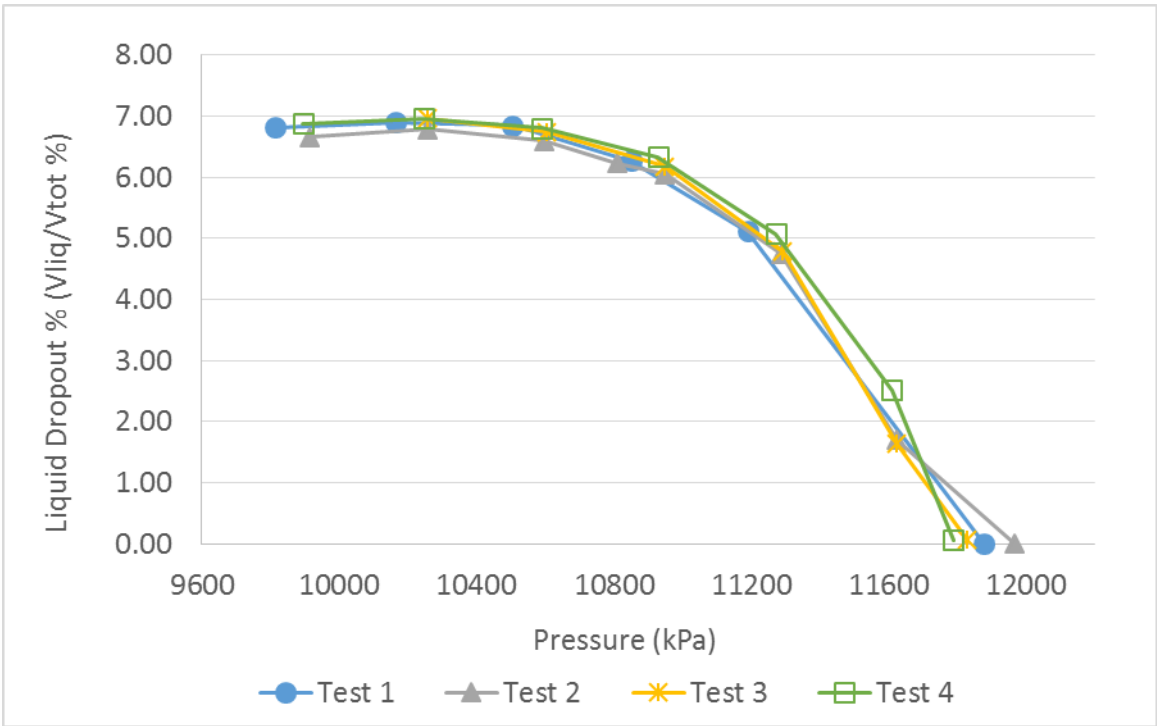


Figure 3.7: The liquid dropout percentages of the diverse CCE tests for Mix 5 at 60 °C

3.4.1 Limitations in performing PVT experiments

While performing PVT experiments, there are practical limitations in measuring physical and chemical properties of the samples. For example, measurements of liquid volumes during CVD tests are, in general, systematically lower than the actual value (Trengove et al., 1991). One reason for this discrepancy could be that the measurement was taken before the phases reached equilibrium (i.e. before the stabilization time). The waiting time recommended before measuring the liquid and gas levels is half an hour; nevertheless, some authors claim that most of the liquid only drains completely to the base of the cell after 2.5 hours (Trengove et al., 1991). Another reason for the lower liquid levels could be due to errors in sampling. For example, a large pressure drop while sampling may cause changes in the equilibrium system, therefore affecting the liquid levels.

When performing CCE or CVD tests with lean gases, two difficulties are present. The small amount of liquid collected at each pressure stage makes it difficult to measure the liquid level due to the curved liquid phase meniscus. The other difficulty is that there is not enough liquid remaining in the cell in the last depletion stage; therefore, sampling and analysing its composition is a challenging task. The liquid composition analysis of the last depletion stage is used for comparing its value with the one obtained by mass balance.

3.4.2 Validation of PVT Experimental Test Results

The quality of compositional data is of critical importance considering PVT tests results are widely used in the oil and gas industry for areas such as reserve estimation, facilities design, gas hydrates prediction, and sales gas valuation. The validation of compositional PVT results is mainly conducted to check the consistency or quality of the experimental data. Inconsistencies are corrected in order to obtain a true description of the fluid under study. When nonlinear regression techniques are used to adjust the EOS parameters, the experimental data should be validated in order to reduce the amount of time spent attempting to match inconsistent data. The experimental data that required validation are obtained from CVD tests. These tests provide volumetric and compositional data for each pressure stage, and this information was used for adjusting the EOS parameters.

In a CVD test, gas and liquid volume measurements are performed in every pressure stage as well as volume and composition analyses of the vapour extracted. Information about the liquid condensate (such as composition and moles) is obtained by material balance using the measured data.

The validation procedure makes it possible to correct the main PVT inconsistencies. These inconsistencies could be negative equilibrium constants (K_i), crossing the equilibrium constant curves when $\log K_i$ for each component are plotted against pressure, or jumps in these curves. In the next section, the methodology used to validate the experimental data is described.

Method to validate PVT experimental Results

The validation procedure consists of performing a simple material balance to obtain the mole fractions of the liquid phase remaining in the PVT cell for each pressure stage of the CVD tests so that the equilibrium constants (K -values) can be calculated. The molecular weight of the liquid and of the C_7^+ fraction in the liquid can also be obtained using the mass balance results. Once all these data are calculated, a series of control checks can be performed in order to verify the consistency of the experimental PVT data. According to the literature, there are six different control routines to scan inconsistencies of the experimental PVT data, (Samaniego et al, 2004; and Bashbush, 1981).

The method used in this research to corroborate the consistency of the data was to plot the K -values versus pressure (the step pressures of the CVD tests) for every component. In case of the absence of inconsistencies, the upper curve (higher K -values) should correspond to nitrogen (N_2), followed by the curves of methane (C_1) and carbon dioxide (CO_2). Then, it follows either the curve of ethane (C_2) or the curve of hydrogen sulfide (H_2S) (depending on the fluid and reservoir temperature). Underneath the remaining component curves should be in increasing order of the molecular weight (or normal boiling points). The K value of the isobutene and isopentane should always be higher than those corresponding to the “normal” components. If the order of the curves is switched or the curves are not parallel among them, it indicates there are inconsistencies.

Once the inconsistencies are found through a control checks, they need to be fixed. The procedure chosen to solve the inconsistencies, such as negative K -values or crossing equilibrium constant curves, has two main steps. In the first step the main inconsistencies are fixed, and in the second step it is verified that the summation of the gas mole percentages of all components is equal to 100. The correction of the inconsistencies modifies the component compositions for those components showing the inconsistencies. Therefore, the new K_i values need to be checked for possible existing inconsistencies and the addition of the moles percentages should be equal to 100%, if not a new adjustment need to be performed.

Another manner to find if there are inconsistencies is to plot of $\log K_i$ versus boiling temperature (T_b) for all the components of the mixture. This graph should closely follow a straight line. The order of the K ratios of the components should be the same than the described for the K -values vs. pressures curves. When inconsistencies are observed, a regression technique is employed. Thus, a minimum least square regression is fitted to the data and used to correct the K_i ratios calculated with the original PVT data. The values of the K_i of the components should follow a descending order, with nitrogen being the largest one. When this order is altered, the original K_i is changed for the corresponding K_i values given by the straight line at the T_b for the particular component under evaluation. After the K_i order of the components is fixed, the gas mole fractions (y_i) are calculated from the new K_i values. This process is repeated for each pressure stage of the CVD test. Several combinations of K -values could match the measurements

at each pressure, however, the set of K -values that will match all the available data is necessary to identify. The Jones and Erbar method could be used to determine the final K -values that represent the experimental results and to ensure that they meet the summation of the gas mole fractions up to 100 percent (Jones and Erbar, 1970).

The procedure chosen to solve the inconsistencies in this research is described through an example in the Appendix A.

Small variations in the measured amount of liquid condensing from the gas at each stage have a disproportionately large effect on the calculated gas z -factor; losses of liquid result in the z -factor being underestimated (Trengove et. al, 1991). Therefore, the composition changes should remain as small as possible.

3.5 Simulation of the filling of a CNG tank in the laboratory

Simulating the filling of a CNG tank was attempted in the laboratory using the PVT cell, a pistoned cylinder, and connection lines. An exposed junction thermocouple was attached to a specially designed end cap containing a cavity to fit the thermocouple. This setting allowed an instantaneous measurement of the temperature inside the tube of the cell since the thermocouple was in direct contact with the fluid being charged. Since the fluid being loaded into the cell was a synthetic gas mixture at high pressure, the thermocouple selected needed to be able to tolerate high pressures. The thermocouple

selected was a type K Mineral Insulated Thermocouple, Exposed Junction with Epoxy seal, 310SS, with a diameter of 3.0 mm and length of 1000 mm complete with STD Plug Temp -50 to 200 °C.

The gas to be sent to the PVT cell was kept in a piston cylinder at high pressure (24,130 kPa or 3,500 psia) and at a temperature of 40 °C to ensure that only one phase was present. All the lines that connected the cylinder to the PVT equipment were also maintained at high temperatures by means of heating tapes to avoid condensation during the transfer operations. Before transferring the gas, all the lines and the pistoned tube of the PVT cell were put under vacuum. The transfer began by filling the lines; once the line had reached the cylinder pressure, the valve to the PVT cell was opened slightly to minimize the Joule-Thompson effect. The oil pump was used to control the volume flow of the gas at a constant rate into the cylinder (500 cc/hr), while the volume of the cell was kept constant. The schematic of the glass tube of the PVT cell is shown in Figure 3.8. Since the cell was under vacuum, some liquid dropout was initially observed, but as the pressure inside the cell increased, the fluid passed from a two-phase state to single-phase state. The simulation of the unloading of the tank was performed by opening the output valve and controlling the flow of the gas using the oil pump. Therefore, the loading and unloading of the gas were controlled during the experiments. The composition of the gas sample charged into the PVT cell is illustrated in Table 3.5.

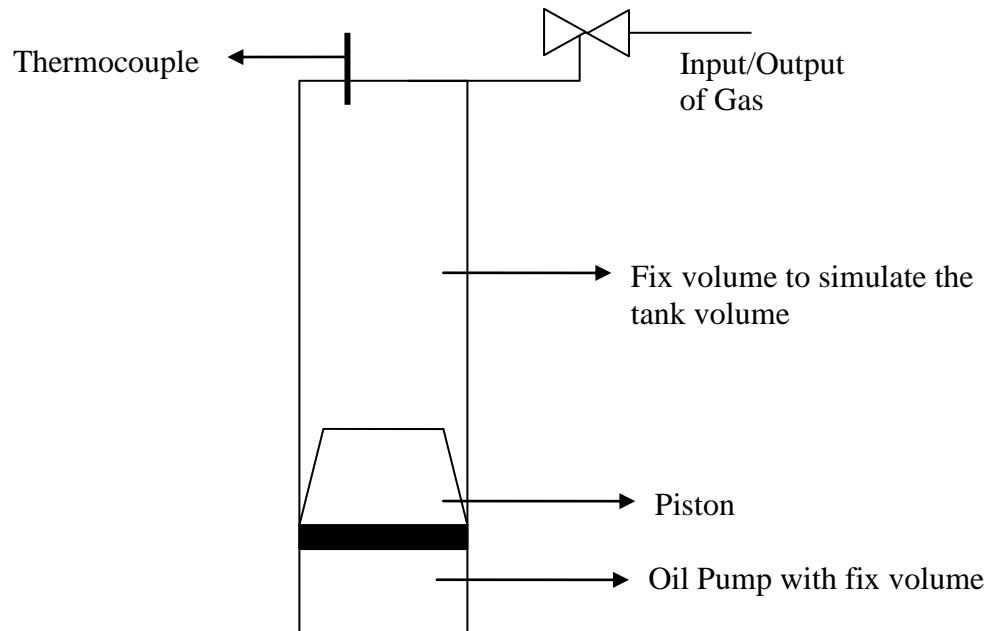


Figure 3.8: Schematic of the glass tube inside the PVT cell, where the gas is charged

Table 3.5: Molar composition of the gas charged to the PVT cell for the simulation of the loading and unloading of a CNG tank

Component	Mole Percentages
Methane	73.960
Ethane	16.354
Propane	5.909
i-Butane	1.121
n-Butane	1.363
i-Pentane	0.615
n-Pentane	0.456
Hexanes	0.172
Myclo-pentane	0.003
n-Octane	0.030
Octanes	0.016
Decanes plus fraction	0.001

During the loading and unloading of the PVT cell, several parameters were measured instantaneously and recorded. These parameters were: cell and oil pump pressures (in psig), volume of oil displaced (in cc), instantaneous temperature inside the tube (in °C), and time. Figure 3.9 illustrates the pressure and temperature changes inside the glass tube of the cell during the experiments. As seen from Figure 3.9, a Joule-Thomson effect was not observed when the gas entered the tube. Instead, the temperature remained constant, and then it increased only 2 °C during the last part of the loading. The temperature increase could be due to gas compression in the cell when loading. When the gas is being charged into the cell, cooling can happen across the valve but as the gas enters the cell, it compresses and it could warm up. The Joule-Thomson effect was small compared to larger heat transfer between system and surroundings. The large difference between the radius and body mass of the tube and the steel body surrounding the tube causes substantial heat exchange. The same behaviour was observed during the unloading operation. The drop of temperature between the loading and the unloading experiments is due to the above mentioned heat exchange.

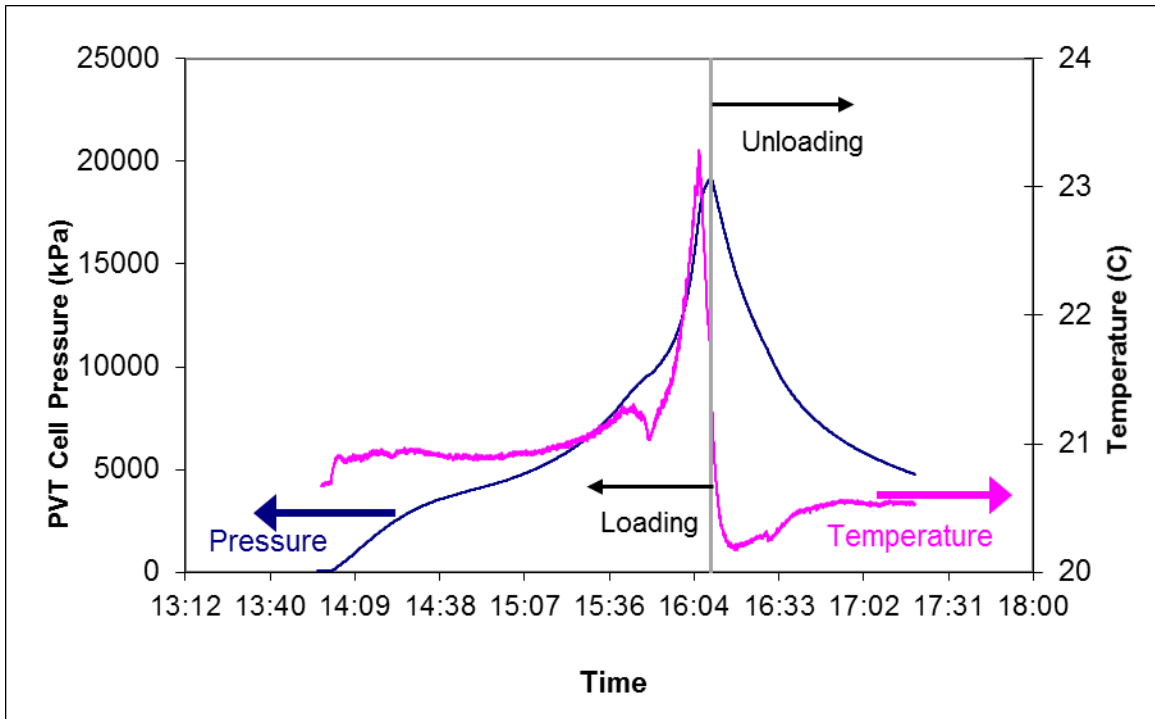


Figure 3.9: Change of pressure and temperature inside of the PVT Cell with time during the loading and unloading of the cell with gas.

A diagram of the radio of the glass tube and the steel cell are shown in Figure 3.10. The large difference in radio created the large heat exchange. Therefore, this equipment was not useful to simulate the loading and unloading operations of a CNG tank with natural gas mixtures of the type encountered in CNG operations.

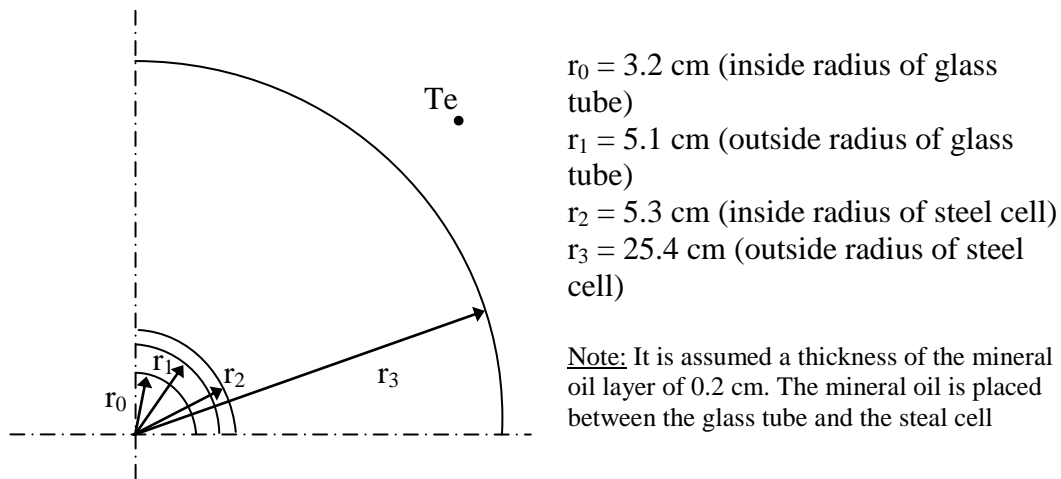


Figure 3.10: Schematic showing the glass tube and the steel cell relative radius.

3.6 Tuning the EOS

The experimental data acquired in this research is then used to compare them with the predictions of EOS's. In Chapter 4, a detail analysis of the deviation of the EOS predictions with respect to experimental data is presented for diverse thermodynamic properties. As discussed in Chapter 2, EOSs could be inaccurate for predicting certain properties (such as liquid dropout) as the amount of heavy hydrocarbons increases in the gas mixtures. Tuning the EOS to improve the predictions is employed to overcome these inaccuracies. In this research, PVTPro software is employed to perform the tuning of the EOS. PVT Pro software is designed to simulate standard PVT laboratory measurements, and to analyze experimental or field data. The software has rigorous model tuning capabilities for multiple samples, using a multivariable regression package to match

simulation results with measured saturation pressures and fluid properties. Diverse EOS models are included in this software, such as PR EOS with volume translation for liquid density correction (1978), PR EOS (1976), and SRK EOS (1972). A detail explanation of the regression technique will be addressed in Chapter 5.

3.7 Conclusions

In this chapter the experimental procedures as well as the equipment employed were described. It demonstrated the importance of validating the CVD experimental data since these data will be used later to modify the parameters of the EOS's in order to provide better predictions. The experimental errors in the measurements made in the lab were indicated through some examples.

The gas samples were used to conduct CCE and CVD to obtain dew points, density, compressibility, and liquid dropout measurements. Experience is needed in order to conduct these tests properly. For instance, dew point formation can be hard to detect. The first drop forms very quickly and, for certain gas compositions, large liquid dropouts are detected immediately after this point. In the case of CVD tests, where part of the depleted gas is removed to reach the reference volume in each pressure stage, it is important to keep the same equilibrium system while sampling so that the compositions are not altered. This is achieved by raising the cell pressure 345 kPa (50 psi) higher before sampling. In addition, after obtaining the measurements and compositions from the CVD

tests, it is very important to conduct a validation of the PVT experimental results to check the consistency and/or quality of the experimental data. Inconsistencies are corrected to obtain a true description of the fluids and to reduce the amount of time spent attempting to match inconsistent data when performing tuning of the EOSs. This compositional validation is critical since these experimental data are used to tune the thermodynamic models for improving their predictions.

The small scale filling of a CNG tank was attempted in the laboratory using the PVT system; however, unsuccessful results were obtained. The enormous heating loss along the walls of the glass tube did not allow for accurate predictions of the real behaviour of the gas inside a tank when it was loaded from vacuum to high pressure and when the gas was unloaded.

CHAPTER 4

EVALUATION OF EQUATIONS OF STATE

This chapter presents an evaluation of the predictions of the two most widely used thermodynamic models in the oil and gas industry, namely the Peng-Robinson (PR) and the Soave-Redlich-Kwong (SRK) equations of state (EOS) (Dustman et al., 2006). The thermodynamic properties evaluated are: dew points, gas densities in the supercritical fluid region and in the two-phase region, liquid dropout, and compressibility. The limitations of PR and SRK for accurately predicting the thermodynamic properties mentioned are considered in this chapter.

4.1 Dew Points

In general, the RK family of equations predict dew points better than the PR family, when experimental values are compared to the predicted values (Nasrifar, 2005). Nevertheless, both equations have limited application in dew point predictions where there is a large presence of heavy hydrocarbons (Coats, 1986).

The specific shape and location of the phase diagrams of gas mixtures are influenced by their hydrocarbon and non-hydrocarbon components. The dew point curve will be located at higher temperatures and pressures when the amount of heavier hydrocarbons is larger in the gas sample. Studies (Jarne et al., 2004) have shown that the increment of

certain components can reduce or increase the chance of condensation of a gas sample. For instance, an increase in the concentration of methane (C_1), ethane (C_2), or carbon dioxide (CO_2) increases the solubility of heavier hydrocarbons in the vapour phase of the gas, therefore reducing the risk of condensation for a given pressure. Consequently, the dew point curve will shift to lower pressures and/or temperatures for a given gas mixture by increasing these components. By contrast, it was also found that increasing the concentration of nitrogen or hydrocarbon with more than two carbon atoms produces the opposite effect. In this study, two samples were evaluated and the range of pressure and temperature used (1.2×10^5 and 81.8×10^5 Pa, and from -59.56 to -11.76 °C) were within the conditions of transporting natural gas by pipelines.

Experimental data was employed to evaluate the accuracy of the EOSs on predicting dew points.

In order to assess the effect of the composition on the dew points and the corresponding applicability of the EOSs, experimental data were used for comparison with EOS predictions. Some of the data corresponded to synthetic gas samples (prepared in the laboratory) and others to natural gas samples from the field. The experimental data produced in this research was using only synthetic gas samples, which were made as indicated in section 3.2 of this thesis. These synthetic gas samples produced in our laboratory were called Mix followed by a number, and the synthetic gas samples obtained were: Mix 1, Mix 2, Mix 3, Mix 4, and Mix 5.

In addition, experimental data collected from literature was employed for obtaining a wider evaluation of the EOS and composition effect on dew points. The synthetic gas samples obtained from the literature were named SNG followed by a number, such as SNG1, SNG2, etc. The compositions of all these data are showed on the Table 4.2 together with their references. The experimental dew points collected were then compared with the predictions of the PR and SRK equations.

4.1.1 Deviation of EOS predictions for synthetic gas samples

The accuracy of the PR and SRK models in predicting dew points as well as the effect of the composition on the shape of the dew point curve are evaluated in this section. For this purpose, experimental data obtained in our laboratory and experimental data from the literature were employed. The compositions of the synthetic gas samples prepared in our laboratory are indicated in Table 4.1 and in Table 4.2 for the synthetic gas samples from literature. The experimental errors of the synthetic gas samples obtained in this research are indicated in section 3.4, and the experimental errors of the data obtained from literature are indicated in Appendix C.

Table 4.1: Compositions of synthetic gas samples prepared in our laboratory

Mixture	Mix 3	Mix 4
Component	% Molar	% Molar
CH ₄	84.083	83.687
C ₂ H ₆	7.223	7.595
C ₃ H ₈	4.441	4.748
iC ₄ H ₁₀	1.042	0.231
nC ₄ H ₁₀		1.45
iC ₅ H ₁₂	0.423	0.316
nC ₅ H ₁₂	0.493	0.331
nC ₆ H ₁₄	0.658	0.037
nC ₇ H ₁₆	---	0.045
nC ₈ H ₁₈	---	0.058
N ₂	---	0.391
CO ₂	1.637	1.111
C ₁ +C ₂	91.306	91.282
C ₃ ⁺	7.057	7.216
C ₅ ⁺	1.574	0.787

Table 4.2: Composition of synthetic gas mixtures in molar percentages from literature

	SNG1	SNG2	SNG3	SNG4	SNG5	SNG6	SNG7	SNG8	SNG9	SNG10
	(a)	(b)	(d)	(a)	(a)	(a)	(c)	(a)	(c)	(b)
N ₂		0.77					0.86		0.67	1.56
CO ₂		1.70								25.91
CH ₄	84.28	84.45	89	93.60	93.51	96.61	86.48	94.09	89.96	69.11
C ₂ H ₆	10.07	8.68	7	2.63	2.97	0.00	9.83	4.47	8.22	2.62
C ₃ H ₈	4.03	3.30		0.00	1.01	0.00	2.39	0.00	0.90	0.42
iC ₄ H ₁₀	0.60	0.29		1.49	1.05	1.53	0.18	0.00	0.11	0.11
nC ₄ H ₁₀	1.03	0.59	4	1.49	1.47	1.48	0.23	0.00	0.13	0.10
iC ₅ H ₁₂	0	0.08		0.80	0	0.39	0.01	1.45	0.01	0.03
nC ₅ H ₁₂		0.09					0.01		0.00	0.02
nC ₆ H ₁₄		0.05								0.11
nC ₇ H ₁₆										
nC ₈ H ₁₈										
C ₁ +C ₂ %	94.35	93.13	96.00	96.23	96.48	96.61	96.31	98.56	98.18	71.73
C ₃ ⁺ %	5.7	4.4	4.0	3.8	3.5	3.4	2.8	1.4	1.2	0.8
C ₅ ⁺ %	0.0	0.22	0.0	0.8	0.0	0.39	0.02	1.45	0.01	0.17

Note: a) (Morch et al., 2006) ; b) (Jarne et al., 2004) ; c) (Avila et al., 2002b) ; d) (Blanco et al., 2000)

CCE tests were conducted and the experimental dew points were measured and compared with the PR and SRK predictions. In the case of Mix 3, the dew points were determined at 0, 10, and 20.7 °C and they are illustrated in Figure 4.1, together with PR and SRK' predictions indicated by the pink and red lines, respectively. The dew points at 0 °C fall close to the cricondenbar and the others fall between the cricondenbar and cricondentherm zones.

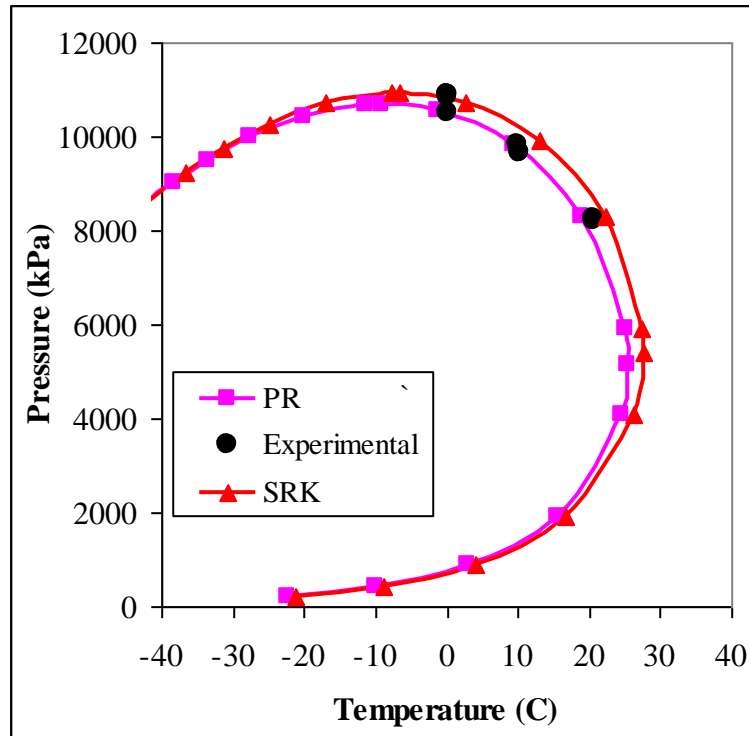


Figure 4.1: Experimental and predicted dew point curves for Mix 3 (Experimental data from this research)

The values of the experimental and predicted dew points are indicated in Table 4.3 as well as the percentage error in the predictions. The average percentage error of the EOS predictions decreases with temperature: nevertheless, all the errors are below 5 %. PR prediction percentage errors have an average of 1.7% while SRK prediction percentage errors have an average of 3.3%. It is important to mention that the experimental errors are taken into consideration in this analysis.

Table 4.3: Dew points predicted by PR and SRK vs data measured for Mix 3 at diverse temperatures during CCE tests

Temperature (°C)		PR	SRK	Experiment
20.7	P (MPa)	7.79	8.7	8.22
	Error %	3.7	4	
20.6	P (MPa)	7.81	8.75	8.24
	Error %	3.8	4.3	
10.3	P (MPa)	9.7	10.22	9.65
	Error %	0.4	4	
10.2	P (MPa)	9.7	10.24	9.66
	Error %	0	4	
10	P (MPa)	9.71	10.252	9.81
	Error %	0.7	3.1	
0	P (MPa)	10.58	10.84	10.79
	Error %	1.4	0.3	

During CCE test with Mix 4, dew points were determined at 0 and 10 °C. The experimental errors associated with these data points were discussed in Chapter 3, section 3.4. The experimental dew points and the phase envelopes predicted by PR and SRK are illustrated in Figure 4.2. In addition, the average percentage errors of the predicted dew points by PR and SRK are indicated in Table 4.4 together with the experimental values.

As for the previous sample, the average errors of the EOSs are below 5 %, where PR prediction errors have an average of 3.6% and SRK prediction errors 2.5 %.

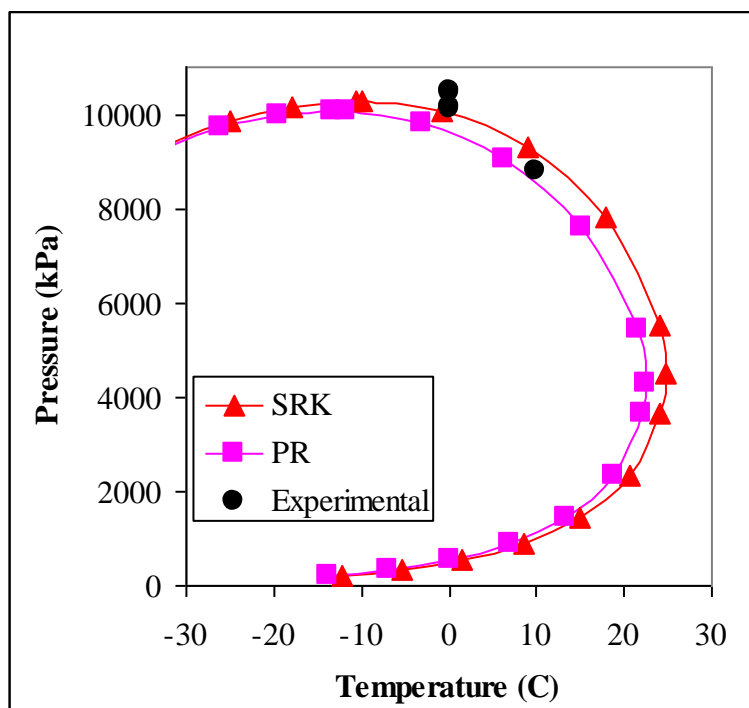


Figure 4.2: Experimental and predicted dew point curves for Mix 4 (Experimental data from this research)

Table 4.4: Dew points predicted by PR and SRK vs data measured for Mix 4 at 0 and 10 °C during CCE tests.

Temperature (°C)		PR	SRK	Experiment
0	P (MPa)	9.62	10.01	10.34
	Error %	5.1	2.2	
10	P (MPa)	8.56	9.15	8.8
	Error %	2	2.7	

Mix 3 and Mix 4 are moderately rich gas samples and are of similar compositions. The EOSs predicted accurately the dew points for these two samples. Although these samples contain a large amount of heavy hydrocarbons (C_3^+ above 7%), the percentages of CO_2

are 1.1 and 1.6 % for Mix 3 and Mix 4, respectively. In general, CO₂ increases the solubility of the heavier hydrocarbons in the vapour phase and dew point curves shift to lower pressures. The impact of CO₂ on hydrocarbons for the vapour phases resulted in better predictions. . The shift of the dew point curves predicted by EOS to lower pressures reduce the differences between the predicted and experimental points. Similar behaviour was observed for gas samples SNG2 and SNG10 (see Figures 4.4 and 4.12). In contrast, for moderately rich samples containing only hydrocarbons (and no CO₂), EOSs predict dew points inaccurately, such as for the cases of SNG4 and SNG6 (see Figures 4.6 and 4.8)

In order to illustrate the effect of non-hydrocarbons in the synthetic gas samples, the dew point curves for the SNG1 and SNG2 samples will be discussed. Figures 4.3 and 4.4, indicate the experimental and EOS predicted dew points for SNG1 and SNG2, respectively. Both samples contain similar amounts of methane and comparable amounts of ethane. However, SNG1 contains a larger amount of heavier hydrocarbons and no non-hydrocarbons, while SNG2 contains significant amounts of CO₂ and N₂. When comparing experimental and predicted dew point curves for SNG1, the experimental curve deviates from the predicted curve above the cricondenbar pressure. This deviation could be attributed to the large amount of heavier hydrocarbons (C₃⁺) and the absence of CO₂, which shifts the dew point curve to lower pressures and temperatures. The deviation between experimental and predicted dew points supports Nasrifar and Bolland (2005) analysis that established the inaccuracies of the existing thermodynamic model in

predicting the behaviour of rich gases above cricondenbar conditions. In the case of SNG2, which has similar heavier hydrocarbon content to SNG1, the experimental data agree closely with the predictions. Based on experimental observations, the agreement among the experimental and predicted points seems to be due to the large concentration of carbon dioxide (CO₂) present in the sample. CO₂ concentration seem to counter the effect of the heavier hydrocarbons' concentration, producing predicted dew point curves closer to the experimental ones. No theoretical explanation can be provided at this stage. In order to explain the effect of CO₂ further analysis needs to be conducted, where heavy hydrocarbons and CO₂ are varied.

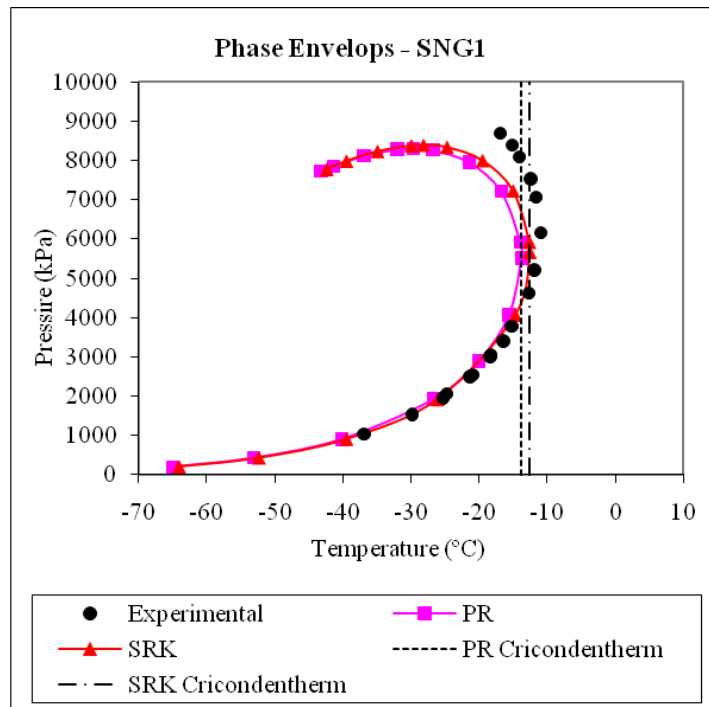


Figure 4.3: Experimental and predicted dew point curves for SNG1 (Experimental data from Morch et al., 2006)

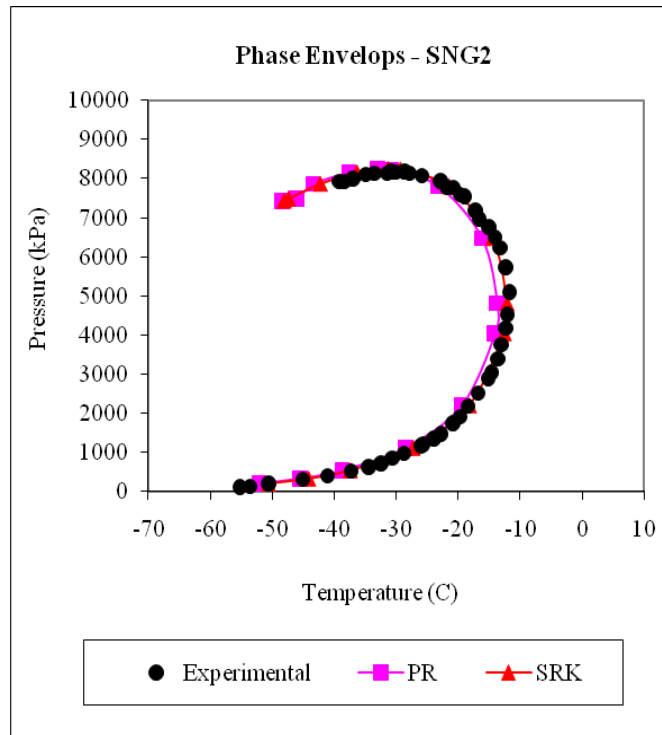


Figure 4.4: Experimental and predicted dew point curves for SNG2 (Experimental data from Jarne et al., 2004)

In order to evaluate the effect of the heavy hydrocarbon components (C_3^+ and C_5^+ fractions), samples with only hydrocarbon components (SNG3 and SNG4) are compared. Both samples contain similar amount of methane plus ethane ($C_1 + C_2$) but differ in the amount of heavier hydrocarbons. SNG3 has a slightly larger amount of C_3^+ fraction, while SNG4 contains a larger C_5^+ fraction. Figures 4.5 and 4.6 illustrate the comparison among the experimental and predicted dew point curves for samples SNG3 and SNG4. It is clear from these figures that the predicted curves for both samples have larger deviations from the experimental curves at pressures above the cricondentherm point. However, the SNG4 sample also has a clear deviation at pressures below the cricondentherm point. This deviation is likely due to the amount of iso-pentane (iC_5)

(normal-pentane is not present in the sample). A similar trend is observed between SNG5 and SNG6 samples, which are illustrated in Figures 4.7 and 4.8, respectively. In addition, the prediction of dew point for sample SNG8 (sample with the largest amount of C_5^+) deviates from the experimental data along the whole dew point curve, which is illustrated in Figure 4.9.

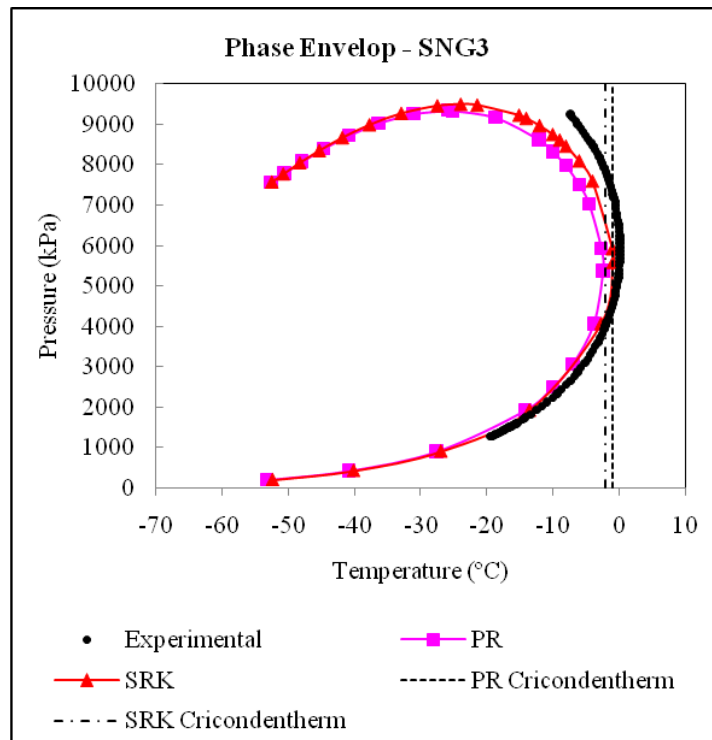


Figure 4.5: Experimental and predicted dew point curves for SNG3 (Experimental data from Blanco et al., 2000)

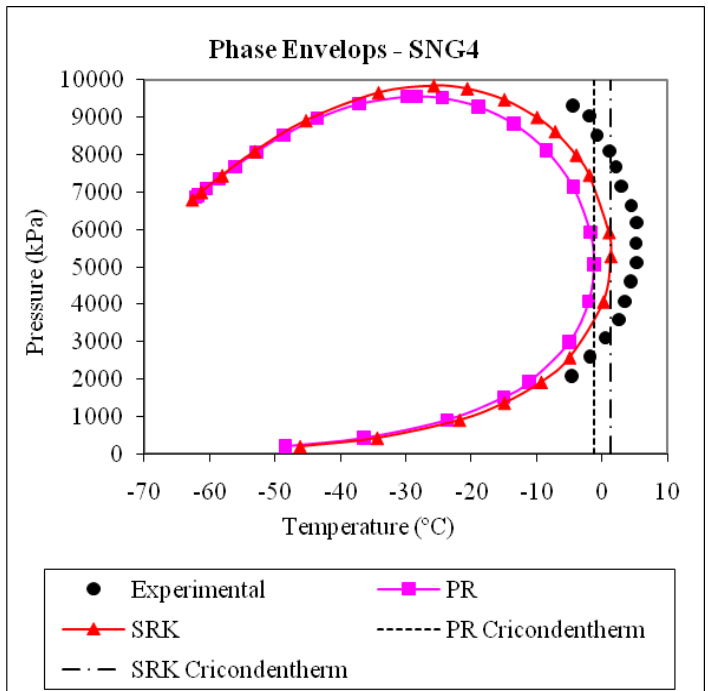


Figure 4.6: Experimental and predicted dew point curves for SNG4 (Experimental data from Morch et al., 2006)

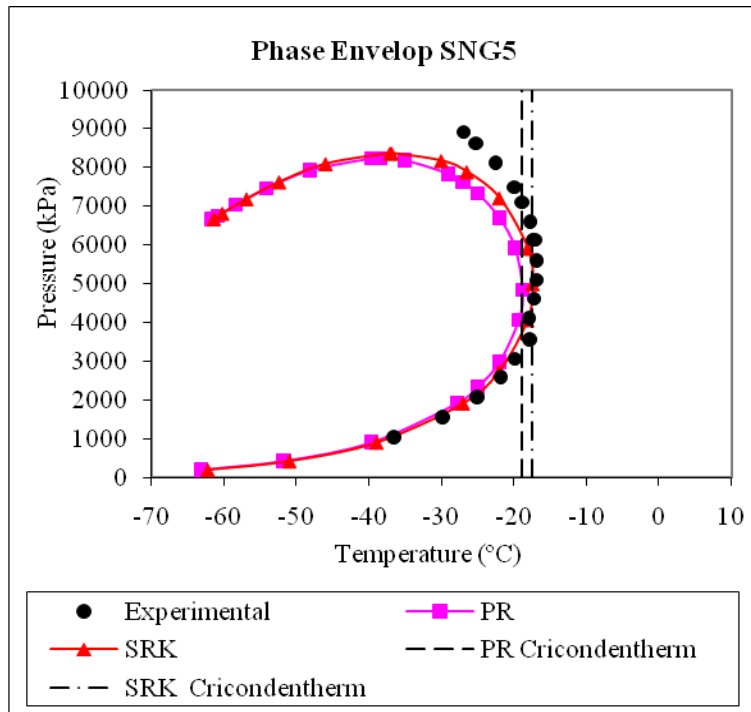


Figure 4.7: Experimental and predicted dew point curves for SNG5 (Experimental data from Morch et al., 2006)

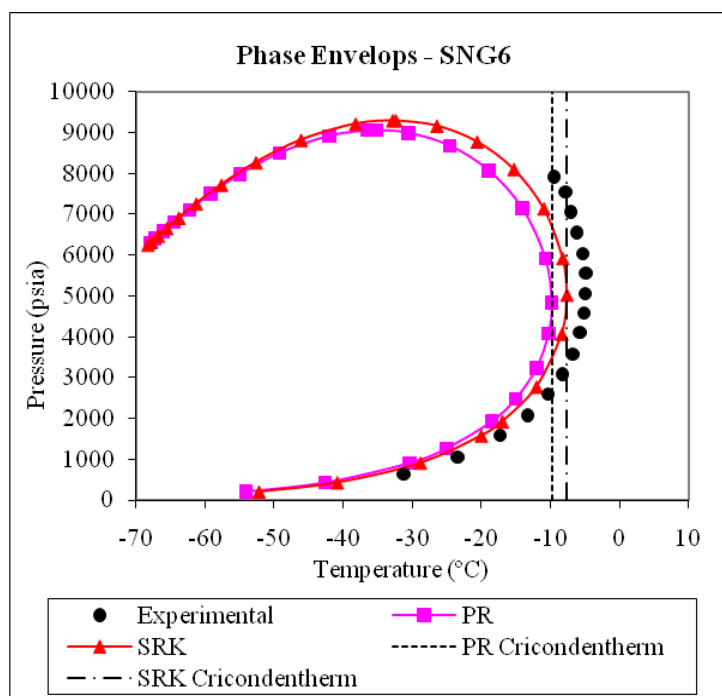


Figure 4.8: Experimental and predicted dew point curves for SNG6 (Experimental data from Morch et al., 2006)

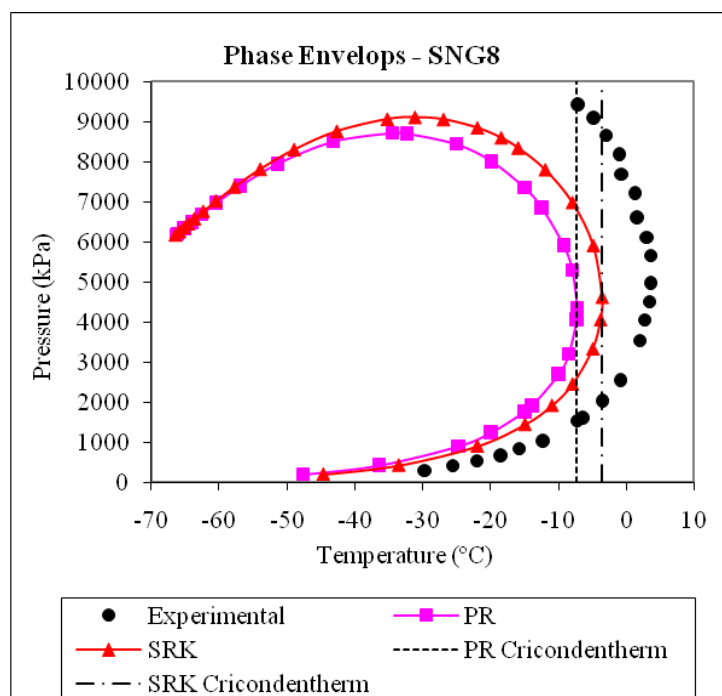


Figure 4.9: Experimental and predicted dew point curves for SNG8 (Experimental data from Morch et al., 2006)

The effect of nitrogen (N_2) on the dew point curve can be observed from the analysis of dew points for samples SNG7 and SNG9. It should be noted that N_2 is the only non-hydrocarbon component in these mixtures. For these two samples, the model predictions agree with the experimental values for pressures below the cricondentherm point. However, above the cricondentherm, the experimental dew points deviate significantly from the predicted curves. As temperature decreases, the differences between the experimental and the predicted curves above the cricondenbar point are reduced. In Figures 4.10 and 4.11 the phase envelopes for SNG7 and SNG9 samples are shown.

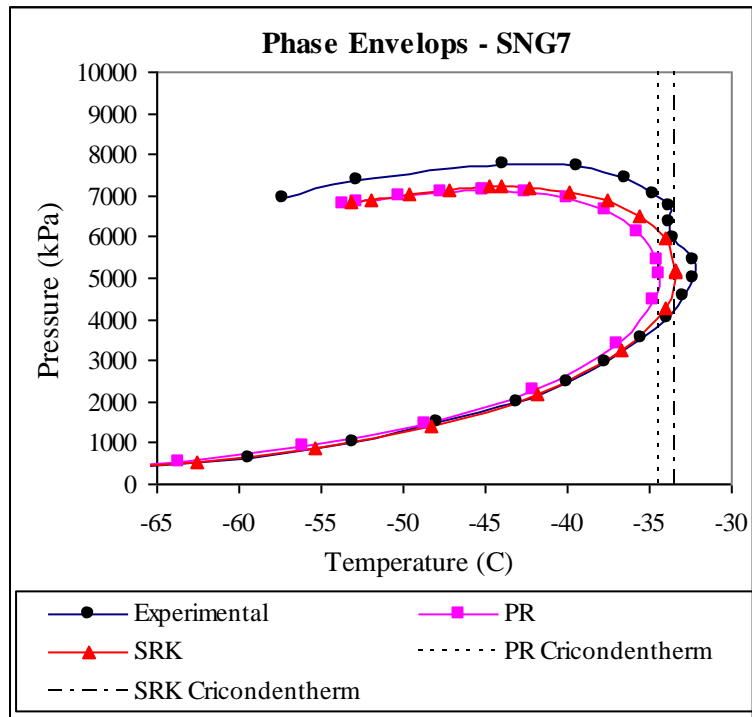


Figure 4.10: Experimental and predicted dew point curves for SNG7 (Experimental data from Avila et al., 2002)

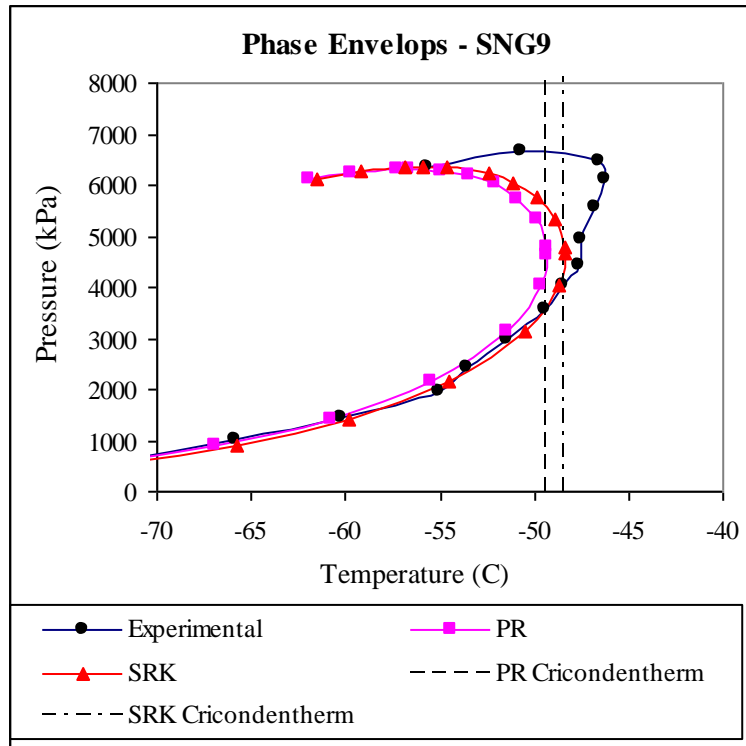


Figure 4.11: Experimental and predicted dew point curves for SNG9 (Experimental data from Avila et al., 2002)

Unfortunately, there are not enough data for samples with only CO_2 as the non-hydrocarbon component. Therefore, a major conclusion or observation cannot be reached at this point. However, there is one sample, SNG10, with a large percentage of CO_2 (more than 25%) that can be evaluated. In addition to having this large percentage of CO_2 , this sample also has a moderate amount of C_5^+ (0.17%). The experimental dew points and the model predicted dew points strongly correlate over the whole range of pressures and temperatures evaluated. As discussed, CO_2 increases the solubility of the heavier hydrocarbons as well as methane and ethane. EOSs could therefore predict the effect of CO_2 more accurately than the effect of N_2 on the gas samples, where major

deviations between predicted and experimental values were observed. In Figure 4.12 the dew point curves for this gas sample are presented.

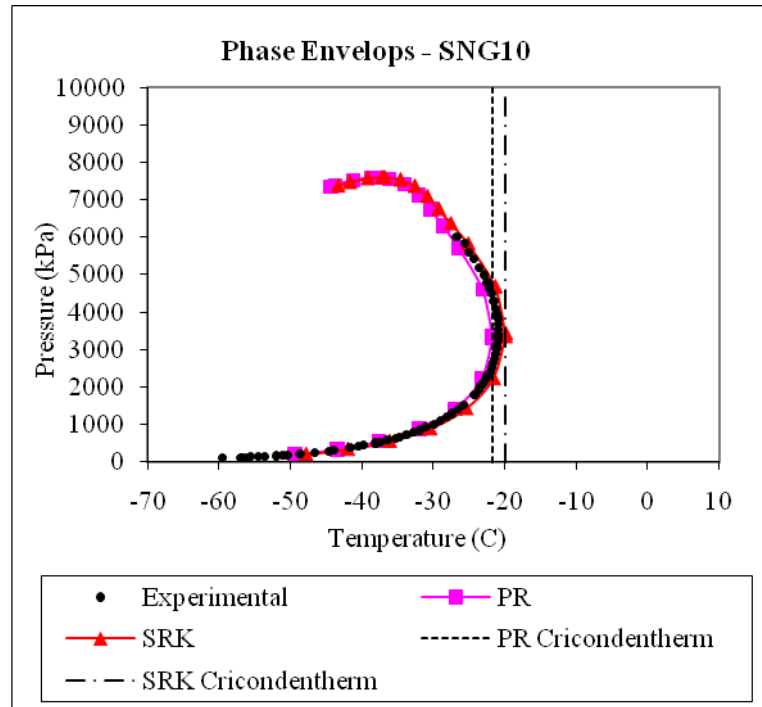


Figure 4.12: Experimental and predicted dew point curves for SNG10 (Experimental data from Jarne et al., 2004)

In general, SRK better predicts the dew points as compared to PR over the diverse range of compositions analysed. Overall, the accuracy of the predictions can vary significantly for the same gas at different conditions of pressure and temperature. For example, the region of the phase envelopes between cricondenbar and cricondentherm is the area with major deviations among predicted and experimental dew points. In addition, the accuracy of the EOS predictions can be strongly affected by the concentrations of certain components in the gas sample. For instance, large concentrations of heavy hydrocarbon

and non-hydrocarbons components in the gas sample will decrease the accuracy of EOS predictions along the dew point curve as demonstrated by mixtures SNG6 and SNG8.

4.1.2 Deviation of EOS predictions for field natural gas samples

The dew point predictions of the PR and SRK models for natural gas samples taken from actual gas reservoir were also evaluated, and their compositions are shown in Table 4.5. These natural gas samples are named NG followed by a number. The compositions of the natural gas samples as well as the experimental results were taken from literature, since no such samples were available in our laboratory.

Table 4.5: Composition of natural gas samples in molar percentages

	NG1	NG2	NG3	NG4	NG5	NG6	NG7	NG8	NG9	NG10	NG11	NG12
	a	a	b	a	a	a	a	a	a	a	a	a
N₂	0.87	0.34	3.91		0.38	0.71	0.39	0.08	0.15	0.41		
CO₂	0.82	2.17	0.75		0.45	8.64	3.47	2.44	0.18	0.97		0.1
C₁	64.04	70.64	70.20	82.38	83	70.85	80.19	82.1	86.57	86.16	91.35	95.22
C₂	10.57	10.76	9.22	4.28	3.76	8.53	6.28	5.78	3.83	3.55	4.03	1.68
C₃	5.75	4.94	2.76	3.51	1.44	4.95	2.75	2.87	1.97	1.54	1.53	0.91
iC₄	1.35		0.66	1.61	0.89	0.75	0.43	0.56	0.49	0.46		0.26
nC₄	2.37	3.02	0.98	3.03		1.26	0.88	1.23	0.72	0.46	0.82	0.33
iC₅	1.06		0.40	0.6	4.36	0.41	0.31	0.52	0.34	0.26		0.16
nC₅	0.98	1.35	0.42	0.68		0.4	0.35	0.6	0.4	0.2	0.34	0.11
nC₆	1.01	0.9	0.82	0.99	3.08	0.46	0.53	0.72	0.57	0.35	0.39	0.25
C7+	11.18	5.88	9.873	2.92	2.63	3.04	4.42	3.1	4.78	5.64	1.54	0.98
C₂+C₁	74.61	81.4	79.42	86.66	86.76	79.38	86.47	87.88	90.4	89.71	95.38	96.9
C₃⁺	23.7	16.1	15.9	13.3	12.4	11.3	9.7	9.6	9.3	8.9	4.6	3.0
C₅⁺	14.2	8.1	11.5	5.2	10.1	4.3	5.6	4.9	6.1	6.5	2.3	1.5
MWC7+	186	153	192.8	125	106	155.3	171	132	200	253	138.78	122.6
SG C7+	0.807	0.810	0.803	0.740	0.733	0.831	0.813	0.774	0.820	0.850	0.796	0.723
Ideal kg/m³	805	808	801	739	732	829	811	772	818	848	795	722

Note 1: a) (Nasrifar, 2005); b) (Yang et al., 1996)

Note 2: The experimental errors reported in the papers are described in Appendix C

For the above gas compositions, the EOSs underestimate the dew points for all the gas samples, except for NG6. The predictions show a wide range of deviations from more than 30% of error to less than 10% error. Large deviations were observed for samples containing a dense C_7^+ fraction. In two cases (NG1 and NG3), the EOS predicts bubble point instead of a dew point, and this can be attributed to the large amount of C_7^+ fractions present (11.17 and 9.87 %, respectively). The absolute percentage of errors for the PR and SRK dew point prediction for the natural gas samples as well as the experimental and predicted saturation pressures are outlined in Table 4.6.

Table 4.6: Absolute percentage of error for PR and SRK dew point predictions for natural gas samples.

Natural Gas	Temperature	Pressure	PR	% Abs	SRK	% Abs
	C	kPa	kPa	Error	kPa	Error
NG7	148.9	54269	30675	43	33212	39
NG6	118.9	39852	24283	39	25890	35
NG9	106.7	60329	44292	27	47126	22
NG10	132.8	81565	61687	24	66645	18
NG11	93.9	26462	20546	22	22415	15
NG2	135.6	33467	26428	21	27869	17
NG8	82.5	28103	23842	15	25111	11
NG4	4.4	21339	19305	10	19671	8
NG5	15.6	18278	19574	7	19974	9
Average				23		19

Note: For the experimental dew point of NG1 and NG3, PR and SRK equations predicted bubble points instead of dew points, so they are not included in the table.

Overall, SRK presents a better prediction of the dew points than PR, and this behaviour is observed over a wide range of gas compositions.

4.2 Liquid Dropout

Liquid Dropout is the ratio of liquid volume over total volume of a gas sample under the two-phase equilibrium conditions. This ratio is measured during CCE tests (see Chapter 3) performed at a constant temperature while the pressure is reduced in steps.

An accurate prediction of the behaviour of gas condensate under different conditions (pressure and temperature) is crucial for the optimum design and operation of process facilities (Aminian, 2004).

As shown in this section, the PR and SRK equations predictions differ from experimental data with respect to liquid dropouts, even for simple gas compositions (synthetic gas samples with normal octane as the heaviest hydrocarbon component). The liquid dropouts predictions of the PR and SRK equations were compared with the experimental values for two gas samples; a synthetic rich gas sample prepared in the laboratory (Mix 5) and a field natural gas sample obtained from literature data (NG3), which general compositions are indicated in Table 4.7 (see Tables 3.1 and 4.5 for complete compositions). Figure 4.13 and 4.14 compare experimental and predicted liquid dropout of the PR and SRK models versus pressure for Mix 5 at two different temperatures 40 and 60 °C, respectively.

Table 4.7: Compositions of the gas samples employed to study the performance of the PR and SRK models for liquid dropout prediction.

Components	Synthetic gas sample (Mix 5) a	Field gas sample (NG3) b
CO ₂	---	0.75 %
N ₂	----	3.91 %
C ₁	64 %	70.20 %
C ₃ ⁺	25 %	15.95 %
C ₅ ⁺	6 %	11.51 %
C ₇ ⁺	1 %	9.87 %

Note: a) It is a synthetic gas sample prepared in the laboratory with n-octane as the heaviest component; the complete composition is shown in Table 3.1 b) The field gas samples contain hydrocarbons heavier than normal octane; the complete composition of this sample is shown in Table 4.5 as NG3 (Yang et al., 1996).

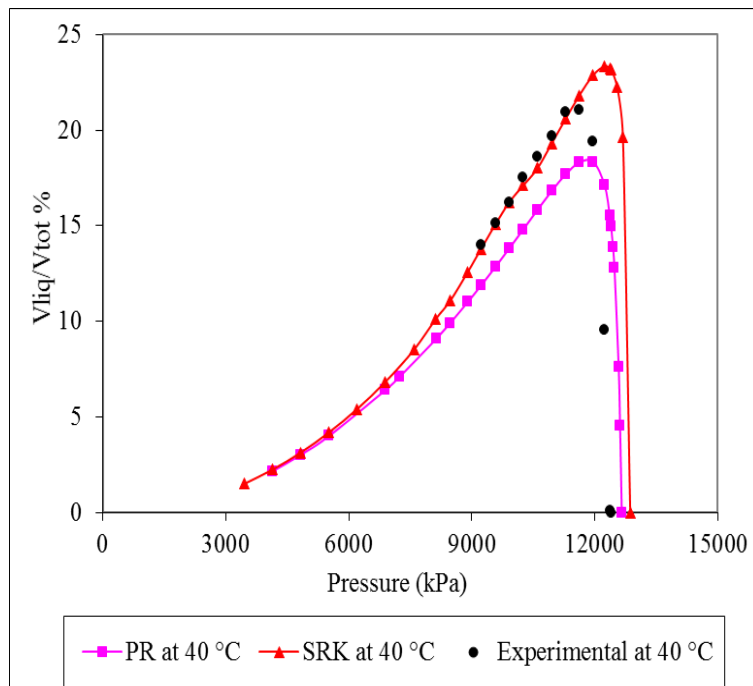


Figure 4.13: Predicted liquid dropout of PR and SRK versus pressure for the synthetic gas (Mix 5) at 40 °C

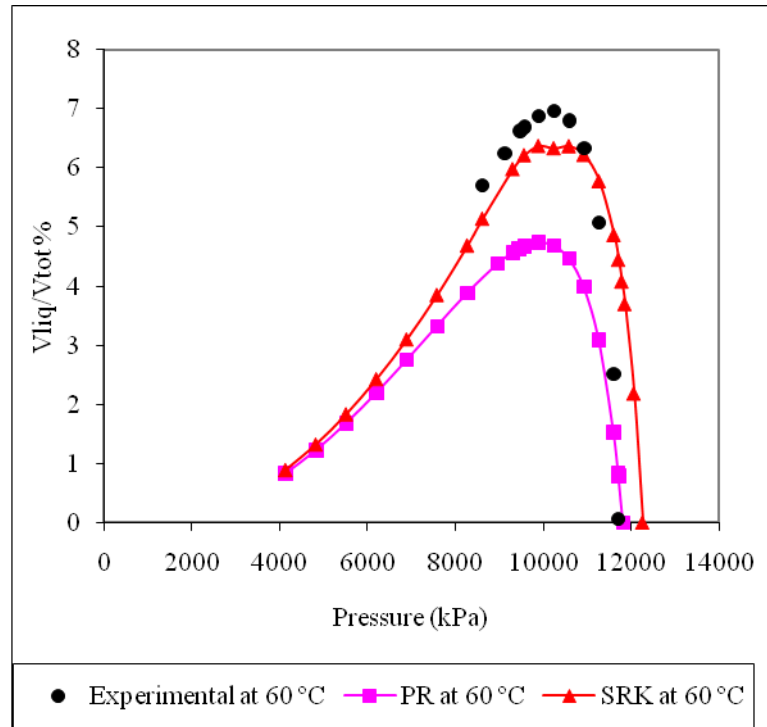


Figure 4.14: Predicted liquid dropout of PR and SRK versus pressure for the synthetic gas (Mix 5) at 60 °C.

At the dew point, there is not liquid accumulation, only a first drop is form. For gas samples with large contain of heavy hydrocarbons, a large liquid accumulation is observed at pressures just below the dew point pressure (especially between the cricondenbar and cricondentherm conditions) when performing a CCE test. Figures 4.13 and 4.14, illustrate the models' predictions, and it can be seen that the largest differences among predictions and experimental point occurred at pressures close to the dew point. In this case, The PR equation predicted lower percentages of liquid dropouts ($V_{liq}/V_{tot}\%$) than the experimental values for both temperatures; however more pronounced at higher temperatures (60 °C). Instead, the SRK model predicts lower liquid

dropout percentage tends to over predict the liquid dropout at lower temperatures and under predict the liquid dropout at higher temperatures.

Natural gas frequently contains a large amount of heavier hydrocarbons in the heptane plus fraction. This fraction was therefore characterized to obtain a more accurate prediction by the models. Although the characterization improved the predictions noticeably, the EOS still indicated large errors in predicting liquid dropouts. Figure 4.15 compares experimental and predicted liquid dropout percentages versus pressures at 156 °C for NG3.

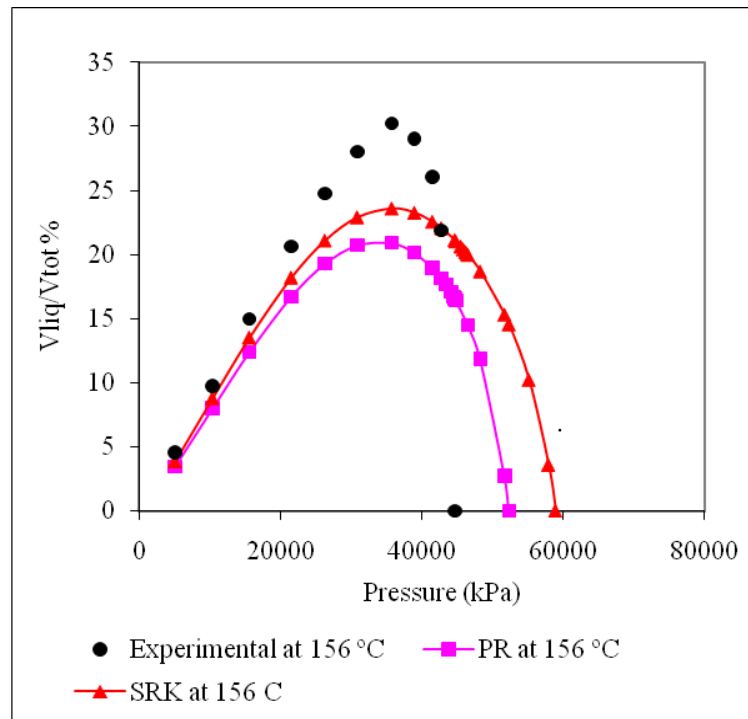


Figure 4.15: Predicted liquid dropout of PR and SRK versus pressure for the natural gas sample at 156 °C.

In this case, both EOS over predicted the dew point pressure, and therefore the amount of liquid dropout above this point. At pressures lower than the experimental saturation pressure, both models under predict the liquid dropout percentages. Similar differences were observed over the temperature range analysed.

4.3 Density

Density is critical for the design of pipeline and flow equipment involved in CNG transfer operations. During the loading of a high pressure tank, the gas can undergo various phase transitions. Phase behaviour will depend on the composition of the gas and on the loading conditions. Density is one of the few measurable properties that could be benchmarked against EOS predictions to check the accuracy of the predictions. If a model predicts the density properly, it is probably effective in predicting pressure and temperature changes during loading and unloading operations.

In this section, the performance of the PR and SRK models to predict fluids/gas density under a range of pressures and temperatures is evaluated. In the first part, the densities of supercritical fluids are evaluated and then the gas densities in the two phase region are evaluated.

4.3.1 Density in the supercritical fluid region

Experimental density for a range of synthetic gas samples were obtained from the literature and also from measurements in our laboratory. The compositions of the gas samples used for density determinations together with their molecular weights, propane and pentanes plus fractions are shown in Table 4.8.

Table 4.8: Compositions of synthetic gas samples, together with their molecular weights and propane and pentanes plus fractions

Mixture	Mix 5 a	Mix 4 a	RG2 b	G2 c	GU2 b	GU1 b	NIST2 b	NIST1 b	G3 c	G1 c
CH ₄	0.6441	0.8369	0.8590	0.9036	0.8120	0.8130	0.9064	0.9658	0.9244	0.9835
C ₂ H ₆	0.1098	0.076	0.0850	0.0571	0.0431	0.0329	0.0455	0.0182	0.0129	0.0051
C ₃ H ₈	0.1282	0.0475	0.0230	0.0112	0.0089	0.0064	0.0083	0.0041	0.0035	0.0015
iC ₄ H ₁₀	0.0248	0.0023	0.0035	0.0017	0.0015	0.0010	0.0010	0.0010	0.0005	0.0003
nC ₄ H ₁₀	0.0329	0.0145	0.0035	0.0030	0.0016	0.0010	0.0016	0.0010	0.0004	0.0002
iC ₅ H ₁₂	0.0215	0.0032	0.0003	0.0003	0.0005	0.0005			0.0001	0.0001
nC ₅ H ₁₂	0.018	0.0033	0.0005	0.0006	0.0003	0.0005			0.0002	0.0001
nC ₆ H ₁₄	0.011	0.0004		0.0006	0.0004	0.0006			0.0001	0.0001
MecycloC ₅										
nC ₇ H ₁₆	0.0043	0.0005								
nC ₈ H ₁₈	0.0054	0.0006								
N ₂		0.0039	0.0101	0.0004	0.0570	0.1358	0.0313	0.0027		0.0000
CO ₂		0.0111	0.0150	0.0001	0.0759	0.0099	0.0047	0.0059		0.0000
He				0.0147					0.0575	0.0084
O ₂				0.0065					0.0005	0.0007
MW		19.99	18.77	17.84	19.83	18.67	17.61	16.78	17.01	16.31
C1+C2 %	75.39	90.98	94.4	96.07	85.51	84.59	95.19	98.4	93.73	98.86
C3+ %	24.61	7.24	3.07	1.78	1.32	1.01	1.09	0.61	0.48	0.23
C5+ %	6.02	0.79	0.075	0.189	0.12	0.17	---	---	0.041	0.025

Note : a) Gas samples made in our lab ; b) (Magee et al., 1997); c) (Capla et al., 2002)

For most of the above mixtures, experiments were performed in the gas or supercritical region. The ranges of temperatures and pressures are -23 to 77 °C and 0 to $34,575$ kPa ($5,000$ psia), respectively (Magee et al.; 1997). The natural gas mixtures employed were prepared gravimetrically at National Institute of Standard and Technology (NIST), and the compositions chosen were representative of the compositions encountered in gas industry operations in North America and in Europe. The density measurements were obtained at NIST obtained with an isochoric gas expansion method, and they had an uncertainty of approximately 0.05 per cent. The experimental values of density were compared to those predicted by the EOS, and then the absolute percentage errors (APE) were calculated. The results are summarized in Figures 4.16 and 4.17 for the gas sample RG2. Where the APE curves of PR presented a minimum, the APE curves of SRK presented a maximum. For instance, the PR prediction and experimental data show the best agreement around $13,688$ kPa ($2,000$ psia) for the curves at -23 , -10 , 2 and 7 °C. In the case of SRK, the lowest error occurs at $8,274$ kPa ($1,200$ psia) and the largest error between $13,688$ kPa ($2,000$ psia) and $20,684$ kPa ($3,000$ psia). Overall, the maximum APE for PR and SRK models were 7 % and 6%, respectively. The APE curves of PR and SRK for the rest of the gas samples mentioned in Table 4.5 are in Appendix C, as well as the figures of the phase envelopes with the isotherms used to calculate the gas densities.

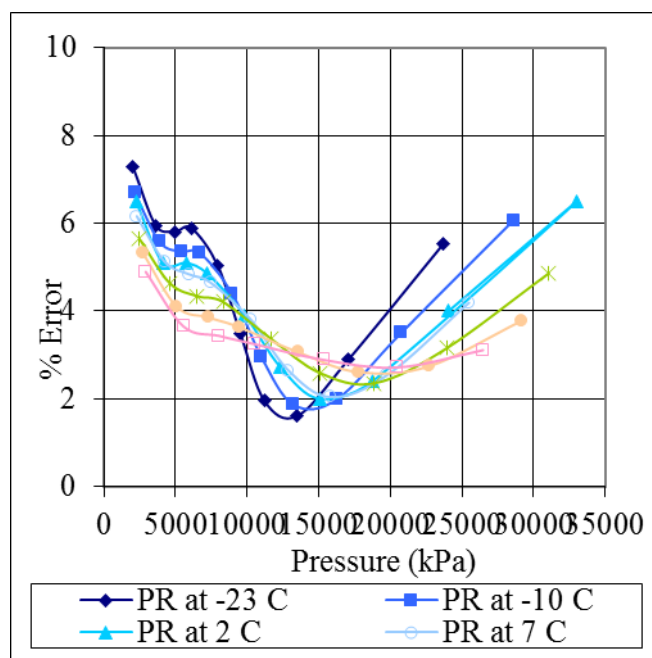


Figure 4.16: Percentage errors of molar density predictions of PR in supercritical region as a function of temperatures for RG2 gas sample.

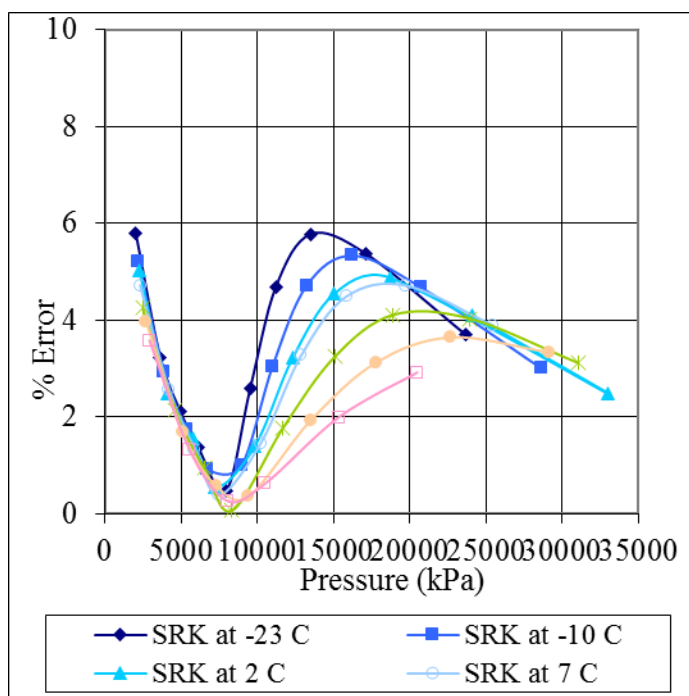


Figure 4.17: Percentage errors of molar density predictions of SRK in supercritical region as function of temperatures for RG2 gas sample.

For the gas samples that cover the same range of pressure and temperature conditions, the average APE of the densities predictions of the PR and SRK equations were calculated and summarized in Table 4.9.

Table 4.9: Average absolute percentage errors of PR and SRK in predicting gas densities for gas samples.

Gas Sample	Average Absolute % Error in predicting gas densities	
	PR	SRK
RG2	4.1	3.9
GU1	4.2	2.3
GU2	4.3	2.8
NIST1	3.8	2.7
Average	4.1	2.9

For rich and moderately rich gas samples (Mix 6 and 4, respectively), the densities were evaluated in the supercritical fluid region to determine the accuracy of the EOS predictions. For the moderately rich gas (Mix 4) the range of pressures and temperatures covered were 13,688 to 27,478 kPa (2,000 to 4,000 psia) and -10 to 10 °C, and for the rich gas 13,688 to 34,372 kPa (2,000 to 5,000 psia) and 10 to 60 °C. The absolute percentage error between predicted and measured values was also calculated. The curve of APE versus pressure showed the same trend as mentioned for the previous cases. The figures showing the APE versus pressure for this gas samples are given in Appendix C, together with the phase envelope and the isotherms.

Another set of experimental gas densities (Capla et al., 2002) was compared. In this case, the range of pressures and temperatures were 864 to 15,067 kPa (140 to 2200 psia) and -20 to 50 °C, respectively. The APEs were calculated for all the temperatures, and showed a different trend compared to the previous cases. Below 6,793 kPa (1,000 psia), the APEs decrease for the PR and SRK predictions. However, above 6,793 kPa (1,000 psia) all the curves showed the same trend as the cases mentioned earlier. It is important to state that the methods of measuring density were different. Magee et al. (1997) used an isochoric gas expansion method, while Capla et al., (2002) used a vibrating-tube apparatus, an Anton Paar equipment consisting of a DMA 512 P measuring cell and a DMA 60 analysis unit. The uncertainty in the density measurements was of $\pm 10^{-3}$ kg/m³. The uncertainty of the temperature measurement of the densimeter cell was estimated to be about ± 10 mK at $T = 298$ K. While, the accuracy of the pressure measurements were around $\pm 0.0025\%$ for the range of 0 to 20 MPa. The experimental method used by the author of this thesis to measure gas densities of Mix 4 and Mix 5 used a vibrating-tube apparatus. The plots of APEs versus pressure and the phase envelopes with the isotherms are given in Appendix D.

Overall, it was found that in the gas phase region and in the supercritical fluid region, the PR and SRK models have average errors less than 8% in gas density predictions.

4.3.2 Gas Densities in the two phase region

To study the accuracy of the PR and SRK models in predicting gas densities in the two phase region, three gas mixtures were used, two moderately rich gases (Mix 3 and Mix 4) and one rich gas (Mix 6).

CVD tests were performed at 10 and 0 °C with Mix 3 and the densities of gas samples were measured with the Anton Paar densitometer (refer Section 3.4 for experimental errors). Table 4.10 compares the experimental densities with the predicted ones by the PR and SRK equations. It is observed that as the pressure decrease for a given temperature the error in the predictions increase; at 10 °C the errors in the prediction are largest than at 0 °C. Overall, the SRK equation had the lower deviation from experimental values than the PR equation.

Table 4.10: Average percentage errors of PR and SRK in predicting gas densities for Mix 3 during CVD tests at 10 and 0 °C

CVD Tests	Exp. ρ (g/cc)	PR		SRK	
		ρ (g/cc)	Error %	ρ (g/cc)	Error %
5.7 MPa; 10 °C	0.0499	0.0553	7.2	0.0535	5
2.9 MPa; 10 °C	0.0189	0.0245	18.3	0.0241	17.2
7.79 MPa; 0 °C	0.0941	0.0993	3.8	0.0947	0.4
3.39 MPa; 0 °C	0.0283	0.0319	8.5	0.0313	7.1

The gas density was also measured for Mix 4 while performing CVD tests at 0 °C. In this case, two CVD tests were performed under the same conditions and the gas density were measured. Table 4.11 gives the experimental densities and the predicted densities for both tests. The results for both tests are similar, which enforce the accuracy of the results.

Table 4.11: Average percentage errors of PR and SRK in predicting gas densities for Mix 4 during CVD tests at 0 °C

P (MPa); n ° Test	Exp. ρ (g/cc)	PR		SRK	
		ρ (g/cc)	Error %	ρ (g/cc)	Error %
7.2 MPa; Test 1	0.0875	0.0875	1.1	0.0836	4.3
5.4 MPa; Test 1	0.0616	0.0598	2.1	0.0577	4.5
3.7 MPa; Test 1	0.0402	0.0374	5	0.0366	6.7
7.2 MPa; Test 2	0.0879	0.0872	0.5	0.0834	3.7
5.4 MPa; Test 2	0.0613	0.0597	1.9	0.0577	4.3
3.7 MPa; Test 2	0.041	0.0374	6.5	0.0365	8.1

CVD tests were also performed with Mix 5 and the absolute percentage error of the PR and SRK gas density predictions at 40 and 60 °C are summarized in Figures 4.18 and 4.19.

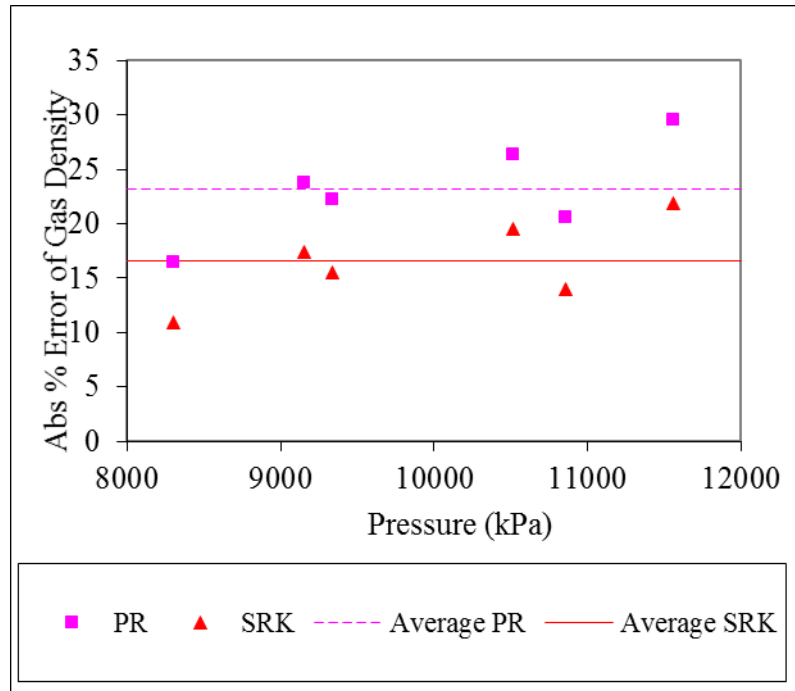


Figure 4.18: Average percentage errors of PR and SRK in predicting gas densities during CVD Test for Mix 5 at 40 °C.

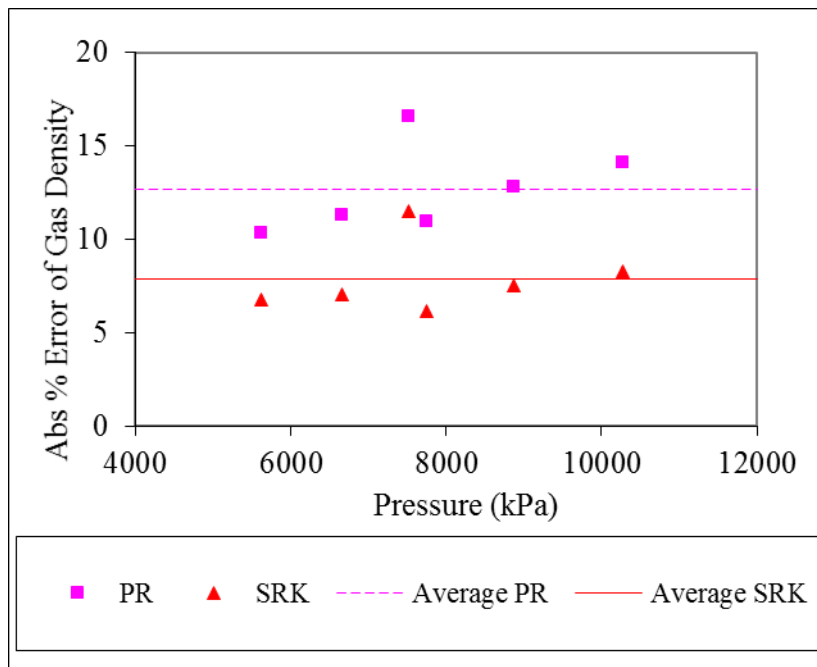


Figure 4.19: Average percentage errors of PR and SRK in predicting gas densities during CVD Test for Mix 5 at 60 °C.

The absolute percentage error of the PR and SRK gas density predictions for the moderately rich gas range between 10 and 15%, while the errors for the rich gas samples are between 8 and 30%, depending on the pressure and temperature.

In this section the original predictions of the EOS are illustrated. In Chapter 6, the improvement in the EOS predictions after tuning will be presented.

4.4 Compressibility in the supercritical region

Compressibility and gas density are inversely proportional as indicated by Equation 4.1. By obtaining the experimental value of one of these properties, the other one can be obtained using Equation 4.1.

$$\rho = \frac{P MW}{Z R T} \quad (4.1)$$

where ρ is gas density (kg/m^3), MW is molecular weight (kg/kgmol), R is the universal gas constant ($\text{m}^3 \text{ kPa/ K mol}$), T ($^{\circ}\text{K}$) is temperature and Z is the compressibility factor.

Experimental gas compressibility data in the supercritical region for the natural gas sample NG3 (see Table 4.5) was used to evaluate EOS predictions. The experimental compressibility was measured between 44,000 and 61,000 kPa and at temperatures of 137, 146, and 177 $^{\circ}\text{C}$ (Yang et al., 1996). These temperatures were selected randomly by

the author of the paper from where the experimental data was obtained The absolute percentage errors in the predictions were calculated and they are illustrated in Figure 4.20. PR and SRK showed absolute percentage errors between 6 and 13 %, with SRK giving better predictions.

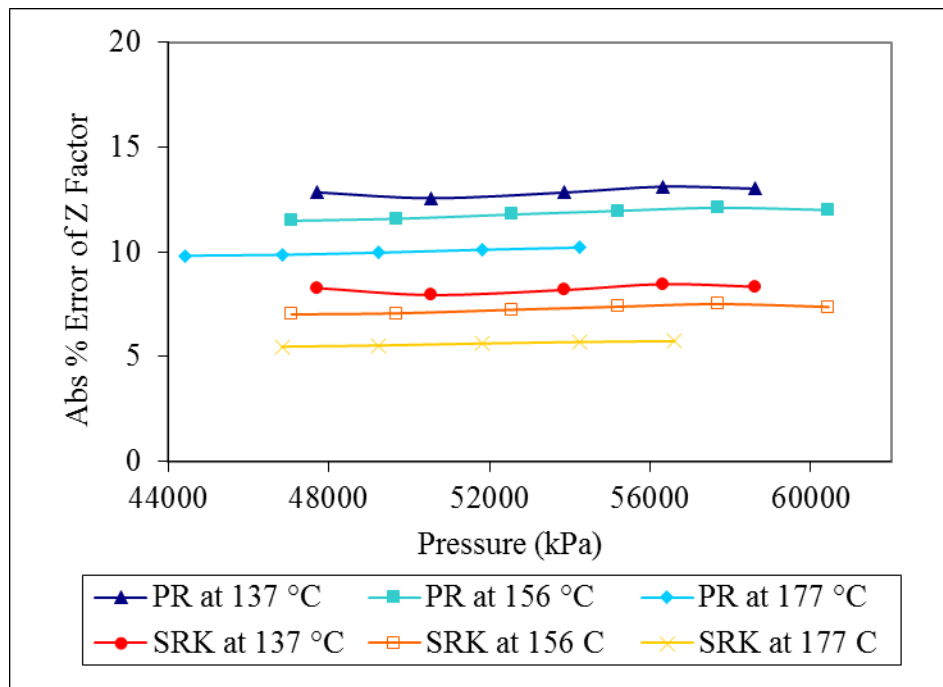


Figure 4.20: Average percentage errors of PR and SRK in predicting compressibility of natural gas sample NG3 in the supercritical region as function of temperatures and pressures.

Although the errors in predicting compressibility (or density) are relatively low, even small errors can have significant impacts in the calculation of gas loaded into CNG tanks.

For instance, in the process of loading gas in CNG processes, the amount of gas that can be charged into a tank will be calculated according to density at the final pressure and temperature conditions. An error of 10% in the density prediction could result in a significant error in the calculation of the mass (or moles) of gas that can be charged to the tank.

4.5 Conclusions

In this chapter, the limitations of the most commonly used models for predicting phase behaviour were demonstrated. The thermodynamic properties considered were dew points, liquid dropout, gas density, and compressibility. These properties were evaluated for synthetic gas samples as well as for natural gas samples.

The gas composition plays an important role in the EOS predicting gas properties and vapour-liquid equilibrium conditions. As the concentration of heavy hydrocarbons increases, the errors in the EOS predictions also increase. For lean and moderately rich gases PR and SRK predict dew points accurately. However, for rich gases the dew points predictions have larger errors compared to experimental values. PR, in general, has errors 5-8% larger than SRK. When the gas under evaluation contains a dense C_7^+ fraction, the errors in the dew point predictions could go from 10 to 50 %. Overall, SRK provides a better prediction of the dew points than PR, and this behaviour is observed over a wide range of gas compositions.

The accuracy of dew points predictions can vary significantly for the same gas at different conditions of pressure and temperature. The region of the phase envelopes between cricondenbar and cricondentherm is the area with major deviations among predicted and experimental dew points.

For synthetic gases, the model predictions for liquid dropout show the largest errors at pressures close to the dew points. PR tends to under predict the liquid dropouts except close to the dew points, while SRK tends to overpredict liquid dropout at lower temperatures and underpredict the liquid dropout at higher temperatures. In the case of natural gas samples, the characterization of the C_7^+ fraction improved the predictions noticeably; nevertheless the EOS still indicated large errors.

The PR density predictions of gas in the supercritical region have a range of error between 2 and 8 %, while SRK have errors between 0 and 6 %, depending on the pressure and temperature conditions. In the two phase region, the errors of the PR and SRK in predicting gas densities vary depending on the type of gas, temperature and pressure. For moderately rich gases, the errors are between 10 and 15%, while for rich gases they lie between 8 and 30%. In both cases, PR always indicated larger errors than SRK.

CHAPTER 5

MATHEMATICAL MODEL

In the previous chapter, deviations were observed between experimental data and the predictions of the EOSs. When measured and predicted PVT data do not match, an adjustment of the model parameters is commonly applied to eliminate the deviations. The adjustment of the model parameters is a process commonly called ‘tuning of EOS’ during which the parameters that require modification are identified and new values are found. In this chapter, descriptions of the two mathematical models used for the tuning process are presented and a complete explanation of this process is also given.

5.1 Mathematical Models descriptions

The two most common EOSs used in the industry are the Peng-Robinson (PR) and Soave-Redlich-Kwong (SRK) (Dustman et al., 2006) equations. Therefore these two equations, or a modification of these equations, are used for tuning purposes in this research. The general form of the equation is given by equation 5.1:

$$P = \frac{RT}{V + \nu_1} - \frac{a_c \alpha(T)}{(V + \nu_2)(V + \nu_3)} \quad (5.1)$$

Where, R is the gas constant, T is temperature, P is pressure, V is molar volume, a_c is the attractive parameter at the critical temperature, α is the attractive parameter temperature dependence, and ν_1 , ν_2 and ν_3 are volume correction parameters. The volume correction parameters are shown in Table 5.1 for some EOSs (Pedersen & Christensen, 2007). The SRK and PR equations only make use of one volumetric correction parameter, while the Peneloux-modified SRK and PR equations make use of two parameters.

Table 5.1: Expression of volume correction parameters for generalized EOS equation 5.1.

EOS	Constant values		
	ν_1	ν_2	ν_3
SRK ^[8]	$-b$	0	B
PR ^[9,10]	$-b$	$(1 + \sqrt{2})b$	$(1 - \sqrt{2})b$
SRK-P ^[11]	$-b$	c	$b + 2c$
PR-P ^[12]	$-b$	$c + (1 + \sqrt{2})(b + c)$	$c + (1 - \sqrt{2})(b + c)$

SRK: Soave-Redlich-Kwong (Soave, 1972); PR: Peng-Robinson (Peng & Robinson, 1976, 1978); SRK-P: Soave-Redlich-Kwong-Peneloux (Peneloux et al., 1982); PR-P: Peng-Robinson –Peneloux (Jhaveri & Youngren, 1988).

In Table 5.1, the mathematical expressions of the volume correction parameters introduce parameter b , which is the molecular co-volume, and parameter c , which is a volume translation or volume shift parameter. The mathematical expression for a_c , $\alpha(T)$, b and c are given by Equations 5.2 to 5.7, and the values of the constants in these equations are indicated in Table 5.2 for the EOS mentioned previously:

$$a_c = \frac{cte_1 R^2 T_c^2}{P_c} \quad (5.2)$$

$$b = \frac{cte_2 RT_C}{P_C} \quad (5.3)$$

$$\alpha(T) = \left[1 + m \left(1 - \sqrt{\frac{T}{T_C}} \right) \right]^2 \quad (5.4)$$

$$m = m_1 + m_2 \omega - m_3 \omega^2 \quad (5.5)$$

where, ω is the acentric factor.

$$c = \frac{C_1 RT_C (C_2 - Z_{RA})}{P_C} \quad (5.6)$$

$$Z_{RA} = 0.29056 - 0.08775 \omega \quad (5.7)$$

Where, Z_{RA} is the Rackett compressibility factor (Rackett, 1976)

Table 5.2: Values of the constant of the EOS parameters (Pedersen & Christensen, 2007)

Constant	EOS			
	SRK	PR	SRK-P	PR-P
cte_1	0.4274	0.45724	0.4274	0.45724
cte_2	0.08664	0.07780	0.08664	0.07780
m_1	0.48	0.37464	0.48	0.37464
m_2	1.574	1.54226	1.574	1.54226
m_3	0.176	0.26992	0.176	0.26992
C_1	---	---	0.40768	0.50033
C_2	---	---	0.29441	0.25969

Since natural gas is a multi-component mixture, mixing rules are applied to calculate the parameters a , b , and c . The most widely applied mixing rules are the Van der Waals one fluid prescription (PVTPro, 2003); however these rules are not applicable for non-polar mixture components. The mathematical expressions of this mixing rule are given by Equations 5.8, 5.9, and 5.10.

$$a_c = \sum_{i=1}^N \sum_{j=1}^N x_i x_j \sqrt{a_i a_j} (1 - k_{ij}) \quad (5.8)$$

where, k_{ij} is the binary interaction parameter (BIP) between components i and j , x is the molar fraction, and N is the total number of components.

$$b = \sum_{i=1}^N x_i b_i \quad (5.9)$$

$$c = \sum_{i=1}^N x_i c_i \quad (5.10)$$

BIP is an adjustable parameter with an indefinite physical meaning and its value depends on the EOS used (Danesh, 1998). A BIP value of zero is given to similar hydrocarbons and non-zero for combinations between complex hydrocarbons and between non-hydrocarbons (such as N_2 , CO_2) and hydrocarbons (PVTPro, 2003).

5.2 Equation Tuning Process based on Experimental Results

Zuo and Zhang (2000) developed a regression technique to fit the PVT data and studied the phase behaviour for single and multiple samples of reservoir fluids. This technique is used in the development of the PVTPro software; therefore, it will be used in this research to tune the EOS. The following paragraphs explain the technique in detail.

5.2.1 Method to tune parameters of EOS

The potential tuneable parameters for a given EOS are critical temperature (T_C), critical pressure (P_C), acentric factor (ω), binary interaction coefficients (k_{ij}), dimensionless volume shift parameter (V^t), and exponent (θ) in the binary interaction coefficient correlation between hydrocarbons. The binary interaction coefficients correlation between hydrocarbon components i and j is given in Equation 5.11.

$$k_{ij} = 1 - \left(\frac{2(V_{ci})^{1/6}(V_{cj})^{1/6}}{(V_{ci})^{1/3} + (V_{cj})^{1/3}} \right)^\theta \quad (5.11)$$

where, V_C is the critical molar volume. The dimensionless volume shift parameter is defined in Equation 5.12.

$$\tilde{V}_i^t = \frac{c_i}{b_i} \quad (5.12)$$

where, c and b stand for the volume shift parameter and the co-volume of the EOS. The V^t parameter can be calculated using the correlation developed by Jhaveri and Youngren (1988) for light components (C_1 - C_6 , N_2 , CO_2). For heavier components V^t can be obtained by matching the density of each component at atmospheric pressure or using the correlation expressed in Equation 5.13:

$$\tilde{V}_i^t = d_1 + d_2 V_i^t \quad (5.13)$$

where, d_1 and d_2 are two adjustable parameters (the default values are $d_1=0$ and $d_2=1$). The tuning of the EOS parameters is made by using experimental data. The PVT experimental data for the regression of the parameters are saturation points, gas phase compressibility factors, phase densities, relative gas and oil volumes, liquid drop out curves, and phase compositions (Pedersen & Christensen, 2007). This information is obtained from saturation (dew/bubble point) pressure tests, constant composition expansion (CCE), constant volume depletion (CVD), differential liberation (DL), separator (SEP), and P-T flash tests. It is important to emphasize that saturation pressure, volumetric, and viscosity data can be fitted separately or simultaneously as they are independent of each other as well the aforementioned parameters.

In every regression calculation, an objective function is required. For EOS parameter tuning, which is a nonlinear minimization problem, the objective function (F) used is the one proposed by Zuo & Zhang (2000) and is given by Equation 5.14.

$$F(\vec{x}) = \sum_{i=1}^M \left(w_i \frac{e_i^{\text{exp}} - e_i^{\text{cal}}(\vec{x})}{e_i^{\text{exp}}} \right)^2 \quad (5.14)$$

where, x is the vector of adjustable parameters with N (number of adjustable parameters) dimension. M , w_i , e^{exp} , e^{cal} are the number of data points, the weighing factor, the experimental and calculated values, respectively.

The lower bound X_{\min} and the upper bound X_{\max} are used to scale the adjustable parameters X , and these are related as shown in Equation 5.15. The value of x_j always falls between zero and one.

$$x_j = \frac{X_j - X_j^{\min}}{X_j^{\max} - X_j^{\min}} \quad (5.15)$$

In order to determine the sensitivity of the objective function with respect to the adjustable parameters, the function is differentiated with respect to each adjustable parameter. The parameters that present the larger absolute values of gradients are more sensitive, so these are more likely to be adjustable variables.

5.2.2 Steps in tuning EOS

The tuning of the EOS was performed using the PVTPro 5.1 software, which employs the regression technique explained in the previous section. The adjustments of the EOS

parameters were made separately for each gas mixture and then results were compared. The general steps followed to tune the EOS using the PVTPro software are described below:

- 1- Selecting the EOS: The EOS with volumetric translation and mixing rules are first selected together with the standard conditions (101 kPa and 15.56 C). The EOSs used were PR (1978) and SRK (1972), while the Van der Waals Mixing Rule with Temperature Independent k_{ij} was selected.
- 2- Adding the gas composition: The gas mixture composition used in the experimental tests is then added. The k_{ij} of all the components are modified according to the k_{ij} that appear in Hysys, The reason for changing the k_{ij} in PVTPro is that Hysys will be then used to evaluate the accuracy of the modified EOS in predicting thermodynamic properties, so the k_{ij} should be the same for the tuning and for evaluating the EOS in the two software packages.
- 3- Entering experimental data: All the experimental data from the CCE and CVD tests are entered in the PVTPro software. In the case of the CCE test, the type of fluid (oil or gas condensate), the temperature and pressure of the test as well as the diverse ratios of volumes (such as V_{liq}/V_{tot} , V_{liq}/V_{sat} , V_{tot}/V_{sat}) for each pressure step, are indicated. The dew point pressure is referred to as saturation pressure and the total volume at this pressure is called the saturated volume, and it is taken as reference. With the CVD test, the general parameters of the test such as the type of fluid (Oil or Gas condensate), the temperature and pressures of the test are indicated. For each pressure step, diverse experimental data can be added,

such as: moles of vapor depleted, total moles depleted, liquid moles before depletion, vapor moles before depletion, moles remaining, % liquid dropout ($V_{liq}/V_{sat}\%$), gas density, gas molecular weight, gas Z factor.

- 4- Calculating the prediction of EOS for the experimental conditions added: Once all the experimental data are added, the PVTPro software is used to calculate the EOS predictions for the conditions of the experimental tests.
- 5- Selecting experimental data for tuning: The tuning of the EOS was done by simultaneously employing saturation pressure and volumetric data from CCE and CVD tests, so that the resulting modified parameters improve the predictions of both properties. The experimental data that can be used for tuning are:
 - a. From CCE tests: liquid volume percentages ($\%V_{liq}/V_{tot}$) and the relative volume (V_{tot}/V_{sat}) at each pressure step of a CCE test.
 - b. From CVD tests: liquid volume percentage ($\%V_{liq}/V_{tot}$) and total vapor depleted at each pressure step of a CVD test.

Each experimental data used for tuning can have an assigned weight percentage. A group of data such as $\%V_{liq}/V_{tot}$ points, can also have assigned a general weight in the tuning. The reason of the weight percentages is to decrease the relative weight of experimental data points which may be slightly inaccurate. For example, the experimental $\%V_{liq}/V_{tot}$ of a gas condensate can present certain inaccuracies if sufficient time was not taken for the measurement (such as being less than 30 min). In this case, a lower weight percentage can be assigned to that particular set of data. In this research, a general criterion was

adopted for assigning the weight percentage values, thus a value of 100 was assigned to each experimental data used in the tuning and the data that was not reliable due to experimental errors was not used for tuning.

Figure 5.1 illustrates a screenshot of the software where the data for tuning is selected and the relative weight percentages are designated.

- 6- Selecting the parameters: Twenty combinations of k_{ij} are selected. Overall, they were the combination between hydrocarbons from nC_3 to nC_8 for the synthetic gas samples, and between the C_1 - C_2 and the pseudo components of the heavy fraction for field natural gas samples. Also, the upper and lower values for each pair of k_{ij} are added in this step. The volume translation coefficients are also selected for tuning. In this step the lower bound X_{min} and the upper bound X_{max} for each parameter selected are assigned. In this research, a value of zero was selected for the lower bound and a value of one for the upper bound.
- 7- Performing sensitivity analysis: In this step, the software performs a sensitivity analysis and based on the result orders the tuneable parameters according to the decreasing order of $|\partial F/\partial x_j|$. An iteration limit and an error tolerance are assigned for performing the sensitivity analysis.
- 8- Modifying sensitivity analysis results: The software lists all the sensitive parameters as adjustable parameters for tuning. In this step, parameters which were not sensitive for tuning can be selected to be included in the regression.
- 9- Performing the model tuning: The software performs a nonlinear regression with a designated iteration limit and an error tolerance. The results are then displayed

in a table indicating the calculated result before and after tuning and the percentage deviation before and after tuning for each experimental data. Also general average relative deviations before tuning and after tuning are determined in order to compare the general change in the predictions. The software also shows the new values for the optimized parameters.

10- Evaluation of the EOS: The new value of the modified parameters of the EOS can now be introduced in the process simulator HYSYS to evaluate the performance of the EOS.

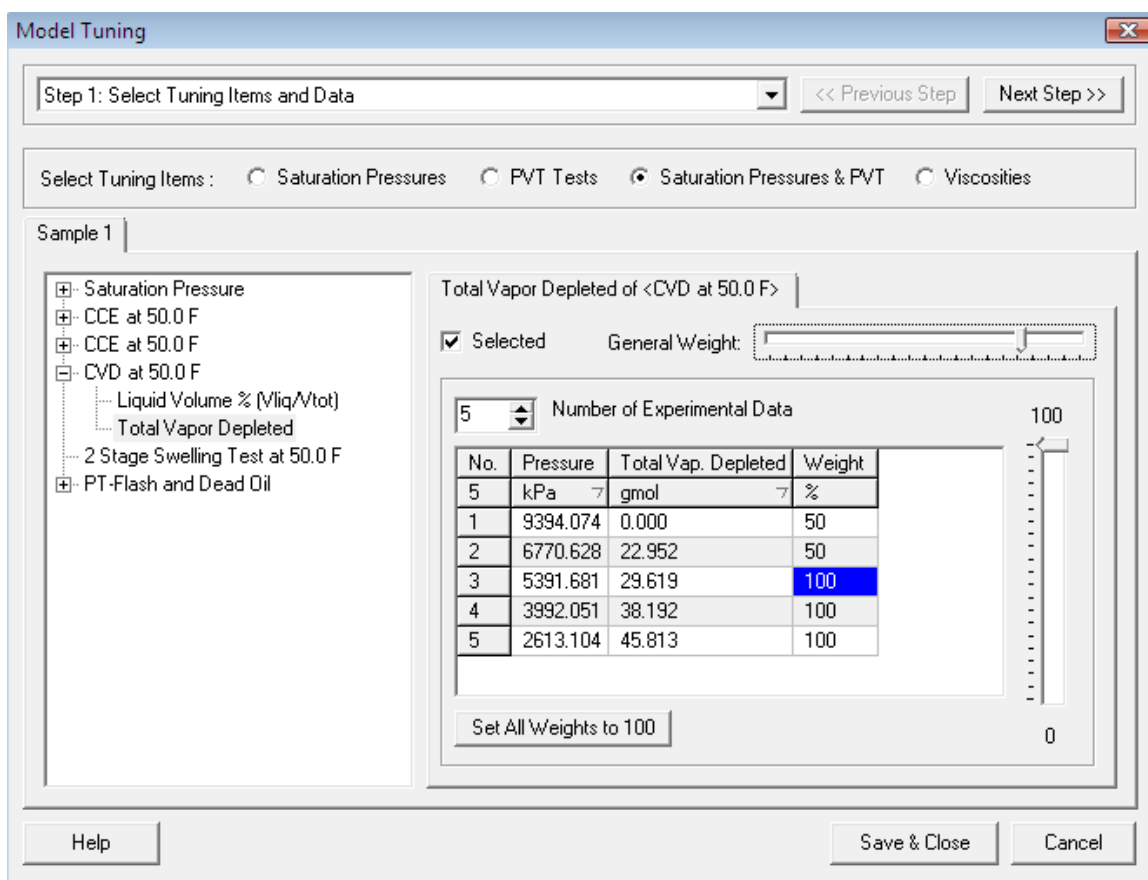


Figure 5.1: Screenshot of PVTPro.5.1 software where the data for tuning are selected and the relative weight percentages are designated.

5.2.2 Mathematical model solution

Once the values of the adjusted parameters are found, they are included in the EOSs to evaluate their performance. The thermodynamic basis in the HYSYS process simulation software allows for changes in the k_{ij} values as well as the volume correction parameters of the built-in EOS models. Therefore, the adjusted parameters obtained with the regression technique (such as k_{ij} , d_1 and d_2) can be introduced into the HYSYS simulator, which in turn would enable the user to study the performance of the tuned EOS. As a result, the predictions of the EOS with tuned model parameters can be compared to those of the original models. The tuned models can then be employed to investigate the performance of the EOS on the loading and unloading operations of a CNG tank by dynamic simulations in HYSYS.

5.3 Conclusion

In this chapter, the mathematical models employed to predict the thermodynamic behaviour of gas samples were described. Since the thermodynamic models have errors in their predictions when compared with measured data, a process of tuning of EOS was proposed and explained. The tuning procedure consists of the identification and modification of the EOS parameters in order to improve their predictions. The evaluation of the performance of the tuned models could be completed using the HYSYS process simulator, where the new EOS parameters' values can be introduced. Thus, HYSYS is used to obtain the predictions of the EOS, before and after tuning. These

results can then be compared against experimental data and evaluate their differences and improvements.

CHAPTER 6

PROPOSED APPROACH FOR IMPROVEMENT OF THE EOS PREDICTIONS

In Chapter 4 the limitations of PR and SRK for predicting natural gas behaviour under temperatures and pressures typically encountered in offshore reservoirs was demonstrated. In this chapter a methodology to improve their predictions is presented. The thermodynamic properties evaluated in this chapter are the same as in Chapter 4. Using experimental data, we performed regression analysis on the EOS in order to evaluate the parameters that required adjustments. In the regression analysis, the same procedure was followed to choose the tuning parameters for all the cases. As a result, a significant improvement in the EOS predictions was achieved through the modification of a few parameters.

6.1 Dew Points

Binary interaction parameters (k_{ij}) play a major role in the calculation of dew points since they affect the vapour-liquid equilibria (VLE) of mixtures. As a general rule, the k_{ij} are estimated empirically (by curve fitting). With the right set of k_{ij} for all the binary combinations in a mixture, the dew points can be accurately predicted. By contrast, having the wrong set of k_{ij} could lead to erroneous predictions of the dew points.

Binary interaction parameters (k_{ij}) are independent of the mixture and only depend of the two components involved. Nevertheless, it was found that modifying certain k_{ij} will improve the dew point predictions of the EOS for gas samples with large content of heavy hydrocarbons. Since a small amount of experimental data was used to tune the EOS's parameters, the modified k_{ij} only represented the given mixture under evaluation. In the case of disposing a larger amount of experimental data, a more general modified k_{ij} could be obtained and in that case this value will be independent of the gas mixture.

During the regression analysis, the deviations of the initial predictions could be reduced by modifying a certain k_{ij} and volume translation coefficients. In the case of synthetic gas samples, by adjusting just one binary interaction parameter (k_{ij}), predictions were significantly improved. The k_{ij} to be modified was selected after performing a regression analysis on the experimental values. When the initial EOS predictions between cricondentherm and cricondenbar points were sharply deviating from experimental data, the predictions could be improved by modifying the k_{ij} for methane and propane (k_{C1C3}). This was observed for the synthetic gas samples SNG1, SNG5, SNG7 and SNG9, whose compositions are indicated in Table 4.2. The new values of the k_{C1C3} , after tuning, were different for each sample. In order to find an optimized value for this binary interaction coefficient, a large amount of experimental data were required. Figures 6.1 and 6.2 show the dew point curves of PR and SRK before and after tuning together with the experimental values for samples SNG1 and SNG 5, respectively.

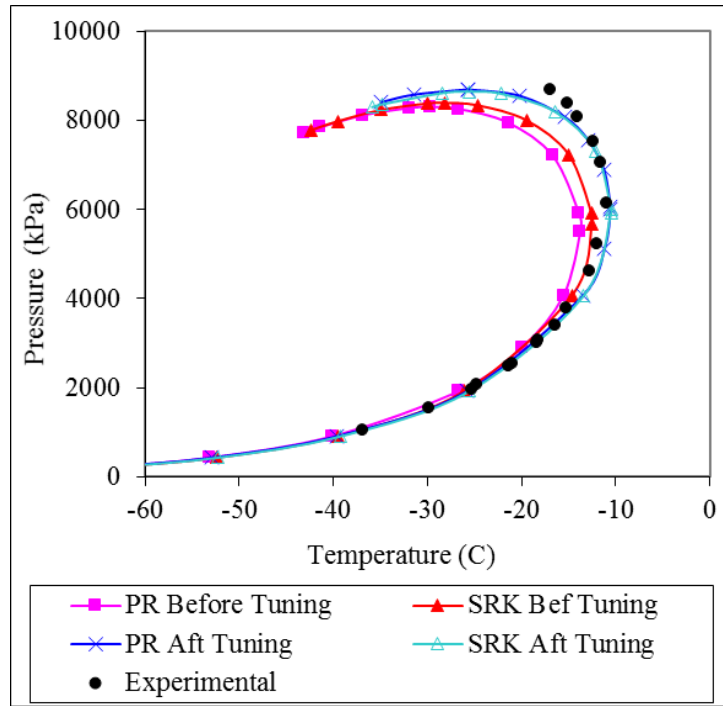


Figure 6.1: Dew point curves of PR and SRK before and after tuning together with the experimental values for samples SNG1

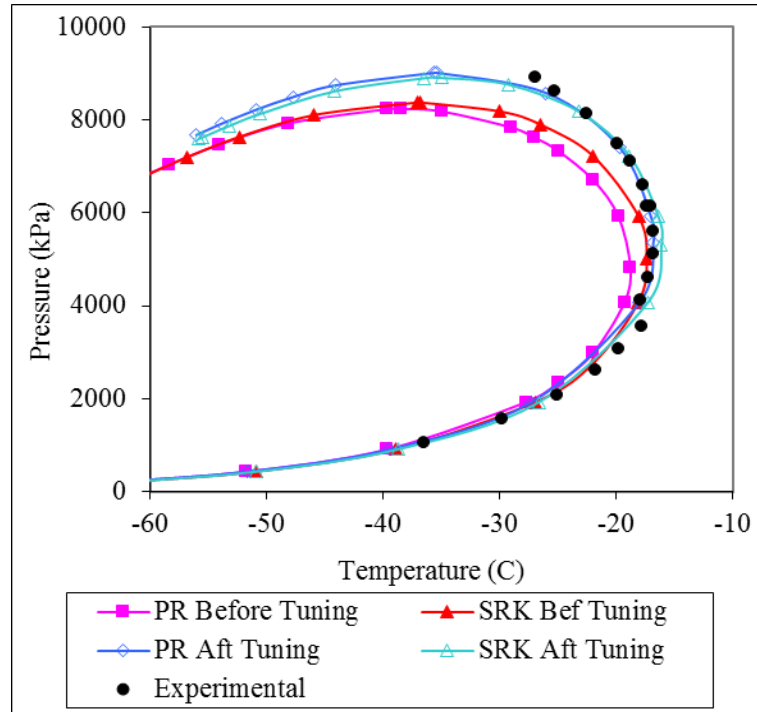


Figure 6.2: Dew point curves of PR and SRK before and after tuning together with the experimental values for samples SNG5

The absolute percentage errors of the temperature predicted at the experimental saturated pressures of PR and SRK for SNG5 are shown in Figure 6.3. For the two examples mentioned, the larger errors occur at high pressure, i.e. the area between the cricondentherm and cricondenbar points. All the samples that showed this trend did not contain a significant amount of pentane plus components. After modifying the k_{ij} parameter (k_{C1-C3}), both equations reduced the errors in their predictions and both showed a good performance for the pressures considered.

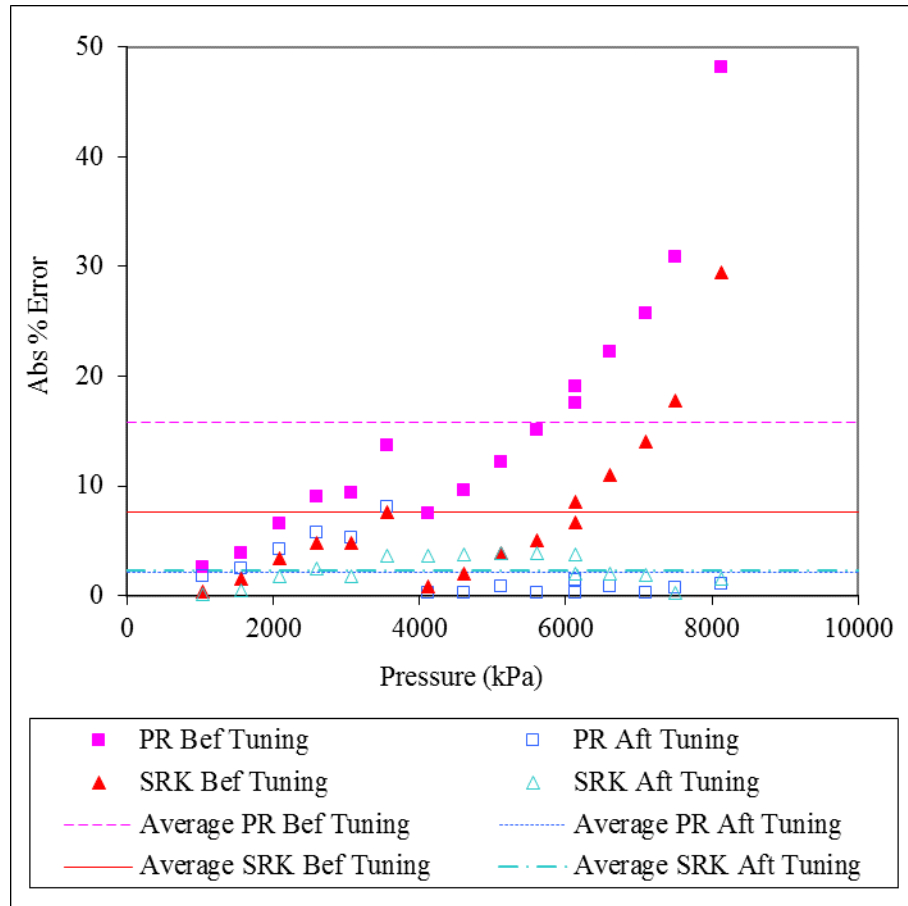


Figure 6.3: Absolute percentage errors of the temperature predicted at the experimental saturated pressure of PR and SRK for SNG5.

For those synthetic gas samples where the deviation between experimental and predicted points start at pressures below the cricondentherm point, the k_{ij} for propane and pentanes (k_{C3-ic5} or k_{C3-nC5}) improved the predictions. Since SNG4 and SNG6 did not contain propane, the k_{ij} between normal butane and iso-pentane ($k_{nC4-ic5}$) showed the best improvement in the dew point predictions. Figures 6.4 and 6.5 give the dew point curves of PR and SRK before and after tuning together with the experimental values for samples SNG4 and SNG6.

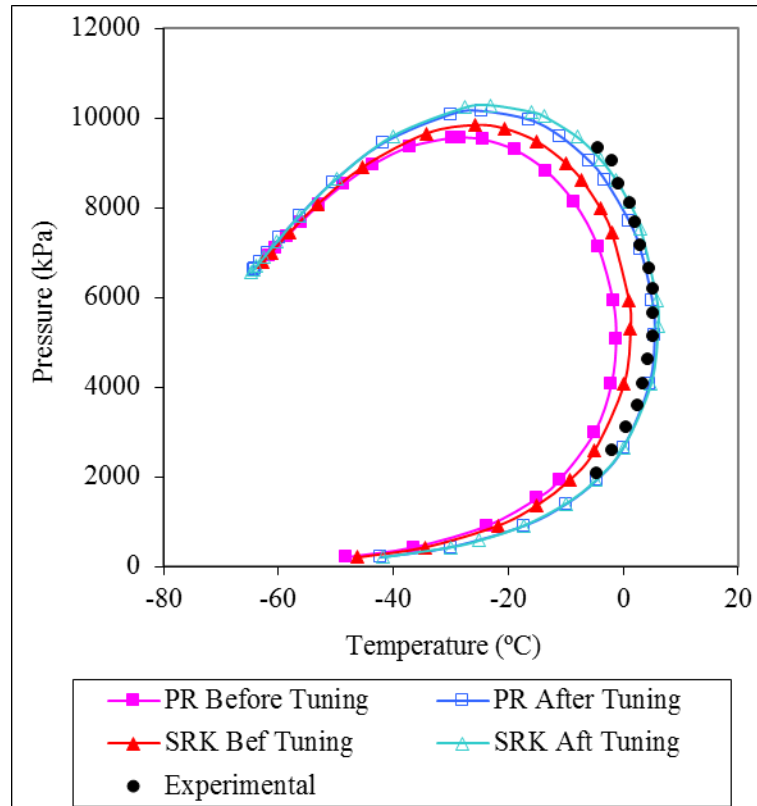


Figure 6.4: Dew point curves of PR and SRK before and after tuning together with the experimental values for samples SNG4

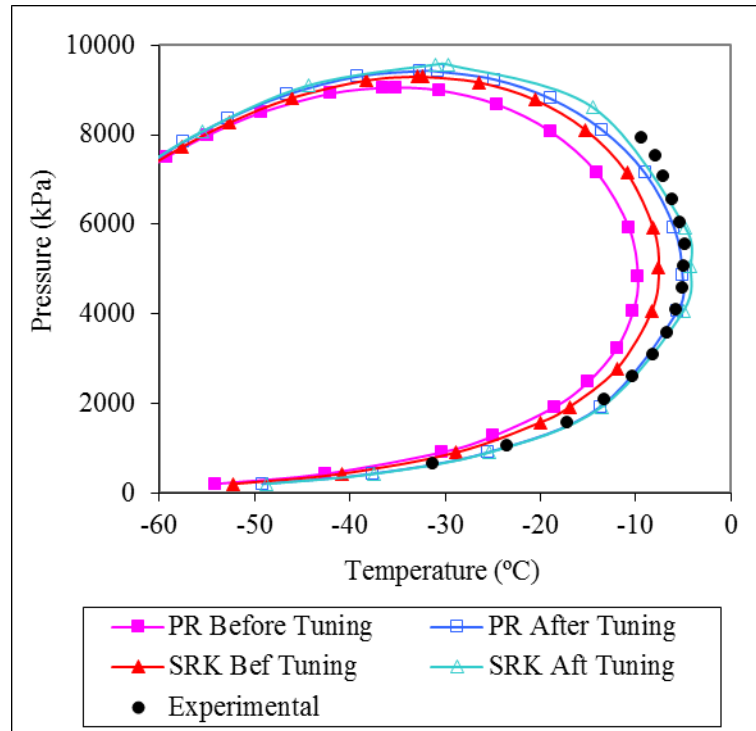


Figure 6.5: Dew point curves of PR and SRK before and after tuning together with the experimental values for samples SNG6

Figure 6.6 indicates the absolute percentage errors of the temperature predicted at the experimental saturated pressure of PR and SRK for SNG6. Another sample presenting deviations between experimental and predicted points that start at pressures below the cricondentherm point is SNG8. In the latter case, the sample only contains methane, ethane and iso-pentane, and the k_{ij} that improved the prediction was between iC_5 and C_2 . Figure 6.7 illustrates the predictions before and after tuning.

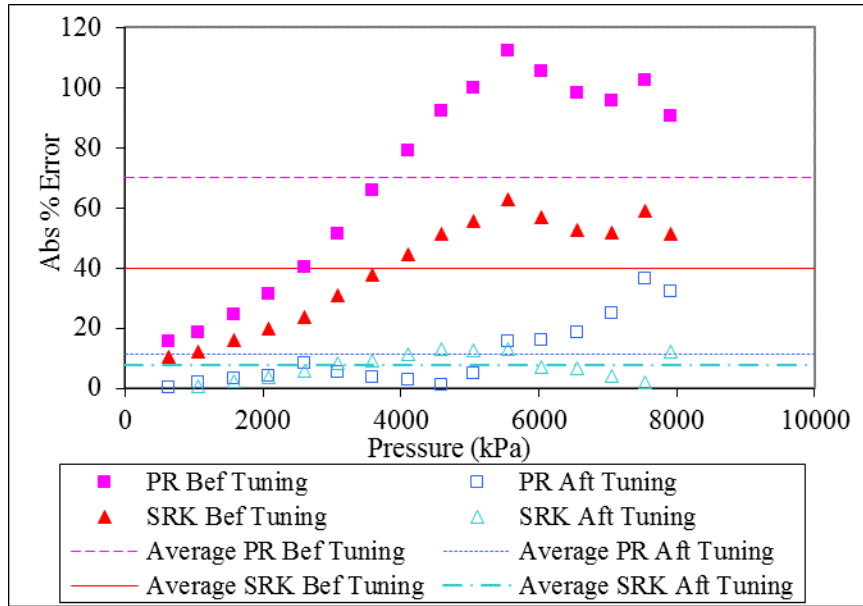


Figure 6.6: Absolute percentage errors of the temperature predicted at the experimental saturated pressure of PR and SRK for SNG6

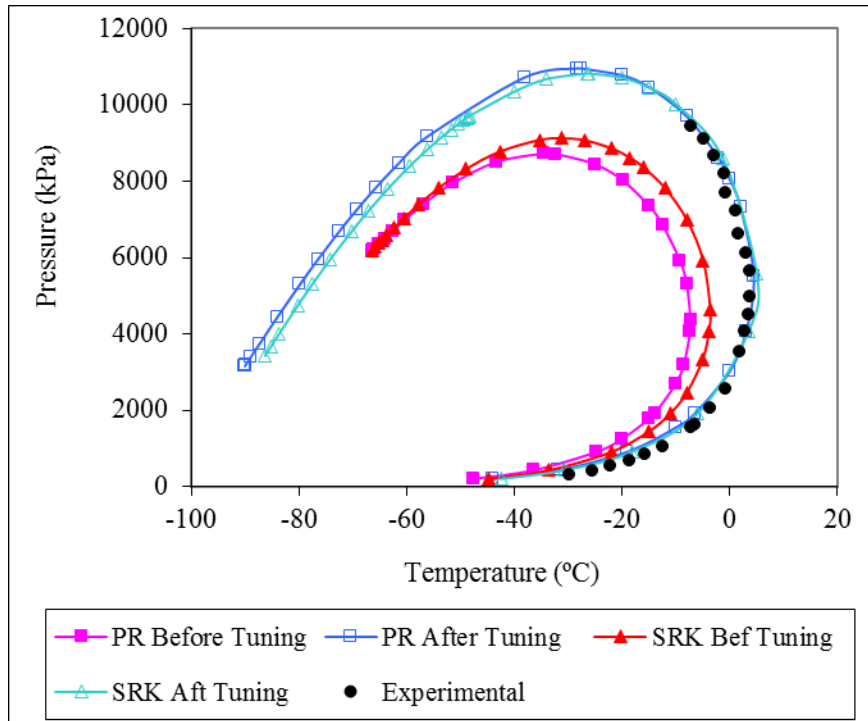


Figure 6.7: Dew point curves of PR and SRK before and after tuning together with the experimental values for samples SNG8

The k_{ij} tuned values involved in improving the predictions of the dew points for PR and SRK equations are indicated in Table 6.1, and 6.2, respectively. All the original k_{ij} for these two equations are shown in Appendix E.

Table 6.1: The k_{ij} tuned values involved in improving the predictions of the dew points for PR

k_{ij}	SNG4	SNG8	SNG6	SNG5	SNG1
C1-C3				-0.65	-0.25
C2-iC5		-0.33			
nC4-iC5	-0.11669		-0.095		

Table 6.2: The k_{ij} tuned values involved in improving the predictions of the dew points for SRK

k_{ij}	SNG4	SNG8	SNG6	SNG5	SNG1
C1-C3				-0.6	-0.2
C2-iC5		-0.288			
nC4-iC5	-0.088		-0.07		

For natural gas samples, as mentioned in Chapter 2, the characterization of the heptanes plus fraction (C_7^+) gives a better dew point prediction and also reduces the computational time during the regression analysis. NG3 was characterized and its plus fraction was divided into five pseudo components, which noticeably improved the EOS predictions.

The characterization of the C_7^+ fraction of the gas provides the main thermodynamic properties of each pseudo components, i.e. critical properties (T, P, V, and acentricity), molecular weight (MW), normal boiling point, and ideal liquid density. These properties

were then used to create hypothetical components for the process simulator (HYSYS). By default, HYSYS creates a k_{ij} for each components combination, according to their thermodynamic properties. However, using the k_{ij} generated by HYSYS leads to errors in phase behaviour predictions. A regression analysis indicated that by finding the right values for the k_{ij} between the last two pseudo hydrocarbon components and methane, nitrogen, and carbon dioxide, as well as setting the remaining k_{ij} between hydrocarbon components and pseudo hydrocarbon components to zero, the dew point predictions improved significantly. The k_{ij} generated by Hysys and the k_{ij} modified after tuning are indicated in Appendix E. The phase envelopes of the EOS before and after modifying the k_{ij} (C_1 - $C_{\text{pseudo}4}$, C_1 - $C_{\text{pseudo}5}$, N_2 - $C_{\text{pseudo}4}$, N_2 - $C_{\text{pseudo}5}$, CO_2 - $C_{\text{pseudo}4}$, CO_2 - $C_{\text{pseudo}5}$) are shown in Figure 6.8. The absolute percentage error of the EOS to predict the saturation pressures are indicated in Figure 6.9.

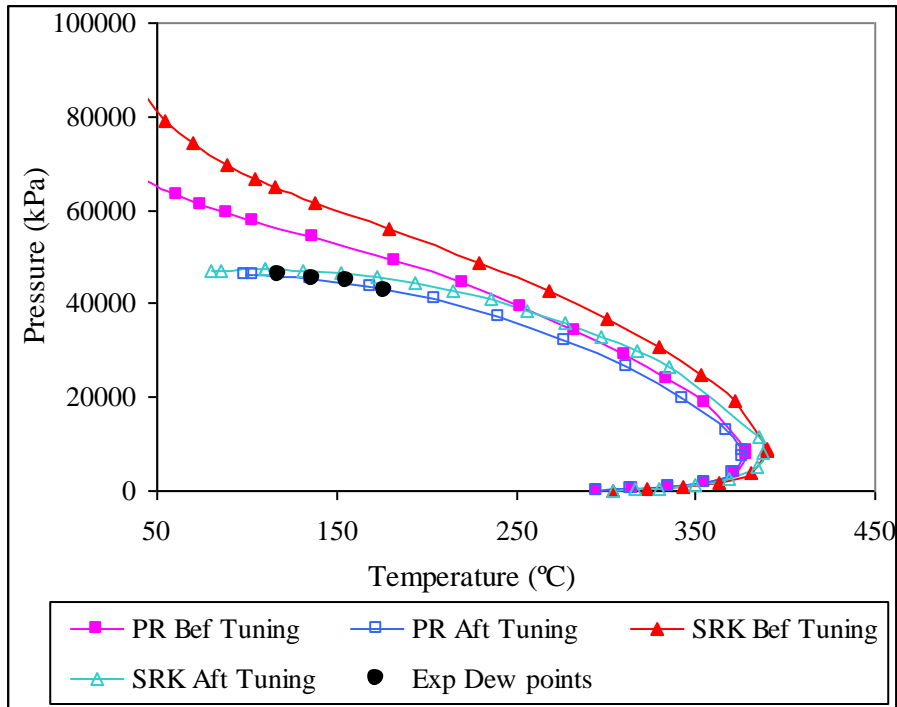


Figure 6.8: PR and SRK predicted dew point curves for NG3 before and after tuning together with the experimental values

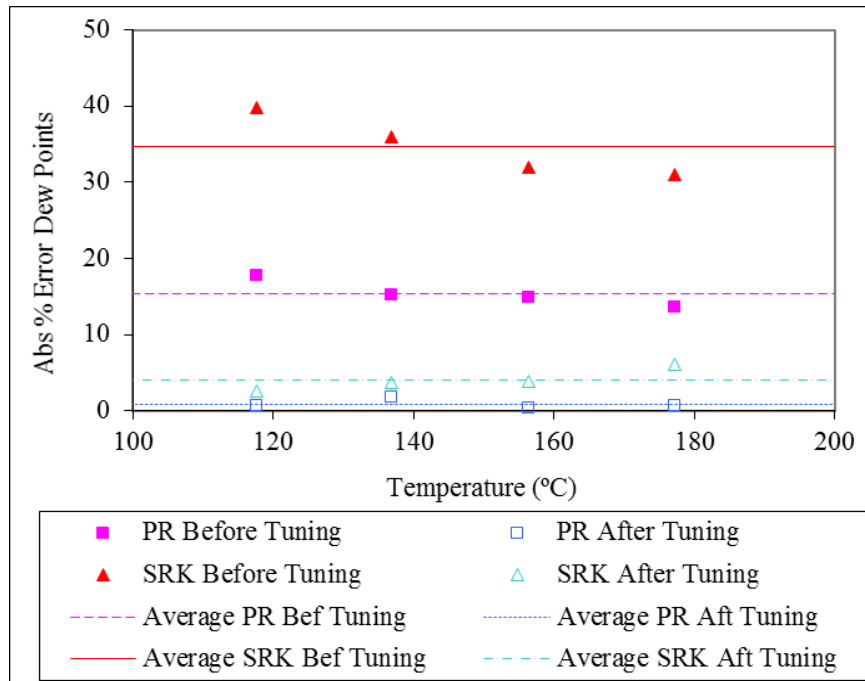


Figure 6.9: Absolute percentage errors of the temperature predicted at the experimental saturated pressure of PR and SRK for NG3.

6.2 Liquid Dropout

In order to reduce the errors of the EOS and improve their predictions, these equations were tuned. In this section, the two examples outlined in Chapter 4, Section 4.2 were used to show the impact of the tuning process on the model predictions. From the regression analysis, it was found that the parameters that required a modification to improve the liquid dropout predictions were the two constants (d_1 and d_2) used to calculate the volume translation of each component (see Equation 5.13). The dimensionless volume shift parameter is independent of the mixture and only will depend on the component involved.

After introducing the new volume translation parameters of the components (calculated using the new constant values), the predictions of the liquid dropout by the EOS were improved. The new volume translation parameters of each component are indicated in Appendix E. Figures 6.10 through 6.12 display the experimental and predicted values before and after tuning liquid dropout versus pressure at different temperatures for the synthetic gas sample (Mix 5). The predictions for both models, PR and SRK, were improved noticeably as shown in the following Figures.

In addition, the average percentage errors of the PR and SRK predictions for liquid dropout were calculated. Overall, the results indicated that PR has larger errors before and after tuning than SRK for the samples evaluated, and their values are shown in Table

6.3. As mentioned in previous chapters, SRK was designed to improve the liquid density; therefore, better performance in predicting liquid dropout is expected.

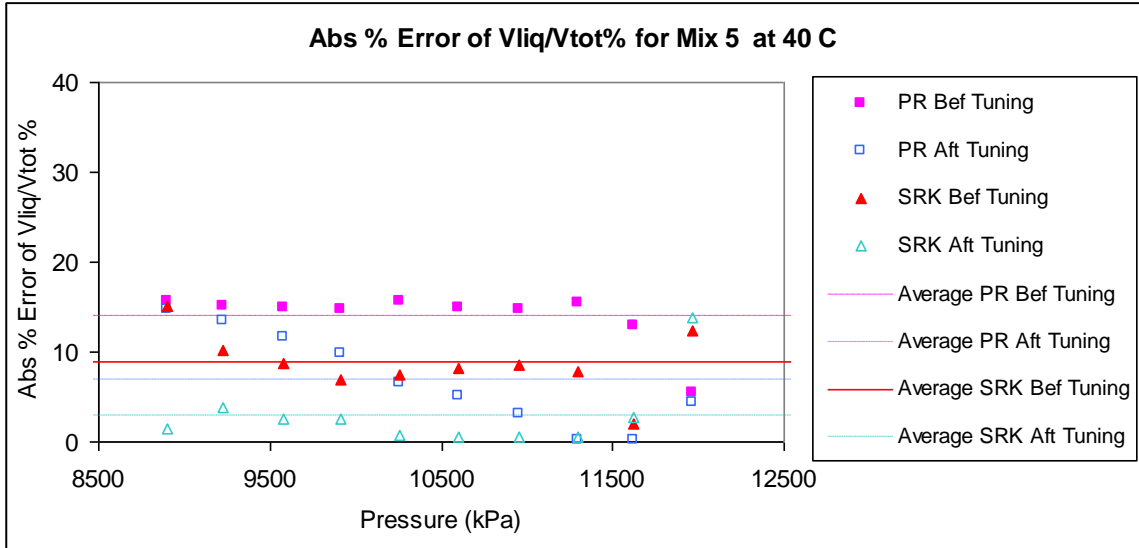


Figure 6.10: Absolute percentage of error for Liquid dropout during CCE Tests at 40 °C for Mix 5

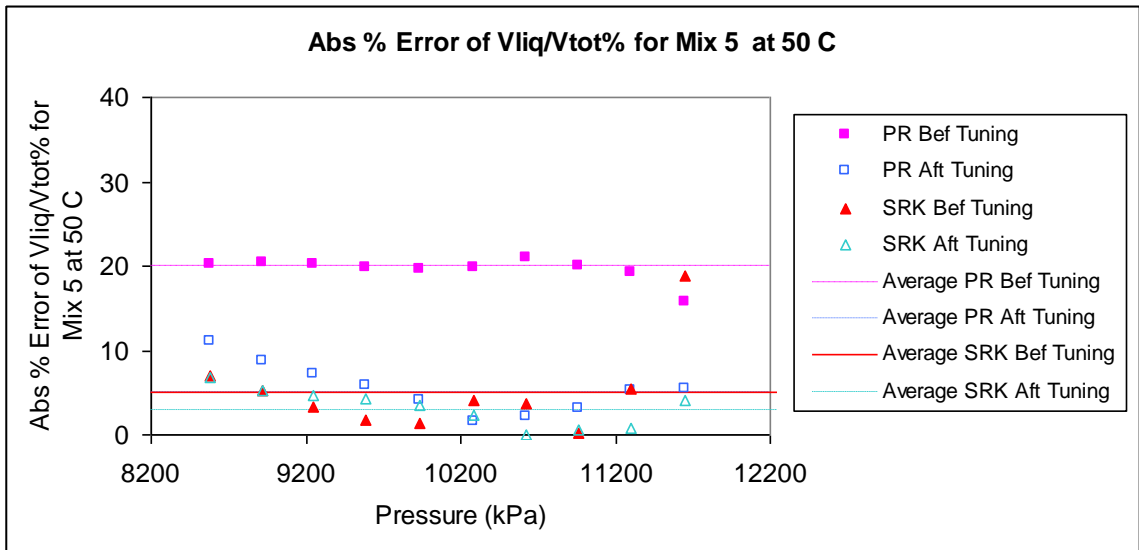


Figure 6.11: Absolute percentage of error for Liquid dropout percentage during CCE Tests at 50 °C for Mix 5

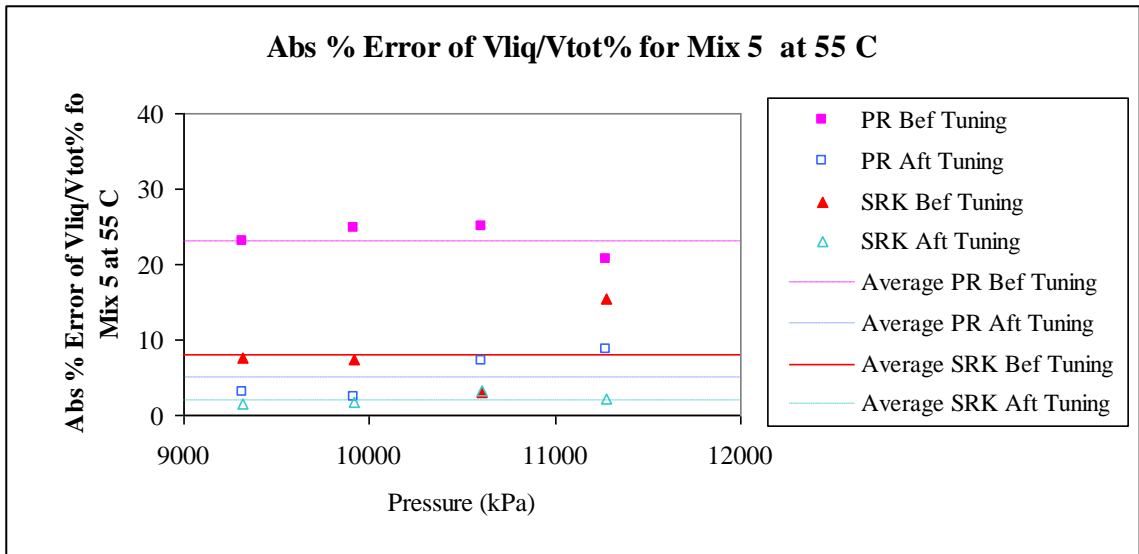


Figure 6.12: Absolute percentage of error for Liquid dropout percentage during CCE Tests at 55 °C for Mix 5

Table 6.3: Average percentage of errors for liquid dropout calculations for the PR and SRK predictions for Mix 5 during CCE Tests at diverse temperatures

Temperature of CCE Test	Average Absolute % Error in predicting Liquid Dropout			
	PR		SRK	
	Before Tuning	After Tuning	Before Tuning	After Tuning
40 °C	14	7	9	3
50 °C	20	5	5	3
55 °C	23	5	8	2
Average	19	6	7	3

In addition to the synthetic gas sample, a natural gas sample (sample NG3 see Table 4.2) was used to evaluate the accuracy of the EOS in predicting liquid dropouts. This gas sample contained a large amount of heavier hydrocarbons grouped in the heptane plus

fraction. Before performing the regression analysis, the heptane plus fraction was therefore characterized. Although the characterization improved the predictions noticeably, the EOS still showed large errors in predicting liquid dropouts. A tuning process was performed to both EOS and, as a result, the constants d_1 and d_2 were used to calculate the dimensionless volume shift parameter (V') (see Equation 5.13). After recalculating the volume translation parameters of each component, the EOS predictions matched the experimental values more closely. The volume translation parameters of each component before and after tuning the EOS are indicated in Appendix E. Figure 6.13 illustrates the experimental liquid dropout percentages before and after tuning predicted versus pressures at diverse temperatures.

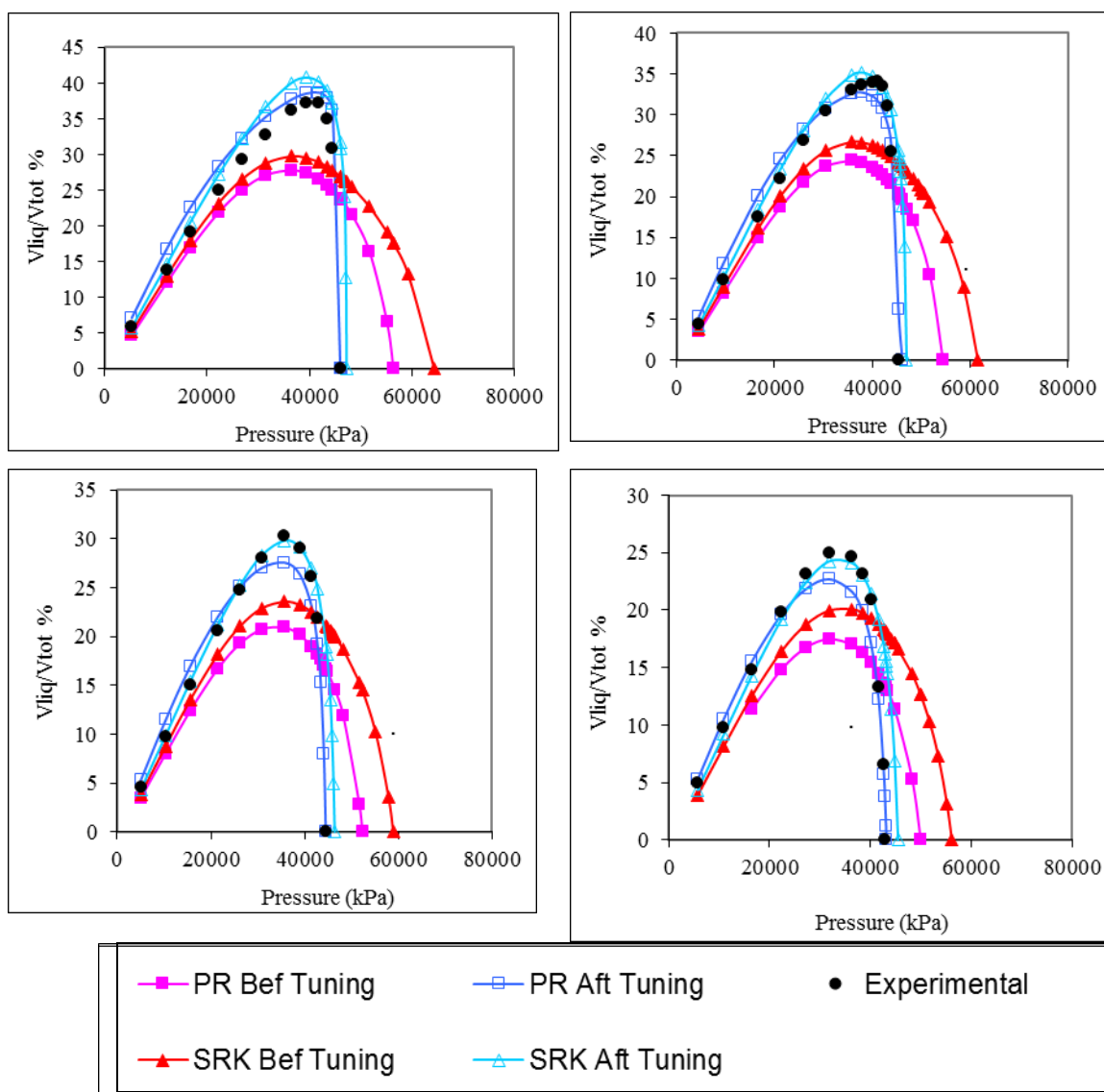


Figure 6.13: Liquid dropout percentages versus pressures during CCE Tests at different temperatures for the natural gas sample. (Left top: 117 °C, right top: 136 °C, left bottom: 156 °C, right bottom: 177 °C)

The average percentage errors of the PR and SRK are summarized in Table 6.4, which shows that the SRK had smaller errors before and after tuning than the PR. This is likely due to the large concentration of heavy hydrocarbons.

Table 6.4: Average percentage errors of PR and SRK in predicting liquid dropout for a field gas sample during CCE Tests at diverse temperatures

Temperature of CCE Test	Average % Error in predicting Liquid Dropout			
	PR		SRK	
	Before Tuning	After Tuning	Before Tuning	After Tuning
117 °C	19	12	13	10
136 °C	24	15	8	5
156 °C	23	14	10	3
177 °C	25	19	9	8
Average	23	15	10	7

6.3 EOS Parameter modified for improvement of the dew point and liquid dropout predictions

The tuning process showed that modifying the Peneloux parameters (see Chapter 5 for equations) improves the prediction of the liquid dropouts markedly, and the modification of the k_{ij} improves the dew point predictions. The k_{ij} needing to be modified depends on the gas composition, as indicated in the previous section with diverse synthetic gas samples. In the case of synthetic gas samples, the modification of just one k_{ij} was enough to obtain better predictions of the dew points. In most of the cases, the modified k_{ij} was a combination of propane and a heavier hydrocarbon component. In general, the k_{ij} were for propane and pentanes (C₃-C₅), propane and normal hexane (C₃-nC₆), or propane and n-octane (C₃-nC₈). For instance, diverse CVD and CCE tests data of Mix 5 were tuned and as a result several combinations of new k_{ij} values (for C₃-nC₅, C₃-nC₆, and C₃-nC₈) were obtained. Tables 6.5 and 6.6 list the various combinations for the diverse tuning

tests of the tuned k_{ij} values for PR and SRK respectively, and also list the average value for each k_{ij} . As mentioned before, it cannot be assumed that these average values are the final k_{ij} values for these hydrocarbon combinations. These values were obtained using the samples evaluated in this thesis, and in order to obtain general k_{ij} value for the three combinations mentioned, more experimental data and tuning is required.

Table 6.5: Diverse combination of new k_{ij} values for C₃-nC₅, C₃-nC₆, and C₃-nC₈ when PR was tuned

new k_{ij}	Test 1	Test 2	Test 3	Average
C ₃ -nC ₅	0.16724	0.14801	0.14268	0.15265
C ₃ -nC ₆	0.04540	0.15435	0.08597	0.09524
C ₃ -nC ₈		0.03714	0.02066	0.02890

Table 6.6: Diverse combination of new k_{ij} values for C₃-nC₅, C₃-iC₅ when SRK was tuned

new k_{ij}	Test 1	Test 2	Average
C ₃ -iC ₅	0.47501	0.48699	0.48100
C ₃ -nC ₅	0.14273		

By contrast, natural gas samples required more than one k_{ij} to be modified in order to improve the prediction of the dew points. The k_{ij} 's that required modification were the k_{ij} 's of the two heaviest pseudo components with methane, nitrogen, and carbon dioxide. The rest of the k_{ij} for these two pseudo components were set to zero.

Once the correct k_{ij} and Peneloux parameters were found for a specific composition, they were updated into the PR and SRK parameters. The equation with the new parameter values (k_{ij} and volume translation parameters of each component) was then used to calculate diverse thermodynamic properties, such as liquid dropout, dew points, and/or density, at different conditions of temperature and pressure.

6.4 Density

As shown in Section 4.3, the standard EOSs have large errors for gas density predictions in the two-phase region. The EOS errors in predicting gas density for a moderately rich gas were between 10 and 15%, and for a rich gas between 8 and 30%, depending on pressure and temperature. Since the errors of the EOS in predicting gas density were, in general, larger than 10%, a regression analysis was performed to improve predictions. The modified parameters were the same as those targeted for improving liquid dropout predictions (Peneloux parameters). The predictions before and after modifying the Peneloux parameters and the k_{ij} are shown in Figures 6.14 to 6.16, for Mix 4 and Mix 5. The values of k_{ij} and Peneloux parameters employed to improve the liquid dropout and dew point predictions are the same ones that were used to improve the density predictions.

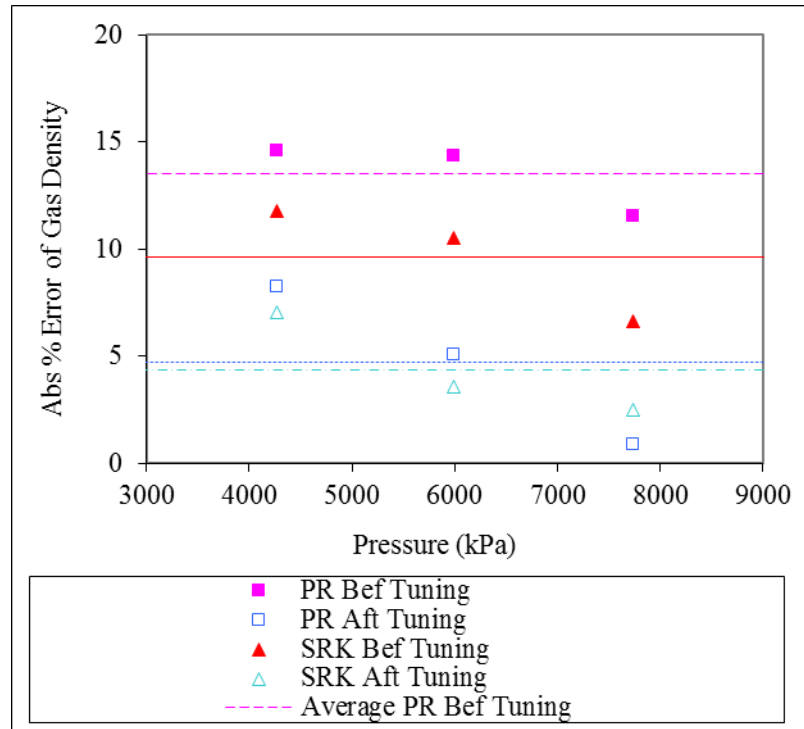


Figure 6.14: Absolute percentage errors of gas density predictions of PR and SRK for Mix 4 during CVD test at 0 °C

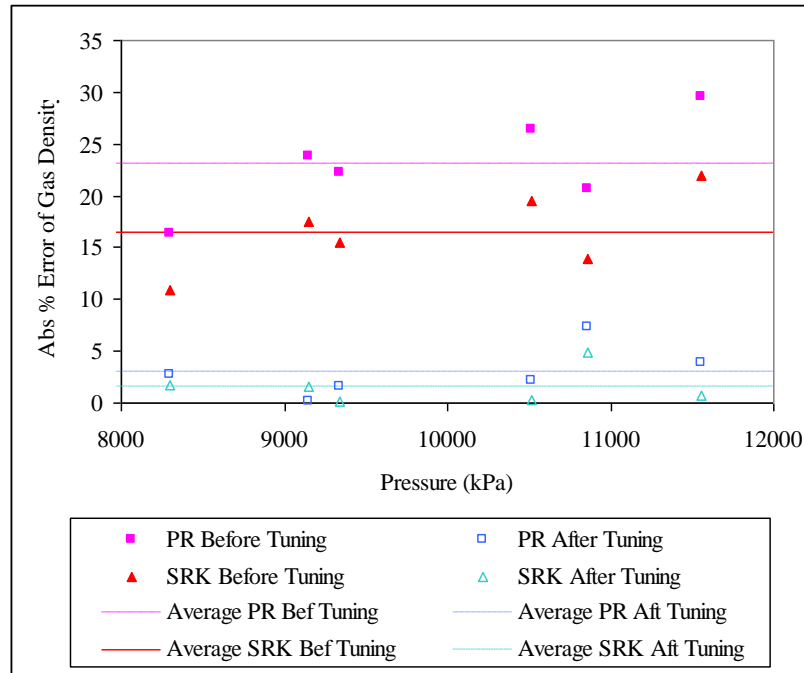


Figure 6.15: Absolute percentage errors of gas density predictions of PR and SRK for Mix 5 during CVD test at 40 °C

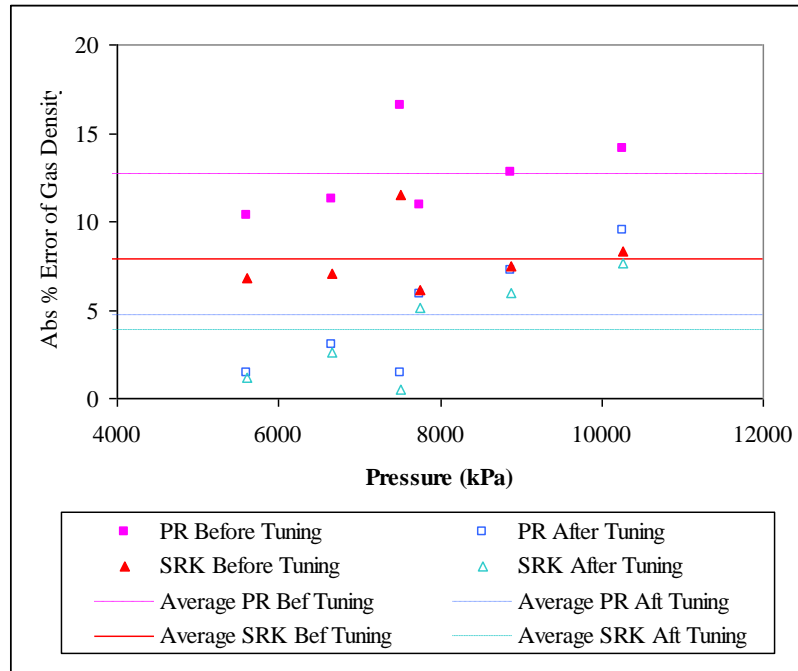


Figure 6.16: Absolute percentage errors of gas density predictions of PR and SRK for Mix 5 during CVD test at 60 °C

6.5 Compressibility

Experimental gas compressibility data in the supercritical region for natural gas sample NG3 (see Table 4.2) was used to evaluate the performance of PR and SRK in predicting compressibility. The experimental compressibility was measured between 44 and 61 MPa and at 137, 146 and 177 °C. These experimental data were then compared with the predictions of the PR and SRK equations. Since the errors in the predictions were around 10%, a regression analysis was conducted to improve the performance of the models.

Gas compressibility and gas density are related (as indicated by Equation 4.1). Therefore the same parameters (i.e. such the Peneloux parameters) were tuned for both properties. The PR and SRK predictions of compressibility before and after modifying the Peneloux parameters inside the models were calculated and then compared with the experimental data. The absolute percentage errors of the predictions with respect to the experimental data were also determined, and are illustrated in Figures 6.17 and 6.18 for PR and SRK, respectively.

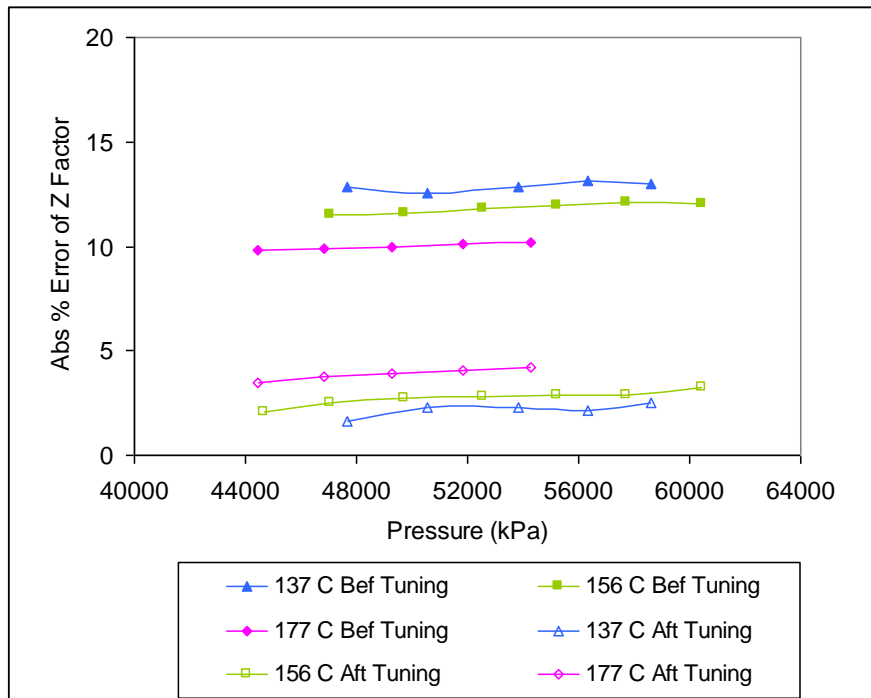


Figure 6.17: Absolute percentage errors of compressibility predictions of PR for NG3

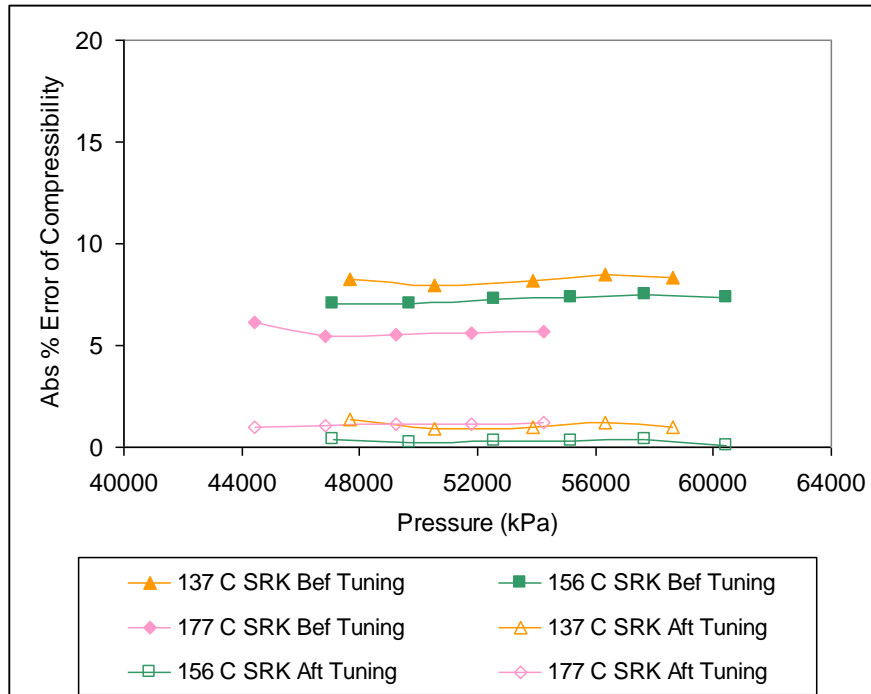


Figure 6.18: Absolute percentage errors of compressibility predictions of SRK for NG3

The average percentage errors for PR and SRK in predicting compressibility before and after modifying certain parameters are illustrated in Table 6.7.

Table 6.7: Absolute percentage errors of PR and SRK in predicting compressibility

Abs % errors in predicting compressibility				
	PR		SRK	
Temperature (°C)	Before Tuning	After Tuning	Before Tuning	After Tuning
136.95	12.9	2.2	8.2	1.1
156.35	11.8	2.8	7.3	0.3
177.15	10.0	3.9	5.6	1.1
	11.6	3.0	7.0	0.8

6.6 Conclusion

In this chapter it was shown that by modifying just a few EOS parameters, a remarkable improvement in the EOS predictions was achieved. While this study showed that there is not a general parameter that can be targeted for all cases, the following observations were made. In the case of synthetic gas samples, modifying one k_{ij} parameter improved the dew point predictions. In the case of natural gas samples, the modification of the k_{ij} among the heaviest pseudo hydrocarbon components and methane and the non-hydrocarbon components (such as N_2 and CO_2) resulted in improvement in predictions. Nevertheless, a good characterization of the plus fraction before the tuning process is recommended to save time in finding the right combination of parameters for improvements. In addition, the density predictions can be improved by modifying the Peneloux parameters. In order to improve the liquid dropout predictions, k_{ij} and Peneloux parameters needed to be changed together. It is important to stress that the Peneloux parameters do not interfere with the dew point predictions and their modification will not affect them. A set of k_{ij} and Peneloux parameters were found for each composition and these values were used to improve the predictions of the thermodynamic properties, independent of pressure or temperature.

CHAPTER 7

DYNAMIC SIMULATION OF LOADING AND UNLOADING CNG TANKS

The previous chapters addressed the errors of EOSs predictions for thermodynamic properties, such as liquid dropouts. In Chapter 6 methods were presented to improve the predictions of the EOS. This chapter will evaluate the possibility of transporting rich gases with minimum treatment offshore by using CNG technology and address the importance of model accuracy in predicting liquid dropouts in simulating the loading and unloading of CNG tanks. The accuracy of model predictions will be particularly critical in cases where rich gases are encountered. Hence, the effect of a liquid content on the loading and unloading operations of a CNG tank will be examined. Because the loading and unloading processes differ for different CNG technologies, a general evaluation of loading and unloading operations will be provided. The methodology presented in this chapter is based on the modelling of loading and unloading processes for several gas sample, and the technique presented will provide general recommendations for the design of loading and unloading systems and operations.

7.1 Methods to Adjust Gas Composition

The feed composition could be adjusted using diverse methods including flashing, turbine expansion, adsorption, refrigeration, and membranes. The type of technology selected for offshore remote locations is limited to the space on the platform, chemical and operating requirements, and possible environmental considerations. Each method has main advantages and disadvantages when located in remote locations (Beronich et al. b, 2006). Marine CNG technology is looked as an alternative for remote locations and stranded reservoir so the minimum treatment required is a plus. The focus of the thesis is to evaluate how to the composition of the gas affect the loading and unloading operations, so a simple flashing method was selected to adjust the composition and not further evaluation was made about which method employ for this purpose.

7.2 Dynamic Simulations of Loading and Unloading a CNG Tank

In order to evaluate how diverse parameters (such as gas composition, feed stream conditions, and loading arrangement) affect the loading and unloading operations of a CNG tank, a process simulator, Hysys, was employed to perform dynamic simulations. The dynamic simulation of the loading and unloading of a CNG tank involves a pressure valve to control the molar flows as well as a CNG tank.

7.2.1 Principal assumption to perform the dynamic simulations

The principal assumptions for performing the dynamic simulations were that:

- The molar flow of the feed stream in the loading operation was controlled to keep it constant.
- The molar flow of the output stream in the unloading operations was controlled to keep it constant.
- The conditioning of the gas to be loaded, such as; making its composition adequate (by removing the heavy hydrocarbons when necessary), compressing the gas to the loading pressure, and making the gas temperature to desired value, were not included in the dynamic simulations.
- The conditions of temperature, pressure, molar flow rate, and composition of each feed stream remained constant during the loading operation.
- There was no H₂S or CO₂ removal.
- The conservation equations accounted for changes occurring over time (by including an accumulation term that differentiated with respect to time).
- Lumped models were used for all the unit operations. This meant that all the physical properties were assumed to be equal in space.
- A holdup model was used to predict the how the holdup and the output streams of an equipment reacted to input changes to the holdup over time;
 - The holdup model is used to calculate the material and energy accumulation, the thermodynamic equilibrium and the heat transfer.
 - A separator is considered as a single holdup, and the valves is considered that has a negligible holdup.

- The pressure and flow profiles were calculated using volume balance equations, resistance equations, and pressure-flow specifications given as input data.
- The system was not adiabatic and not isothermal

7.2.2 Conservation Relationships

The mass balance equation has an accumulation term, which is the only term that varies with time. The general mass balance equation is indicated in Equation 7.1.

$$\text{Rate of accumulation of mass} = \text{mass flow rate into system} - \text{mass flow rate out of system} \quad (7.1)$$

The mass balance equation for a tank is indicated in Equation 7.2.

$$\frac{d(\rho_V V_V + \rho_L V_L)}{dt} = F_{inV} \rho_{inV} + F_{inL} \rho_{inL} - (F_{oV} \rho_V + F_{oL} \rho_L) \quad (7.2)$$

In this equation, F_{inV} is the vapour molar flow rate of the feed entering the tank, F_{inL} is the liquid molar flow rate of the feed entering the tank, ρ_{iV} is the density of the vapor feed entering the tank, ρ_{iL} is the density of the liquid feed entering the tank, F_{oV} is the vapour molar flow rate of the stream exiting the tank, F_{oL} is the vapour molar flow rate of the stream exiting the tank, ρ_V is the vapour density of the stream exiting the tank, ρ_L is

the liquid density of the stream exiting the tank, V_V is the volume of the vapor phase in the tank, and V_L is the volume of the liquid phase in the tank.

The component balances are described as shown in Equation 7.3:

$$\begin{aligned} & \text{Rate of accumulation of component } j \text{ in vapor phase} + \text{Rate of accumulation of} \\ & \text{component } j \text{ in liquid phase} = \text{Flow of component } j \text{ into system} - \text{Flow } j \text{ out of system} \end{aligned} \quad (7.3)$$

For a multi component feed with a perfectly mixed tank, the balance for the component j is indicated in Equation 7.4:

$$\frac{d(C_{jV}V_V + C_{jL}V_L)}{dt} = F_{inV}C_{jinV} + F_{inL}C_{jinL} - (F_{oV}C_{jV} + F_{oL}C_{jL}) \quad (7.4)$$

In equation 7.4, C_{jinV} is the concentration of j in the inlet vapour stream, C_{jinL} is the concentration of j in the inlet liquid stream, C_{jV} is the concentration of j in the vapor outlet stream, and C_{jL} is the concentration of j in the liquid outlet stream.

For a system with N_c components, there will be a total mass balance equation and a $N_c - 1$ component balance equation.

The energy balance equation is defined as expressed in Equation 7.5.

Rate of accumulation of total energy = Flow of total energy into system – Flow of total energy out of system + Heat added to system across its boundary + Heat generated by reaction – work done by system on surroundings (7.5)

The assumptions made for the energy balance equation 7.5 are:

- The potency energy can be ignored
- The inlet and outlet velocity are not high, therefore kinetic energy term are negligible
- There is no shaft work (no pump), therefore work is equal to zero.

The general energy balance for a two phase system for a large tank is shown in Equation 7.6.

$$\frac{d}{dt} [\rho_V V_V H + \rho_L V_L h] = F_{inV} \rho_{inV} H_{inV} + F_{inL} \rho_{inL} h_{inL} - (F_{oV} \rho_V H + F_{oL} \rho_L h) + Q_L \quad (7.6)$$

In equation 7.6, Q_L is the heat loss across the wall. If this equation is employed for a small tank a thermal mass term should be added since its effect is significant.

The heat loss was calculated using a simple model, which is described in Equation 7.7.

$$Q_L = UA(T_f - T_{amb}) \quad (7.7)$$

In this equation, U is the overall heat transfer coefficient, A is the overall heat transfer area, and T_f and T_{amb} are fluid and ambient temperatures, respectively.

7.3 Dynamic Simulation Conditions

Dynamic simulations of the loading and unloading of a CNG tank were performed using the process simulator Hysys. For the purpose of this study, the most recent version was required (version 7.2). The latest version includes a new parameter called the Dense Phase Tuning (DPT) parameter, in which value can be set between 0.5 and 2. By modifying this parameter in the "Phase Order" tab at the Fluid Package property view (Basis Environment) in Hysys, the predicted liquid and vapour phase boundaries in the supercritical region can be switched. The old problem of erroneously predicting liquid instead of gas in this region is consequently avoided.

The conditions chosen to perform the loading and unloading operation of a CNG tank with gas is affected by numerous factors, including gas composition, tank size, initial temperatures and pressures, flow rates, and final pressure of the tank. The following sections will evaluate the effect of gas composition, initial gas temperature, and molar flow rates on the loading and unloading operations.

Diverse gas compositions were used for dynamic simulation of the loading and unloading operations of a CNG tank. The compositions ranged from a moderately rich gas to a rich gas, and they are listed in Table 7.1.

Table 7.1: Compositions of the gas samples

Component	Natural Gas 1 (NG1)	Natural Gas 2 (NG2)	Synthetic Gas 1 (SNG1)	Synthetic Gas 2 (SNG2)	Synthetic Gas 3 (SNG3)
N₂	3.91	5.05	0.39		---
CO₂	0.75	0.75	1.11		---
C₁	70.20	82.35	83.69	79.57	65.71
C₂	9.22	8.75	7.60	9.77	10.96
C₃	2.76	2.00	4.75	7.77	12.59
iC₄	0.66	0.36	0.23	1.00	2.37
nC₄	0.98	0.45	1.45	1.09	3.09
iC₅	0.40	0.11	0.32	0.40	1.86
nC₅	0.42	0.09	0.33	0.28	1.55
nC₆		---	0.04	0.10	1.05
MCycloC₅	---	---	---	---	0.02
nC₇	---	---	0.05	0.01	0.4
nC₈	---	---	0.06	0.01	0.4
C₆	0.82	0.07	---	---	---
C_{7-C₉}	1.41	0.02	---	---	---
C_{10-C₁₃}	1.82	---	---	---	---
C_{14-C₁₈}	0.95	---	---	---	---
C_{19-C₂₆}	0.73	---	---	---	---
C_{27-C₈₀}	4.97	---	---	---	---
C₃⁺	15.9	3.10	7.22	10.66	23.33
C₅⁺	11.5	0.18	0.79	0.80	5.28
C₇⁺	9.88	0.02	0.10	0.02	0.80

In the dynamic simulations presented in this chapter, tuned EOS were employed rather than the original EOS. As illustrated in previous chapters, the original EOS present inaccuracies in predicting the dew points, especially when high concentration of heavy hydrocarbons are present in the gas. In case of moderate rich or lean gas, the performances of the tuned and original EOSs do not differ noticeably since the heavy hydrocarbons content is significant.

Figure 7.1 illustrates the PR and SRK predicted dew point curves of three gas samples; NG2, SNG1, and SNG2, used in the dynamic simulations in this chapter. The similarity between the dew point curves of PR and SRK equation is because they were generated with the tuned EOS. Using the original EOS would create larger difference in the predictions between the equations, when high content of heavy hydrocarbons are present in the gas samples.

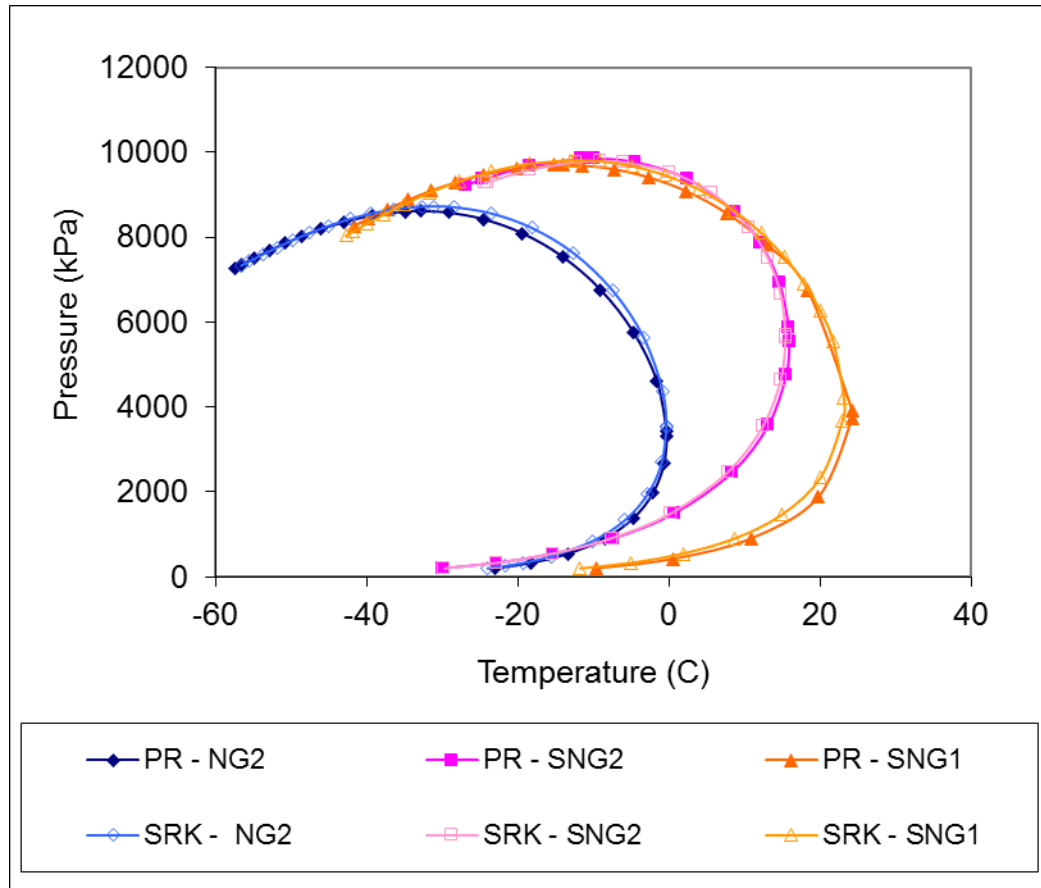


Figure 7.1: Dew point curves of the original gas samples before flashing employed for the study of the dynamic loading and unloading of a CNG tank.

7.4 Simulations of Loading Operation of a CNG Tank

The objective in this section is to evaluate the implications of loading gases with diverse liquid content into a CNG tank, and provide recommendations for proper loading conditions, while taking into account the liquid content of the gas. Dynamic simulations of the loading of a CNG tank (under diverse conditions) were performed and the accumulation of liquids during these operations were analysed. The reason for evaluating the accumulation of liquids inside the tank is due to the possibility of facing remaining liquid inside the tank after unloading it. The loading time was chosen as the parameter of comparison among all cases evaluated.

During the dynamic simulations of the loading of a CNG tank, the impact of several process parameters such as the temperature of the feed stream (feed temperature), the pressure of the feed stream (feed pressure), gas compositions, and molar flow rates, on loading CNG tanks, were evaluated. When a specific parameter was under evaluation, other parameters not under evaluation were fixed, allowing for a more accurate comparison of the effects. Evaluating these diverse parameters makes it possible to identify which conditions are more appropriate for each case. Although this specific analysis does not include the capital and operational costs, they should be considered for a complete evaluation. While certain cases have a shorter loading time, they may also require additional equipment, which produces a higher cost. The effect of process parameters will be further discussed in greater detail in the following sections.

7.4.1 Feed Pressure for the loading of a CNG tank

This section studies three alternatives for loading the tank using different feed pressure arrangements, named 1P, 2P, and 3P. In the first alternative, 1P, the tank was fed at a constant high pressure (26,207 kPa). In the second alternative, 2P, the tank was fed in series with two feed streams, which vary in their pressures. The first feed stream had a low pressure (6,900 kPa), and it was used to feed the tank until the pressure inside approximated its pressure. The feed was then switched to the second feed stream, with a higher pressure (26,207 kPa). The two pressure steps were chosen to feed the tank in order to reduce the Joule-Thomson effect, so less liquid condenses inside the tank. In the third alternative, 3P, the tank was fed with three feed streams in series, and they differed in their pressures. The tank was fed until the pressure inside approached the actual feed pressure. The first stream had a low pressure (6,900 kPa or 1,000 psia), the second stream a medium pressure (15,172 kPa or 2,200 psia), and the third a high pressure (26,207 kPa or 3,800 psia). By comparing different feed pressures, it was possible to determine if time could be saved by alternating the feed pressure during the loading. Figures 7.2 to 7.4 illustrate via a flow diagram these alternatives, and tables 7.2, 7.3, and 7.4 indicate the conditions of the feed stream for each of the three arrangement.

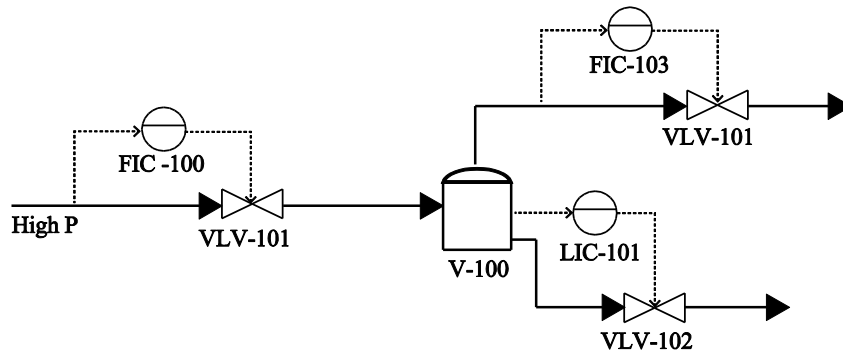


Figure 7.2: Flow diagram of loading a CNG tank with one feed stream a constant high pressure (arrangement named 1P)

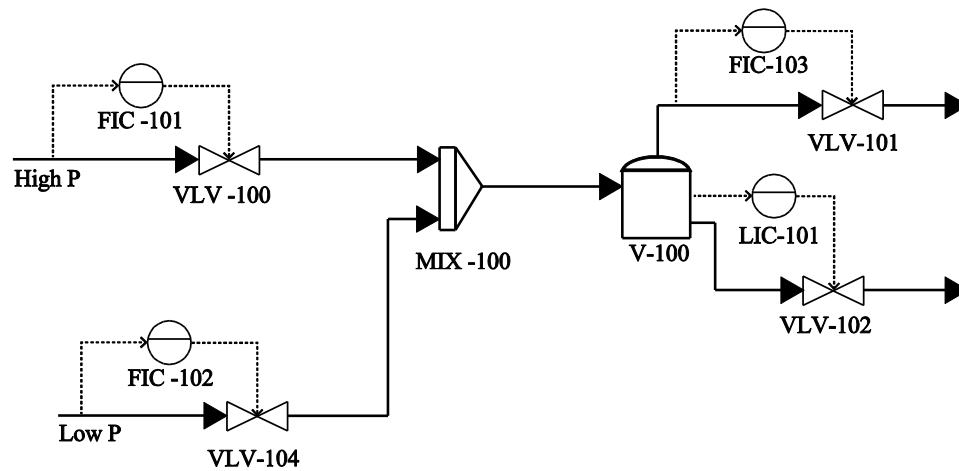


Figure 7.3: Flow diagram of loading a CNG tank with two feed streams in series, one with a low pressure and the other one with a high pressure (arrangement named 2P)

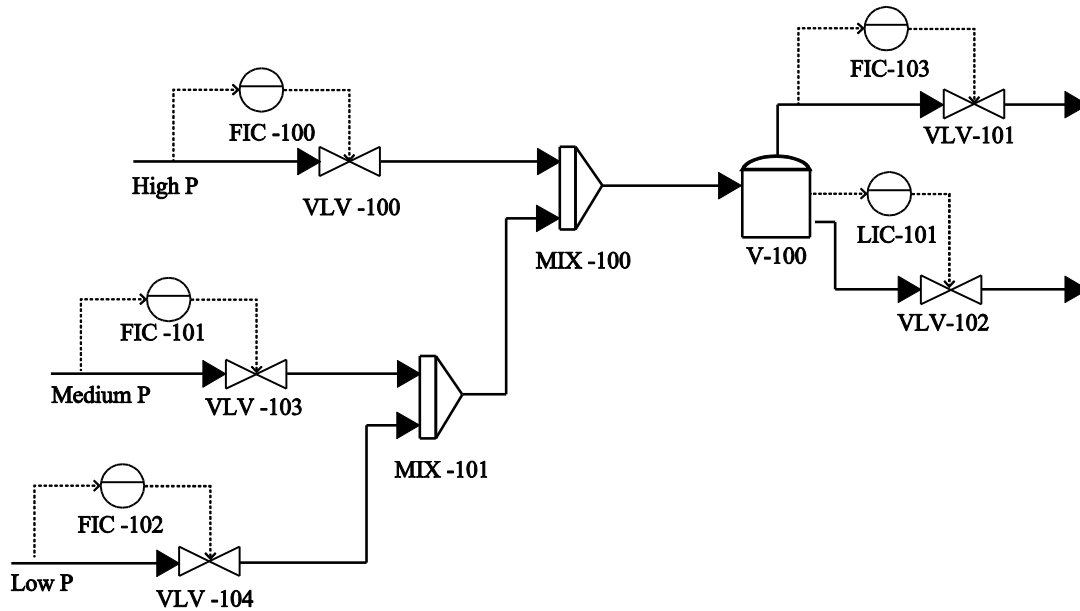


Figure 7.4: Flow diagram of loading a CNG tank with three feed streams in series, one with a low pressure, the second one with a medium pressure and the last one with a high pressure (arrangement named 3P)

Table 7.2: Conditions of the feed stream for simulating (dynamically) the loading of a CNG tank using 1P arrangement to evaluate the feed pressure arrangement.

Feed stream conditions for loading	
Tank Volume (m ³)	11.8
Loading Arrangement	1P
Temperature (°C)	20
Pressure (kPa)	26,207
Molar Flow (kmol/hr)	5
Name of Gas Loaded	SNG1

Table 7.3: Conditions of the feed stream for simulating (dynamically) the loading of a CNG tank using 2P arrangement to evaluate the feed pressure arrangement.

Feed stream conditions for loading	
Tank Volume (m ³)	11.8
Loading Arrangement	2P
Temperature (°C)	20
Pressure (kPa)	6,900 first pressure 26,207 second pressure
Molar Flow (kmol/hr)	5
Name of Gas Loaded	SNG1

Table 7.4: Conditions of the feed stream for simulating (dynamically) the loading of a CNG tank using 3P arrangement to evaluate the feed pressure arrangement.

Feed stream conditions for loading	
Tank Volume (m ³)	11.8
Loading Arrangement	3P
Temperature (°C)	20
Pressure (kPa)	6,900 first pressure 15,172 second pressure 26,207 third pressure
Molar Flow (kmol/hr)	5
Name of Gas Loaded	SNG1

Figure 7.5 and Figure 7.6 illustrate the different pressures and temperature profiles while loading a CNG tank with Synthetic Gas sample 1 (SNG1) at a feed temperature of 20 °C for three alternatives selected. Loading the tank using three feed pressures (3P) in series saves one hour in loading time compared to using one feed pressure (1P). The longer loading time for the 1P alternative is directly related to larger amount of liquid accumulated inside the tank. The amount of liquid accumulated depends on the temperature inside the tank. The gas loaded using 1P alternative reaches the lowest

temperature, and a lower temperature means a larger accumulation of liquids. Figure 7.7 illustrates the liquid dropout profiles of the three feed pressures alternatives. This figure suggests that adding an extra feed pressure step does not significantly improve the loading time, so 2P alternative would be the more convenient option since compression cost will be lower.

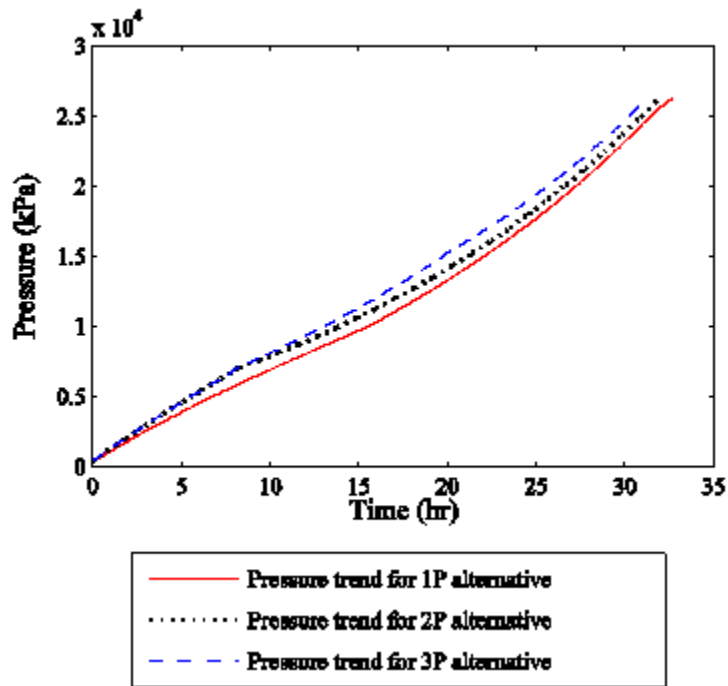


Figure 7.5: Pressure trends of the SNG1 inside a CNG tank during the loading operation with a Feed Stream Temperature of 20 °C using diverse loading alternatives (1P, 2P, 3P)

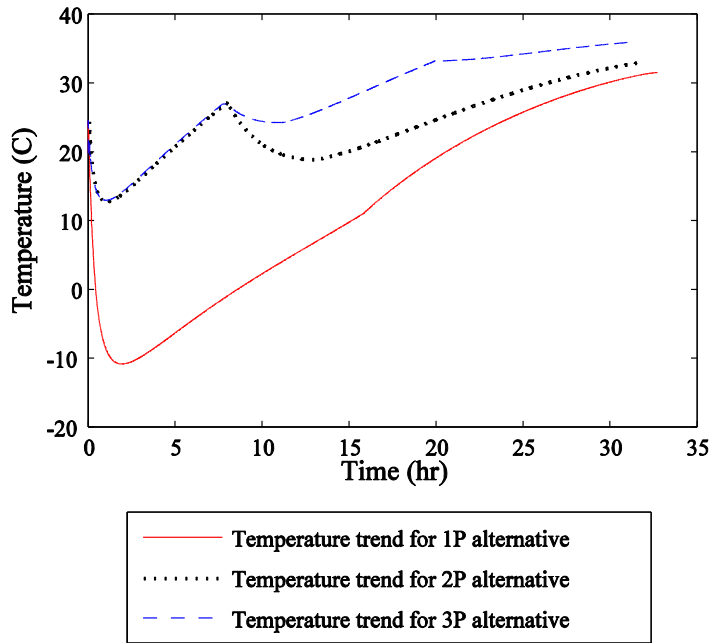


Figure 7.6: Temperatures trends of the SNG1 inside a CNG tank during the loading operation with a Feed Stream Temperature of 20 °C using diverse loading alternatives (1P, 2P, 3P)

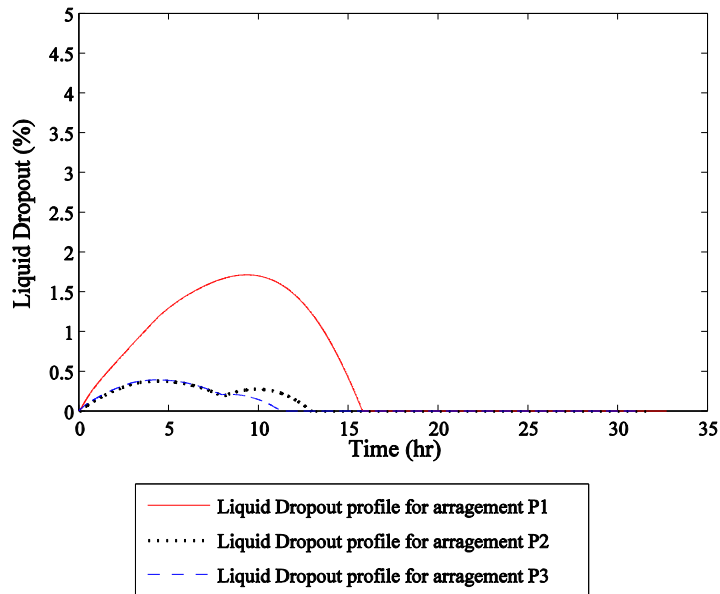


Figure 7.7: Liquid Dropout trends of the SNG1 inside a CNG tank during the loading operation with a Feed Stream Temperature of 20 °C using diverse loading alternatives (1P, 2P, 3P)

7.4.2 Feed Temperature

Two different temperatures for the feed stream (feed temperatures) were selected to illustrate its impact on loading a CNG tank with a moderately rich gas (SNG1) using 1P arrangement. The selected temperatures cover the range of the possible gas temperature at the surface facility, and their values are 20 and 80 °C. These temperatures were selected according to the possible range of temperatures at the facility surface. Figure 7.8 indicates the temperature trends for feed temperatures of 20 and 80 °C, and Figure 7.9 illustrates the liquid dropout trends for these two temperatures.

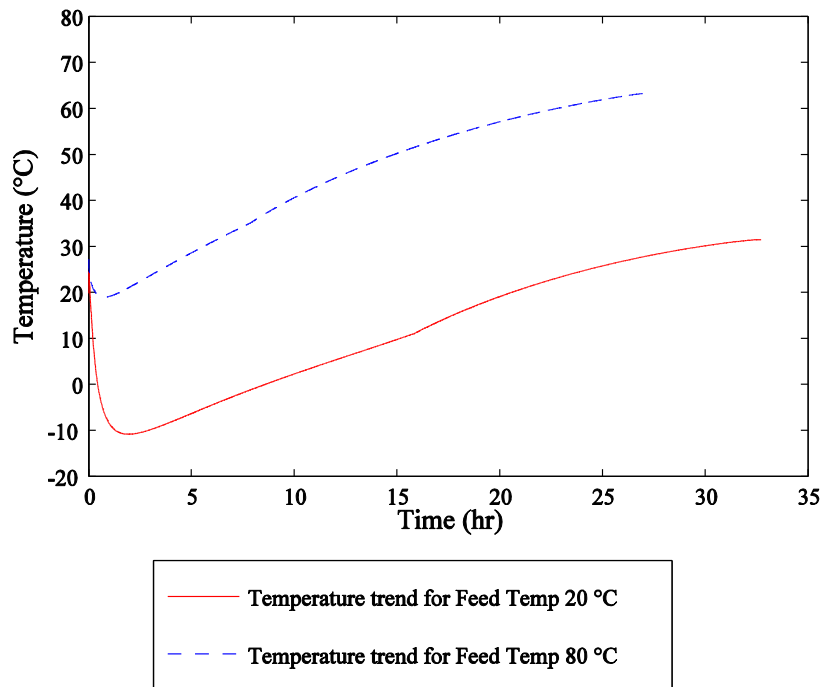


Figure 7.8: Temperatures trends of the SNG1 inside a CNG tank during the loading operation with a Feed Stream Temperature of 20 and 80 °C, using 1P arrangement

The loading of the tank was performed using the arrangement of 1P (previously explained) and the feed pressure was 26,207 kPa. Consequently, the temperature trends in Figure 7.8 have a clear minimum which slowly increase with time. The tank is initially empty, therefore when the high pressure gas enters, it faces a large pressure drop and decreasing its temperature (due to Joule Thomson effect). As the temperature of the feed stream decreases, the gas loaded will reach a lower temperature inside the tank during the loading operation since the rate of change of temperature respect to pressure will be larger, as it is observed from the figure when the tank is loaded with a feed temperature of 20 °C.

When the tank is loaded using the 2P or 3P arrangements, the gas temperature also decreases during loading; however, this decrease is less significant than when 1P arrangement is selected. When 1P arrangement is used for loading the tank, the loaded gas faces a larger pressure delta, which is the difference between the feed stream pressure (26,207 kPa) and the pressure inside the tank (1379 kPa or 200 psi). For 2P and 3P arrangements, the pressure differential that the gas faces is smaller (6,900 kPa minus 1379 kPa), since both arrangements have the same initial pressure for the feed stream.

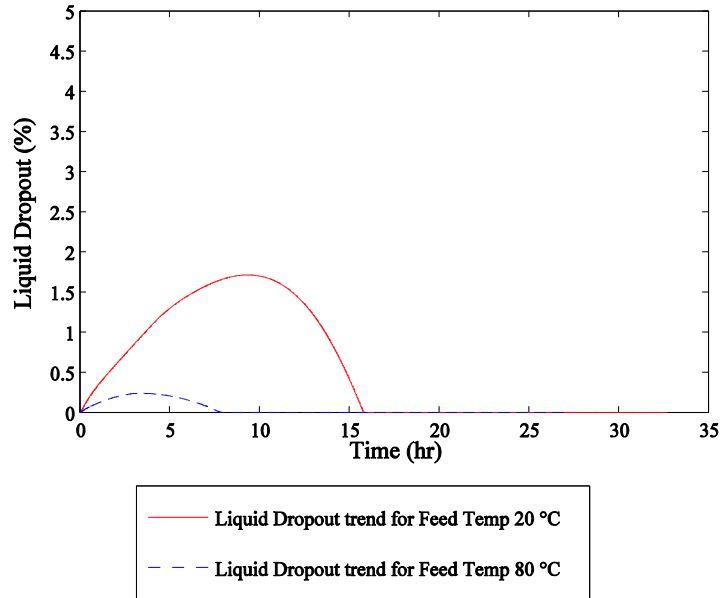


Figure 7.9: Liquid dropout trends of the SNG1 inside a CNG tank during the loading operation with a Feed Stream Temperature of 20 and 80 °C

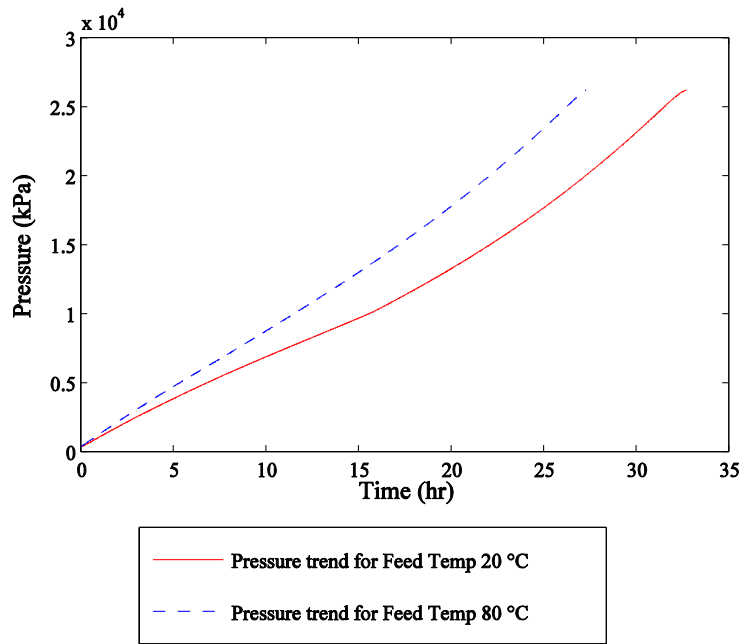


Figure 7.10: Pressure trends of the SNG1 inside a CNG tank during the loading operation with a Feed Stream Temperature of 20 and 80 °C

Figure 7.10 indicates the pressure trend of the SNG1 inside a CNG tank while loading it for the two feed stream temperatures. It is observed that the preferred final pressure (26200 kPa) inside the tank is reached faster at 80 °C. When loading the tank with a feed stream temperature of 80 °C, at the preferred final pressure inside the tank (26200 kPa), the final gas temperature was 63.27 °C and its density was 11.15 kgmol/m³. When loading the tank with a feed stream temperature of 20 °C at the preferred final pressure inside the tank (26200 kPa), the final gas temperature was 31.43 °C and its density was 13.20 kgmol/m³. Therefore, the lower feed temperature (20 °C) loaded a denser gas, and to reach the final desired pressure inside the tank (26,200 kPa) a larger amount of mass was required to be loaded, which required a longer loading time. In this example, the final loading times for the feed temperatures 20 and 80 °C were 32.62 and 27.27 hours, respectively. As a result for this case, the loading time can be reduced by increasing the feed temperature.

At the final pressure inside the tank (26200 kPa) the gas densities are 14 kgmole/m³ when loading with a constant feed temperature of 20 °C and 10.3 kgmole/m³ with a constant feed temperature of 80 °C. The total moles loaded in the first case are 165 and in the second case 121. Therefore, a larger amount of gas can be loaded into the CNG tank employing a lower feed temperature. In this particular case a 37% more of moles could be loaded.

7.4.3 Molar Flow

The effect of the molar flow on the loading of a CNG tank was evaluated with two different molar flow rates of 5 and 10 kgmole/hr for the feed stream. Although doubling the molar flow reduced the loading time by half, it also reduced the temperature inside the tank. This can be explained from the energy balance and ignoring the heat loss, work and potential energy, expressed in equation 7.7.

$$m \left(\frac{v_{in}^2 - v_{out}^2}{2} \right) = m(H_{out} - H_{in}) \quad (7.7)$$

In equation 7.7, m is the mass flow rate, v is the velocity, and H is the enthalpy. Assuming that H only depends on the temperature, as the velocity increases the delta velocity indicated in the previous equation will increase and will be positive, therefore the enthalpy difference has to increase ($H_{in} > H_{out}$) for the right side to be positive, which will produce a temperature drop.

As a result, the loading time can be reduced by increasing the feed molar flow only up to a value where the lowest temperature reached by the gas is within the tank materials temperature specification (ASME B31.3-2010 - Standard for Process Piping). Figures 7.11, 7.12 and 7.13 illustrate the pressure, temperature, and liquid dropout trends of SNG1 during the loading a CNG tank with two different molar feed flows, 5 and 10 kgmol/hr, with a feed stream temperature of 40 °C, and 1P arrangement.

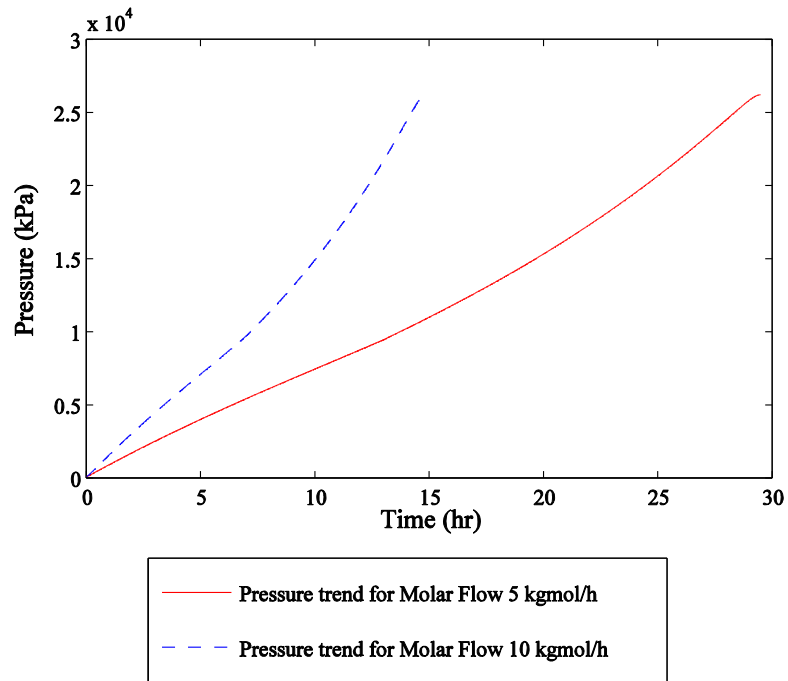


Figure 7.11: Pressure trends of SNG1 inside a CNG tank during loading it with a Feed Molar Flow of 5 and 10 kgmol/hr and 40 °C.

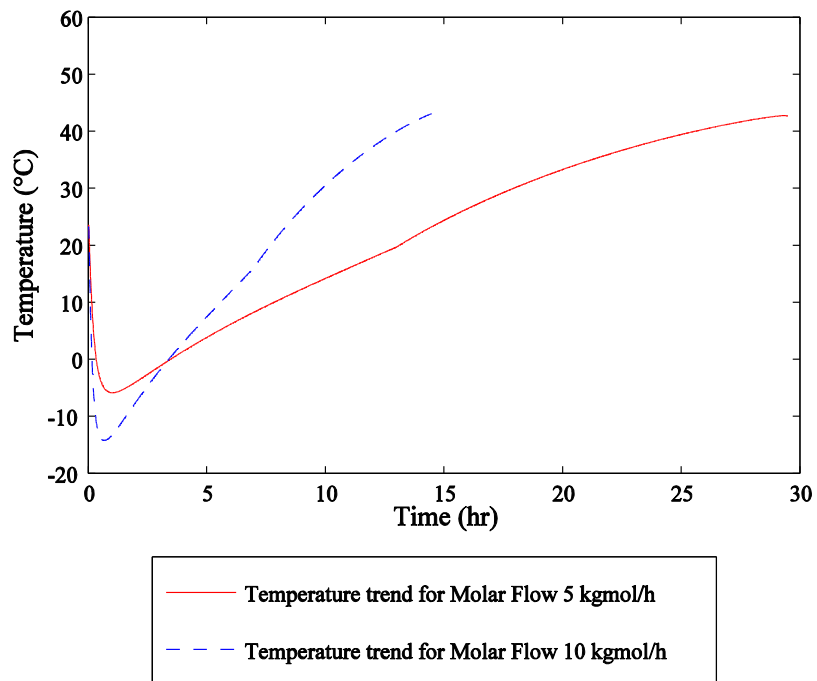


Figure 7.12: Temperature trends of SNG1 inside a CNG tank during the loading operation with a Feed Molar Flow of 5 and 10 kgmol/hr and 40 °C.

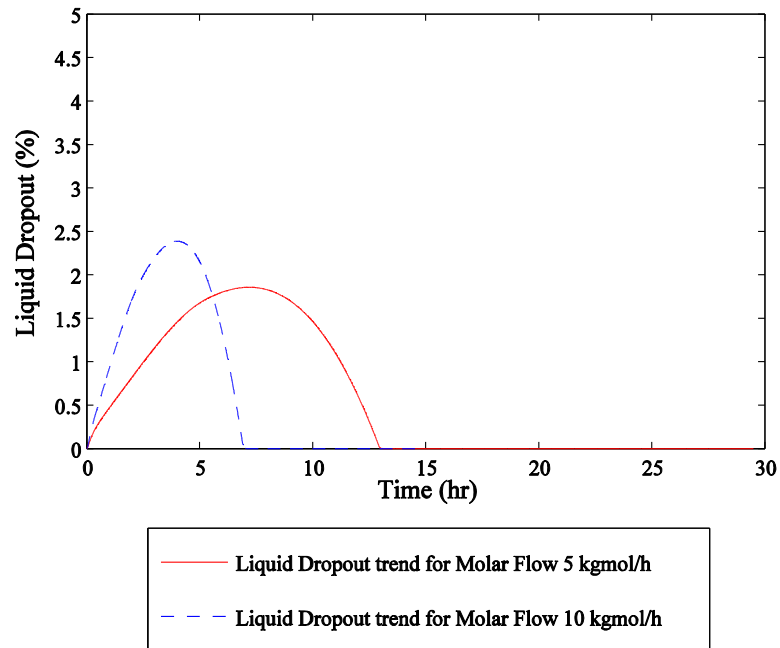


Figure 7.13: Liquid Dropout trends of SNG1 inside a CNG tank during the loading operation with a Feed Molar Flow of 5 and 10 kgmol/hr and 40 °C.

7.4.4 Gas Composition

This section evaluates the effects that heavier hydrocarbons have on the loading of a CNG tank. Three gas compositions with different content of heavier hydrocarbons were used to compare the time required for loading a CNG tank for each of them. The gases used were NG2, SNG1, and SNG2, and their compositions are indicated in Table 7.1. The loading conditions chosen were: a feed molar flow of 5 kgmol/hr, the 2P arrangement for the feed pressure, and a feed temperature of 40 °C. The varying temperature and pressure for each gas sample inside the tank during the loading operation are illustrated in Figure 7.14 and Figure 7.15. The liquid trends during the unloading operation will be illustrated in section 7.4.

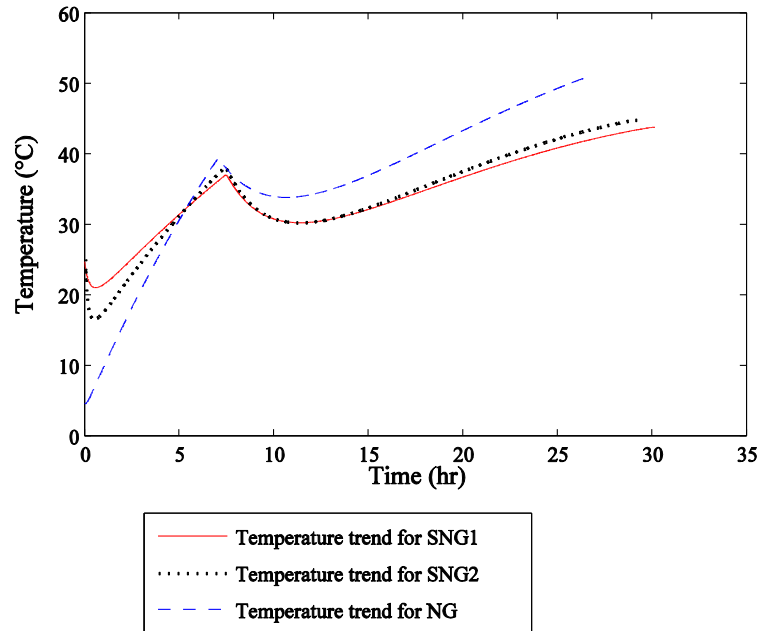


Figure 7.14: Temperature trends of the three different gases: NG2, SNG1, and SNG2 inside a CNG tank during the loading operation with a feed flow of 5 kgmol/hr and feed temperature of 40 °C.

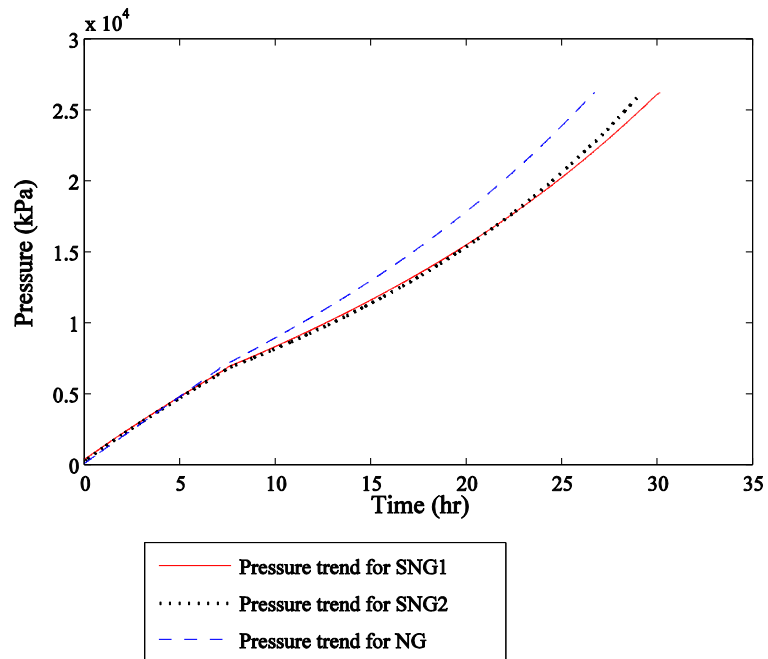


Figure 7.15: Pressure trends of the three different gases: NG, SNG1, and SNG2 inside a CNG tank during the loading operation with a feed flow of 5 kgmol/hr and feed temperature of 40 °C.

As shown in the Figure 7.15, the richest gas (SNG1) takes longer to be loaded since it contains larger amount of heavy hydrocarbons and its density is larger. In this example, the final loading times for the gases NG, SNG2 and SNG1 were 26.75, 29.07 and 30.16 hours, respectively. Thus, the content of heavy hydrocarbons is a main factor to be considered in the design of the loading and unloading operations of a CNG tank.

Table 7.5 indicates the gas density of the diverse gases at the final pressure inside the CNG tank (26200 kPa) and 40 °C as well as the total moles loaded inside the tank, which has a volume of 11.8 m³.

Table 7.5: Gas density of the diverse gases at the final pressure inside the CNG tank (26200 kPa) and 40 °C as well as the total moles loaded inside the tank

	NG2	SNG1	SNG2
C3+ (mole percentage)	3.10	7.22	10.66
C5+ (mole percentage)	0.18	0.79	0.80
C7+ (mole percentage)	0.02	0.10	0.02
Gas density (kgmole/m ³)	12.12	12.54	12.84
Total moles loaded into the CNG tank	143	148	151

7.5 Unloading Conditions

Two main factors were evaluated during the unloading operations: the amount of liquid remaining inside the tank at keel pressure (final pressure reached in the tank), and the lowest temperature reached by the gas inside the tank. Reducing the temperature inside

the tank may require more expensive materials to construct a CNG tank, so the lowest temperature inside the tank should be checked. Moreover, a large amount of liquid remaining inside the tank at the keel pressure will need to be removed to avoid an economic loss. An option to recover the liquid could be adding a drain at the bottom of the tanks, so the liquids could be discharged. Also, if liquid remains in the bottom of the tank (as the liquid vaporizes during unloading and depressurization operation) the composition of the released gas to the line will differ from the one originally charged. In Chapter 2 it was shown that EOSs present errors in predicting liquid dropouts. Therefore, in order to have an accurate estimation of the amount of liquid remaining inside the tanks, tuned equations should be employed for the simulations of these operations. The scope of this thesis did not include measuring the maximum heavy hydrocarbon content that a gas sample can contain, in order to be loaded into a CNG tank without producing a large amount of liquid remaining inside the tank after unloading, and therefore requires further evaluation. It is recommended to load a gas with a dew point of between -13 and -10 °C at 26200 kPa to meet the pipelines conditions until further evaluations are made for the CNG tanks in order to drain liquids from it.

In order to evaluate how diverse unloading conditions affect the performance of the operation, dynamic simulations were performed for the unloading operations. For this purpose some of the gases described in Table 7.1 were employed for simulating the unloading operation from a CNG tank. As for the loading operation the molar flow was the controlled variable to evaluate the performance of the loading operation under diverse

conditions the output molar flow was the controlled variable for the discharge of the CNG tank. Diverse factors were evaluated for the unloading operations including gas compositions, initial gas temperatures inside the tank, and discharge molar flows. The parameters of comparison to evaluate the performance of each case were the unloading time, the lowest temperature reached inside the tank during the unloading operation, and the liquid level at keel pressure. These factors are evaluated in the following sections

7.5.1 Effect of initial temperature

The unloading operation of a CNG tank will occur at a different pressure and temperature than the final conditions of the loading operation. During transportation, the heat exchange between the tanks and environment causes a decrease in the temperature of the tank and, therefore, of loaded gas. The initial temperature for unloading is assumed to be around 20 °C, however, it may be lower or higher. The unloading temperature trends of the gas inside the CNG tank under two initial gas temperatures were determined and compared. The initial gas temperatures selected for this analysis were 20 °C and 33 °C, and both temperature trends are shown in Figure 7.15 for SNG1. The Figure indicates that when the keel pressure of 1188 kPa was reached, the final temperature inside the tank was 6.64 °C for the initial temperature of 33 °C and 4.48 °C for the initial temperature of 20 °C. Also, the unloading times required were 30.15 and 32.37 hr for the initial temperature of 33 and 20 °C, respectively.

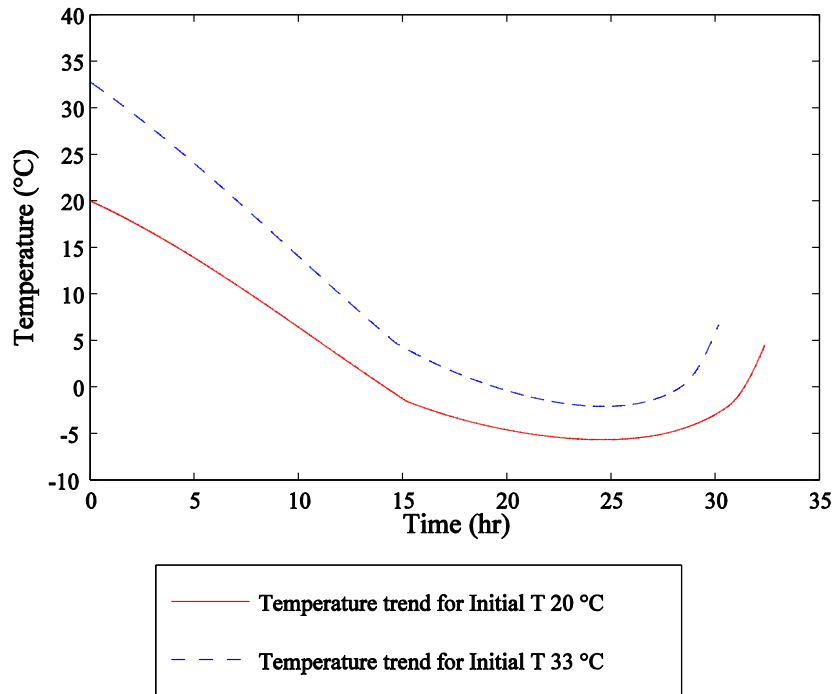


Figure 7.16: Temperature trends for SNG1 inside the CNG tank during the unloading operation for two initial gas temperatures, which values were 20 and 33 °C.

Figure 7.26 suggests that by increasing the initial unloading temperature of the gas, the time required for its discharge decreases, and the final minimum temperature inside the tank increases. Figure 7.17 indicates the liquid dropout trends for the two initial unloading temperatures. When the initial unloading temperature is higher, lower amount of liquid remains inside the tank when at keel pressure. The liquid percentages remaining inside the CNG tank at the keel pressure of 1188 kPa are 0.236% and 0.306%, for the Initial temperature of 33°C and 20 °C, respectively. The pressure trends are indicated in Figure 7.18.

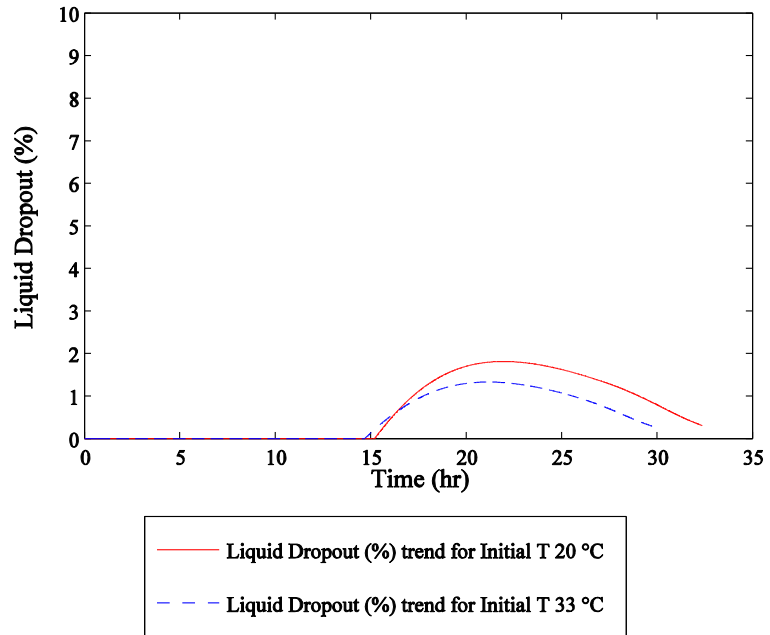


Figure 7.17: Liquid dropout trends for two initial gas temperatures during the unloading operations of SNG1. The initial temperatures are 20 and 33 °C.

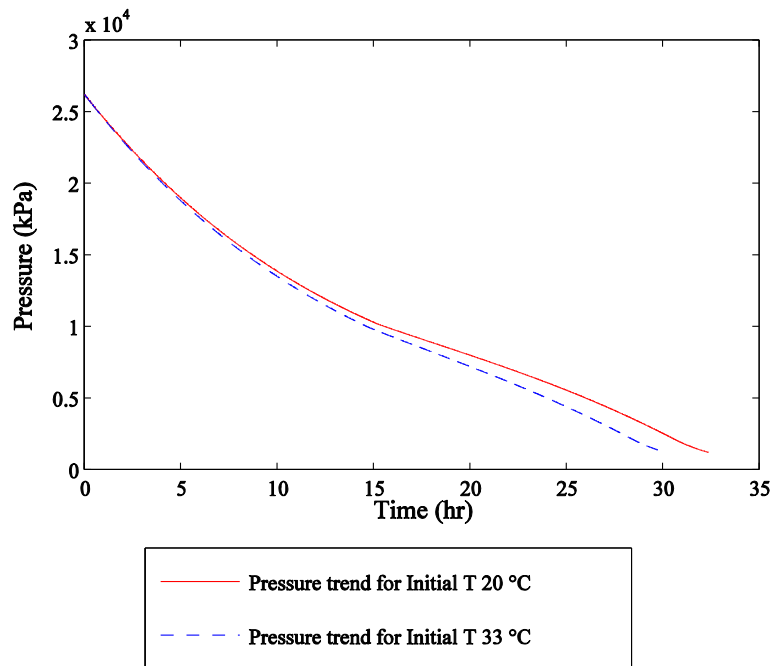


Figure 7.18: Pressure trends for two initial gas temperatures during the unloading operations of SNG1. The initial temperatures are 20 and 33 °C.

7.5.2 Effect of gas composition

In order to evaluate the effect of heavy hydrocarbon content in the gas, the unloading of two different gases (NG2 and SNG2) from a CNG tank were compared. The conditions selected for the unloading operation were an initial gas temperature and pressure of 20 °C and 26,206 kPa (3800 psia), and molar flow rate of 5 kgmol/hr. As a result, the leaner gas, NG2, reached the keel pressure at a very low temperature (below -60°C) inside the tank when compared to the richer gas SNG2 (which reached the keel pressure at a final temperature of around -10°C). Figure 7.19 indicates the temperature trend during the unloading of the two gases NG2 and SNG2.

When the liquid content remaining inside the CNG tank at the keel pressure was compared, both gases presented similar amounts (0.85% for the richer gas SNG2 and 0.74% for the leaner gas NG2), although during the unloading the richer gas had a larger accumulation. The liquid dropout trends during the unloading operation of the two gases mentioned are shown in Figure 7.20. The small difference of the liquid remaining inside the tank after unloading indicates that the heavy hydrocarbon content should be removed only until certain extend. For these two gases the C_3^+ content for the heavier sample (SNG2) was 10.7 % while it was 3.1% for the leaner sample (NG2). The C_5^+ fraction were 0.8% and 0.18% for SNG2 and NG2, respectively. The C_7^+ fraction was the same for both samples.

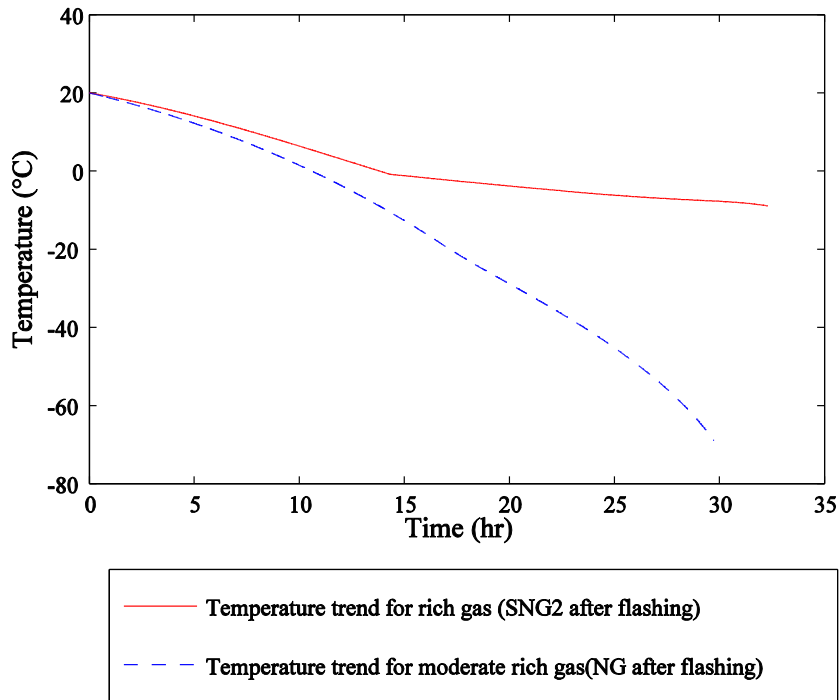


Figure 7.19 Temperature trends during the unloading of SNG2 and NG2. Initial gas temperature and pressure are 20 °C and 26,206 kPa (3800 psia).

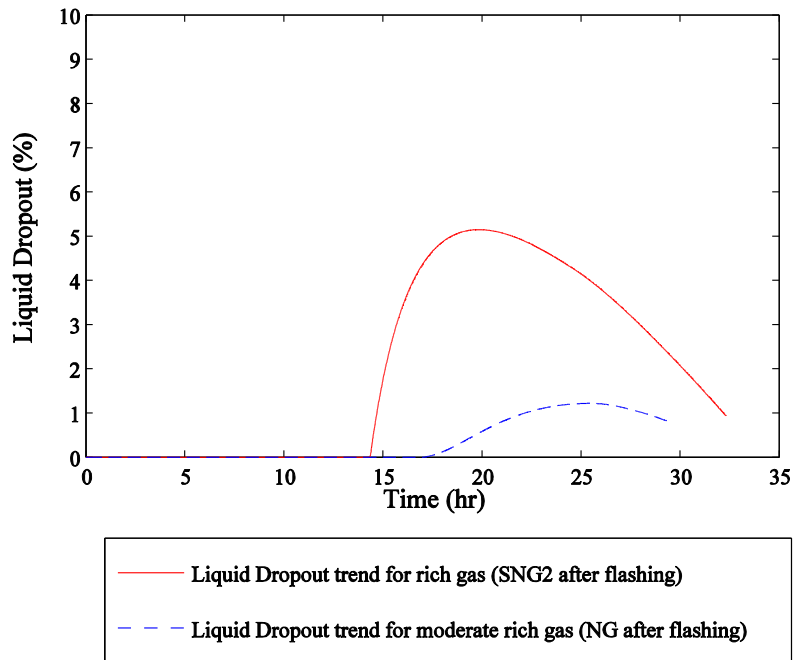


Figure 7.20: Liquid dropout trends during the unloading of SNG2 and NG2. Initial gas temperature and pressure are 20 °C and 26,206 kPa (3800 psia).

The liquid dropout trend of a lean gas (SNG2) during the unloading operation was also compared to liquid dropout trend of a rich gas (SNG3) during the unloading operation. Figure 7.21 indicates the liquid dropout trends during the unloading for these two gas samples. From this figure, it is observed that unloading the richer gas (SNG3) cause a large accumulation of liquids inside the tank. Therefore, the gas should be flashed to remove partially the liquid content before loading. The C_3^+ content for the heavier sample (SNG3) was 23.33% compared to the 10.66% observed in the moderately rich sample (SNG2). These samples also differed largely in their C_5^+ fraction content, which were 5.28% and 0.8%, for SNG3 and SNG2, respectively.

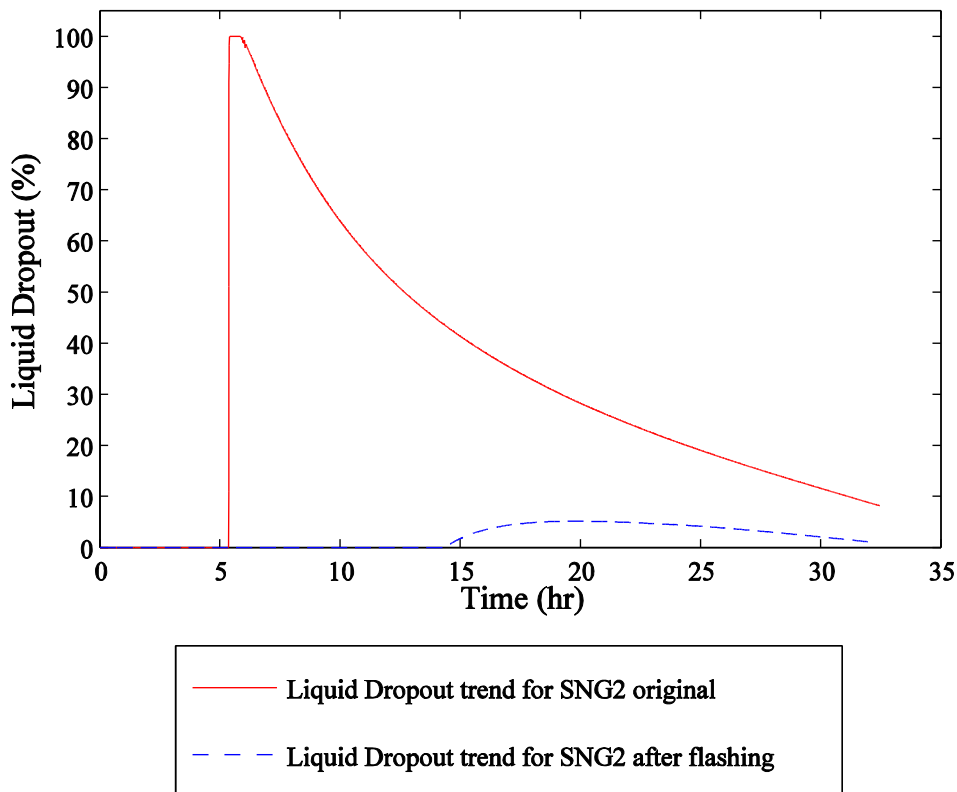


Figure 7.21: Liquid dropout trends during the unloading operation for the original gas sample SNG2 and the same sample but after flashing it.

Two criteria should be used to determine how much liquid is required to be removed from the gas. The first criterion is that the liquid dropout should not be so large as to interfere with the loading. This last case is illustrated in Figure 7.21, where the quantity of liquid accumulated for SNG3 became so large that at one point during the loading, the tank was almost full with condensate. The second criterion concerns the volume of liquid remaining in the tank after unloading the gas. If liquid remains inside the tank, it indicates the composition of the unloaded gas is different than the one loaded. Also, for the next loading operation, the composition of the gas to be loaded will be modified by this liquid.

Since the unloading of a very rich gas could cause liquid to remain inside the tank, and the unloading of very lean gas could cause very low temperatures inside the tank, neither are desired. Therefore, the concentration of heavier hydrocarbons present in the gas to be loaded needs to be balanced so that the loading and unloading operations can proceed properly.

7.5.3 Effect of molar flow

The effect of the molar flow rates during the unloading of a CNG tank filled with SNG1 gas was evaluated. Two flow rates were selected for this purpose, 5 and 10 kgmol/hr. By doubling the molar flow, the unloading time was reduced by half, however, the temperatures dropped lower inside the tank. Therefore, the flow rate can be increased to reduce the loading time but as there is possibility of dropping temperatures inside the

tank, the temperature should always be checked. The temperature profiles of the unloading of a CNG tank with SNG1 gas sample under two different molar flows are shown in Figure 7.22.

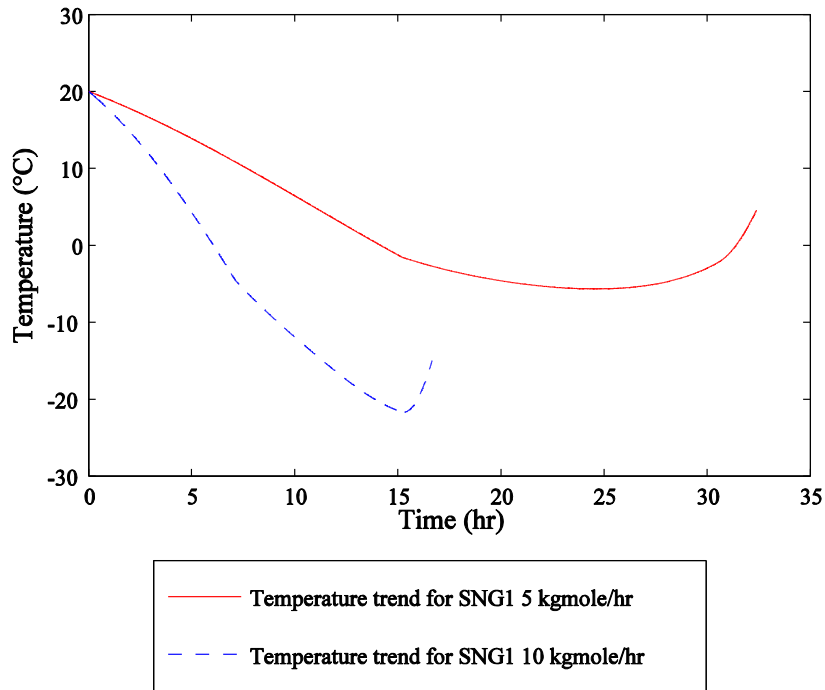


Figure 7.22: Temperature trends during the unloading of CNG tank with SNG1 for two discharge molar flow rates of 5 and 10 kgmol/hr.

7.6 Impact of Gas Composition

When rich gases were loaded into and unloaded from a tank without flashing the feed in an inlet separator, several difficulties were encountered; a large accumulation of liquid remains inside the tank after unloading the gas, and a longer loading time is required.

Therefore, it is recommended that very rich gas samples are first flashed in a separator to remove the liquids prior to loading the remaining gas into the tank.

7.6.1 Consequences of an incorrect prediction by the EOS when flashing a rich gas

As it was illustrated in Chapter 4, EOSs do not accurately predict the ratio of liquid to gas after a flash has been completed. In order to estimate the possible amount of gas that can be loaded after flashing a rich gas, an accurate liquid dropout prediction is highly important. The consequences of inaccurately predicting liquid dropout by the EOS are illustrated in this section by comparing the EOS's predictions, before and after tuning, for flashing a *rich gas* (NG1 in Table 7.1).

In general, the gas from the reservoir arrive to the surface facility on offshore at a temperature around 35 °C and a pressure close to 6890 kPa. However, these conditions will vary since they depend on the reservoir conditions (temperature, pressure, age, etc). The rich gas to be loaded is then flashed to remove the liquid content using a single flash separator at the conditions that the gas arrived to the facility surface (see results in Tables 7.5). Larger amounts of liquid could be removed at pressures close to the dew point, but it requires gas compression. Figure 7.23 illustrates the operations required prior to load rich gas samples into a CNG tank. As mentioned, the gas arrives at 35 °C and 70 bar. It is then flashed, and the remaining gas is compressed (to 20,000 26200 kPa) and cooled to the desired temperature for loading it into a CNG tank.

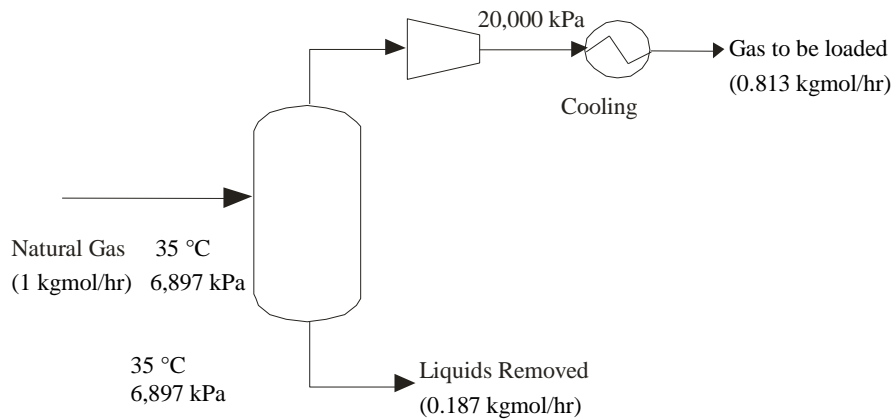


Figure 7.23: Process flow diagram of flashing a NG1 sample at 35 °C and 6,897 kPa (the molar flows are the one obtained with the original PR)

A molar flow rate of 1 kgmole/hr of gas at 35 °C and 6890 kPa was flashed and the predicted gas and liquid molar flow rates with their respective composition were obtained using the original, tuned PR, and SRK equations. The liquid dropout percentages (the percentage ratio of liquid over total volume) at the flashing conditions were then calculated.

The resulting gas from the flashing was then ready to be loaded into a CNG tank with a volume of 11.78 m³. The total moles of gas that can possibly be loaded were calculated using the predicted gas densities by the original and the tuned EOS. The densities were calculated using the gas compositions obtained for EOS. The final conditions of the loading operation were assumed as 40 °C and 26,200 kPa. Table 7.6 indicate the results of the flashing using the original and tuned EOS. It also indicates the predicted total gas moles that can be loaded when using each of EOSs.

Table 7.6: Results of flashing NG1 sample (composition in Table 7.1) at 35 °C and 6,897 kPa in an equilibrium flash separator

Component	PR				SRK			
	Gas Stream		Liquid Stream		Gas Stream		Liquid Stream	
	Before Tuning	After Tuning	Before Tuning	After Tuning	Before Tuning	After Tuning g	Before Tuning g	After Tuning g
N ₂	4.70	4.74	0.49	0.48	4.70	4.75	0.46	0.46
CO ₂	0.81	0.82	0.49	0.48	0.81	0.81	0.49	0.49
C ₁	81.64	81.85	20.54	21.99	81.69	81.89	19.89	22.27
C ₂	9.33	9.21	8.73	9.25	9.34	9.23	8.70	9.17
C ₃	2.17	2.10	5.30	5.47	2.17	2.09	5.36	5.49
iC ₄	0.39	0.37	1.86	1.87	0.38	0.37	1.88	1.87
nC ₄	0.49	0.47	3.11	3.12	0.48	0.46	3.17	3.14
iC ₅	0.13	0.12	1.59	1.57	0.12	0.11	1.64	1.59
nC ₅	0.11	0.11	1.77	1.73	0.11	0.10	1.80	1.74
C ₆	0.11	0.10	3.90	3.78	0.10	0.09	3.96	3.79
C _{7-C9}	0.11	0.11	21.83	21.03	0.10	0.09	22.05	20.96
C _{10-C13}	0.01	0.01	11.76	11.31	0.00	0.00	11.85	11.24
C _{14-C18}	0.00	0.00	8.29	7.97	0.00	0.00	8.35	7.92
C _{19-C26}	0.00	0.00	6.30	6.07	0.00	0.00	6.35	6.02
C _{27-C80}	0.00	0.00	4.04	3.89	0.00	0.00	4.07	3.86
C ₃ ⁺ %	3.52	3.38	69.75	67.81	3.46	3.31	70.45	67.62
C ₅ ⁺ %	0.47	0.44	59.48	57.35	0.43	0.40	60.05	57.11
C ₇ ⁺ %	0.12	0.11	52.22	50.27	0.10	0.09	52.66	50.00
Molar Flow (kgmol/hr)	0.813	0.805	0.187	0.195	0.814	0.804	0.186	0.196
	Before Tuning		After Tuning		Before Tuning		After Tuning	
Liquid Dropout %	10.5		15.1		10.1		12.39	
Gas Molar Density (kgmol/m ³) at 40 °C and 26,200 kPa	12.13		9.72		11.30		11.97	
Moles of Gas Loaded in a CNG tank of 11.78 m ³	143		115		133		141	

Note: the volume of the tank is 11.78 m³ and the Feed molar flow is 1 kgmole/hr

The difference between the original and tuned EOS predictions indicated in Table 7.5 is significant. This discrepancy is due to the high heavier hydrocarbon content in the gas

sample. As discussed in the previous chapters, EOS predictions become less accurate as the amount of heavier hydrocarbons increases in the gas sample, which is also evidenced in this example.

7.7 Original vs Tuned EOSs

A comparison for CNG loading and unloading simulations based on the original and the tuned EOS (Equation of State) was not provided because they only differed slightly in the liquid dropout trend. The gas was flashed before being loaded into the CNG tank, so there was not a large accumulation of liquids during the loading and unloading operations. As it was indicated in Chapter 4, for lean and moderate rich gases EOSs predict accurately the thermodynamic properties (dew point, liquid dropout, gas density). In addition, the temperature and pressure trends were equal since the same conditions for both cases were employed. The tuned equations of state did not impact predictions when the gas was flashed since most of the heavy hydrocarbons were removed. A robust optimization on the tuned parameters is required to properly analyze the impact of the tuned EOS and this could be done as a future work.

Major discrepancies between the original and tuned EOSs predictions occur when predicting properties for rich gases. As it was mentioned in the previous paragraph, the rich gases are flashed before loading into a CNG tank, and the predictions of the original and tuned EOS for this separation differ. In Section 7.5, this difference is illustrated by comparing the total amount of gas loaded into a CNG tank using the original and the

tuned EOS. The original EOSs predicted a larger gas molar density when compared with the tuned EOS predictions. Therefore, the original EOS predicted that a larger amount of gas could be loaded into the CNG tank.

A large difference between the original and the tuned EOS could be observed if a rich gas was loaded into the CNG tank. This Chapter indicated that when loading a rich gas into a CNG tank a significant amount of liquid was formed inside the tank, and a large amount of liquids remained in the tank at the keel pressure. For this reason, rich gases were mostly not used in the loading and unloading of a CNG tank simulations.

7.8 Conclusions

In this chapter, it was illustrated how inaccurate and improper predictions of phase behaviour by EOS could result in a wrong estimation of the gas volume and composition when a rich gas is flashed to remove the liquids. Therefore, tuning the EOS is highly recommended for proper estimation of the gas that could be transported employing CNG marine technology in cases of condensate reservoirs.

In addition, diverse gas compositions were used to perform dynamic simulations of the loading and unloading of a CNG tank to evaluate the effect of the heavy hydrocarbon content of the gas on these operations. For this purpose, diverse parameters were analyzed and several observations were made, which will be addressed in the following paragraphs.

When a lean gas was loaded, relatively low temperatures (below -20°C) were reached inside the tank as compared to richer gases. Therefore, special materials for the CNG tanks may be required to tolerate such low temperatures. To avoid using special materials, the unloading operation can be stopped at a higher pressure to prevent the tank from reaching very low temperatures. However, this option may be unattractive because of the residual gas in the tank. Another possibility to avoid the low temperatures could be intermittent unloading. This procedure stops the unloading operation to allow the temperature of the gas inside the tank to increase by heat exchanging with the environment. Stopping the unloading operation will also increase the loading time, therefore it needs to be evaluated for each case.

When gases with high concentrations of heavy hydrocarbon were unloaded, it was generally observed that large amounts of liquid remained inside the tanks at keel pressure. A solution could be heating the tanks to increase the initial gas temperature (to re-evaporate the liquids), however, this option is likely expensive. Another solution could be to drain the liquid remaining inside the tank, which requires the tanks to be properly designed for this operation.

Overall, it was concluded that the amount of liquid formed inside the tank during the loading and unloading operations is very important. For larger accumulations of liquid inside the tank more time was required to complete these operations. However, heavier

hydrocarbons contained in the gas should be removed only to a certain extent. Removing all the heavier hydrocarbons may produce very low temperatures during the unloading operation, and not removing these components could cause an accumulation of liquids inside the tank when at keel pressure. In order to know the optimum heavy hydrocarbon recovery an optimization is required for each specific case.

CHAPTER 8

CONCLUSIONS AND RECOMMENDATIONS

8.1 Concluding Summary

Exploitation of stranded gas reservoirs (where the gases contained a large amount of condensate), associate gas from offshore production platforms, and condensate gas reservoirs for short to medium distances are the most promising applications of marine CNG transportation technologies. While marine transportation of gas in the CNG form could be an option to produce these reservoirs, the amount of condensate allowed to be loaded into the CNG tanks needs to be studied. Transporting rich gases with minimum treatment offshore by using CNG technology would be the most appealing option. The first step in the evaluation was to assess the performance of the EOS in accurately predicting the thermodynamic properties of rich and moderately rich gases. This work involved performing experiments to first evaluate the EOS, and based on the obtained data, to tune the EOS and improve certain thermodynamic properties (such as density and dew point predictions). Then simulations of the loading and unloading operations of a CNG tank were performed.

8.1.1 Dynamic Simulations of Loading and Unloading a CNG tank

Diverse gas compositions were used to perform dynamic simulations of the loading and unloading of a CNG tank to evaluate the effect of the heavy hydrocarbon content of the gas on these operations. From all the simulations performed, several observations were made. First, when unloading lean gases, very low temperatures were reached inside the tank. Therefore, special materials for the CNG tanks may be required to tolerate these low temperatures. To avoid using special materials, the discharge can be stopped at a higher pressure to prevent the tank from reaching extremely low temperatures. However, this option may not be profitable because unsold gas remains in the tank, and the capacity of the tank is reduced for the next load. Another way to avoid low temperatures may be intermittent unloading, which facilitates a temperature increase inside the tank between discharges, but it will increase the loading time. Another observation was that large amounts of liquid remained inside the tanks at keel pressure when gases with a high content of heavy hydrocarbons were unloaded. A possible solution may be heating the tanks to increase the initial gas temperature (to re-evaporate the liquids); however, this option may be unpractical and expensive. Another option to recover the liquid could be adding a drain at the bottom of the tanks, so the liquids could be discharged. The issue associated with the liquid remaining at the bottom of the tank is that as the liquid vaporizes during unloading and depressurization operation, the composition of the released gas to the line will differ from the one originally charged.

Overall, it was observed that the amount of liquid formed inside the tank during the loading and unloading operations affected the time required for these operations. The accumulation of liquid inside the tank was directly related with the density of the gas, which depends on the gas composition as well as of the temperature and pressure. For instance, when the same gas was loaded using two different feed stream temperatures, the loading time required for each case, as well as the amount of liquid accumulated inside the tank during the loading operation was different. For larger accumulations of liquid inside the tank more time was required to complete these operations.

Although denser gases or gases with larger content of heavy hydrocarbons required longer loading time, heavier hydrocarbons contained in the gas sample should be removed only to a certain extent. Removing all the heavier hydrocarbons may produce very low temperatures during the unloading operation, and not removing these components could cause an accumulation of liquids inside the tank (when at keel pressure), thus modifying the final gas composition unloaded.

Conducting dynamic simulations of loading and unloading of CNG operations in a process simulator can determine the applicability of certain potential reservoirs for marine CNG transportation technologies. The current commercial process simulation packages lack the ability for accurately predicting the behaviour of gas under the temperature and pressure conditions of the CNG operations (high pressures and low temperatures, and two phase region). By modifying some parameters of the EOS, a

noticeable improvement is obtained and an accurate evaluation of the CNG applicability for a particular reservoir can be conducted.

The experimental simulation of the loading and unloading of a CNG tank with the PVT cell in the laboratory was attempted. Unfortunately, results were unsuccessful since the set up used for the experiment did not properly represent the loading of a CNG tank and different effects were observed. An instantaneous measurement of the temperature and pressure of the gas was obtained, but the Joule-Thompson effect was not detected.

8.1.2 Experimental Approach

Experiments were conducted in an advanced laboratory with sophisticated equipment including a PVT cell, a densitometer, and a gas chromatograph. Diverse gas compositions were made in the laboratory to perform the experiments. For this purpose, it was developed, with relatively high accuracy, a new and simple method to prepare gas sample. The composition of the gas samples in the laboratory, although not exact, was ideal and comparable to the desired gas composition required for the purpose of this research. A combination of results from the CCE and CVD tests were employed to modify the parameters of the EOS and improve their predictions. Before using the CVD experimental data for tuning the EOS, a validation procedure was also required in order to check the consistency and/or quality of the experimental data.

8.1.3 EOS Performance

In the first part of this thesis, an evaluation of the current thermodynamic models, (mainly PR and SRK models) was conducted to determine the errors in their predictions. During the evaluation of the EOS predictions, a distinction between synthetic gas samples and natural gas samples was made. The synthetic gas samples are thoroughly characterized in terms of composition, while natural gas from reservoirs may not be. Most of the literatures emphasize the inaccuracy of the EOS in predicting the thermodynamic properties of natural gas samples due to the uncertainty of the uncharacterized fraction properties. However, this study demonstrated that EOS are also inaccurate for predicting synthetic gases rich in heavy hydrocarbons, where the heavy fraction is fully characterized.

In general, as the amount of condensate increases in any gas composition (either for a synthetic gas or a natural gas sample), the EOS errors in predicting dew point pressures and liquid dropout become larger. This was demonstrated by comparing experimental and predicted properties for diverse gas composition. The observations made during the analysis are summarized below.

a) Dew points

In this research, some new correlations were found between the shape of the dew point curve and the gas composition.

After evaluating the performance of the PR and SRK equations of state (for predicting dew points for a number of different gas compositions) it was found that these equations do account adequately for the heavier hydrocarbons. Although this is well known, this study focused on CNG conditions where the degree of inaccuracy has not been explored and the impacts of small inaccuracies can be significantly dramatic. In some cases, the effect of a large amount of heavy hydrocarbons on the dew point curve was countered by a large amount of CO₂, resulting in EOS predictions in better agreement with the experimental results. However, when a gas sample contained a large amount of heavy hydrocarbons and no CO₂, the predictions of the EOS were very inaccurate. In the case of a sample containing only hydrocarbon components, such as in gas samples with butanes as the heaviest hydrocarbons, the greatest deviations between the predictions and the experimental dew points occurred at pressures above the cricondetherm. When the gas samples contained pentanes or heavier hydrocarbon components, the EOS dew point predictions deviated at all pressures. Therefore erroneous conclusion could be made if we only account for the effect of the heavy hydrocarbons (without including the non-hydrocarbons components), on the shape of the dew point curve. For samples containing only N₂ as non-hydrocarbon component, EOS dew point predictions correlate with the experimental values for pressures below the cricondetherm, but above this point the experimental points deviate sharply from the predicted curves.

Overall, the SRK equation is a better predictor of the dew points than the PR equation. In general, EOSs underestimate the dew point pressures. Larger deviations were observed

between experimental and predicted dew points for natural gas samples, especially those samples with a dense C_7^+ fraction (above 800 kg/m^3). In some cases, EOS predicts bubble point instead of dew point, and this can be attributed to the large amount of C_7^+ fractions.

In samples containing a plus hydrocarbon fraction, the proper characterization of the plus fraction significantly improves the predictions. It was observed that when the C_7^+ fraction was not characterized, the dew point pressures were under-predicted, and when the C_7^+ fraction was characterized, the dew point pressures were overestimated but contained smaller errors. In addition, there is an optimum number of components after lumping (usually between 6 and 12), and it was found that characterizing the plus fraction into six pseudo components provided the maximum improvement of the predictions. Adding more pseudo component did not improve the predictions. The Pedersen characterization method for the plus fractions was selected since several studies (refer to Chapter 2) proved that it was the best method.

b) Liquid dropout

The magnitude of the error in liquid dropout predictions was a function of the gas composition. In the case of synthetic gas samples, the error was more noticeable for temperatures between the cricondenbar and cricondentherm, as the amount of condensate increased in the compositions. Overall, the PR and SRK models tended to under predict liquid dropout, except for pressures and temperatures close to the dew points. While

characterizing the plus fraction in natural gas samples improved the predictions, the predictions were still inaccurate. The errors in the predictions were larger close to the dew point pressure, but as the pressure decreased the predictions became more accurate.

c) Gas Density

The gas density was measured in the one phase region (gas or supercritical region) and in the two phase region, and different results were obtained. In the one phase region, all the gas density predictions were on the gas phase and supercritical region, and overall the errors in the predictions were below 10%. PR and SRK density predictions for the synthetic gas samples showed opposite trends, except for very low pressure. The absolute percentage error (APE) curves for these two equations were compared and where the APE curves of PR presented a minimum, the APE curves of SRK presented a maximum. As expected, the SRK equation predicted smaller errors as it was originally designed to predict gas densities more accurately. In the two phase region, the gas density predictions deviated significantly (for moderate rich gases the APE was between 10 and 15%, and for rich gases between 8 and 30%), depending on the pressure and temperature conditions. The larger errors in the two phase region could be the result of an incorrect prediction of liquid dropout. Although the errors in predicting density (or compressibility) were relatively low in the one phase region, these small errors can have significant impacts. For instance, in the process of loading gas in a CNG tank, the amount of gas that can be charged will be calculated according to density at the final pressure and temperature conditions, which is in the supercritical region. An error of

10% in the density prediction could result in a significant error in the estimated volume of gas loaded into a CNG tank.

8.1.4 Method to Improve EOS predictions

A regression technique to fit the PVT data and study the phase behaviour for single or multiple samples of reservoir fluids was conducted. The properties measured and analyzed for improvements were dew point pressures, gas densities, compressibility, and liquid dropout. These properties are very important for determining the optimal design conditions for safety and efficiency on load, store, and unload CNG vessels. Therefore, a methodology for improving EOS predictions was proposed.

Binary interaction parameters (k_{ij}) play a major role in the calculation of dew points since they affect the vapour-liquid-equilibrium (VLE) of mixtures. When the k_{ij} between hydrocarbons were set to zero, dew point predictions were overestimated. The modification of the k_{ij} improves the dew point predictions, and they need to be made in accordance with the gas composition. In the case of synthetic gas samples, the modification of just one k_{ij} of the models was enough to obtain better predictions of the dew points. In most of the cases, the k_{ij} modified was a combination of propane and pentanes (C₃-C₅), propane and normal hexane (C₃-nC₆), or propane and n-octane (C₃-nC₈). For example, it was found that initial EOS predictions that sharply deviated from experimental data between cricondentherm and cricondenbar were improved by modifying the k_{ij} for methane and propane ($k_{C_1C_3}$). For those deviations starting at

pressures below the cricondentherm, the modification of k_{ij} for propane and pentanes ($k_{C_3iC_5}$ or $k_{C_3-nC_5}$) improved the predictions. In the case where the gas sample did not contain propane, the k_{ij} between normal butane and iso pentane ($k_{nC_4-iC_5}$) showed the best improvement in the dew point predictions. On the contrary, natural gas samples required more than one k_{ij} modification in order to improve the prediction of the dew points. The k_{ij} s of the two heaviest pseudo-component with methane and the non hydrocarbon components (N_2 and CO_2) were modified (for the C_7^+ fraction lumped into 6 pseudo components), and for the remaining pseudo components the k_{ij} between hydrocarbon components were set to zero.

The tuning process showed that modifying the Peneloux parameters (see Chapter 5 for equations) markedly improved the prediction of the liquid dropouts. Most literatures recommend modifying the critical properties (such as critical temperature) of the plus fraction after characterization to improve liquid dropout predictions. However, modifying the critical properties of the plus fraction can affect the values of other thermodynamic properties. Therefore, the modification of the Peneloux parameters is recommended based on this study since this parameter will only modify the liquid dropout and density (and compressibility) predictions.

The EOS prediction errors in gas density in the two-phase region were improved by modifying the Peneloux parameters and the k_{ij} . Since gas compressibility and gas density are related (as indicated in Equation 4.1), the same parameters (i.e. such the Peneloux

parameters) were modified and a great improvement in compressibility predictions were obtained for both models (the APE were 3% and 0.8% for PR and SRK respectively).

The performance of the EOS was tested using the process simulator HYSYS, which allowed modifying adjusted parameters obtained with the regression technique, such as k_{ij} , d_1 and d_2 . The software was used to produce EOS predictions with and without modification of some parameters and compared against experimental data to evaluate differences and improvements.

The method for improving the EOS predictions first involves performing experimental tests to obtain dew point pressures, gas densities, and liquid dropout measurements. A comparison between experimental and EOS predictions is conducted to determine the types and magnitudes of deviations. After this evaluation, an adjustment of the parameters is performed (with a regression technique) based on the recommendations made in the previous paragraphs about which parameters to modify.

8.2 Objectives Reached

The objective of the proposed work was to accurately predict the loading and unloading behaviour of the gas for marine CNG transportation technologies, and to evaluate the applicability of rich and moderate gases for this technology. For this purpose, an accurate thermodynamic model that predicts natural gas behaviour under the complete operation

range of CNG loading and unloading operations was necessary. As demonstrated in previous chapters, the two most common thermodynamic models used in the Oil and Gas industry, PR and SRK, inaccurately predict the thermodynamic properties of the gas samples. In order to create a general modification of these thermodynamic models, an enormous amount of experimental results and tuning work were required. Before began conducting the PVT tests, many technical challenges, as well as difficulties fine tuning the equipment were faced. Therefore, several extensive preliminary tests were required prior to PVT testing

This research presented a methodology to properly conduct an evaluation for each reservoir that could possible to be developed based on marine CNG technology. It was shown that unlike transportation using pipeline technology, extensive offshore hydrocarbon dew pointing may not necessarily be required. The gas with relatively high NGL content could be stored in CNG tanks and shipped to destination for further processing and NGL recovery. This would improve the economics of gas transportation using the marine CNG technology.

The proposed work addressed research areas and matters related to the following: thermodynamic models, experimental operations of PVT cells, gas chromatography, densitometry, tuning and optimization techniques, process modeling/simulation and liquid-vapour equilibrium studies, advanced thermodynamics, and mathematical modeling.

8.3 Major Contributions

The area of Newfoundland and Labrador as well as many other regions around the world possess a large number of stranded gas reservoirs that currently cannot be exploited due to economical and technical reasons. This thesis addresses Marine CNG technology as an option to monetize stranded natural gas reservoir (more particularly condensate reservoirs). Employing this technology the natural gas can be transported from offshore to onshore by shipping in the form of compressed natural gas (CNG).

Loading and unloading the gas into and from high pressure storage vessels (tanks) on board of ships involves significant technical problems. During these operations, the gas experiences phase changes, and variation in temperature and pressure. The accurate predictions of these changes are necessary to facilitate a safe and optimal operation. The accuracy of the predictions requires reliable equation of state (EOS). This research evaluates the accuracy of the most widely used EOS by the industry, namely PR and SRK, for diverse gas compositions. It demonstrated that their accuracy is reduced as the amount of heavier hydrocarbons increases in the gas composition (even for gas compositions where all the components are known).

A methodology to evaluate a gas reservoir for Marine CNG technology is presented. The methodology is demonstrated through three main steps:

- Performing experiments,
- Evaluating and tuning the equations of states, and

- Performing dynamic simulations to model the loading and unloading operations of a CNG tanks

To improve the predictions of equations of states, the binary interaction parameters (BIN) and the Peneloux parameters were proposed to be tuned. The k_{ij} could also be adjusted and depended on the gas composition. It was shown that for cases where the gas contained a heavy hydrocarbon fraction (C_7^+), this fraction could be characterized into six pseudo components and by tuning the k_{ij} between methane and the first two pseudo component and setting the rest to zero better predictions could be achieved.

8.4 Recommendations

To determine the suitability of a certain gas reservoir for marine CNG transportation, a complete analysis of the gas behaviour during the loading and unloading operations is required. The extent of condensate removal before loading the gas to the CNG tanks also needs to be evaluated. This research proposed a methodology to determine the proper design of the loading and unloading systems and to estimate if a gas reservoir could potentially be developed based on marine CNG technologies. In order to properly implement the proposed methodology, a more sophisticated system than just a PVT cell will be needed. To verify the accuracy of thermal modeling and gas behaviour, a properly designed test tank is required in order to simulate the actual large scale of CNG tanks. Therefore, the heating loss that a CNG tank will experience in a ship should be represented in the small test cylinder used in the laboratory. The overall thermal phenomena including gas cooling and heat transfer should be measurable during the lab

tests. Knowing the real temperature-pressure behavior during the loading and unloading operations will help to improve the thermodynamic models and therefore obtain a proper design of these operations.

An optimization on the EOS adjustable parameters is required in order to attain the best possible values that will improve the EOS predictions (such as k_{ij} or Peneloux parameters). To achieve this optimization, an extensive number of experimental data is required. Depending on the type of gas, the predictions of the EOS for the gas behaviour and properties will deviate differently respect to actual values. Therefore, it is recommended to conduct an optimization tests on the adjustable parameters for each type of gas separately. For instance, lean gases, moderate rich gases, and rich gases may all have different values' parameters to predict accurately the thermodynamic properties and behaviour of the gases. It is also recommended to evaluate the thermodynamic behaviour of gases with different percentages of non-hydrocarbon components, such as N_2 or CO_2 , since, as it was illustrated in this research, these components could enormously affect the predictions depending on their compositions in the gas samples. All these evaluations could only be achieved with a large database of experimental results for each type of gas.

Chapter 7 illustrates through dynamic simulations the temperature, pressure and liquid dropout changes of the gas during the loading and unloading operations of a CNG tank. The dynamic simulations were performed evaluating the effect of diverse operating parameters (such as temperature of the feed, pressure of the feed, molar flow rate) one at

a time. As a future work, it is recommended to evaluate the interaction among the parameters, which can be achieved employing a formal method of design of experiments.

REFERENCES

Abdi M., Hawboldt K., and Hussain A., "Gas Behaviour during Loading and Unloading: Need for Standard Gas Behaviour Tests", at the International Marine CNG Standards Forum, 7-9 November 2006.

Aminian K., Brannon A., and Ameri S., "Evaluation of a Depleted Gas-Condensate Reservoir for Gas Storage", at the 2004 SPE Eastern Regional, Charleston, West Virginia, U.S.A 15-17 September 2004, SPE 91483.

Anton Paar, Instructional Manual DMA HPM Density Measuring Cell for High Pressure and High Temperatures, 2005a.

Avila S., Blanco S., Velasco, I., Rauzy E., and Otin S. "Thermodynamic Properties of Synthetic Natural Gases. 1. Dew Point Curves of Synthetic Natural Gases and Their Mixtures with Water and with Water and Methanol: Measurement and Correlation" J. Ind. Eng. Chem. Res., 2002a, 41, 3714-3721.

Avila S., Blanco S., Velasco I., Rauzy E., and Otin S., "Thermodynamic Properties of Synthetic Natural Gases. 2. Dew Point Curves of Synthetic Natural Gases and Their

Mixtures with Water and Methanol. Measurement and Correlation”, Energy & Fuels 2002b, 16, 928-934

Bashbush J.L; “ A Method to Determine K-Values From Laboratory Data and Its Applications”, paper SPE 10127 presented at the 56th Annual Fall Technical Conference and Exhibition of the SPE of AIME, held in San Antonio, Texas, USA, 5-7 October 1981.

Beronich E., Abdi M., and Hawboldt K., “Prediction of natural gas behaviour in loading and unloading operations of marine CNG transportation systems”, Journal of Natural Gas Science and Engineering (May 2009). (a)

Beronich E., Abdi M., and Hawboldt K., “Recovering Natural Gas Liquids in Atlantic Canada’s Offshore Petroleum Production Projects”, the 85th GPA Annual Convention in Grapevine, (March 2006). (b)

Biopact Team, “A quick look at CNG ships”, News from September 05, 2007

Capa L., Buryan P., Jedelsy J., Rottner M., and Linek J. “Isothermal p V T measurements on gas hydrocarbon mixtures using a vibrating-tube apparatus”. J. Chem. Thermodynamics 2002, 34, 657-667.

Coats, K., and Smart G. “Application of a Regression-Based EOS PVT Program to Laboratory Data”, SPE Reservoir Engineering, 1986, 277-299.

Dandekar A., and Patil S.; “Insights into Tuning of Equations of State Models of Natural Gas (LNG & CNG) and Liquefied Petroleum (LPG) Bearing Petroleum Reservoir Fluids”; The Seventeenth International Offshore and Polar Engineering Conference, Lisbon, Portugal July 1-6, 2007.

Dandekar A. Y., “Effect of Fluid Characterization on CVD Liquid Drop-out Predictions of Gas Condensate Fluids Using an Equations of State Model”, Energy Sources, Part A: Recovery, Utilization, and Environmental Effects, 30:16, 1548-1562, 2008.

Danesh, Ali.; ”PVT and phase behaviour of petroleum reservoir fluids”. Elsevier Science, 1998.

Dustman T., Bergman D., and Bullin J.; “An Analysis and Prediction of Hydrocarbon Dew Points and Liquids in Gas Transmission Lines”, at Gas Processors Association (GPA) Annual Meeting, Grapevine, TX, U.S.A March 5-8, 2006.

EIA (Energy Information Administration) - International Energy Outlook 2011.

Elsharkawy A., "Characterization of the Plus Fraction and Prediction of the Dewpoint Pressure for Gas Condensate Reservoirs", at the 2001 SPE Western Regional Meeting, Bakersfield, California, USA, SPE 68776, 26-30 March 2001.

Hine L., "CNG vs LNG for Tobago gas play", LNG Unlimited Newsletter, 22 December, 2011.

Esmail T., and Qallaf A.; "Compositional and PVT Analysis for Determining Liquid Dropout in Pipelines", at the Abu Dhabi International Petroleum Exhibition and Conference, Abu Dhabi, UAE, January, 2009.

Hanrahan Michael; "Marine CNG – The Evolution of New Natural Gas Technology", Gas Processors Association (GPA) Europe, Conference Paper, September 2008.

Jarne C., Avila S., Blanco S. T., Rauzy E., Otin S., and Velasco I. "Thermodynamic Properties of Synthetic Natural Gases. 5. Dew Point Curves of Synthetic Natural Gases and Their Mixtures with Water and with Water and Methanol: Measurement and Correlation" J. Ind. Eng. Chem. Res., 43, 209-217, 2004.

Jhaveri B. and Youngren G.; “Three Parameter Modification of the Peng-Robinson Equation of State to Improve Volumetric Predictions”, SPE Reservoir Eng., 1033, 1988.

Jones D.; and Erbar J.; “Computer Determination of Data-Matched Equilibrium Ratios”, Journal of Petroleum Technology, August 1970.

Katz D., “Overview of Phase Behaviour of Oil and Gas Production”, Journal of Petroleum Technology, Vol 228, 1205-1214, 1983.

Liang B., Balasubramanian S., Wang B., Jensen C., Yang A., and Kennedy D.; “PVT characterization and compositional modelling of gas condensate and volatile oil reservoirs”, International Journal Oil, Gas and Coal Technology, Vol. 4, N° 1, 2011.

Magee J. W., Haynes W. M., and Hiza M. J. “Isochoric (p, ρ , T) measurements for five natural gas mixtures from T= (225 to 350) K at pressures to 35 MPa”, J. Chem Thermodynamics 29, 1439-1454, 1997.

Manning, Manning, F. S. and Thompson R. E., Oilfield Processing of Petroleum, Vol. One: Natural Gas, PennWell Books, Tulsa, Oklahoma, 1991.

Morch O., Nasrifar Kh., Bolland O., Solbraa E., Fredheim A., and Gjertsen L.; “Measurement and modeling of hydrocarbon dew points for five synthetic natural gas mixtures”. *Fluid Phase Equilibria* 239, 138-145, 2006.

Nasrifar K. and O. Bolland. “Predicting Natural Gas Dew Points from 15 Equations of State”. *Energy & Fuel*, 19, 561-572, 2005.

Nasrifar K., and Bolland O.; “Predicting Natural Gas Dew Points from 15 Equations of State”, *Energy & Fuels* 19, 561-572, 2005.

Nasrifar K., and Bolland O., “Prediction of Thermodynamic Properties of Natural Gas Mixtures using 10 Equations of State Including a New Cubic Two-constant Equation of State”, *Journal of Petroleum Science and Engineering*, 51, 253-266, 2006.

Pedersen K., and Christensen P., “Phase Behaviour of Petroleum Reservoir Fluids”. Taylor & Francis Group, 2007.

Pedersen, K.S., Fredenslund, Aa. and Thomassen, P.: *Properties of Oils and Natural Gases*, Gulf Publishing Co., Houston, Texas, 1989.

Peneloux A., Rauzy E., and Freze R; “A consistent correction for Redlich-Kwong-Soave volumes” *Fluid Phase Equilibria* 8, 7-23, 1982.

Peng D., and Robinson D.; "A new two-constant equation of state", *Ind. Eng. Chem. Fundam.* 15, 59-64, 1976.

Peng D., and Robinson, D.; "The characterization of the heptanes and heavier fractions for the GPA Peng-Robinson Programs", GPA Research Report RR-28, 1978.

Rynn P., Patel H., and Serratella C.; "ABS Development of a Guide for Compressed Natural Gas Carrier", Offshore Technology Conference, Houston, Texas, 30 April-3 May, 2007.

Rackett H.; "Equation of state for saturated liquids", *J.Chem. Eng. Data* 15, 59-64, 1976.
Soave G.; "Equilibrium constants from a modified Redlich-Kwong equation of state", *Chem. Eng. Sci.* 27, 1197-1203, 1972.

Samaniego-V. F.; Bashbush, B.J.L.; Leon, G.A.; Mazariegos, U.C.; Corona, B.A., Castillo, P.P.F.; "On the Validation of PVT Compositional Laboratory Experiments", paper SPE 91505 presented at the SPE Annual Technical Conference and Exhibition held in Houston, Texas, USA, 26-29 September 2004.

Trengove R.D.; Hann, J.H.; and Skates J. R.; "The impact of PVT Data Quality on Hydrocarbon Recovery Predictions", paper SPE 22988 presented at the SPE Asia-Pacific Conference held in Australia, 4-7 November 1991.

Valsgård S., Lothe P., Strom N., Mørk K., Ng E. and Roper N.; “CNG - A Competitive Ship Transport Solution for Natural Gas”, Singapore Maritime & Port Journal, 2004.

Whitson, C.H., Anderson, T.F. and Soreide, I.: “C7+ Characterization of Related Equilibrium Fluids Using the Gamma Distribution,” Presented in Chorn, L.G. and Mansoori, G.A.: C7+ Fraction Characterization, Taylor & Francis New York Inc., New York 35, 1989.

Whitson, C.H., Anderson, T.F. and Soreide, I.: “Application of the Gamma Distribution Model to Molecular Weight and Boiling Point Data for Petroleum Fractions,” Chem. Eng. Comm. 96, 259, 1990.

Yang T., Chen W., and Guo T. “Phase behaviour of a near-critical reservoir fluid mixture”. J. Fluid Phase Equilibria, 128, 183-197, 1996.

Zuo J., and Zhang D.; “Plus Fraction Characterization and PVT Data Regression for Reservoir Fluids near Critical Conditions”, SPE - Asia Pacific Oil and Gas Conference, Proceedings - SPE Asia Pacific Oil and Gas Conference and Exhibition, p 1235-1246, 2000.

APPENDIX A

A.1 Initial Mass Balance for first CVD sample using experimental data

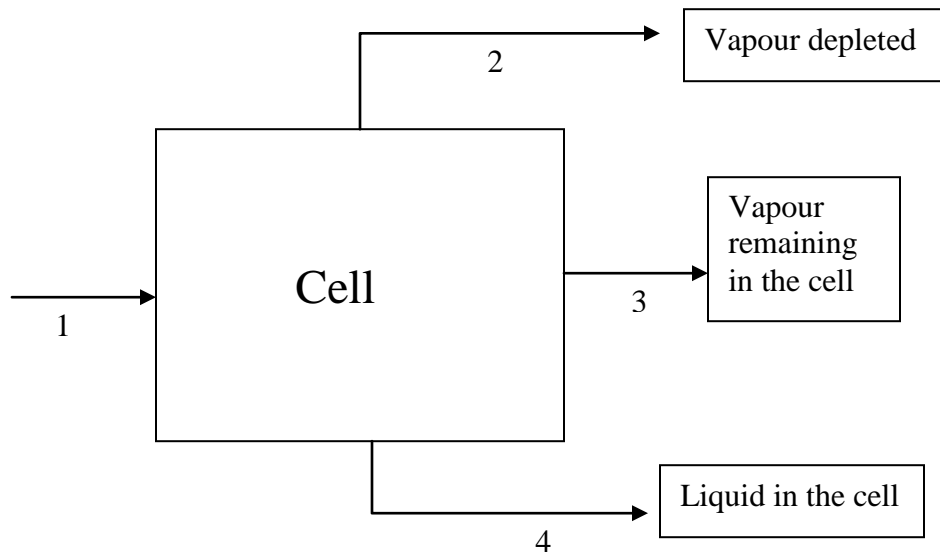


Figure A.1: Block diagram of the streams involved in a CVD test

Data:

n_1 = moles of component 1

V_1, V_2, V_3 = Molar volume of components 1, 2 and 3

Y_{j1}, Y_{j2}, Y_{j3} = vapor molar fraction of component j for vapor streams 2 and 3 (stream 2 and 3 have the same composition)

ρ_2 = gas density of stream 2

MW_j = molecular weight of component j

Unknown:

n_2, n_3, n_4 = total moles in streams 2, 3 and 4

X_{j4} = liquid molar fraction of component j

K_j = equilibrium constant of component j

A.1.1 System of equations to solve unknown

$$MW_2 = \sum_{i=1}^j Y_{j2} * MW_j \quad \text{Molecular weight of stream 2}$$

$$n_2 = \frac{V_2 * \rho_2}{MW_2} \quad \text{Moles depleted (stream 2)}$$

$$Z_2 = \frac{P * V_2}{n_2 * R * T} \quad \text{Compressibility factor of gas depleted}$$

$$n_3 = \frac{P * V_3}{Z_2 * R * T} \quad \text{Gas moles remaining in the cell (stream 3)}$$

$$n_4 = n_1 - n_2 - n_3 \quad \text{Liquid moles in the cell (stream 4)}$$

$$X_{j4} = \frac{n_1 * Y_{j1} - n_2 * Y_{j2} - n_3 * Y_{j3}}{n_4} = \frac{n_1 * Y_{j1} - Y_{j2} * (n_2 + n_3)}{n_4} \quad \text{Liquid Fractions (stream 4)}$$

$$K_j = \frac{Y_{j2}}{X_{j4}} \quad \text{Equilibrium constants}$$

A.1.2 Result of Mass balance using experimental data for First CVD sample

Table A.1: Mass Balance Results for First CVD sample

Pressure (psia)	Vol After Sampling			Vapor Displaced				Total Moles remaining in the cell	ZGD from gas depleted	Vapor Moles in the Cell	Liquid Moles in the Cell
	Total (cc)	Liquid (cc)	Vapor (cc)	Volume (cc)	Density (g/cc)	MW	Moles (gmoles)				
1676	55.74	12.44	43.30	5.55	0.1436	24.78	0.0322	0.270	0.766	0.2510	0.0192

Note: The values in blue are measured values (MW is measure through gas composition and calculated)

Table A.2: Liquid fractions and K-values resulting from mass balance

	Moles Fractions			K-values
	MW	Vapor	Liquid	
C1	16.04	0.703	-0.235	-2.9866
C2	30.07	0.107	0.149	0.7181
C3	44.10	0.112	0.367	0.3050
i-C4	58.12	0.019	0.108	0.1759
n-C4	58.12	0.000	0.516	0.0000
Neopentane	72.15	0.024	-0.355	-0.0681
i-C5	72.15	0.013	0.140	0.0959
n-C5	72.15	0.011	0.124	0.0867
C6	84.00	0.006	0.090	0.0626
n-C7	100.20	0.001	0.048	0.0274
n-C8	114.00	0.001	0.076	0.0074
N2	28.01	0.003	-0.027	-0.1150
		1.000	1.000	

It can be observed that three components have negatives liquid fractions.

A.1.3 Checking consistency of the data

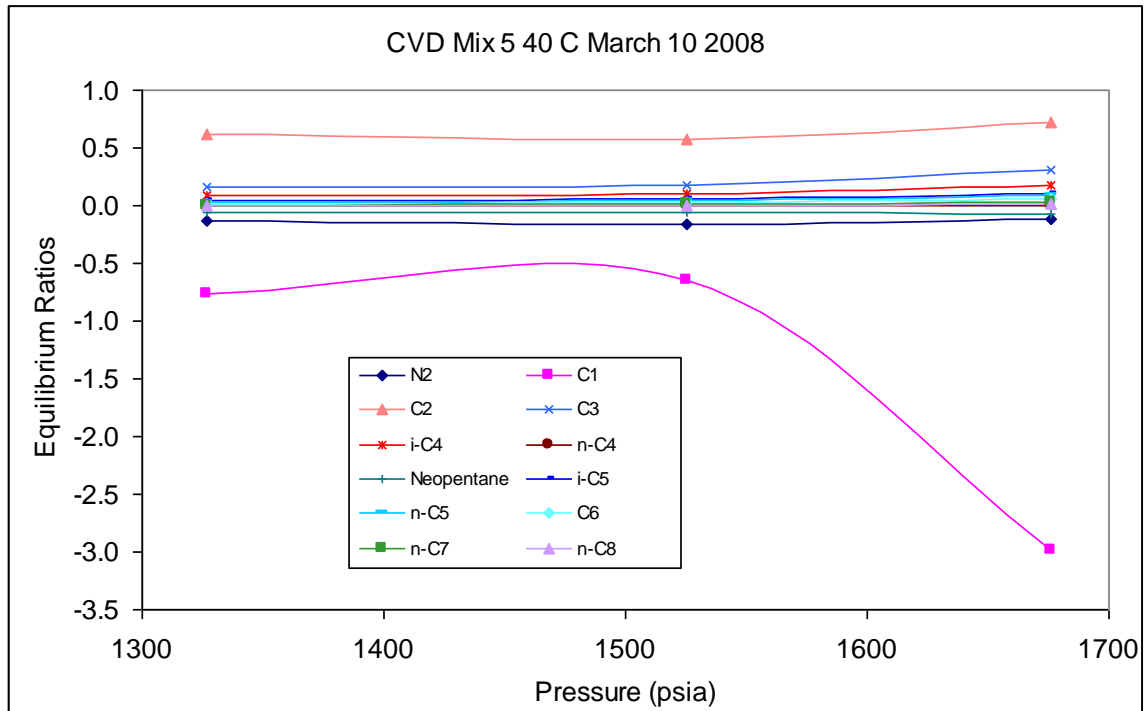


Figure A.2: Plot of the K values obtained through the material balance procedure versus pressure.

The curves illustrated in Figure A.2 should plot in a parallel-like trend with no humps inconsistent or crossings. The upper curve (higher K-values) should correspond to nitrogen (N₂), followed by the curves of methane (C₁) and carbon dioxide (CO₂). Then, it follows either the curve of ethane (C₂) or the curve of hydrogen sulfide (HS₂) (depending on the fluid and reservoir temperature). Underneath the remaining component curves should plot in increasing order of the molecular weight (or normal boiling points). The K value of the isobutene and isopentane should always be higher than those corresponding to the “normal” components.

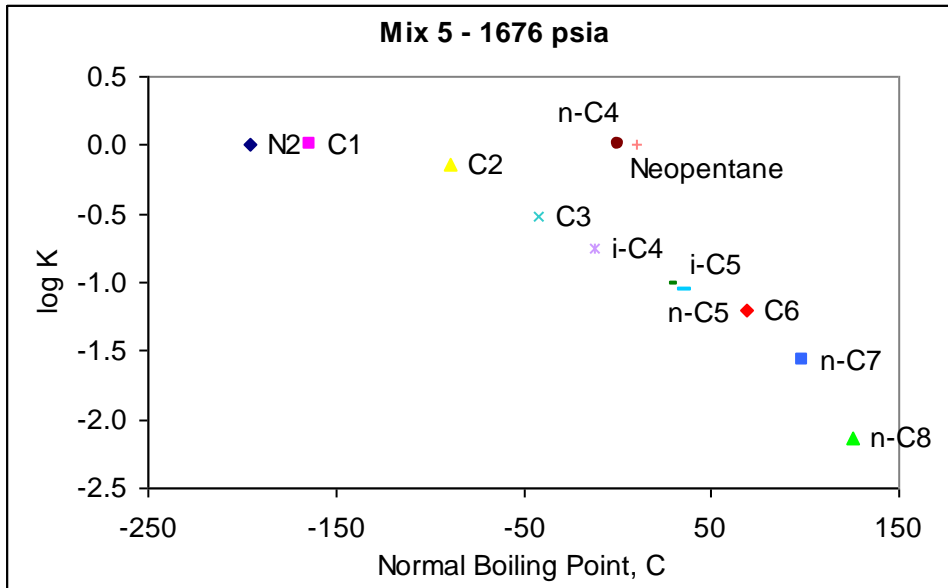


Figure A.3: Plot of Log K versus Normal Boiling Point to check consistency of the data

Figure A.3, which illustrates log K-values versus normal boiling points of the different components of the hydrocarbon mixture is also a sensitivity data check. This graph should closely follow a straight line and humps indicate errors in the measurements. The order of the K ratios should be the same that expressed for Figure A.2. It can be observed from Figure A.3, that nC4 and Neopentane fall out of an imaginary straight line as well as N2 and C1.

A.1.4 New K-values to re-calculate the mass balance

The new values of K are obtained using a least squares straight line (see Figure A.4). These values are used to calculate again the mass balance and modify slightly the vapor

mole fractions obtained experimentally through gas chromatography in order to have consistency in all the data.

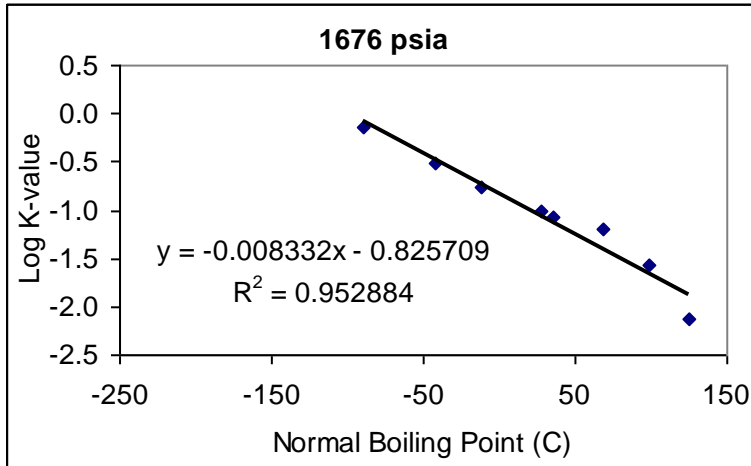


Figure A.4: Correction graph of Log K_j versus normal boiling points.

A.2 Experimental Procedures

Steps to prepare a gas mixture

In order to prepare a gas sample in the laboratory, initial calculations are required to estimate the amount of each component needed for the desired composition. Therefore, the first steps for preparing a gas mixture involve calculations and then some measurements. The steps that need to be followed to prepare a gas sample using the experimental set up outlined in Section 3.2 are described as follow:

- 1- The steps to prepare a gas sample mixture using the above described experimental set up is described below. The first steps are the initial calculation required to estimate the amount of each component added into the sample cylinder. The following steps refers to the actual preparation of the sample. Select the composition of the gas mixture desired to prepare in the laboratory.
- 2- Use Hysys to calculate the mass density of the mixture at the final temperature (room temperature) and pressure in the sample cylinder. (Note: the highest pressure is restricted by the highest pressure of the methane cylinder. In the case another gas sample cylinder is available, methane and any other gas can be sent to this cylinder and compressed to a higher pressure). Knowing the mass density, calculate the total mass of the mixture (M) for the volume of the gas sample cylinder (629 cc) at the final temperature and pressure selected. Then, calculate the mass of each component (m_i) by multiplying the mass fraction times total mass ($m_i = x_i * M$).
- 3- In Hysys, create a new case and place a stream with a close loop and fix volume (volume of the sample cylinder). Use this case to calculate the pressures built inside the sample cylinder every time a new component is added (employ mass flow). The first components added are the liquid components (iC_5 , nC_5 , nC_6 , nC_7 , nC_8). Then, the following heavier gas component is added and the pressure inside the sample cylinder is calculated. The order of adding the gas components is: nC_4 , iC_4 , C_3 , C_2 , CO_2 , N_2 , and finally C_1 .

Note: It could be possible that for a particular component, the pressure calculated is higher than its available pressure in the pure gas cylinder in the laboratory. In that case, the gas mixture composition needs to be reviewed and modified according the maximum pressures available in the pure gas cylinders of each individual component. This recalculation could be avoided if an extra sample cylinder is available in the lab. Each gas component can be sent from its pure gas cylinder to a secondary sample cylinder to be compressed up to the required pressure.

- 4- Once all the pressures and mass for each component are known, the gas mixture can be prepared. The first step is to clean with solvent, and vacuum the high pressure gas sample cylinder to ensure there are not any traces of previous gas samples remaining inside the cylinder. Then, the empty weight of the sample cylinder is measured and registered for reference.
- 5- With the sample cylinder ready, the components of the mixture can start to be added. Liquid hydrocarbon components (pentanes, normal hexane, normal heptane, and normal octane) are placed into a beaker; with a syringe they are taken and injected in a plastic line, which has one end connected to the sample cylinder and the other end opened. When the valve of the sample cylinder is opened to introduce the liquids, only liquid should be sucked into the cylinder (under vacuum). After transferring the liquids, the pressure and the weight of the sample cylinder should be measured to check if these values match with the calculated ones. As more components are added into the cylinder, reaching the

equilibrium takes longer time and the pressure keeps changing until the equilibrium is reached. Therefore, measuring the weight of the sample cylinder could be more effective than measuring the pressure.

- 6- After adding the liquids, the sample cylinder is connected to the gas preparation setup illustrated in Figure 3.3, and all the lines should be evacuated. There are five valves between the pure gas cylinders and the sample cylinder that each gas component will encounter. The first valve is the one in the pure component cylinder, the second valve is placed in the panel to facilitate the addition of the pure gases directly from the panel instead from each pure gas cylinder (there are one valve in the panel for each component, see Figure 3.3), The third valve is the high precision valve to control the flow. The fourth valve connects the two pressure gauges and the line to the sample cylinder, and the fifth valve is the actual valve on the sample cylinder. The positions of all these valves should be close before adding a new component; they should be opened one by one from the pure gas cylinder until the sample cylinder.
- 7- The gaseous components are added one by one in an ascending vapour pressure order, starting from butanes, propane, and ethane, continuing with carbon dioxide, nitrogen, and finally methane. After adding a new gas component, it is necessary to give time to the components for mixing (it is a non-ideal mixture and equilibrium is not reach instantaneously). In order to accelerate the time to reach equilibrium, the extremes of the sample cylinder are moved up and down so the ball (piston) contained inside moves and helps the components to mix.

After giving sufficient time for the gas mixture to reach equilibrium (in general several hours may be needed if the sample contains large amount of condensates), a gas sample should be taken and sent to the gas chromatogra

Table A.3: Recalculation of the K-values using the least squares straight line illustrated in Figure 3.

1676 psi				
Components	Boiling Point (°C)	New Log K	Old K-values	New K-values
N2	-195.0	0.799	-2.9866	6.296
C1	-164.0	0.541	0.7181	3.473
C2	-89.0	-0.144	0.3050	0.718
C3	-42.0	-0.516	0.1759	0.305
i-C4	-11.7	-0.755	0.0000	0.176
n-C4	-0.5	-0.822	-0.0681	0.151
Neopentane	10.0	-0.909	0.0959	0.123
i-C5	28.0	-1.018	0.0867	0.096
n-C5	36.1	-1.062	0.0626	0.087
C6	69.0	-1.203	0.0274	0.063
n-C7	98.4	-1.562	0.0074	0.027
n-C8	125.5	-2.131	-0.1150	0.007

The new values of K are used to re-calculate the moles fractions.

APPENDIX B

In order to determine the value of the density of a gas sample the densitometer was calibrated using pure gas samples of well known density, such as nitrogen. The densities were measured at temperature constant and changing the pressure. As a result, a set of parallel lines were obtained after plotting density versus period. Figure B.1. illustrates these curves for each temperature measured (-10, 0, 10, 40 and 60 °C).

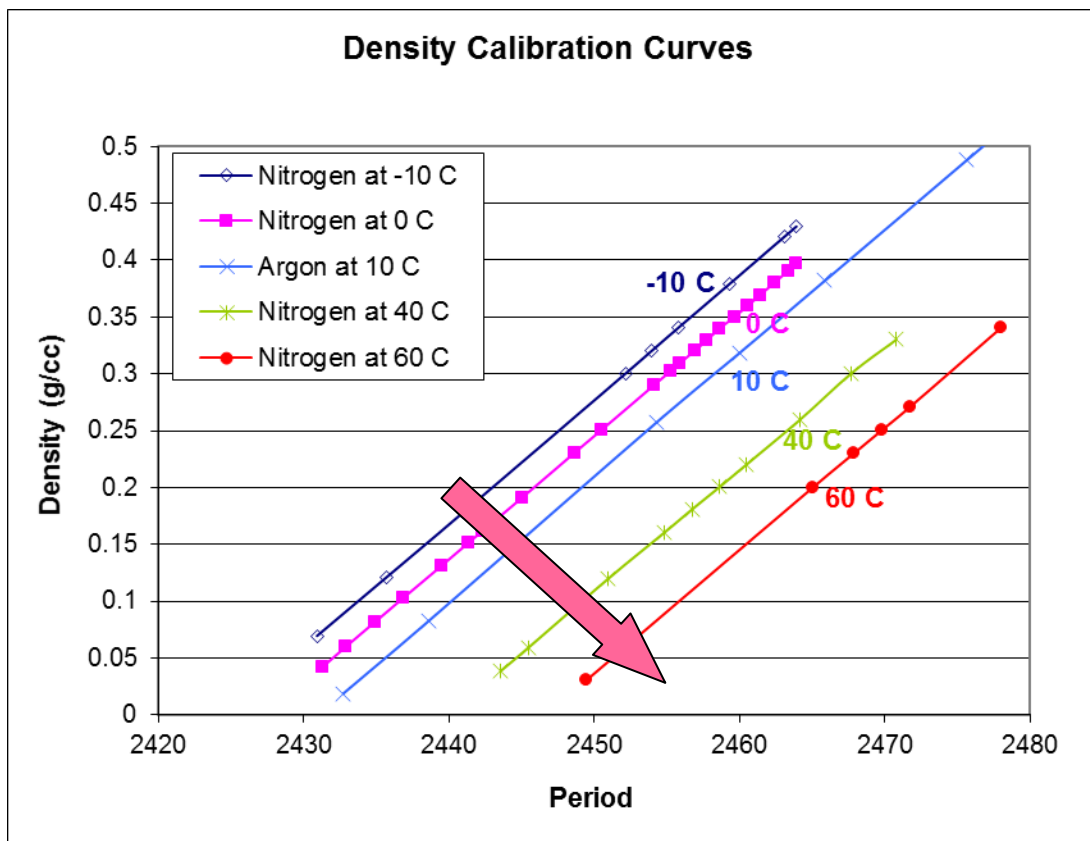


Figure B.1: Nitrogen density curves for diverse temperatures

The equations representing each line are indicated in Table B.1.

Table B.1: Equations of the calibration curves of Nitrogen at diverse temperatures

Temperature (°C)	Equation for the density
-10	$y = 0.010924395 x - 26.487470627$
0	$y = 0.010866573 x - 26.377669006$
40	$y = 0.010744715 x - 26.118083246$
60	$y = 0.010649931 x - 26.052813037$

All the lines are linear and only vary slightly in the slopes and the constants. Therefore, it was assumed that the density varies linearly with the pressure at a constant temperature.

The common form of a linear equation in the two variables x and y is indicated in equation B.1:

$$y = a.x + b \tag{B.1}$$

Using all the equations, the dependencies of the slope and the constant with the temperature were evaluated. Both variables were plotted against temperature and the tendency curves were obtained. Figures C.2 and C.3 show the curves of the slope and constant versus temperature, respectively.

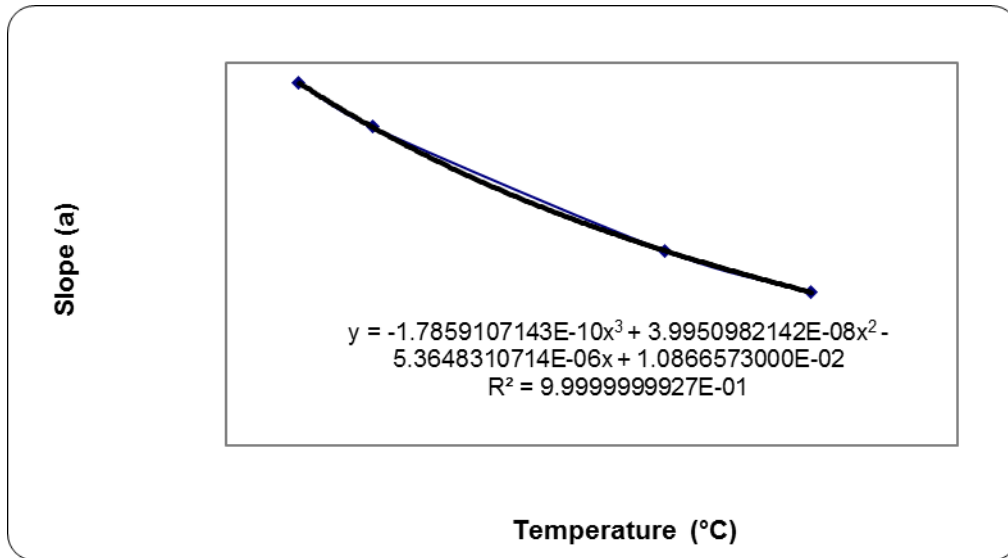


Figure B.2: Dependency of the slope with the temperature

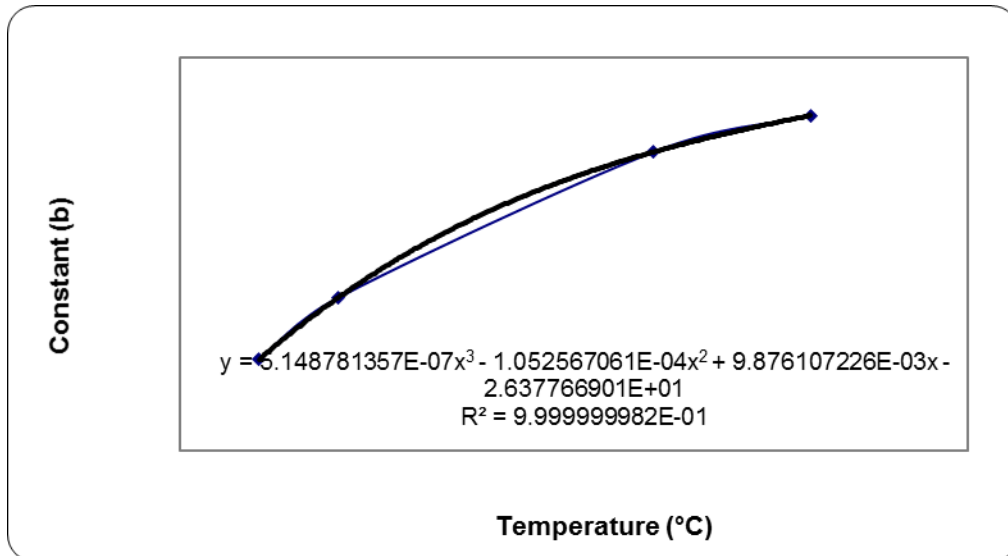


Figure B.3: Dependency of the constant with the temperature

The determination of the dependency of the slope with the temperature can be obtained from Figure B.2 and it is indicated in Equation B.2.

$$a(T) = -1.7859107143E^{-10} * T^3 + 0.000000039950982142 * T^2 - 0.0000053648310714 * T + 0.01086657$$

(B.2)

The determination of the dependency of the constant with the temperature can be obtained from Figure C.3 and it is indicated in Equation B.3.

$$b(T) = 0.0000005148781357 * T^3 + 0.000105256706 * T^2 - 0.009876107226 * T - 26.37766901$$

(B.3)

The density is calculated as indicated in Equation C.4:

$$\rho = a(T).Period + b(T) \tag{B.4}$$

APPENDIX C

C.1 Experimental Errors of the data of synthetic gas samples obtained from the literature

C.1.1 Experimental data obtained from literature for evaluating Dew Points

a) SNG1, SNG4, SNG5, SNG6, y SNG8

Reference: “Measurement and modeling of hydrocarbon dew points for five synthetic natural gas mixtures” Ø. Mørcha, Kh. Nasrifar, O. Bolland, E. Solbraa, A.O. Fredheim, L.H. Gjertsen *Fluid Phase Equilibria* 239 (2006) 138–145

In order to evaluate the effect of hydrocarbons on the dew points, the gas mixtures evaluated only contained hydrocarbon components without the presence of non-hydrocarbon components (such as nitrogen and carbon dioxide). The synthetic natural gases were all gravimetrically calibrated and the relative uncertainty in the compositional analysis was less than 0.5% for all components. The composition were verified by chromatography using the procedures in GPA 2286-95 and ASTM D5134/92, and they are expressed in Table C.1.

The dew points were measured with a dew point mirror and cooling system manufactured by Chandler Engineering; and the uncertainty for the temperature was ± 0.1 on the range of -103.15 to 146.85 °C. The ranges of temperature and pressure used to

measure the dew points were from -38.15 to -11.75 °C and from 0.3 to 10 MPa, respectively.

The dew point curve was recreated by measuring around 20 dew point between a high pressures (close to the cricondenbar point) to a low pressure. All the measurements were taken twice to verify their repeatability, and the maximum deviation between two measurements, along the range of pressure taken, was less than 1 K.

Table C.1: Gas compositions

Component	SNG1 (SNG2 on the paper)	SNG4 (SNG5 on the paper)	SNG5 (SNG1 on the paper)	SNG6 (SNG3 on the paper)	SNG8 (SNG4 on the paper)
Methane	0.84280	0.93600	0.93505	0.96611	0.94085
Ethane	0.10067	0.02630	0.02972	---	0.04468
Propane	0.04028	---	0.01008	---	---
i-butane	0.00597	0.01490	0.01050	0.01527	---
n-butane	0.01028	0.01490	0.01465	0.01475	---
n-pentane	---	0.00795	---	0.00385	0.014470

Note: The compositions for the gases were validated in the Statoil R&D laboratory using gas chromatography.

b) SNG2 (gas 2) y SNG10 (Gas 1)

Reference: “Thermodynamic Properties of Synthetic Natural Gases. 5. Dew Point Curves of Synthetic Natural Gases and Their Mixtures with Water and with Water and Methanol: Measurement and Correlation”, C. Jarne, S. Avila, S. T. Blanco, E. Rauzy, S. Otin, and I. Velasco, *Ind. Eng. Chem. Res.* 2004, 43, 209-217

Composition:

The two synthetic gases (SNG2 and SNG10) were prepared according to the gravimetric method (International Standard ISO 6142: 1981) by Abello-Linde. The compositions of these gas mixture and their accuracy specified by the supplier are listed in Table C.2.

Table C.2: Composition of Synthetic Natural Gases (SNG2 and SNG10) in % mol and Relative Accuracy Specified by the Supplier

Component	SNG2 (Gas 2 on paper)	SNG10 (Gas 1 on paper)
Nitrogen	0.772 ± 2%	1.559 ± 1%
CO ₂	1.700 ± 1%	25.908 ± 1%
Methane	84.446 ± 0.2%	69.114 ± 0.2%
Ethane	8.683 ± 1%	2.620 ± 1%
Propane	3.297 ± 1%	0.423 ± 2%
i-butane	0.293 ± 2%	0.105 ± 2%
n-butane	0.589 ± 2%	0.104 ± 2%
i-pentane	0.084 ± 2%	0.034 ± 2%
n-pentane	0.086 ± 2%	0.023 ± 2%
n-hexane	0.050 ± 2%	0.110 ± 2%

Dew point measurement:

The dew points were measured with a chilled mirror instrument. The uncertainty on the dew point temperature was less than ± 1 K and the pressure transmitter presented a maximum error of 0.1% in the calibrated range. The ranges of pressure and temperature used to measure the dew points were within the typical conditions for transporting natural gas on pipelines and these were from 1.2×10^5 to 81.8×10^5 Pa and -59.56 to -11.76 °C.

c) SNG7 (gas 3) y SNG9 (Gas 1)

Reference: “Thermodynamic Properties of Synthetic Natural Gases. 2. Dew Point Curves of Synthetic Natural Gases and Their Mixtures with Water and Methanol. Measurement and Correlation”, Susana Avila, Sofia T. Blanco, Inmaculada Velasco, Evelyne Rauzy, and Santos Otin, Energy & Fuels 2002, 16, 928-934

Composition:

The synthetic natural gases were prepared according to the gravimetric method (International Standard ISO 6142:1981), by Air-Liquide and Abello'-Linde. The compositions of the SNG mixtures and their accuracy specified by the supplier are listed in Table C.3.

Table C.3: Composition of Synthetic Natural Gases (%mol) and Absolute or relative Accuracy by the supplier

Component	SNG7 (Gas 3 on paper)	SNG9 (Gas 1 on paper)
Nitrogen	0.862 ± 2%	0.67 ± 0.02%
Methane	86.4838	89.9584
Ethane	9.832 ± 1%	8.22 ± 0.17%
Propane	2.388 ± 1%	0.90 ± 0.02%
i-butane	0.183 ± 2%	0.11 ± 0.01%
n-butane	0.231 ± 2%	0.13 ± 0.01%
i-pentane	0.0139 ± 2%	0.0084 ± 0.0002%
n-pentane	0.0063 ± 2%	0.0032 ± 0.001%
n-hexane		

Dew point measurement:

The dew point values are measured by means of a chilled mirror instrument and the range of pressure and temperature selected for the measurements were from 1.4 to 77.7×10^5 Pa and from -73.25 to 10.95 °C, respectively. An MBW Dew Point Instrument, Mod. DP3-D-HP-K2 was used and the uncertainty on the dew temperature was better than ± 0.1 K. The pressure transmitter has a maximum error of 0.1% in the calibrated range.

d) SNG3 (gas 1)

Reference: “Dew points of ternary methaneqethaneqbutane and quaternary methaneqethaneqbutaneqwater mixtures: measurement and correlation”, Sofia T. Blanco, Susana Avila, Inmaculada Velasco, Evelyne Rauzy, Santos Otin, Fluid Phase Equilibria 171, 2000. 233–242

Composition:

The synthetic gas mixture composed by methane, ethane, and butane was supplied by Air Liquide and its composition was verified by chromatographic analysis. The composition of this ternary mixture was 7 ± 0.14 vol.% of ethane, 3.99 ± 0.08 vol % of butane, and 89 vol% of methane.

Dew point measurement:

Experimental dew points were measured for the range of pressure and temperature of 4.77×10^5 and 99.45×10^5 Pa and temperatures from -22.23 to 15.39 °C. The dew point values were measured by means of a chilled mirror instrument, an MBW dew point instrument mod. DP3-D.

The uncertainty in the dew temperature was ± 0.4 K, and the pressure transmitter presented a maximum error of 0.2% in the calibrated range.

C.2 Experimental Errors of the data of natural gas samples obtained from the literature

C.2.1 Experimental data obtained from literature for evaluating Dew Points

a) NG3

The dew point pressures were measured several times but the errors are not reported in the paper.

APPENDIX D

Density

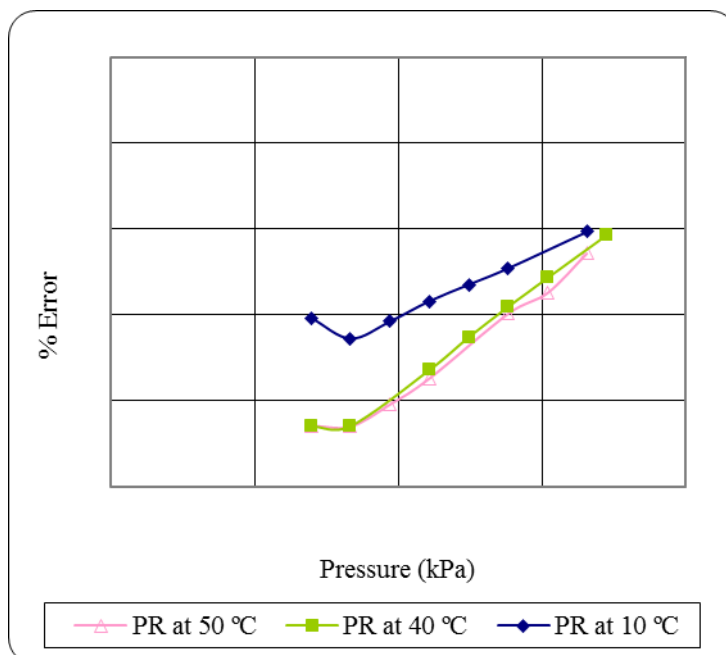


Figure D.1: Percentage errors of mass density predictions of PR in supercritical region at diverse temperatures for Mix 5

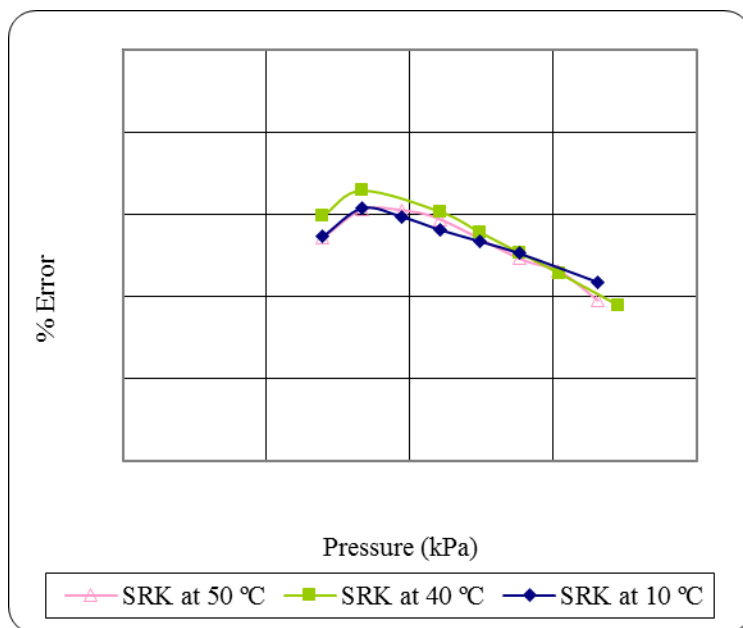


Figure D.2: Percentage errors of mass density predictions of SRK in supercritical region at diverse temperature for Mix 5

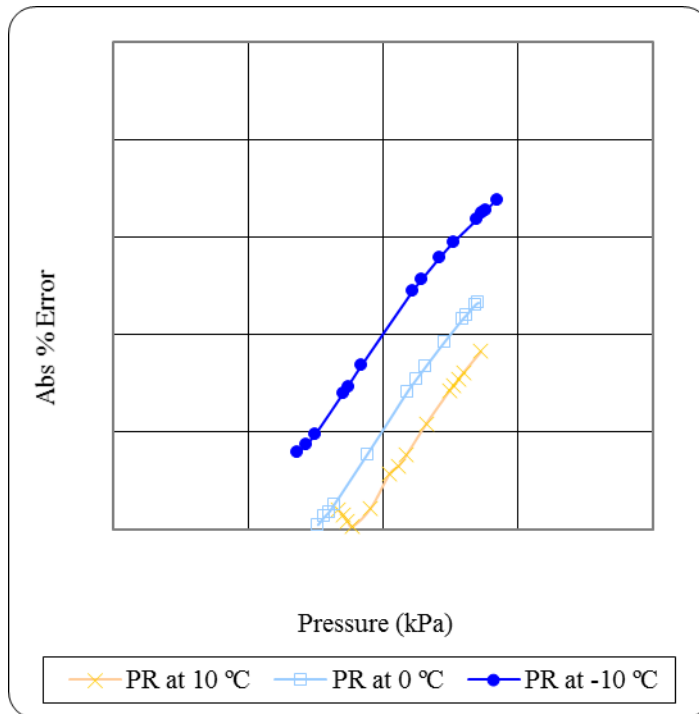


Figure D.3: Percentage errors of mass density predictions of PR in supercritical region at diverse temperature for Mix 4

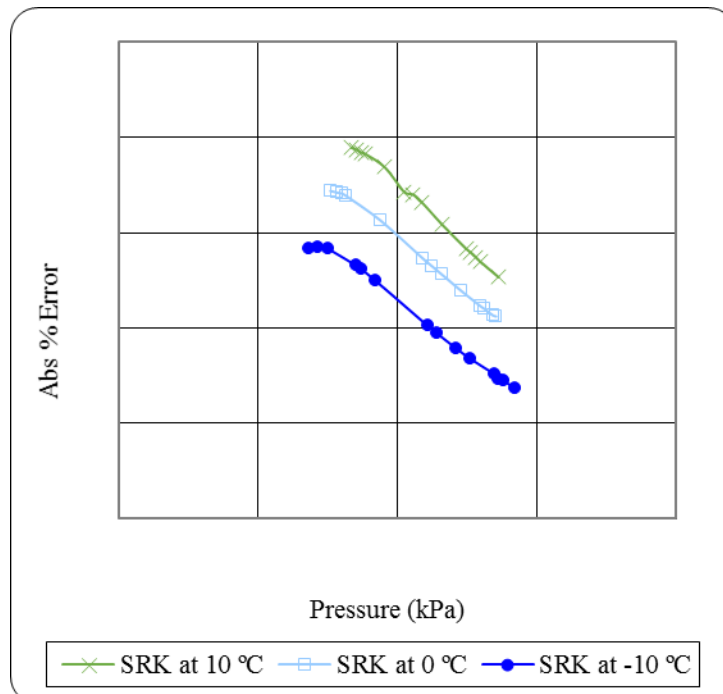


Figure D.4: Percentage errors of mass density predictions of SRK in supercritical region at diverse temperature for Mix 4

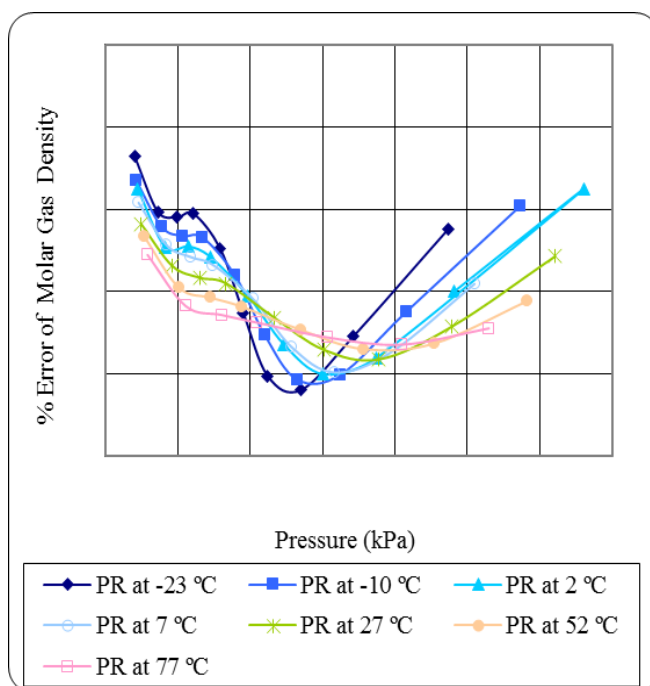


Figure D.5: Percentage errors of molar density predictions of PR in supercritical region at diverse temperature for RG2

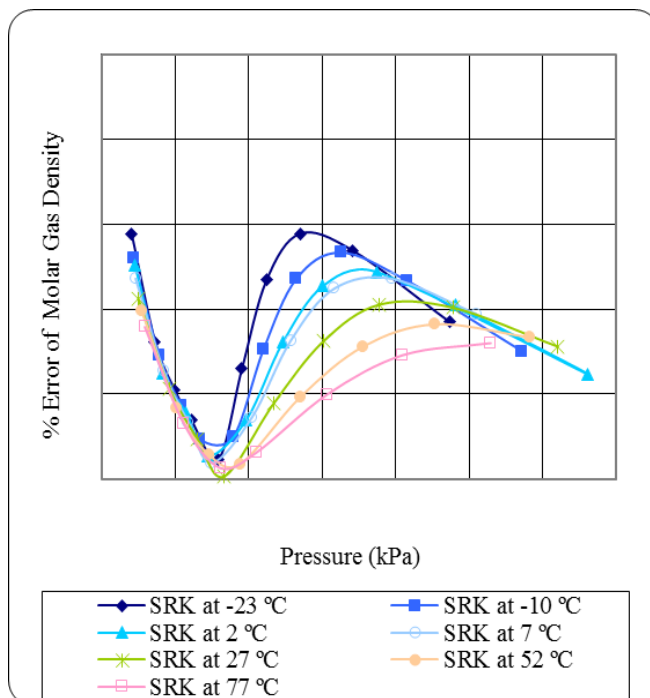


Figure D.6: Percentage errors of molar density predictions of SRK in supercritical region at diverse temperature for RG2

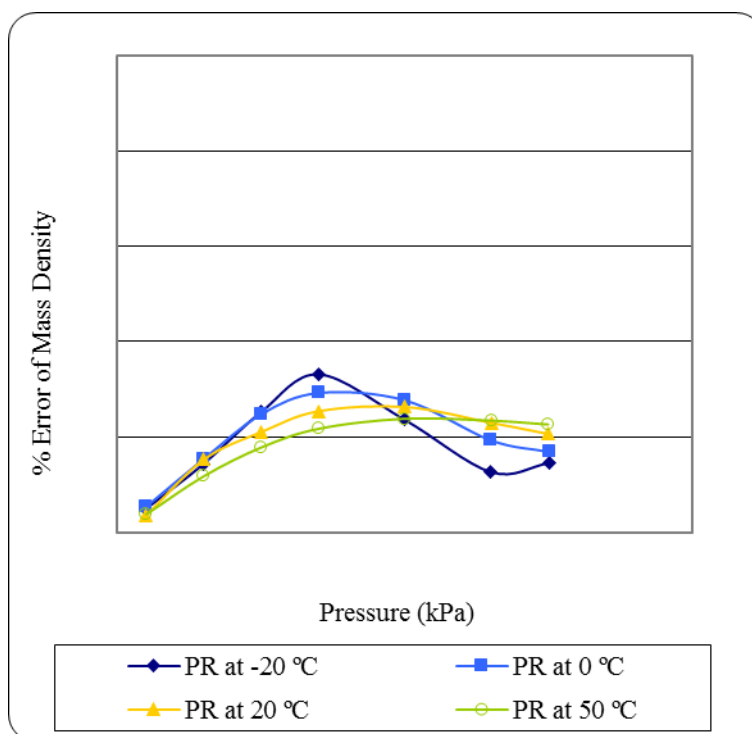


Figure D.7: Percentage errors of mass density predictions of PR in supercritical region at diverse temperature for Gas2

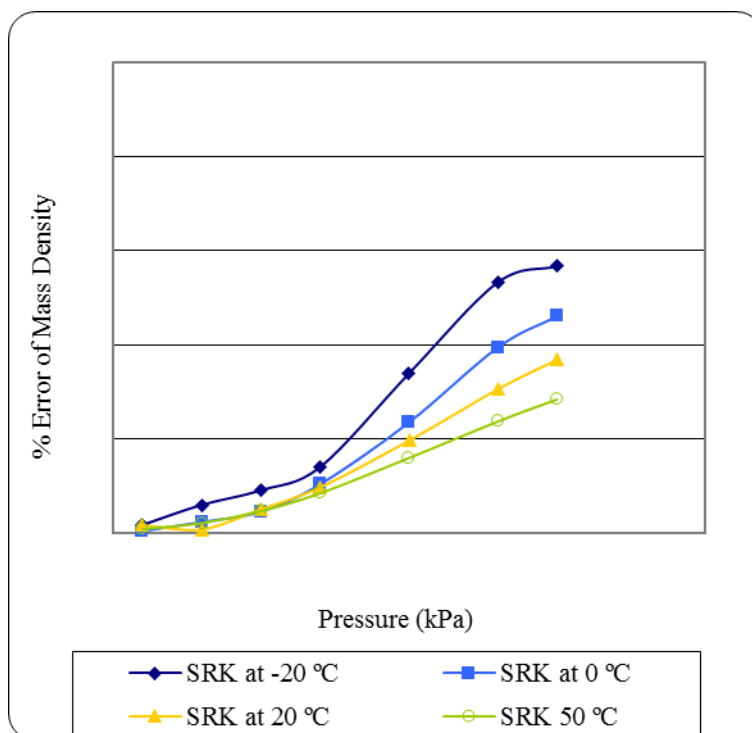


Figure D.8: Percentage errors of mass density predictions of SRK in supercritical region at diverse temperature for Gas2

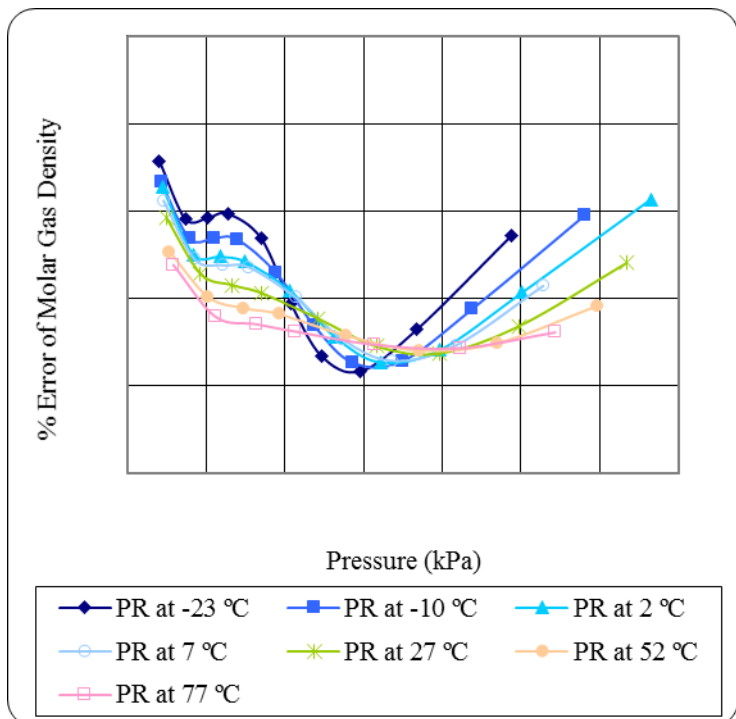


Figure D.9: Percentage errors of molar density predictions of PR in supercritical region at diverse temperature for GU2

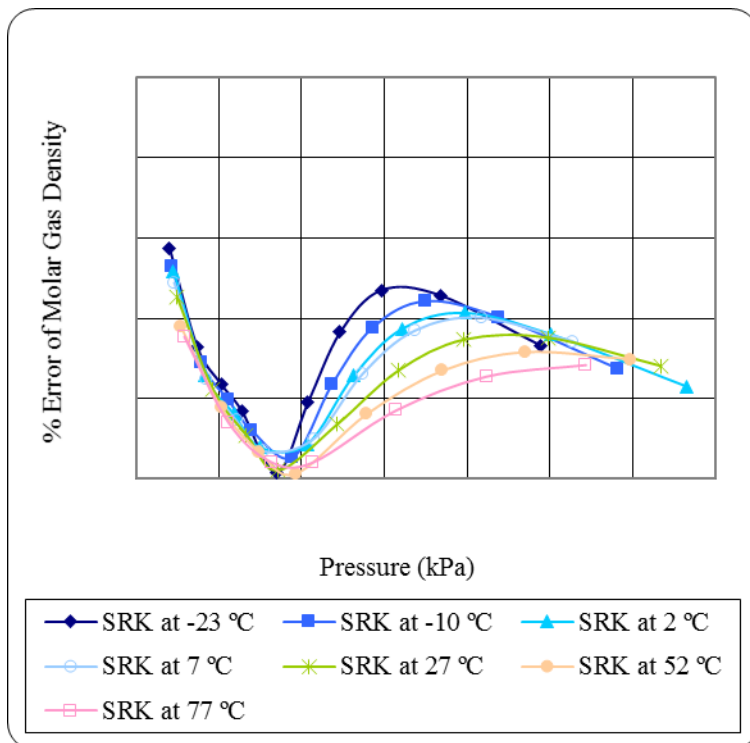


Figure D.10: Percentage errors of molar density predictions of SRK in supercritical region at diverse temperature for GU2

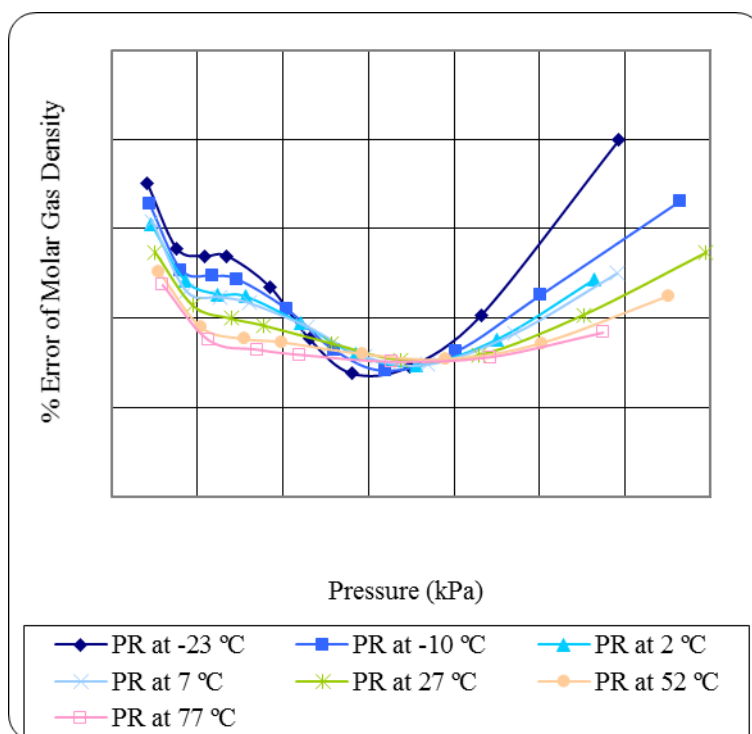


Figure D.11: Percentage errors of molar density predictions of PR in supercritical region at diverse temperature for GU1

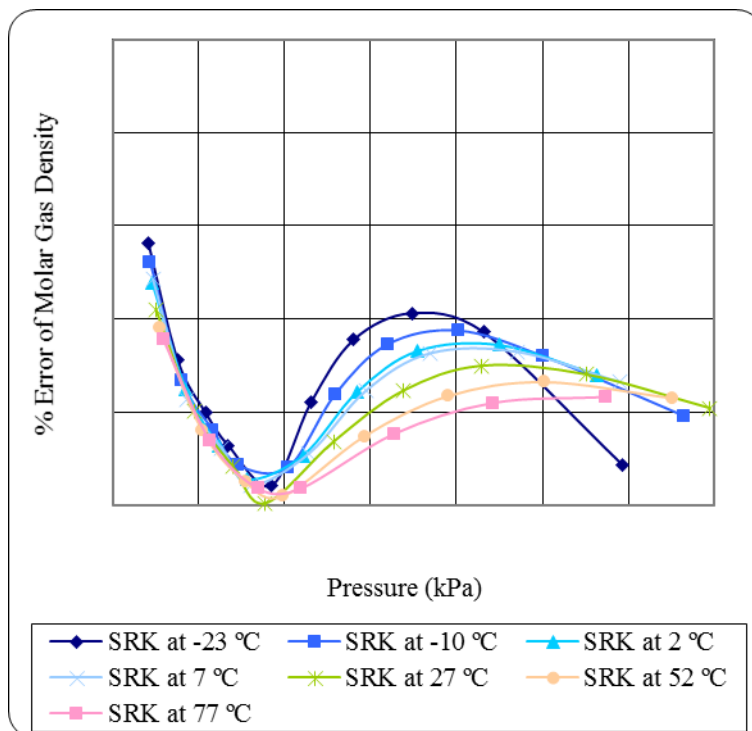


Figure D.12: Percentage errors of molar density predictions of SRK in supercritical region at diverse temperature for GU1

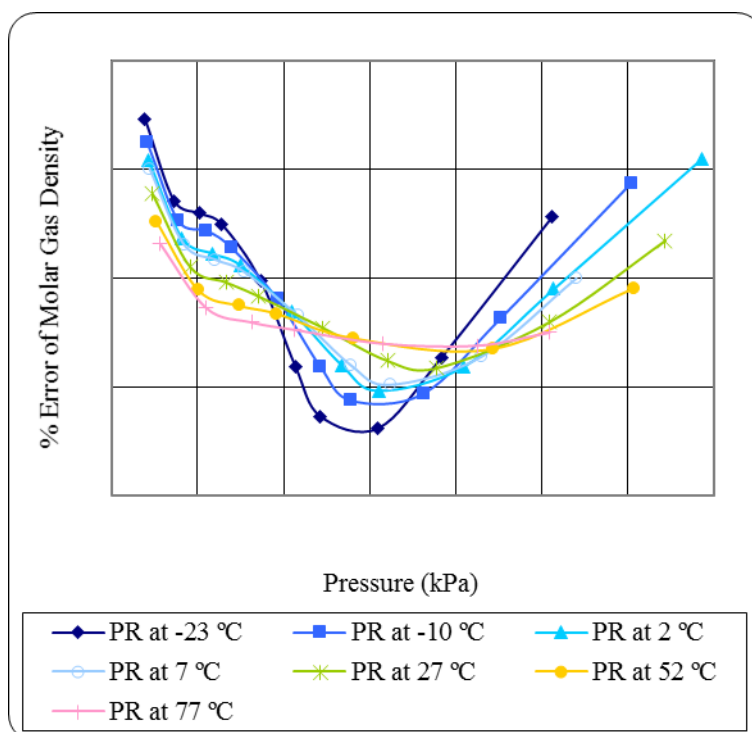


Figure D.13: Percentage errors of molar density predictions of PR in supercritical region at diverse temperature for NIST1

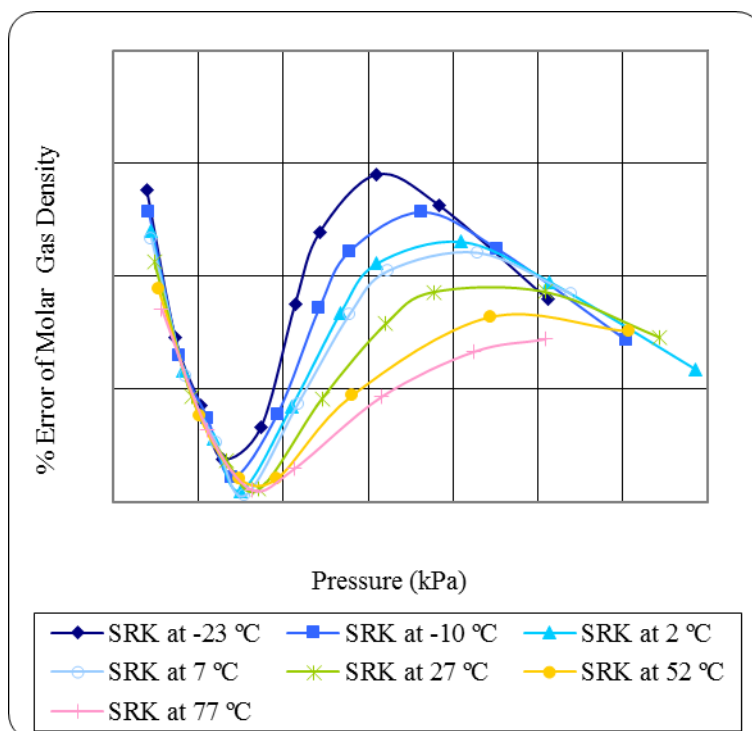


Figure D.14: Percentage errors of molar density predictions of SRK in supercritical region at diverse temperature for NIST1

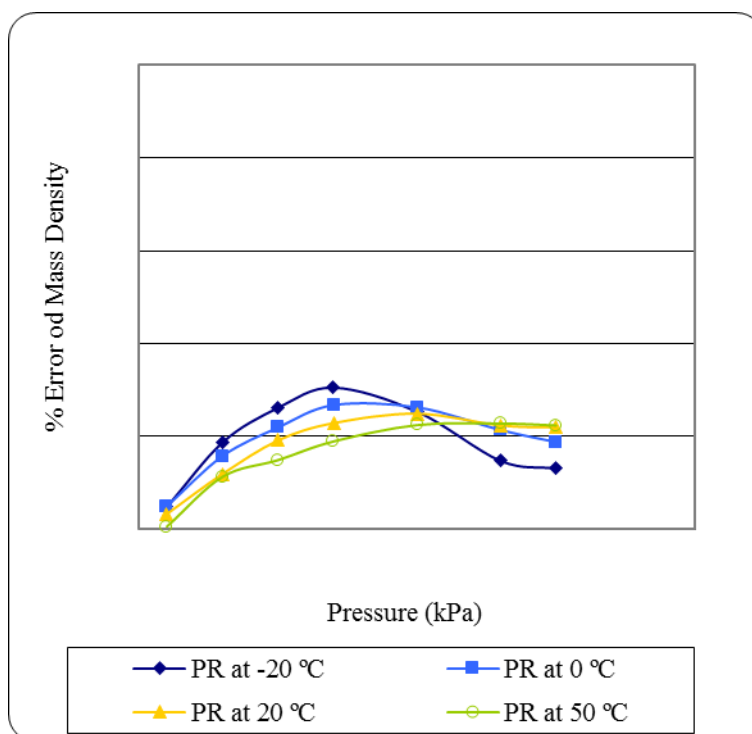


Figure D.15: Percentage errors of molar density predictions of PR in supercritical region at diverse temperature for Gas3

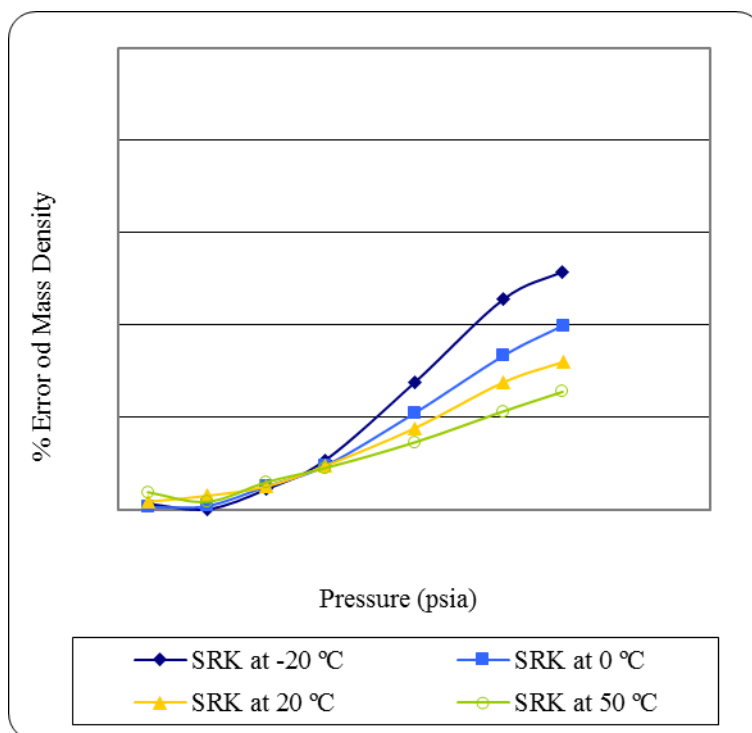


Figure D.16: Percentage errors of molar density predictions of SRK in supercritical region at diverse temperature for Gas3

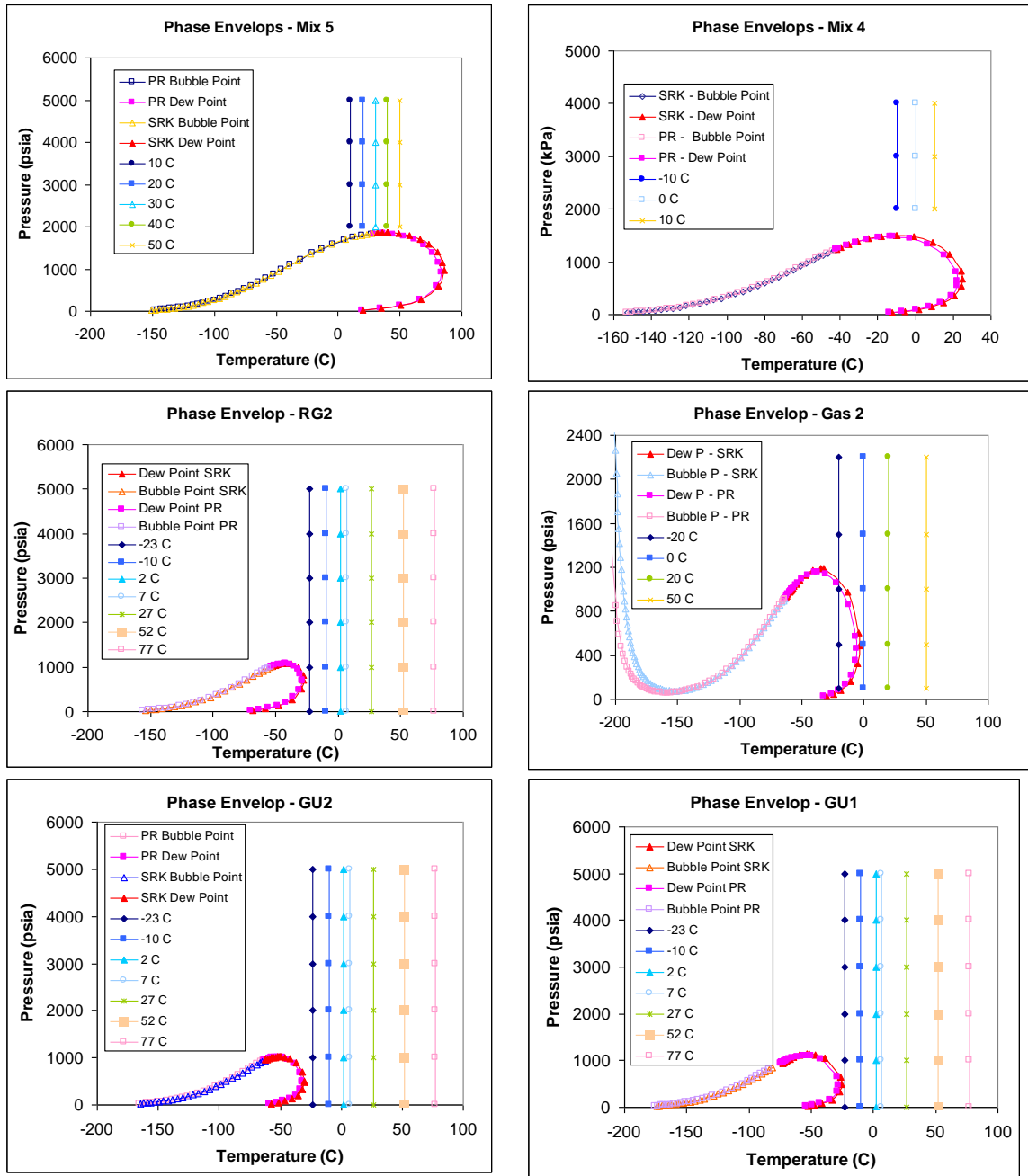


Figure D.17: Phase envelopes of the synthetic gas samples used in this study are indicated together with the isothermal where densities were measured.

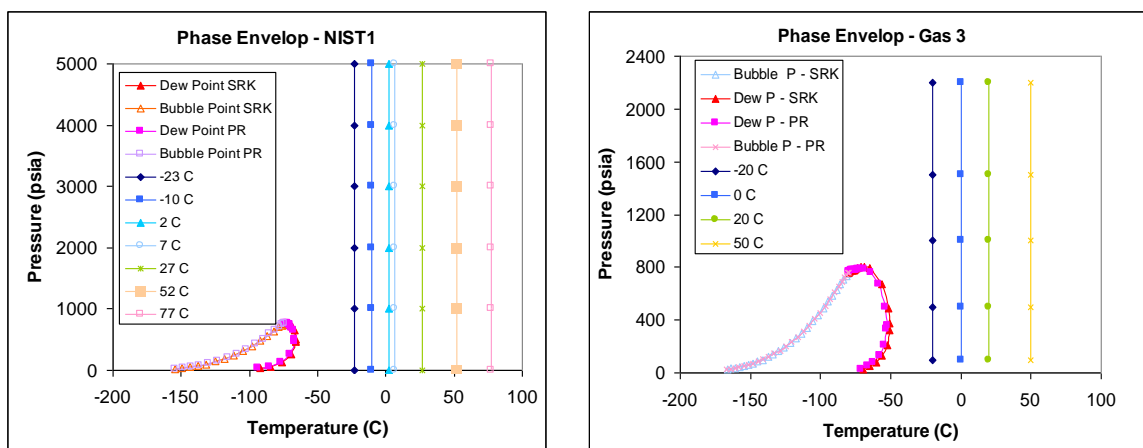


Figure D.18: Phase envelopes of the synthetic gas samples used in this study are indicated together with the isothermal where densities were measured.

APPENDIX E

E.1 Binary Interaction Parameters (k_{ij})

E.1.1 Original k_{ij} for PR and SRK used for synthetic gas samples

The original k_{ij} of PR and SRK equations are indicated in Tables E.1 and E.2, respectively.

Table E.1: k_{ij} for PR equation

	CO ₂	H ₂ S	CH ₄	C ₂ H ₆	C ₃ H ₈	iC ₄ H ₁₀	nC ₄ H ₁₀	iC ₅ H ₁₂	nC ₅ H ₁₂	nC ₆ H ₁₄	McyloC5	nC ₇ H ₁₆	nC ₈ H ₁₈
N ₂	-0.020	0.1676	0.0360	0.0500	0.0800	0.0950	0.0900	0.0950	0.1000	0.1490	0.1000	0.1439	0.1000
CO ₂		0.1000	0.1000	0.1298	0.1350	0.1298	0.1298	0.1250	0.1250	0.1250	0.1010	0.1199	0.1150
H ₂ S			0.0850	0.0840	0.0750	0.0500	0.0600	0.0600	0.0650	0.0600	0.0450	0.0600	0.0550
CH ₄				0.0022	0.0068	0.0131	0.0123	0.0176	0.0179	0.0235	0.0187	0.0289	0.0342
C ₂ H ₆					0.0013	0.0046	0.0041	0.0074	0.0076	0.0114	0.0081	0.0153	0.0193
C ₃ H ₈						0.0010	0.0008	0.0026	0.0027	0.0051	0.0030	0.0079	0.0109
iC ₄ H ₁₀							0.0000	0.0003	0.0004	0.0016	0.0005	0.0032	0.0052
nC ₄ H ₁₀								0.0005	0.0005	0.0019	0.0007	0.0036	0.0058
iC ₅ H ₁₂									0.0000	0.0004	0.0000	0.0015	0.0029
nC ₅ H ₁₂										0.0004	0.0011	0.0014	0.0028
nC ₆ H ₁₄											-0.0023	0.0003	0.0011
McyloC5												0.0012	0.0025
nC ₇ H ₁₆													0.0002

Table E.2: k_{ij} for SRK equation

	CO ₂	H ₂ S	CH ₄	C ₂ H ₆	C ₃ H ₈	iC ₄ H ₁₀	nC ₄ H ₁₀	iC ₅ H ₁₂	nC ₅ H ₁₂	nC ₆ H ₁₄	McyloC5	nC ₇ H ₁₆	nC ₈ H ₁₈
N ₂	-0.0171	0.1588	0.0312	0.0319	0.0886	0.1315	0.0597	0.0930	0.0936	0.1650	0.1000	0.0800	0.0800
CO ₂		0.1150	0.0956	0.1401	0.1368	0.1368	0.1412	0.1297	0.1347	0.1420	0.1089	0.1092	0.1350
H ₂ S			0.0888	0.0862	0.0925	0.0560	0.0626	0.0650	0.0709	0.0570	0.0450	0.0787	0.0550
CH ₄				0.0022	0.0068	0.0131	0.0123	0.0176	0.0179	0.0235	0.0187	0.0289	0.0342
C ₂ H ₆					0.0013	0.0046	0.0041	0.0074	0.0076	0.0114	0.0081	0.0153	0.0193
C ₃ H ₈						0.0010	0.0008	0.0026	0.0027	0.0051	0.0030	0.0079	0.0109
iC ₄ H ₁₀							0.0000	0.0003	0.0004	0.0016	0.0005	0.0032	0.0052
nC ₄ H ₁₀								0.0005	0.0005	0.0019	0.0007	0.0036	0.0058
iC ₅ H ₁₂									0.0000	0.0004	0.0000	0.0015	0.0029
nC ₅ H ₁₂										0.0004	0.0012	0.0014	0.0028
nC ₆ H ₁₄											-0.0007	0.0003	0.0011
McyloC5												0.0012	0.0025
nC ₇ H ₁₆													0.0002

E.1.2 k_{ij} for PR used for NG3 sample

The k_{ij} of PR equation for the normal component and for the each pseudo components are illustrated in the following two tables, Table E.3 indicated the k_{ij} of PR and the k_{ij} created by Hysys for each components combination, according to their thermodynamic properties of each pseudo components (i.e. critical properties (T, P, V, and acentricity),

molecular weight (MW), normal boiling point and ideal liquid density). Table E.3 indicated the k_{ij} after performing a regression analysis, which has different k_{ij} for the last two pseudo hydrocarbon components.

Table E.3: k_{ij} for PR equation for sample NG3

	N ₂	CH ₄	C ₂ H ₆	C ₃ H ₈	iC ₄ H ₁₀	nC ₄ H ₁₀	iC ₅ H ₁₂	nC ₅ H ₁₂	C ₆	C ₇ -C ₉	C ₁₀ -C ₁₃	C ₁₄ -C ₁₈	C ₁₉ -C ₂₆	C ₂₇ -C ₃₀
CO ₂	-0.020	0.1000	0.1298	0.1350	0.1298	0.1298	0.1250	0.1250	0.1010	0.1010	0.1010	0.1010	0.1010	0.1010
N ₂		0.0360	0.0500	0.0800	0.0950	0.0900	0.0950	0.1000	0.1000	0.1000	0.1000	0.1000	0.1000	0.1000
CH ₄			0.0022	0.0068	0.0131	0.0123	0.0176	0.0179	0.0237	0.0268	0.0421	0.0564	0.0670	0.0772
C ₂ H ₆				0.0013	0.0046	0.0041	0.0074	0.0076	0.0116	0.0138	0.0255	0.0372	0.0461	0.0549
C ₃ H ₈					0.0010	0.0008	0.0026	0.0027	0.0052	0.0068	0.0157	0.0252	0.0328	0.0404
iC ₄ H ₁₀						0.0000	0.0003	0.0004	0.0016	0.0025	0.0087	0.0162	0.0225	0.0289
nC ₄ H ₁₀							0.0005	0.0005	0.0019	0.0029	0.0094	0.0171	0.0235	0.0301
iC ₅ H ₁₂								0.0000	0.0005	0.0010	0.0056	0.0119	0.0173	0.0231
nC ₅ H ₁₂									0.0004	0.0009	0.0055	0.0116	0.0171	0.0228
C ₆										0.0001	0.0029	0.0077	0.0122	0.0171
C ₇ -C ₉											0.0019	0.0060	0.0101	0.0146
C ₁₀ -C ₁₃												0.0012	0.0033	0.0061
C ₁₄ -C ₁₈													0.0005	0.0019
C ₁₉ -C ₂₆														0.0004
C ₂₇ -C ₃₀														

Table E.4: k_{ij} for PR equation after tuning

	N ₂	CH ₄	C ₂ H ₆	C ₃ H ₈	iC ₄ H ₁₀	nC ₄ H ₁₀	iC ₅ H ₁₂	nC ₅ H ₁₂	C ₆	C ₇ -C ₉	C ₁₀ -C ₁₃	C ₁₄ -C ₁₈	C ₁₉ -C ₂₆	C ₂₇ -C ₃₀
CO ₂	-0.020	0.1000	0.1298	0.1350	0.1298	0.1298	0.1250	0.1250	0.1010	0.1010	0.1010	0.1010	0.125	0.125
N ₂		0.0360	0.0500	0.0800	0.0950	0.0900	0.0950	0.1000	0.1000	0.1000	0.1000	0.1000	0.12	0.12
CH ₄			0.0022	0.0068	0.0131	0.0123	0.0176	0.0179	0.0237	0.0268	0.0421	0.0564	-0.0070	-0.0022
C ₂ H ₆				0.0013	0.0046	0.0041	0.0074	0.0076	0.0116	0.0138	0.0255	0.0372	0	0
C ₃ H ₈					0.0010	0.0008	0.0026	0.0027	0.0052	0.0068	0.0157	0.0252	0	0
iC ₄ H ₁₀						0.0000	0.0003	0.0004	0.0016	0.0025	0.0087	0.0162	0	0
nC ₄ H ₁₀							0.0005	0.0005	0.0019	0.0029	0.0094	0.0171	0	0
iC ₅ H ₁₂								0.0000	0.0005	0.0010	0.0056	0.0119	0	0
nC ₅ H ₁₂									0.0004	0.0009	0.0055	0.0116	0	0
C ₆										0.0001	0.0029	0.0077	0	0
C ₇ -C ₉											0.0019	0.0060	0	0
C ₁₀ -C ₁₃												0.0012	0	0
C ₁₄ -C ₁₈													0	0
C ₁₉ -C ₂₆														0
C ₂₇ -C ₃₀														

E.1.3 Volume translation parameters

The volume translation parameters of each component were calculated with the two adjustable parameters d_1 and d_2 , using Equations 5.13. The resulting values of the volume translation parameters before and after tuning the EOS of Mix 5 and NG3 are indicated in Tables E.5 and E.6.

Table E.5: Volume translation parameters of each component for PR equation before and after tuning for Mix 5

New d₁	0.297361										
New d₂	0.059003										
	CH₄	C₂H₆	C₃H₈	iC₄H₁₀	nC₄H₁₀	iC₅H₁₀	nC₅H₁₀	MecycloC₅	nC₆H₁₄	nC₇H₁₆	nC₈H₁₈
Tc (°C)	-82.5	32.3	96.7	134.9	152.0	187.2	196.5	234.7	259.6	267.0	295.4
Pc (MPa)	4.64	4.88	4.26	3.65	3.80	3.33	3.38	3.03	3.79	2.74	2.50
V ^t Tuned (m ³ /kgmol)	0.0077	0.0118	0.0164	0.0212	0.0213	0.0262	0.0266	0.0322	0.0270	0.0380	0.0441

Table E.6: Volume translation parameters of each component for PR equation before and after tuning for NG3

d1	0.7078														
d2	0.0692														
	CH ₄	C ₂ H ₆	C ₃ H ₈	iC ₄ H ₁₀	nC ₄ H ₁₀	iC ₅ H ₁₀	nC ₅ H ₁₀	C ₆	C ₇ -C ₉	C ₁₀ C ₁₃	C ₁₄ C ₁₈	C ₁₉ C ₂₆	C ₂₇ C ₈₀	CO ₂	N ₂
Tc (C)	-82.5	32.3	96.7	134.9	152.0	187.2	196.5	234.4	278.9	343.7	408.9	481.5	610.0	31.0	-147.0
Pc MPa	4.64	4.88	4.26	3.65	3.80	3.33	3.38	3.01	2.86	2.12	1.65	1.40	1.22	7.37	3.39
V	0.0185	0.0283	0.0394	0.0508	0.0509	0.0629	0.0635	0.0771	0.0884	0.1343	0.1904	0.2475	0.3270	0.0187	0.0167